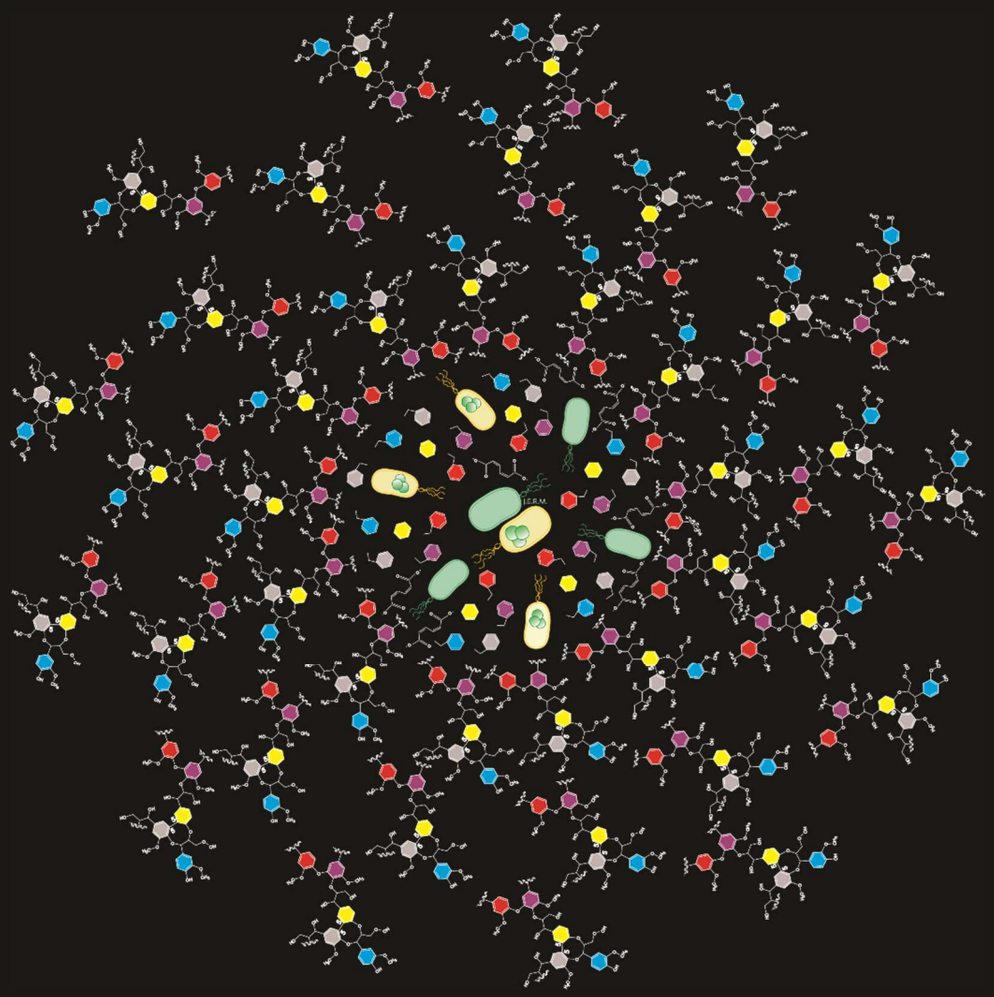

Lignin aromatics valorization by *Pseudomonas putida*

Juan E. Ramírez M.

2021

Juan E. Ramírez M.

Lignin aromatics valorization by *Pseudomonas putida*:

Novel strategies to increase the production of *mcl*-polyhydroxyalkanoate and *cis,cis*-muconic acid

GHENT UNIVERSITY

RWTH AACHEN UNIVERSITY

Lignin aromatics valorization by *Pseudomonas putida*: novel strategies to increase the production of *mcl*-polyhydroxyalkanoate and *cis,cis*-muconic acid

Von der Fakultät für Mathematik, Informatik und Naturwissenschaften der RWTH Aachen University zur Erlangung des akademischen Grades eines Doktors der Naturwissenschaften genehmigte Dissertation

vorgelegt von

Juan Esteban Ramírez Morales

M. Sc. Biochemical Engineering

aus

Medellín,
Antioquia, Colombia

Berichter: Univ.-Prof. Dr.-Ing. Lars M. Blank
Univ.-Prof. Dr.-Ing. Korneel Rabaey
Univ.-Prof. Dr. rer. nat. Miriam Agler-Rosenbaum

Tag der mündlichen Prüfung: 26.10.2021

Diese Dissertation ist auf den Internetseiten der Universitätsbibliothek verfügbar.

Eidesstattliche Erklärung

Juan Esteban Ramírez M.

erklärt hiermit, dass diese Dissertation und die darin dargelegten Inhalte die eigenen sind und selbstständig, als Ergebnis der eigenen originären Forschung, generiert wurden. Hiermit erkläre ich an Eides statt

1. Diese Arbeit wurde vollständig oder größtenteils in der Phase als Doktorand dieser Fakultät und Universität angefertigt;

2. Sofern irgendein Bestandteil dieser Dissertation zuvor für einen akademischen Abschluss oder eine andere Qualifikation an dieser oder einer anderen Institution verwendet wurde, wurde dies klar angezeigt;

3. Wenn immer andere eigene- oder Veröffentlichungen Dritter herangezogen wurden, wurden diese klar benannt;

4. Wenn aus anderen eigenen- oder Veröffentlichungen Dritter zitiert wurde, wurde stets die Quelle hierfür angegeben. Diese Dissertation ist vollständig meine eigene Arbeit, mit der Ausnahme solcher Zitate;

5. Alle wesentlichen Quellen von Unterstützung wurden benannt;

6. Wenn immer ein Teil dieser Dissertation auf der Zusammenarbeit mit anderen basiert, wurde von mir klar gekennzeichnet, was von anderen und was von mir selbst erarbeitet wurde;

7. Ein Teil oder Teile dieser Arbeit wurden zuvor veröffentlicht und zwar in

Ramírez-Morales J. E., Czichowski P., Besirlioglu V., Regestein L., Rabaey K., Blank L. M., Rosenbaum M. Lignin aromatics to PHA polymers: nitrogen and oxygen are the key factors for *Pseudomonas*. 2021. *ACS Sustainable Chemistry & Engineering*, 9, 31, 10579–10590. https://doi.org/10.1021/acssuschemeng.1c02682

Aachen 30.11.2021

Juan Esteban Ramírez M.

"The science knowledge only adds to the excitement, the mystery and the awe of a flower"

Richard P. Feynman

Dedicada a mi familia, especialmente a mi abuelo Alvaro Morales (Q.E.P.D.)

Dissertation supervisors:

Prof. dr. ir. Lars Blank (Thesis Advisor)
Institute of Applied Microbiology (iAMB), Department of Biology, Faculty of Mathematics, Computer Science and Natural Sciences, RWTH Aachen University, Germany

Prof. dr. ir. Korneel Rabaey (Thesis Advisor)
Center for Microbial Ecology and Technology (CMET), Department of Biotechnology, Faculty of Bioscience Engineering, Ghent University, Belgium

Prof. dr. Miriam Agler-Rosenbaum (External promotor)
Leibniz Institute for Natural Product Research and Infection Biology, Hans Knöll Institute (HKI), Jena, Germany; Faculty of Biological Sciences, Friedrich-Schiller-University Jena, Germany

Members of the examination committee:

Prof. dr. Alan Slusarenko (Chair
Department of Plant Physiology, Faculty of Mathematics, Computer Science and Natural Sciences, RWTH Aachen University, Germany

Prof. dr. ir. Marjan De Mey
Centre for Synthetic Biology (CSB), Department of Biotechnology, Faculty of Bioscience Engineering, Ghent University, Belgium

Prof. dr. Ramon Ganigué
Center for Microbial Ecology and Technology (CMET), Department of Biotechnology, Faculty of Bioscience Engineering, Ghent University, Belgium

Dr. René Rozendal
Managing Director Paques Biomaterials, Balk, The Netherlands

Dean of the Faculty of Mathematics, Computer Science and Natural Sciences RWTH Aachen University	**Dean of the Faculty of Bioscience Engineering, Ghent University**
Univ. Prof. Dr. rer. nat. Carsten Honerkamp	Prof. dr. ir. Marc Van Meirvenne
Rector of RWTH Aachen University	**Rector of Ghent University**
Univ. Prof. Dr. rer. nat. Dr. h. c. mult. Ulrich Rüdiger	Prof. dr. Rik Van de Walle

Titel van het doctoraat in het Nederlands:

Lignine-aromaten valorisatie door *Pseudomonas putida*: nieuwe strategieën om de productie van *mcl*-polyhydroxyalkanoaat en *cis,cis*-muconzuur te verhogen

Cover illustration: Juan Esteban Ramírez M

Ramirez-Morales J.E.., Lignin aromatics valorization by *Pseudomonas putida*: novel strategies to increase the production of *mcl*-polyhydroxyalkanoate and *cis,cis*-muconic acid, PhD thesis, **2021**, RWTH Aachen University, Germany ; Ghent University, Belgium.

The author and the promotors give the authorization to consult and to copy parts of this work for personal use only. Every other use is subject to the copyright laws. Permission to reproduce any material contained in this work should be obtained. Copyright ©

Acknowledgements

I want to start by expressing my gratitude to my advisor Prof. Dr. Miriam Agler-Rosenbaum who was always supporting me in all the places where this thesis took place. From a distance or close, you always offered me kindness, patience and of course an excellent scientific guide. Thanks for giving me the opportunity to come to Germany, where I could perform high quality research supported by an excellent funded project. I really appreciate all the valuable time that you invested on improving this thesis. I am also grateful to Prof. Lars Blank who gave me wise scientific advice and the chance to work in an excellent but also very cool research institute (iAMB Aachen). Many thanks to my co-supervisor Prof. Korneel Rabaey who gave me very close scientific and technical guidance while I was doing my secondment at CMET (Ghent), the most international and diverse research group I've been to. Many thanks to Manja for helping me all this time. I really appreciate your easy-going personality, which helped to ease many times the stress generated on dealing with many administrative loads. My gratitude to the European Union's Horizon 2020 research and innovation programme (Marie Skłodowska-Curie grant) for letting me to develop a stronger ''cultural Intelligence'' while doing networking with international peers.

There are now so many good memories with so many nice people that I met in Aachen, Ghent, Leeuwarden and Jena. Thanks to the former Rosenbaum group: Liesa, Simone, Carola, Ivan, Kristina, Ronny, Desy, Valeria, Annika, Lisa, Phillip and Erick. I will remember so many good and funny times spent in the lab, conferences, hikes in the nature, etc. Thanks a lot to many kind, cool and helpful people that I also met in the iAMB group, so many beer and grill mates, some of them with really good talent for baking as well: Dario, Dieter, Carl, Nick, Vinicius, Tobias, Till, Wing-Jin, Christoph, Birthe, Hamed, Philipp, Ulf, Annette, Gisela, Isabel, Nugraha, Hendrik, Mariam, Salome, Maike, Benedikt, and Sebastian. A huge institute! Quiero agradecer el apoyo y buena energía de mis amigos en Aachen, Elpi, Farha, Daniel, que los conocí por hablar español y que incluso viajaron a Colombia y visitaron mi familia. También quiero agradecer a Monika, por su amabilidad y oportuna ayuda.

Thanks to the CMET group, for introducing me a bit in the Belgian beer culture and share so many international experiences: Bárbara, Lotte, José, Eleftheria, Myrsini Sakarika, Suanny, Eline, Jan, Luiza, Jolien, Karel, Antonin, Regine, Tim, Mike, Greet, Ioanna, Jorien, Cindy, Pieter x2, Funda, Florian, Naya, Stephen, Xiaofei, Tyler, Rui, Amanda, Martin, Camille, Xiaoting and Xu. That's another huge research group! Thanks to Shengle, Matthias, Nienke, San, Erick and João for a nice experience at Paques, without you my idea about Friesland it would not have been the same.

I couldn't miss the opportunity to be grateful with my Super W project colleagues, with whom I also shared excellent times in intensive workshops, universities and European cities: Marco, Larissa, Pamela, Shengle again, Yohannis, Amelia, Kazem, Kasper, Philipp, Negar, Aleksandra, Iryna and the funny Mojtaba!.

As I landed finally in Jena, welcoming, kind and helpful friends and colleagues also contributed to the completion of my research: Lars, Svetlana, Santiago, Ana, Ivan again, Carola again, Annika again, Bettina, Ronja, Gundela, Karin, Johann, Dede, Sundar, Bianka, Angel, Stefanie, Furkan, Anthony, Nico, Askan, Zubaish, Michael x2, Uwe, Gudrun, Jan, Karsten, Matthias. For sure thanks to Onyi and Sanowar. Their dedication contributed nicely to my research. En Jena también agradezco la compañía y momentos de relajo junto a Castri. Fue bueno coincidir en la misma ciudad Alamana.

Finalmente, quiero agradecer a mi familia por todo el apoyo en estos casi cinco años, el cual ha sido tan incansable a la distancia. Gracias también a Alina por brindarme su cariño y estar siempre pendiente.

Funding

This work was supported by the European Union's Horizon 2020 research and innovation programme under the Marie Skłodowska-Curie grant agreement No 676070 (SuPER-W).

This project has received funding from the *European Union's Horizon 2020 research and innovation programme under the* Marie Sklodowska-Curie grant agreement No 676070

Table of Contents

Abstract

Lignin, a major component of lignocellulosic biomass, is the most abundant aromatic polymer on the planet. Thus, it represents a renewable and non-fossil source of aromatics, promising to positively impact the transition to a circular bioeconomy. Despite being a chemical treasure box, lignin is still widely underutilized. In the last years, there is an emerging paradigm change towards implementing new biorefineries based on chemo- and/or biocatalytic upgrading of lignin aromatics into valuable products. Especially, in the biocatalytic conversion, the native aromatic catabolic ability of many *Pseudomomas* promises to ease the inherent aromatic heterogeneity of lignin depolymerized mixtures. Simultaneously, some *Pseudomomas* strains can synthesize valuable molecules for the polymer industry like medium chain length polyhydroxyalkanoate (*mcl*-PHA) and *cis,cis*-muconic acid. While enormous progress is underway in metabolic engineering towards improving conversion of aromatics into *mcl*-PHA, there is a significant gap in detailed bioprocess understanding, especially from mixtures of lignin-derived aromatics. Analogously, despite important advances on strain engineering and bioprocess development, limitations related to product accumulation at toxic levels still prevents reaching industrially-relevant productivities of *cis,cis*-muconic acid from lignin substrates. Thus, through understanding the key factors for successful bioconversion and applying this knowledge to implement innovative bioprocess strategies, this thesis intended to increase production of *mcl*-PHA and *cis,cis*-muconic acid from lignin aromatics.

After performing step-wise screenings and parallel cultivations of several known strains of the *Pseudomonas* family, this work clearly confirmed *Pseudomonas putida* KT24440 as the most robust, versatile, and well performing biocatalyst for *mcl*-PHA accumulation from a defined lignin aromatic mixture. In a next step, the detailed resolution of aromatics funneling and microbial metabolic activity was revealed during online measurements of the oxygen consumption. From this experience, oxygen and nitrogen availability were identified as the key factors for a successful biocatalytic upgrading. Overall, the accumulation of *mcl*-PHA was improved in the wild type strain under technically relevant conditions by up to 43% (polymer content in cell biomass, mg *mcl*-PHA mg^{-1} CDW). At this stage, the highest *mcl*-PHA concentration (582 mg L^{-1}) was obtained for a C/N ratio of 60 for oxygen-unlimited conditions (oxygen transfer rate ≥ 20 mmol L^{-1} h^{-1}). In contrast, aromatic intermediates accumulated under oxygen-limited conditions at oxygen transfer rates below 10 mmol L^{-1} h^{-1}. Through this bioprocess characterization, the performance of the biocatalytic funneling in *P. putida* KT2440 became predictable and thus, the experimental conditions were scalable into a 1-L stirred tank bioreactor based on the oxygen transfer rate. Finally, the benefits of implementing simultaneous biocatalyst and bioprocess optimization strategies were demonstrated. A 1.9-fold increment in *mcl*-PHA concentration and a 1.5-fold increment in *mcl*-PHA content were obtained from lignin aromatics.

To alleviate the negative effect of product accumulation at toxic levels, this thesis also implemented an innovative solution establishing an *in-line* extraction of *cis,cis*-muconate produced by a metabolically engineered strain of *P. putida* KT2240. The implementation followed a systematic approach of process development. First, an electrolytic extraction of *cis,cis*-muconate was characterized in terms of flux and Coulombic efficiency from a synthetic media. In parallel, *cis,cis*-muconic acid bioproduction rates were defined in a conventional process and the negative effect of *cis,cis* muconic acid on the culture was confirmed at a threshold concentration of 195 mM (27.7 g L^{-1}). In the middle time, long term electrolytic extractions were performed at a higher scale using fermentation broths as approximation of the final process. This experience served to identify and solve relevant technical drawbacks related to muconic acid precipitation in the anodic chamber. The solution consisted of pH control at 3.5, which was a suitable pH where higher amounts of the muconate isomeric forms *cis,cis*- and *cis,trans*- were found in solution (*i.e.,* not as precipitated form). This was essential to enable higher muconate accumulation in the anolyte. From all the process parameters (*i.e.,* bioproduction rates and extractive electrolytic performance) obtained separately, a final integration was carried out. Through implementing the *in-line* extraction from a bioreactor, the volumetric productivity of *cis,cis*-muconate was increased 15.6 % in respect to a conventional bioprocess run in parallel.

Overall, this study contributed to deepening our understanding of the biocatalytic capability of the promising bacterium *P. putida* KT2440 towards efficient conversions of lignin aromatics for future biorefinery applications. Additionally, the potential of selective removal of *cis,cis*-muconic acid was demonstrated for the first time in a microbial cultivation, contributing as an important step towards implementing a cost-effective bioproduction system.

Kurzfassung

Lignin, ein Hauptbestandteil der Lignocellulose-Biomasse, ist das am häufigsten vorkommende aromatische Polymer auf unserem Planeten. Somit stellt es eine erneuerbare und nicht fossile Quelle für Aromaten dar, die verspricht, den Übergang zu einer zirkulären Bioökonomie positiv zu beeinflussen. Obwohl es sich um eine wertvolle chemische Ressourse handelt, wird Lignin immer noch nicht ausreichend genutzt. In den letzten Jahren hat sich ein Paradigmenwechsel bei der Implementierung neuer Bioraffinerien ergeben und es wird vermehrt Wert auf die chemo- und / oder biokatalytische Aufbereitung von Ligninaromaten zu wertvollen Produkten gelegt. Insbesondere bei der biokatalytischen Umwandlung verspricht die natürliche katabolische Fähigkeit vieler Pseudomonaden Aromaten zu nutzen, die inhärente aromatische Heterogenität von depolymerisierten Lignin-Gemischen zu erleichtern. Gleichzeitig können einige *Pseudomomas*-Stämme wertvolle Moleküle für die Polymerindustrie wie Polyhydroxyalkanoate mittlerer Kettenlänge (*mcl*-PHA) und *cis,cis*-Mukonsäure synthetisieren. Während durch Metabolic Engineering enorme Fortschritte bei der Verbesserung der Umwandlung von Aromaten in *mcl*-PHA erzielt werden, gibt es eine erhebliche Lücke im detaillierten Verständnis von Bioprozessen, insbesondere bei Gemischen von Aromaten aus Lignin. Analog dazu verhindern ,trotz wichtiger Fortschritte bei der Stamm- und in der Bioprozessentwicklung, Limitationen durch toxische Effekte der Produktinhibierung immer noch, dass industriell relevante Produktivitäten von *cis,cis*-Mukonsäure aus Ligninsubstraten erreicht werden. Durch das Verständnis der Schlüsselfaktoren für eine erfolgreiche Biokonversion und deren Umsetzung in innovative Bioprozessstrategien sollte die Produktion von *mcl*-PHA und *cis,cis*-Mukonsäure aus Ligninaromaten gesteigert werden.

Nach schrittweisen Screenings und vergleichenden Kultivierungen mehrerer bekannter Stämme der *Pseudomonas*-Familie bestätigte diese Arbeit eindeutig, dass *Pseudomonas putida* KT24440 der robusteste, vielseitigste und leistungsfähigste Biokatalysator für die Akkumulation von *mcl*-PHA aus einem definierten aromatischen Lignin-Gemisch ist. In einem nächsten Schritt wurde die detaillierte Aromatenverwertung und diemikrobielle Stoffwechselaktivität durch Online-Messungen des Sauerstoffverbrauchs aufgelöst. Durch diese Untersuchungen wurde die Verfügbarkeit von Sauerstoff und Stickstoff als Schlüsselfaktor für eine erfolgreiche biokatalytische Verbesserung identifiziert. Insgesamt wurde die Bildung von *mcl*-PHA im Wildtyp-Stamm unter technisch relevanten Bedingungen um bis zu 43% (mg *mcl*-PHA mg^{-1} CDW) verbessert . Die höchste mcl-PHA-Konzentration (582 mg L^{-1}) wurde für ein C/N-Verhältnis von 60 unter Bedingungen ohne Sauerstofflimitierung erhalten (Sauerstoffübertragungsrate ≥ 20 mmol L^{-1} h^{-1}). Im Gegensatz dazu akkumulierten aromatische Zwischenprodukte unter sauerstofflimitierten Bedingungen bei Sauerstoffübertragungsraten unter 10 mmol L^{-1} h^{-1}. Durch diese Bioprozess-Charakterisierung wurde die Leistungsfähigkeit des biokatalytischen Aromatenumwandlung in *P. putida* KT2440 vorhersehbar und die experimentellen Bedingungen basierend auf der

Sauerstoffübertragungsrate in einen 1-l-Rührkessel-Bioreaktor skalierbar. Schließlich wurden die Vorteile von Strategien zur gleichzeitigen Optimierung von Biokatalysatoren und Bioprozessen demonstriert. Eine 1,9-fache Erhöhung der *mcl*-PHA-Konzentration und eine 1,5-fache Erhöhung des *mcl*-PHA-Gehalts wurden aus Ligninaromaten erzielt.

Um den negativen, toxischen Effekt der Produktakkumulation von *cis,cis*-Mukonsäurezu mildern, wurde in dieser Arbeit auch eine innovative Lösung zur Inline-Extraktion von *cis,cis*-Mukonat etabliert, das von einem genetisch verändertem Stamm von *P. putida* KT2240 gebildet wird. Die Umsetzung folgte einem systematischen Ansatz der Prozessentwicklung. Zunächst wurde eine elektrolytische Extraktion von *cis,cis*-Mukonat hinsichtlich Rate und Coulombischer-Effizienz aus einem synthetischen Medium charakterisiert. Parallel dazu wurden die Bioproduktionsraten von *cis,cis*-Mukonsäure in einem herkömmlichen Bioprozessen definiert und die negative Wirkung von *cis, cis*-Mukonsäure auf die Kultur bei einer Schwellenkonzentration von 195 mM (27,7 g L^{-1}) bestätigt. Anschließend wurden elektrolytische Langzeitextraktionen in höherem Maßstab unter Verwendung von Fermentationsbrühen als Annäherung an den Endprozess durchgeführt. Diese Erfahrung diente dazu, relevante technische Nachteile im Zusammenhang mit der Ausfällung von Mukonsäure in der anodischen Kammer zu identifizieren und zu lösen. Die Lösung bestand aus einer pH-Kontrolle bei 3,5, was ein geeigneter pH war, bei dem höhere Mengen der Mukonsäureisomere *cis,cis*- und *cis,trans*- in Lösung gefunden wurden (d. h. nicht als ausgefällte Form). Dies war entscheidend, um eine stärkere Anreicherung von Mukonat im Anolyten zu ermöglichen. Basierend auf allen Prozessparametern (d. h., den Bioproduktionsraten und der extraktiven Elektrolyseleistung), die aus den getrennten Schritten erhalten wurden, wurde eine endgültige Prozessintegration abgeleitet. Durch die Durchführung der InLine-Extraktion aus einem Bioreaktor wurde die volumetrische Produktivität von *cis,cis*-Muonat gegenüber einem herkömmlichen parallel laufenden Bioprozess um 15,6% erhöht.

Insgesamt trägt diese Studie dazu bei, unser Verständnis der biokatalytischen Fähigkeit des vielversprechenden Bakteriums *P. putida* KT2440 zur effizienten Umwandlung von Ligninaromaten für zukünftige Bioraffinerieanwendungen zu vertiefen. Darüber hinaus wurde erstmals in einer mikrobiellen Kultivierung das Potenzial der selektiven Entfernung von *cis,cis*-Muconsäure nachgewiesen, was einen wichtigen Schritt zur Etablierung eines kostengünstigen Bioproduktionssystems darstell.

Samenvatting

Lignine, een belangrijk bestanddeel van lignocellulose biomassa, is het meest voorkomende aromatische polymeer op aarde. Het vertegenwoordigt een hernieuwbare en niet-fossiele bron van aromaten, met de belofte een positieve invloed te hebben op de overgang naar een circulaire bio-economie. Ondanks dat lignine een chemische schatkist is, wordt het sterk onderbenut. In de afgelopen jaren is er een paradigmaverandering gaande rond de implementatie van nieuwe bioraffinaderijen op basis van chemo- en/of biokatalytische opwaardering van lignine-aromaten tot waardevolle producten. Vooral bij de biokatalytische omzetting belooft het natieve aromatische katabolische vermogen van veel Pseudomonadacea de inherente aromatische heterogeniteit van met lignine gedepolymeriseerde mengsels te vergemakkelijken. Tegelijkertijd kunnen sommige Pseudomomas-stammen waardevolle moleculen voor de polymeerindustrie synthetiseren, zoals polyhydroxyalkanoaat met middellange ketenlengte (*mcl*-PHA) en *cis,cis*-muconzuur. Hoewel er enorme vooruitgang wordt geboekt op het gebied van metabolische engineering om de omzetting van aromaten in *mcl*-PHA te verbeteren, is er een aanzienlijke lacune in het gedetailleerde begrip van bioprocessen, vooral van mengsels van van lignine afgeleide aromaten. Analoog, ondanks belangrijke vooruitgang op het gebied van stam-engineering en bioprocesontwikkeling, voorkomen beperkingen door accumulatie van toxische intermediairen nog steeds het bereiken van industrieel relevante productiviteiten van *cis,cis*-muconzuur uit ligninesubstraten. In dit proefschrift beoogden we de productie van *mcl*-PHA en *cis,cis*-muconzuur uit lignine-aromaten te verhogen door de sleutelfactoren voor succesvolle bioconversie te begrijpen en deze te implementeren in innovatieve bioprocesstrategieën.

Na het uitvoeren van stapsgewijze screenings en parallelle cultivatie van verschillende bekende stammen van de *Pseudomonas*-familie, bevestigde dit werk duidelijk *Pseudomonas putida* KT24440 als de meest robuuste, veelzijdige en goed presterende biokatalysator voor *mcl*-PHA-accumulatie uit een gedefinieerd aromatisch lignine-mengsel. In een volgende stap werd met hoge resolutie de funnelling van aromaten en microbiële metabolische activiteit onthuld tijdens online metingen van het zuurstofverbruik. Op basis van deze ervaring werd de beschikbaarheid van zuurstof en stikstof geïdentificeerd als de belangrijkste factoren voor een succesvolle biokatalytische opwaardering. Over het algemeen was de accumulatie van *mcl*-PHA in de wildtype-stam onder technisch relevante omstandigheden tot 43% (mg *mcl*-PHA mg^{-1} CDW) verbeterd. In dit stadium werd de hoogste *mcl*-PHA-concentratie (582 mg L^{-1}) verkregen voor een C/N-verhouding van 60 voor zuurstofrijke omstandigheden (zuurstofoverdrachtssnelheid ≥ 20 mmol L^{-1} h^{-1}). Daarentegen accumuleerden aromatische tussenproducten onder zuurstofbeperkende omstandigheden bij zuurstofoverdrachtssnelheden van minder dan 10 mmol L^{-1} h^{-1}. Door deze karakterisering van het bioproces werd de prestatie van de biokatalytische trechter in *P. putida* KT2440

voorspelbaar en dus waren de experimentele omstandigheden schaalbaar in een bioreactor met geroerde tank van 1 L op basis van de zuurstofoverdrachtssnelheid. Ten slotte werden de voordelen aangetoond van het implementeren van gelijktijdige strategieën voor biokatalysator- en bioprocesoptimalisatie. Een 1.9-voudige toename in *mcl*-PHA-concentratie en een 1.5-voudige toename in *mcl*-PHA-gehalte werden verkregen uit lignine-aromaten.

Om het negatieve effect van productaccumulatie op toxische niveaus te verminderen, implementeerden we in dit proefschrift ook een innovatieve oplossing voor een *in-line* extractie van *cis,cis*-muconaat geproduceerd door een metabolisch gemanipuleerde stam van *P. putida* KT2240. Eerst werd een elektrolytische extractie van *cis,cis*-muconaat gekarakteriseerd in termen van flux en coulometrische efficiëntie uit een synthetisch medium. Tegelijkertijd werden *cis,cis*-muconzuur-bioproductiesnelheden gedefinieerd in een conventioneel proces en het negatieve effect van *cis,cis*-muconzuur op de cultuur werd bepaald, met een drempelconcentratie van 195 mM (27.7 g L^{-1}). In de tussentijd werden langdurige elektrolytische extracties op grotere schaal uitgevoerd met behulp van fermentatie media als benadering van het uiteindelijke proces. Deze experimenten dienden ook om technische nadelen met betrekking tot muconzuurprecipitatie in de anodekamer te identificeren en op te lossen. De oplossing bestond uit een pH controle op 3.5, wat een geschikte pH was waar grotere hoeveelheden van de muconaat-isomeervormen *cis,cis*- en *cis,trans*- in oplossing werden gehouden (d.w.z. niet in geprecipiteerde vorm). Dit was essentieel om een hogere accumulatie van muconaat in de anoliet mogelijk te maken. Van alle afzonderlijk verkregen procesparameters (d.w.z. bioproductiesnelheden en extractieve elektrolytische prestaties) werd een definitieve integratie uitgevoerd. Door de *in-line* extractie uit een bioreactor te implementeren, werd de volumetrische productiviteit van cis,cis-muconaat met 15.6% verhoogd ten opzichte van een conventioneel parallel lopend bioproces.

Over het algemeen heeft deze studie bijgedragen aan het verdiepen van ons begrip van het biokatalytische vermogen van de veelbelovende bacterie *P. putida* KT2440 naar efficiënte omzettingen van lignine-aromaten voor toekomstige bioraffinagetoepassingen. Bovendien werd het potentieel van selectieve verwijdering van cis,cis-muconzuur voor de eerste keer aangetoond in een microbiële cultuur, wat een belangrijke stap was naar de implementatie van een kosteneffectief bioproductiesysteem.

List of Abbreviations

Abbreviation	Explanation
AEM	Anion exchange membrane
Ag/AgCl	Silver/silver chloride
AroY	Heterologous protocatechuate descarboxilase
BenD	Benzoate 1,2-cis-dihydrodiol
C/N	Carbon to nitrogen ratio (molar based)
CatA	Catechol 1,2-dioxygenase
CatA2	Catechol 1,2-dioxygenase 2
CatB	Muconate cycloisomerase
CatC	Muconolactone isomerase
C-C	Carbon-carbon linkage
CDW	Cell dry weight
C-O	Carbon-oxygen linkage
Ech	Feruloyl-CoA hydratase-lyase
EDTA	Ethylenediaminetetraacetic acid
EQ	Environmental Quotient
Fcs	Feruloyl-CoA-synthase
G	Guaiacyl lignin unit
H	Hydroxyphenyl lignin unit
IEM	Ion exchange membrane
IPTG	Isopropyl β-d-1-thiogalactopyranoside
LB	Lysogeny Broth
lcl-PHA	Long chain length Poly(3-hydroxyalkanoate)
mcl-PHA	Medium chain length Poly(3-hydroxyalkanoate)
MSM	Mineral salt medium
PhaC	Poly(3-hydroxyalkanoate) polymerase
PhaG	(R)-3-hydroxydecanoyl-ACP:CoA transacylase
PhaZ	Poly(3-hydroxyalkanoate) depolymerase
PHB	Poly-3-hydroxybutyrate
PobA	4-hydroxybenzoate 3-monooxygenase
RE	Reference electrode
RQ	Respiratory quotient
S	Syringy lignin unit
scl-PHA	Short chain length Poly(3-hydroxyalkanoate)
TFA	Trifluoroacetic acid
TOM®	Transfer-Rate Online Measurement device
VanAB	Vanillate O-demethylase
Vdh	Vanillin dehydrogenase
β-O-4	Ether bond

Symbols used in calculations

Symbol	Explanation	Unit or constant value
I_o	Initial average scattered light value	h
I_f	Final average scattered light value	h
N_0	Population size at t = 0	-
A	Maximal growth value reached	AU
μ_{max}	Maximum specific growth rate	h^{-1}
λ	Lag phase	h
$Peri$	The relative perimeter	-
n	Shaking frequency	rpm
OTR_{cap}	Oxygen transfer rate capacity	mmol L^{-1} h^{-1}
$Osmol$	Osmolarity	Osmol kg^{-1}
d_0	Orbital throw	cm
d	Shake flask diameter	mm
p_{abs}	Ambient pressure	bar
CTR	Carbon dioxide transfer rate	mmol L^{-1} h^{-1}
$\dot{V}_G$	Gas flow rate	L h^{-1}
V_L	Reactor filling volume	L
V_{norm}	Molar volume of an ideal gas	mol L^{-1}
$y_{O2,in}$	Molar fraction of oxygen (inlet)	-
$y_{CO2,in}$	Molar fraction of carbon dioxide (inlet)	-
$y_{CO2,out}$	Molar fraction of carbon dioxide in the off gas	-
CE	Coulombic or faradic efficiency	%
z	Valence of the element	-
F	Faraday constant	96,485 C mol^{-1}
I	Current appli	A
Δt	Time change (electrolytic process)	
V	Volume of catholyte	L
ΔC	Change of element concentration	M
μ_{set}	Specific growth rate set	0.04 h^{-1}
$Y_{x/s}$	Biomass yield	g g^{-1}
m_s	Maintenance coefficient	g g^{-1} h^{-1}
X_0	Initial biomass concentration	g (cell dry weight) L^{-1}
S_0	Glucose concentration in the nutrient solution	g L^{-1}

Organisms

Short name	**Full name**
E. coli	*Escherichia coli*
P.putida S12	*Pseudomonas putida* S12
P.putida KT2440	*Pseudomonas putida* KT2440
P.putida F1	*Pseudomonas putida* F1
P. taiwanensis VLB120	*Pseudomonas taiwanensis* VLB120
P. aeruginosa PA14	*Pseudomonas aeruginosa* PA14
P. aeruginosa PAO1	*Pseudomonas aeruginosa* PAO1
P. fluorescens	*Pseudomonas fluorescens*

Chapter 1: General Introduction

Contributions:

This chapter was written by .Juan E. Ramírez and reviewed by Lars M. Blank and Miriam A. Rosenbaum.

1.1 Global context

Although feedstocks, water, and land play an essential role in all economic activities, energy is an essential factor in production processes and therefore in economic growth (Stern, 2011). Since the 20th century, the incessant utilization of natural resources like fossil fuels for energy has driven a rapid economic development, which has been reflected in the high living standards for a part of the world population (Crafts, 2000). This fast and ´´easy access`` to the energy contained in fossil fuels is undeniably connected to all the societal advances and surge of novel production systems. However, the prominent progress has not been exempt of constraints and contradictions, generating also environmental and social inequality challenges (Yao *et al.*, 2020). Nowadays, as global warming advances, the need of a transition from a fossil-based economy to renewable models is more than clear, but many of those challenges may persists even when new forms of energy and efficient production systems become available. While some humans may live comfortably and benefit from clean energy and high value products, a poor segment of the population could be exposed to detrimental emissions when using highly-polluting energy. At the same time, this group often is deprived of quality goods, creating a negative impact on human health and welfare and ultimately limiting productive opportunities. Thus, economic growth, while necessary, is not a sufficient condition in itself for achieving equitable health (Taylor, 2009). To have a decentralised, sustainable, and equitable production system, which are the promised advantages of a successful model based on renewable feedstocks and cleaner energetic matrices, it is necessary to avoid lock-ins influenced by the classical linear system, implementing smart policies to pull a truthful paradigm change.

A required action on a more holistic level must be promoted by policy makers and different stakeholders. This can be traduced into joining forces to fund and implement relevant research and innovation projects beyond only promoting incremental changes or upgrades in the already established system. Finally, the efforts may boost the necessary breakthroughs on finding new transition pathways on the roadmap towards implementing sustainable production systems. As original contribution, this doctoral thesis intended to investigate a circumscribed area that represents a great challenge, but at the same time a relevant step towards building a new bio-based production system: The biological conversion of lignin into valuable products. Although this investigation was not expected to lead to an immediate or fundamental paradigm shift, it emerged as an input to expand the current knowledge and to add new perspectives in the field of lignin valorization through biotechnological innovation. The next sections of this introduction chapter elaborate the context and background of conversion of lignocellulosic feedstocks, focusing on the lignin fraction and the ongoing work in applied microbiology and the biotechnological progress to establish an efficient production system of valuable biochemicals from lignin aromatics. Finally, after identifying the main challenges and the gaps to cover, the outline and research approach of this thesis is described.

1.2 Conversion of lignocellulosic biomass and circular bioeconomy

Biomass is usually defined as a biological material derived from living organisms, which originates from carbon dioxide fixation during natural photosynthesis and thus, plays an important role in the global carbon cycle (Houghton *et al.*, 2009). It represents the most abundant source of carbon in the biosphere and is the first candidate to substitute the use of fossilized carbon laid down over millions of years ago (Berner, 2003). Unlike fossil feedstocks, which are inherently finite, biomass can be replenished on a rolling timeframe of years or decades (Roddy, 2013). Although this is a narrow window, the renewable feature positions biomass with a great potential to become an alternative to fossil-based economic growth if bio-based production systems are efficient enough.

In the literature, there is a broad conceptual variety of definitions involving circular economy and its relation to the bioeconomy (Leipold and Petit-Boix, 2018). According to the European Commission the bioeconomy is defined as "production of renewable biological resources and the conversion of these resources and waste streams into value added products, such as food, feed, bio-based products and bioenergy" (European-Commission, 2012). Later on, the circular economy was defined for minimizing the generation of waste and maintaining the value of products, materials and resources for as long as possible (European-Commission, 2015). Recently, from the updated terms, the European-Commission announced that the "European bioeconomy needs to have sustainability and circularity at its heart" (European-Commission, 2018). To achieve a resource-efficient biomass utilization and being aware that a comprehensive circular economy is not possible without the bioeconomy, a combined definition has emerged as circular bioeconomy (Stegmann *et al.*, 2020). In any case, although all these concepts are still in an early stage of development, they have a huge potential to contribute to the final goal: A more sustainable world. Ultimately, this involves resource efficiency and a low carbon footprint, where the supply of non-food biomass like lignocellulosic feedstocks (*i.e.,* wood, straw, grasses, etc.) promises to play a central role.

A general representation of the material and energy flows involved in the production systems of a linear economy and circular bioeconomy is shown in Fig 1A. Lignocellulosic biomass, being a bio-resource platform for novel materials and products, emerges as fundamental factor in the transition to a circular bioeconomy (Fig 1B). As the circular system differs from the linear model on how value is created or maintained, a circular bioeconomy minimizes the "take-make-dispose" standard that follows the current global economy. For this, additional material flows coming from manufacturing biomass as side-streams need to be re-evaluated through the so called cascade processes (Stegmann *et al.*, 2020). Their main goal is to increase the efficiency on biomass utilization by reusing, recycling and ultimately generating energy. This understanding is largely applied in the context of conventional biorefineries, which involve traditional waste-to-energy strategies from woody biomass (Jarre *et al.*, 2020). However, to develop the future biorefining processes that warrant a full value chain of bio-based products,

new developments on increasing the conversion efficiency of all lignocellulosic constituents (*i.e.,* lignin, cellulose and hemicellulose) are required.

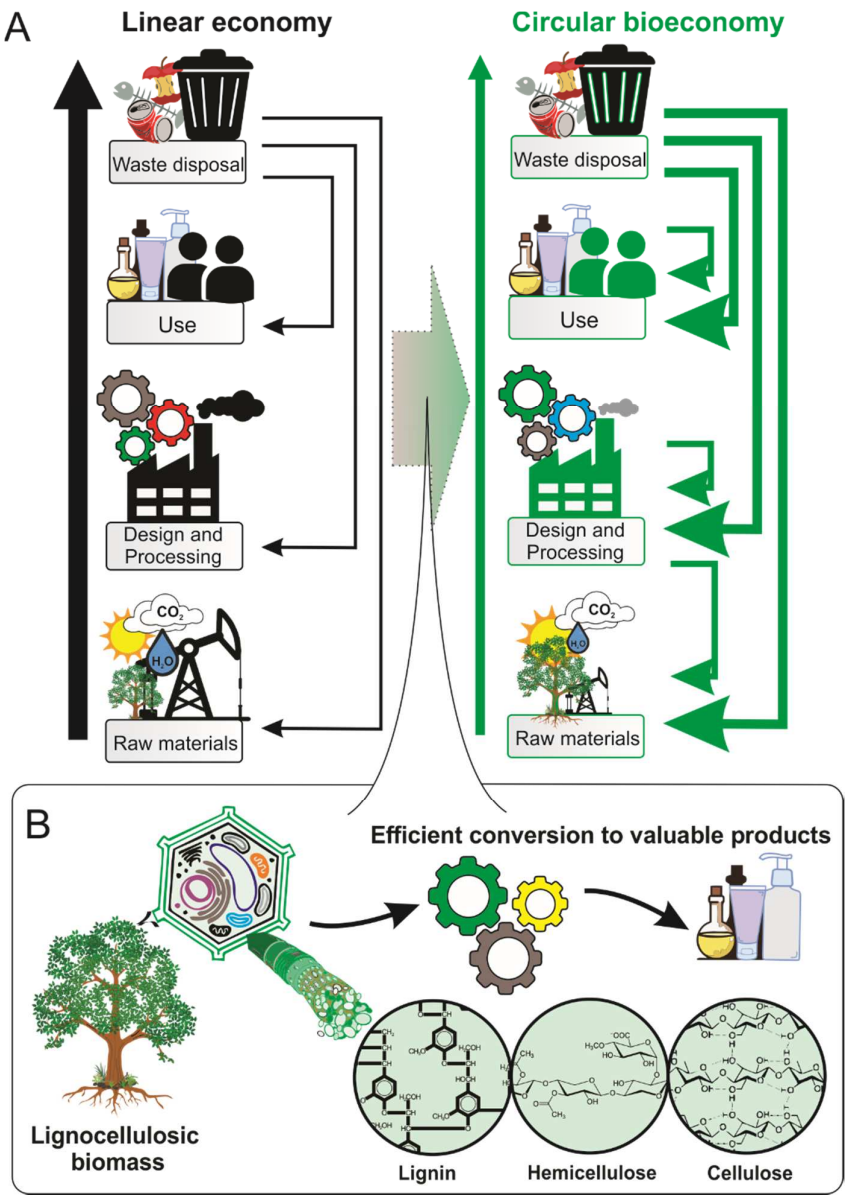

Fig 1.1 Material and energy flows involved in the production systems of a linear economy and a circular bioeconomy. During the transition to a circular bioeconomy (A), efficient conversion of lignocellulosic biomass (*i.e.,* all the natural polymers forming the cell wall like lignin, cellulose and hemicellulose) is essential to guarantee a full value chain of bio-based products (B).

1.2.1 The biorefinery concept

To improve efficiencies of converting lignocellulosic biomass into valuable products, several integrated processes based on biorefinery concepts have been proposed. A biorefinery always involves the integral processing of biomass into a spectrum of marketable products and energy while taking care of environmental, economic, and social sustainability. Biorefineries are classified depending on their components (*i.e.,* platforms, products,

feedstocks, and conversion processes), giving rise to several terminologies (ElMekawy *et al.*, 2013). From them, lignocellulosic feedstock biorefineries embrace the challenge of refining lignocellulosic biomass through several processing steps. First, the raw material is pre-treated mainly with acid or alkaline agents to release cellulose, hemicellulose, and lignin. Cellulose is converted by (enzymatic) hydrolysis into D-glucose (C6). Hemicellulose units are released from an amorphous branched polymer that contains both C5 (xylose, arabinose, and rhamnose) and C6 sugars (glucose, mannose, and galactose). After hydrolysis of cellulose and hemicellulose C6 sugars and some of the C5 sugars serve as substrates for fermentation to produce biofuels (ethanol, butanol, hydrogen, biodiesel, etc.) (Yousuf, 2012; Fan, 2014; Birgen *et al.*, 2019; Bhatia *et al.*, 2021) or chemical blocks like organic acids or value added molecules (Takkellapati *et al.*, 2018). A great example of the efforts applied to increase conversion efficiency of these biomass fractions is the technique called consolidated bioprocessing (CBP), which is used to produce some of the above mentioned products by using a single or a plethora of microorganisms (Olguin-Maciel *et al.*, 2020).

1.2.2 Sustainable chemical processes

To increase the sustainability in the chemical processes occurring in lignocellulosic feedstock biorefineries, concepts like atom efficiency and E-factor have been introduced (Sheldon, 2007; Sheldon, 2012). They account for the amount of waste generated and the negative environmental impact, respectively. Additionally, to evaluate not only the amount of waste but also its hazardous nature, the Environmental Quotient (EQ) can help as quantitative estimation (Sheldon, 2012). In any case, technological advances on increasing chemical yields should decrease waste generation and consequently increase energy efficiency. The chemical composition of the feedstocks is crucial to achieve these desired goals. Lignocellulosic biomass is mainly composed of cellulose (40–60%), hemicellulose (20–35%), and lignin (15–40%), and the rest correspond to proteins, extractives and ash (Hayes, 2013; Zoghlami and Paës, 2019). Thus, as the processing of C6 and some C5 sugars into desired products has been widely implemented, the focus should move on improving lignin conversion. Thereby, catalysis is a central aspect for increasing the rate and atom efficacy of such chemical reactions. The new catalytic routes for upgrading lignin to valuable chemicals have given rise to an additional bio-based production concept: The lignin biorefinery (Paone *et al.*, 2020; Sudarsanam *et al.*, 2020).

1.3 Lignin, a renewable source of aromatics

"Lignine" (derived from the Latin word *lignum*, meaning wood) was the name given to a substance described as fibrous, tasteless and insoluble in water, which can be precipitated from solution using acid (de Candolle, 1813). Lignin is mainly contained in the cell walls of vascular plants (Fig 1.2C), filling the spaces between cellulose and hemicellulose, and acting like a resin that holds the lignocellulose matrix together. It has different biological functions acting as structural material to provide mechanical support, water transport, and resistance

to various stresses, including defence against degradation by external agents (Liu *et al.*, 2018). In the last decades, different scientific efforts have been placed on lignin research for understanding the processes involved in pulp manufacture and looking for new possibilities in commercial applications (Adler, 1957; Zhang and Naebe, 2021). This has helped to elucidate their main structural elements, which are considered a treasure from a chemical point of view (Becker and Wittmann, 2019). Nowadays, lignin is considered the most abundant aromatic polymer on the planet, which make it a promising renewable source of aromatic molecules and that ultimately can be directly valorized or converted to more valued chemicals. However, the greatest challenge for the conversion technologies lies in the heterogeneous structure of lignin.

1.3.1 Chemical structure of lignin

Lignin presents the most complex and heterogeneous chemical structure of the three main polymers found in biomass. The polymeric matrix is based on repeated aromatic units corresponding to three primary monomeric building blocks. They are phenylpropanoid units linked by C-O and C-C bonds: coniferyl alcohol, sinapyl alcohol and p-coumaryl alcohol (Fig 1.2AB). Approximately 50-80% of all the linkages between them are β-O-4 ether bonds (which dictate the lignin reactivity), while others like 5-5, β-5, and β-β' linkages can also occur (Becker and Wittmann, 2019) (Fig 1.2A). The monolignols differ in the number of methoxy groups associated to the aromatic ring and correspond to the three lignin units: G (guaiacyl), S (syringyl) and H (hydroxyphenyl), respectively) (Fig 1.2B) (Korányi *et al.*, 2020). The content and composition of lignin varies depending on the biomass type (Fig 1.2C). The highest lignin content is found in hardwood (*i.e.,* deciduous trees like oak), which is composed approximately 90-95% of coniferyl units (G-type). On the other hand, the composition is almost equally distributed in softwood lignin (*i.e.,* coniferous trees like pine) with 25-50% of coniferyl units (G-type) and 50-75% of sinapyl units (S-type) (Korányi *et al.*, 2020). In addition to G and S units, the lignin of grass (*i.e.,* herbaceous plants like crops) also contains p-coumaryl units (H-type) (Fig 1.2C). Finally, lignified cell walls with the 3 units have been found also in seaweed, specifically in the red alga *Calliarthron cheilosporioides* (Martone *et al.*, 2009). The occurrence of different lignin units and therefore diverse linkages in different kind of biomass will obviously affect lignin deconstruction and therefore the quality and quantity of aromatic molecules obtained. For example, the β-O-4 ether bond makes up approximately half of the lignin in softwood biomass and more than 60% in hardwood. This type of lignin contains less C-C linkages because the presence of additional methoxy groups in the S units prevent their formation (Zakzeski *et al.*, 2010; Ragauskas *et al.*, 2014; Korányi *et al.*, 2020). From this chemical diversity derived of the complex lignin structure, several methods of biomass fractionation, lignin depolymerisation, and aromatic upgrading have been studied in the context of lignin valorization.

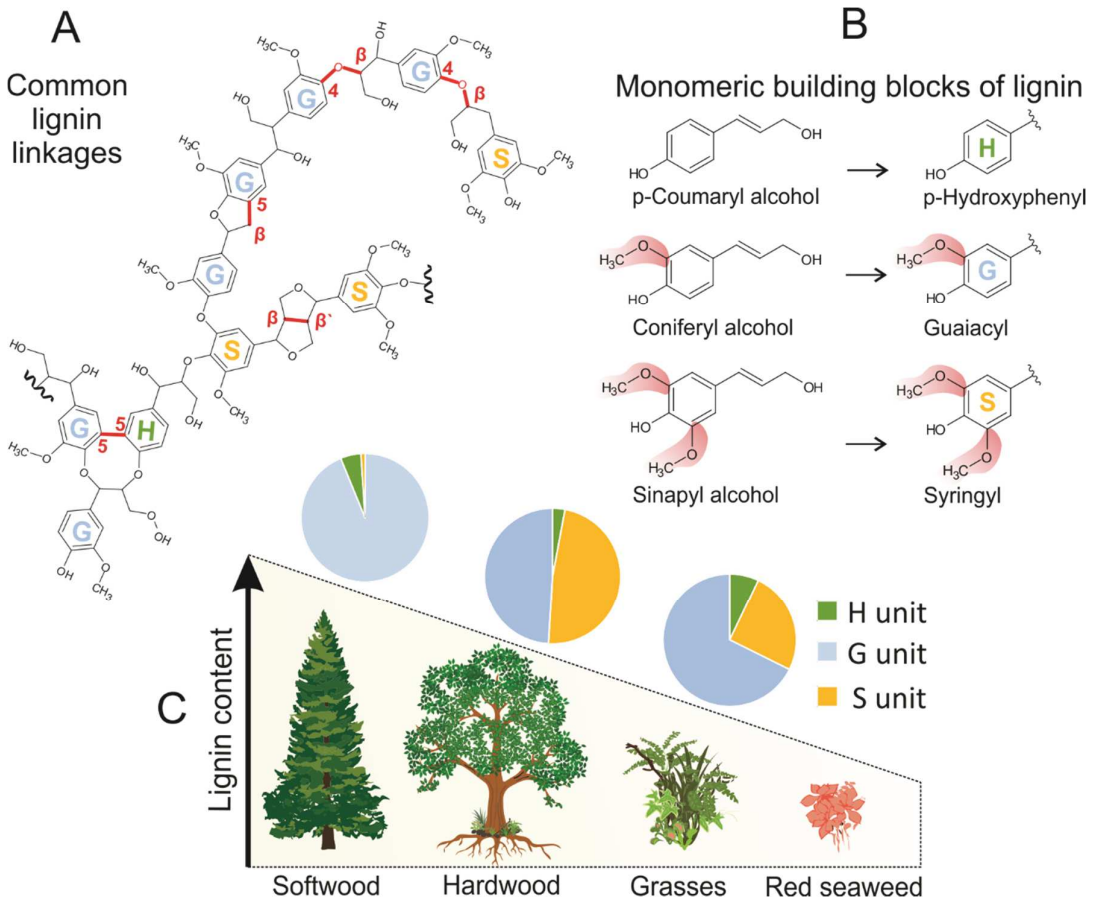

Fig 1.2 Chemical structure of lignin and content in different biomass sources. The polymeric matrix is based on repeated aromatic units linked by C-O and C-C bonds, where the most common are (marked in red): β-O-4 (most reactive linkage), β-O-4, β-5, and β-β' (A). The three primary monomeric building blocks (B) are: coniferyl alcohol, sinapyl alcohol, and p-coumaryl alcohol, which differ in the number of methoxy groups (highlighted in red) and correspond to the units: G (guaiacyl), S (syringyl) and H (hydroxyphenyl), respectively. The content and composition of lignin varies depending on the biomass type (C). Separate parts of this scheme were adapted from (Zakzeski *et al.*, 2010; Ragauskas *et al.*, 2014; Becker and Wittmann, 2019; Zhang and Naebe, 2021).

1.4 Implementing a full value chain from lignin

Targeting high-value chemical compounds implies an efficient lignin processing and conversion, where the combination of three important elements is imperative: Biomass fractionation, lignin depolymerization, and aromatic upgrading to useful chemicals (Schutyser *et al.*, 2018). These steps can be operated in a physically separated fashion, consecutive processes, or in some cases simultaneously.

1.4.1 Biomass fractionation

The first step to implement a value chain from lignin aromatics is the recovery of lignin from biomass. Being aware of the multiple biomass compositions in the feed streams, which in turn depends on the local environment, each lignocellulosic feedstock biorefinery will need to adapt and implement niche-specific production processes. In general, there are four

categories of conventional pre-treatment technologies where lignin is isolated by fractionation: physical (like cavitation, milling and steam explosion), solvent fractionation (using alcohols, organic acids, ethylene glycol, ionic liquids and deep eutectic solvents), chemical (acidic, alkaline, oxidative and reductive catalytic fractionation) and enzymatic. Each pre-treatment process has both advantages and disadvantages and uses different operational conditions that alter in different ways the chemical structure of lignin (Zakzeski *et al.*, 2010). The final lignin product can be isolated as solid residue, precipitate, or even directly as depolymerised product. This is based on the liberation of lignin from the biomass matrix (*i.e.* carbohydrates are obtained as delignified pulp) or based on carbohydrate deconstruction (*i.e.,* lignin recovered either as insoluble residue or precipitate) (Fig 1.3A).

Traditionally, the most common fractionation processes consist of alkaline delignifications. They are carried out in the pulp and paper industry, where the lignin structure is susceptible to rearrange. The target linkages are reactive ether bonds (like β-O-4), which are cleaved by nucleophilic attack by anions such as HS^- to facilitate delignification and to some extent depolymerization. This results in the formation of new stable C-C linkages, and a more condensed and unreactive lignin that is very difficult to valorize (Jardim *et al.*, 2020). An example for this, is the Kraft lignin process, the dominant pulping technique that occurs at high pH using considerable amounts of NaOH and sodium sulfide (Na_2S) at high temperatures. After precipitation, the concentrated lignin-rich solid with a recalcitrant structure is burned to recover heat.

In other methods like sulfite pulping, lignin extraction is carried out at varying pH range from 2 to 13 and using (bi) sulfite salts. This process yields water-soluble lignosulfonates that are also highly degraded but hold a better polymeric property than Kraft lignin (Cao *et al.*, 2019). A third traditional method is soda pulping, which only uses NaOH and antraquinone, generating sulfur-free lignin. Historically, it has been used frequently to produce pulps from non-woody biomass (Schutyser *et al.*, 2018). Another common method is the organosolv processes, which is carried out using solvents and acidic environments, permitting an effective solubilization of lignin and separation of cellulose and hemicellulose. Depending on the severity of conditions applied, it can partially preserve the native structure of lignin (Thoresen *et al.*, 2020). Ethanol organosolv technology has been proposed as alternative in production of second-generation cellulosic ethanol and biochemicals (Zhou *et al.*, 2018). Several other methods for isolating lignin include: Steam explosion, ammonia fiber explosion, dilute acid hydrolysis, enzymatic hydrolysis or a combination of some of them (Wang *et al.*, 2019). The most relevant methods based on carbohydrate deconstruction are based on thermal pretreatments (like fast pyrolysis where lignin depolymerization also occurs), acid catalysed, and enzymatic hydrolysis. In cases where important molecular alteration of the lignin structure limit the conversion into value-added chemicals (as it is the case for most of the isolated lignin), the technical lignin streams serve in macromolecular material applications. Some of them include: Adhesives, coatings, foams, phenolic resins, dispersing

agents, retardants, and lately more interesting materials like multifunctional nanocomposites (Hemmilä *et al.*, 2017; Tian *et al.*, 2017; Glasser, 2019). However, only less than 2% of the industrial lignin waste is used for these material applications and the rest is burned (Cao *et al.*, 2018).

1.4.2 Lignin depolymerisation

After lignin extraction, the next step in creating higher value is breaking down the bonds of the polymeric structure into low molecular weight products (*i.e.,* aromatic monomers, dimers or oligomers). In cases of starting from isolated lignins (*i.e.,* technical lignins), which are partially depolymerized during traditional fractionation processes, the loss of lignin reactivity impede a further depolymerisation. On the other hand, this drawback can be avoided starting from native lignins (Fig 1.3A). Most of the depolymerisation methods involve high temperatures and/or use of catalyst, and generate different mixtures of components. For example, during pyrolysis of native lignin, fractions containing waste carbon (*i.e.,* char), residual lignin, aqueous phase (*i.e.,* alcohols or hydrophilic compounds), gaseous products (*i.e.,* volatile organic compounds, H_2, CO) and oil are commonly generated (Mu *et al.*, 2013). The lignin oil is where most of the target aromatic compounds are found and the residual lignin contains re-polymerized particles. Pyrolysis is a widely-known method for thermal decomposition of lignocellulosics that, despite being simple, is also unspecific, presents low energy yield and produces excessive air pollution. However, important improvements on fast pyrolysis have been implemented at pilot scale, like the case of the bioliq® concept developed at the Karlsruhe Institute of Technology (KIT) (Pfitzer *et al.*, 2016). Other lignin depolymerization processes starting with isolated lignins include: Acid/base catalysed, oxidative, reductive, mechanochemical, photocatalytic, electrochemical, and other thermal methods different than pyrolysis like microwave and hydrothermal liquefaction (Fig 1.3A) (Cao *et al.*, 2019). The latest developments of some of these approaches involve controlling the reaction conditions and catalyst properties to promote selective cleavage/conversion, avoid aromatic ring cleavage and conserve functional groups. This progress would lead to increase the aromatic yield and reduce waste, impacting positively on the atom efficiency (also known as atom economy) and E-factor (both concepts are described in section 1.2.2). Some of the aromatic compounds generated after lignin depolymerisation consist of phenolic monomers like guaiacols, syringols, cresols and catechols (Fernández-Rodríguez *et al.*, 2017; Schutyser *et al.*, 2017). Other aromatics like vanillin and hydroxycinnamic acids can be found after alkaline oxidative cracking (Lyu *et al.*, 2018) or base-catalyzed methods (Rodriguez *et al.*, 2017), respectively.

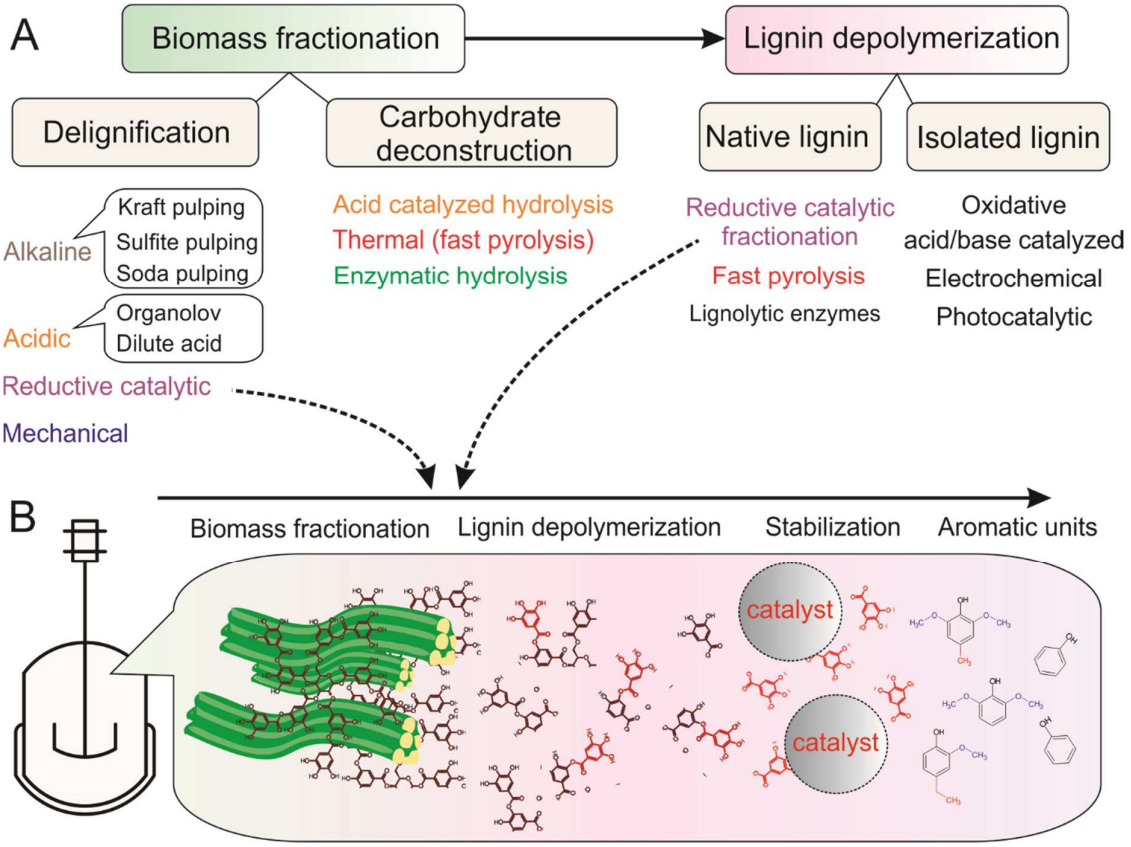

Fig 1.3 Methods of biomass fractionation and lignin depolymerization. The biomass fractionation processes can be classified depending on delignification of cellulose or carbohydrate deconstruction (A). Lignin depolymerization can be achieved from native lignin or isolated (technical) lignin. Through an emerging technology based on reductive fractionation processes, the priority attention is given to the depolymerisation. Due to a rapid stabilization, depolymerized lignin results with minimal condensation, conserving reactive linkages. This concept is also called 'lignin-first' as the first aim is to obtain value from lignin. Parts of the figure were adapted from Renders *et al.*, 2017.

Before 2010, research in lignin depolymerization lagged behind because the focus was given to prioritizing the valorization of cellulose from lignocellulosic feedstocks. Thus, the recalcitrant lignin was mainly discarded. However, with a high priority on creating higher value from lignin, over the last 10 years, lignin conversion gained much attention and significant progress has been made (Korányi *et al.*, 2020). The mayor advances were achieved as one-pot full conversion of native lignin while stabilizing reactive intermediates to protect the native β-O-4 linkages during extraction avoiding repolymerization. This enabled higher yields of desired monoaromatic products (Shuai *et al.*, 2016). Since the introduction of the reductive catalytic fractionation methods during 2014–2015, where the lignin fraction is the central character of biomass, integrated biorefinery approaches reaching the complete valorization of all lignocellulose constituents have been proposed (Korányi *et al.*, 2020). This concept is also called 'lignin-first' and the priority attention is given to the depolymerisation of lignin with minimal condensation (Renders *et al.*, 2017). This process is dependent on a catalyst and involves solvolysis, fractionalization/depolymerization and reductive stabilization

in one-step (Fig 1.3B). It has been implemented in batch and flow-through operating modes (Anderson *et al.*, 2017; Renders *et al.*, 2019), where the common lignin monomers obtained are methoxylated phenols like 4-propenyl- and 4-ethylguaiacols/syringols, although it depends on lignocellulose feedstock and reaction conditions (Sudarsanam *et al.*, 2020). Some up-scaling initiatives of this innovative process are still in development. For instance, a case involving different stakeholders to test this technology is the consortium Biorizon that aims to develop bio-aromatics from lignin and which has recently launched the ALIGN project (Biorizon, 2018).

Lastly, biological organisms have also been studied to depolymerize lignin. The main efforts have concentrated on testing lignolytic enzymes found in white-rot fungi and some bacteria, enabling the possibility to minimize energy demand and hazardous waste generation (Salvachúa *et al.*, 2016; Hämäläinen *et al.*, 2018; Shin *et al.*, 2019; Chan *et al.*, 2020). Bacterial lignin-degraders of the genera *Streptomyces*, *Paenibacillus*, *Rhodococcus*, *Amycolatopsis*, *Oceanimonas*, *Comamonas*, *Pandoraea* and *Pseudomonas* have been isolated from different environments (Becker and Wittmann, 2019). White-rot fungi, the main natural producers of lignolytic enzymes, are hard to cultivate, and present a complex regulation of their biosynthetic pathways. These limitations have redirected the attention on enzymatic breakdown from bacterial sources. A successful case is the extremely alkaline lignin oxidase product LIGNOTM, commercialized by the Finnish company MetGen (Hämäläinen *et al.*, 2018) In general, biocatalytic activity on lignin occurs in a cocktail of oxidative enzymes like laccases, peroxidases and accessory enzymes like H_2O_2-generating oxidases. Peroxidases generate radical mediators that can penetrate the lignin structure helping the initiation of depolymerisation and can act in close proximity or from a distance (de Gonzalo *et al.*, 2016). As laccases present a lower redox potential, they cleave only phenolic lignin units if there is no presence of redox mediators like vanillin and p-coumarate (Abdelaziz *et al.*, 2016). The aromatic monomers that can be found after lignolytic activity include: Ferulate, p-coumarate, phenol, vanillin, guaiacol and cresols (Abdelaziz *et al.*, 2016). The possibility of integrating ligninolytic enzymes and bacterial cultures have been also explored, where lignin depolymerisation was enhanced by the synergetic presence of *Pseudomonas putida* KT2440 (Salvachúa *et al.*, 2016). Recently, outer membrane vesicles (OMVs) were reported to act as extracellular cargo of lignolytic oxidoreductases in *P. putida* KT2240 (Salvachúa *et al.*, 2020).

1.4.3 Lignin aromatics upgrading and funneling

Only few low-molecular weight aromatic compounds obtained after lignin depolymerization can be considered high valued for marketable applications. For instance, vanillin can be used in fragrance preparation or as flavorant (Paul *et al.*, 2021). Nevertheless, the rest of the aromatic monomers need a further upgrading (*i.e.,* modifications or transformations) for final commercialization, which include chemocatalytic and biocatalytic approaches (Schutyser *et al.*, 2018). Due to the low concentrations of single compounds found in the complex aromatic mixtures after depolymerisation an alternative strategy of upgrading called ´´funneling´´ has

been introduced some years ago (Linger *et al.*, 2014). This convergent approach is based on the natural catabolic funnels that some microbes use to catabolize aromatic compounds. Analogously, some chemocatalytic upgrading routes can be considered as funnels as well (Fig. 1.4A) (Rinaldi *et al.*, 2016).

In the chemocatalytic funneling, transformations can modify the phenolic core or side chains of the aromatic molecule. The modifications of the phenolic core reduce functionality and O/C ratio through hydrodeoxygenation in water or alkane solvents, decreasing the product complexity. Two examples of funneling a heterogeneous mixture of lignin aromatics to produce phenol and terephtalic acid are shown and explained in more detail in Fig. 1.4 A. Other molecules like carboxylic acids, alkanes and cyclohexanols can be also obtained and applied as mid-range fuel additives or as polymer building blocks (Schutyser *et al.*, 2018). Recently, some authors have reported extensive reviews on this emerging field (Liu *et al.*, 2020; Wong *et al.*, 2020).

The biocatalytic funneling occurs naturally in microbes and offers a great promise for production of value-added chemicals from lignin. Although this process occurs in aerobic and anaerobic microorganisms, the first kind have been more studied, motivated mainly by bioremediation studies based on degradation of xenobiotic aromatic compounds. During aromatic catabolic pathways (*i.e.,* upper pathways), a large machinery of enzymes funnel (*i.e.,* defunctionalize) monomers, dimers and oligomers into central intermediates like catechol, protocatechuate and gallate (Fig. 1.4B) (Becker and Wittmann, 2019). Some of the upper pathways have been interrupted to accumulate intermediaries with promising applications using metabolic engineering (Kohlstedt *et al.*, 2018; Becker and Wittmann, 2019; Perez *et al.*, 2019). After lignin depolymerisation, diverse aromatics are funneled to central intermediates like catechol, protocatechuate and gallate. In microbes presenting a β-ketoadipate pathway, the ortho-cleavage of the aromatic ring occurs, while other organisms actually have metha-cleavage dioxygenases and degrade aromatic compounds in a β-ketoadipate-independent manner (Becker and Wittmann, 2019). Thus, different ring-cleavage types will generate different metabolites like pyruvate, acetyl-CoA and succinyl-CoA, which modify how carbon flux enters the central metabolism and are thus having an impact on metabolic efficiency based on the redox equivalents generated (Johnson and Beckham, 2015). From these central precursors, microbes can synthetize valuable biochemicals. The next section focuses on target molecules that have been produced after biological upgrading of aromatics.

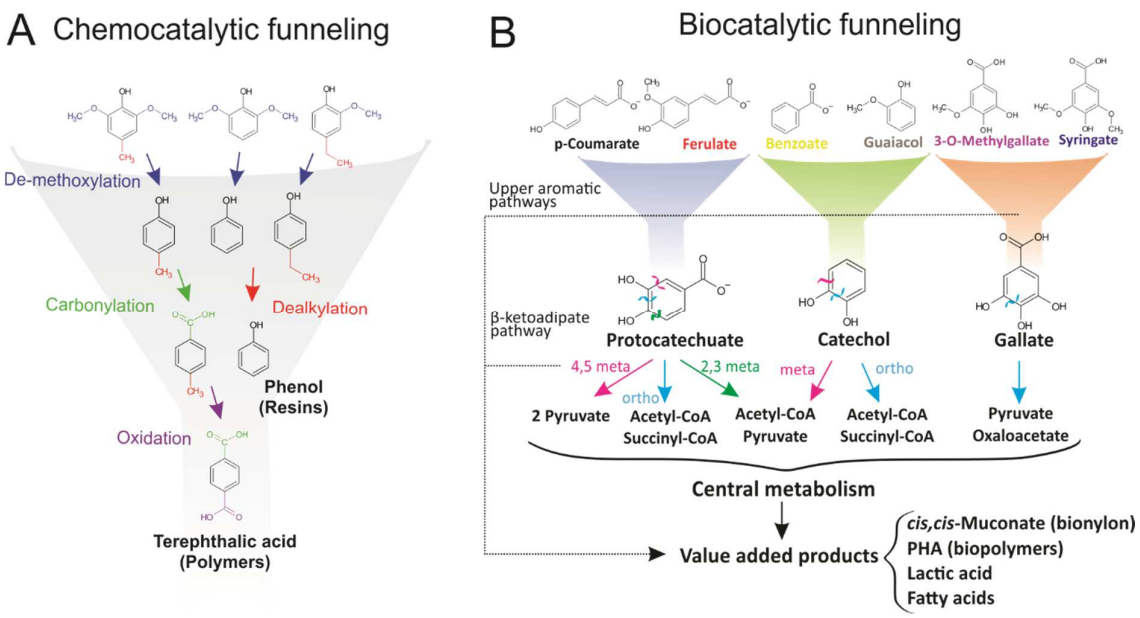

Fig. 1.4 Chemocatalytic and biocatalytic funneling of lignin aromatic mixtures. During the chemocatalytic funneling (A), modifications occur in the phenolic core and/or at side chains (i.e., functional groups) of the aromatic molecule. Defunctualizations and functualizations are applied towards synthesis of target molecules. Phenol, a precursor for resins, is produced performing demethoxylations and dealkylations from a depolymerized stream containing a mixture of aromatics. When introducing functional groups during oxidations, other molecules like terephtalic acid are synthetized. The biocatalytic funneling is based on the enzymatic machinery of some bacteria (B). Lignin aromatics are funnelled through upper pathways into central intermediates like protocatechuate, catechol and gallate. Depending on the type of aromatic cleavage (*i.e.,* ortho or meta), different precursors fuelling the central metabolism can be generated. Different valuable products can be synthetized either from the aromatic catabolic routes or during anabolic pathways. Parts of this figure were adapted form (Becker and Wittmann, 2019; Wong *et al.*, 2020).

1.4.3 Value added chemicals derived from biocatalytic upgrading of lignin aromatics

Over the last years, different studies have reported the production of important molecules from lignin derivatives using microbes. The first report elucidated the catabolic pathways and enzymes in *Sphingobium* sp. SYK-6, which are able to cleave β-O-4 and 5-5 linkages in lignin dimers (Masai *et al.*, 2012). Thus, this bacterium is capable of utilizing various types of lignin-derived biaryls and monoaryls as the sole source of carbon and energy metabolism. From this work on, it became a model bacterium for studying the conversion of lignin to chemicals. The first metabolically engineered strain to covert lignin aromatics into value added chemicals like vanillin was *Rhodococcus jostii* RHA1 (Sainsbury *et al.*, 2013). Another promising molecule is *cis,cis*-muconic acid, a product of the ortho-cleavage of the aromatic intermediate catechol, which can be used as building block for nylon production. Since many years ago, it was known that mutant strains of *Pseudomonas putida* and *Corynebacterium glutamicum* could accumulate *cis,cis*-muconic acid from aromatics like benzene, toluene, benzoic acid, or catechol (Yoshikawa *et al.*, 1990). However, in the last decades important progress was achieved enhancing productivities (Bang and Choi, 1995; Choi *et al.*, 1997; van Duuren *et al.*, 2011; van Duuren *et al.*, 2012; Choi *et al.*, 2020). Recently, the production of *cis,cis* muconate

has been focused in the context of lignin valorization, giving place to important studies involving metabolic engineering and bioprocess development from lignin derived substrates (Vardon *et al.*, 2016; Johnson *et al.*, 2017; Salvachúa *et al.*, 2018). The production of biopolymers like medium chain length polyhydroxyalkanoates (*mcl*-PHAs) has also been demonstrated from single aromatics and/or from alkaline pretreatment liquor (APL) in *Pseudomonas putida* KT2440 (Linger *et al.*, 2014). APL as lignin derived stream has been widely used in this kind of research studies because the aromatic content is likely to be metabolized. These streams containing hydroxycinnamic acids like p-coumaric and ferulic acid, which are naturally incorporated in herbaceous cell walls (de Oliveira *et al.*, 2015), have been recovered by alkaline pretreatment of lignocellulosic waste crops (Karlen *et al.*, 2020). Other products like novel pyridine dicarboxylic acids, bio-based adipic acid, lactic acid and fatty acids are also examples of value-added molecules (Johnson and Beckham, 2015; Mycroft *et al.*, 2015; Zhao *et al.*, 2016; Skoog *et al.*, 2018; Johnson *et al.*, 2019; Perez *et al.*, 2019. Finally, a combination of biological and chemocatalytic steps have demonstrated the production of cyclic-C6-1,4-diacid monomers (Carraher *et al.*, 2017), adipic acid (Vardon *et al.*, 2015), considered fuel-range hydrocarbons (Linger *et al.*, 2014).

From the microbes mentioned above, *Pseudomonas sp.* is shaping up as promising hosts to develop microbial cell platforms to synthetize valuables products like *mcl*-PHAs and *cis,cis* muconic acid. The next section focuses on the potential of this bacterial genus to produce these two valuable products.

1.5 Lignin valorization potential of *Pseudomonas sp.*

Species of the genus *Pseudomonas* represent a group of ubiquitous environmental bacteria with a great metabolic diversity. They are gram-negative and rod-shaped, which were classified for first time at the end of the 19th century (Migula, 1894; Migula, 1900; Palleroni, 2010). Due to the increasing number of genome sequences, this genus is now a focus area for scientific research in medical, plant, environmental and industrial microbiology (Silby *et al.*, 2011; Winsor *et al.*, 2016). Especially, many *Pseudomonas* species are attractive for genetic manipulation, which has derived in a vast number of molecular tools and applications in metabolic engineering (Martínez-García and de Lorenzo, 2017). Due to their great ability to degrade aromatic compounds, they also have gained a lot of attention to metabolize synthetic plastics (Wilkes and Aristilde, 2017) and valorize lignin derivatives (Kumar *et al.*, 2021).

The number of research studies on isolates of wild type *Pseudomonas* strains able to degrade lignin-related compounds have been considerable and are extensively reported in databases like eLignin (Brink *et al.*, 2019). However, due to the great diversity and adaptability of *Pseudomonas*, further approaches towards the selection and evaluation of physiological behaviour of promising strains, who are not only able to uptake, but also to transform depolymerized lignin-derived aromatic streams into valuable compounds, are necessary.

Additionally, since the host selection is crucial for establishing suitable platform strains and microbial factories, additional bacterial properties related to a proper domestication like metabolic robustness, genetic accessibility, fast growth and high productivities, need to be also covered for future viable industrial-scale applications (Becker and Wittmann, 2019). One of the species standing out for combining most of these features is *Pseudomonas putida*.

1.5.1 Pseudomonas putida

Genomic studies on this bacterium show large sets of organized genes involved in mechanisms of aromatic detection, transport, utilization, regulation, chemotaxis, stress-response, and regeneration of reduced cofactors to face unfavourable redox periods (Dos Santos *et al.*, 2004; Blank *et al.*, 2010; Belda *et al.*, 2016; Lin *et al.*, 2019). Additionally, the remarkable aromatic-funnel capacity of *P. putida* has evolved to adapt and tolerate stressful environmental conditions where multiple physicochemical and nutritional scenarios prevail, as has been reflected in studies on bioremediation (Nikel *et al.*, 2014).

From different studies on aromatic degradation, several catabolic pathways of lignin aromatics have been characterized in *P. putida* (Kim *et al.*, 2006; Jiménez *et al.*, 2010; Nogales *et al.*, 2017). Most of the known funneling pathways of the strain *P. putida* KT2440 are shown in Fig. 1.5 (Ravi *et al.*, 2017). The branches that metabolize coniferyl, p-coumaryl, and benzoyl aromatic units are known as upper pathways that end in the central intermediates protocatechuate and catechol. The corresponding enzymes that activate the side chains of p-coumarate, ferulate and benzoate are designated in the figure description. In the case of ferulate catabolism, as additional effort, demethylation of vanillate into protocatechuate generates additional formaldehyde. In the β-ketoadipate pathway, ortho-cleavage of catechol generate *cis,cis* muconate. Afterwards, the carbon flux of both pathways merge into β-ketoadipate, which is further metabolized into acetyl-CoA and succinyl-CoA. From these compounds, it is possible to build biomass and/or reserve molecules like *mcl*-PHA.

1.6 Production of *mcl*-PHA from lignin aromatics

Polymers like *mcl*-PHA are a straight-forward native product of *P. putida*, which are an alternative to fossil-based plastic and can be used as biodegradable polymer in medical and material applications (Prieto *et al.*, 2016). This storage molecule is synthesized intracellularly by the enzymatic polymerization of (R)-3-hydroxyacyl-CoA monomers (C6 to C14) (Wang *et al.*, 2018; Xu *et al.*, 2019b). Granules containing PHA are also called carbosomes (50–500 nm) and contain densely packed hydrophobic polymer (Jendrossek and Pfeiffer, 2014). They are covered by phospholipid monolayers and protein components related to the PHA machinery (Jendrossek and Pfeiffer, 2014).

There are other types of PHA like poly-3-hydroxybutyrate (PHB) (*i.e.,* the most studied in wastewater-cultures) (Amadu et al., 2021), short chain length PHAs (*scl*-PHAs, C3 to C5) and long chain length PHAs (*lcl*-PHAs, C>14) (Muneer *et al.*, 2020). Although these other polymers have their own niche applications like soft plastic for packaging (*i.e.,* in the case of *scl*-PHA), *mcl*-PHA stands out by having more versatility and being more flexible and resistant (*i.e.,* high elasticity and tensile strength) (Mozejko-Ciesielska *et al.*, 2019).

Bacterial strains from *Pseudomonas sp.* generate 3-hydroxyacyl (3HA) precursors for *mcl*-PHA synthesis from different substrates using two pathways (Fig 1.6). Carbon sources like fatty acids can be degraded via β-oxidation process into (R)-3-hydroxyacyl-CoA, the precursor for *mcl*-PHA synthesis. On the other hand, structurally unrelated compounds like sugars, acetate, and aromatic compounds are converted in the central metabolism into Acetyl-CoA. Through *de novo* fatty acid biosynthesis, the resulting carbon flux is then directed through malonyl-CoA and following activation into acyl-ACP and malonyl-ACP (R) intermediates. These intermediates are transformed into (R)-3-hydroxyacyl-ACP and later to (R)-3-hydroxyacyl-CoA by the transacylase PhaG. Finally, the PHA synthase PhaC enable polymerization of these precursors (Mozejko-Ciesielska *et al.*, 2019). In parallel, depending on the environmental conditions, *mcl*-PHA depolymerase (PhaZ) can provide again 3-hydroxyacyl precursors for carbon and energy (Arias *et al.*, 2013). The *de novo* fatty acid biosynthesis pathway is more active when a previous biomass build-up stage was promoted along with a nutritional imbalance like nitrogen limitation (Wang *et al.*, 2018; Xu *et al.*, 2019b).

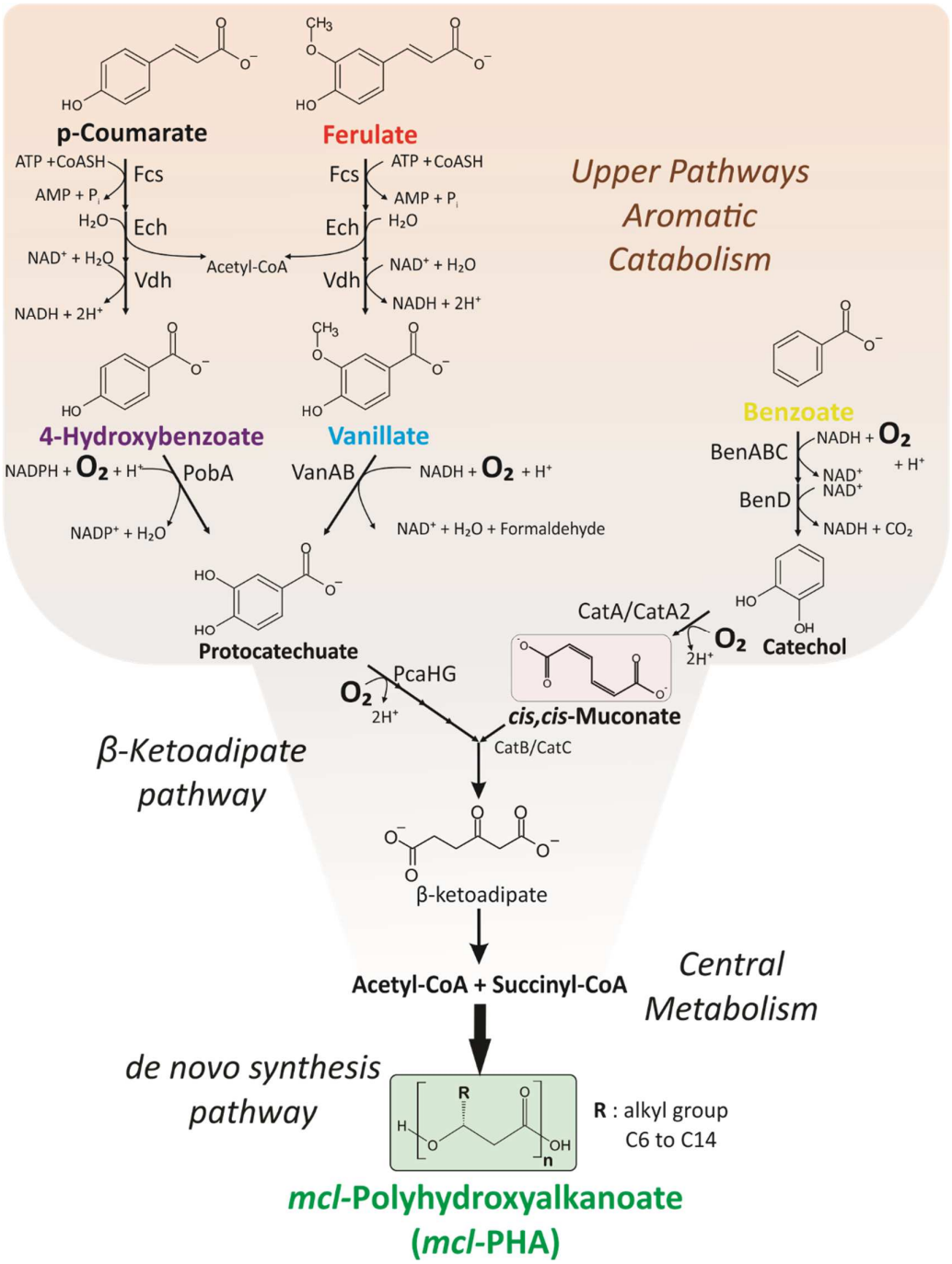

Fig. 1.5 Metabolic pathways to synthesize valuable molecules like *mcl*-PHA and *cis,cis*-muconate from lignin aromatics in *P. putida* KT2440. Aromatic funneling starts with upper pathways where aromatic molecules are activated and then converge into central intermediates like catechol and protocatechuate. Then they are cleaved and metabolized via the β-ketoadipate pathway to access the central carbon metabolism. Finally, part of the carbon flux excess accumulates as *mcl*-PHA by *de novo* synthesis under nitrogen limiting conditions. Fcs, feruloyl-CoA-synthase; Ech, feruloyl-CoA hydratase-lyase; Vdh, vanillin dehydrogenase; PobA, 4-hydroxybenzoate 3-monooxygenase; VanAB, vanillate O-demethylase; BenABC, benzoate 1,2-dioxygenase; BenD, benzoate 1,2-*cis*-dihydrodiol dehydrogenase; CatA and CatA2, catechol 1,2-dioxygenase ; CatB, muconate cycloisomerase; CatC, muconolactone isomerase; PcaHG, protocatechuate 3,4-dioxygenase. Adapted from Ravi *et al.*, 2017.

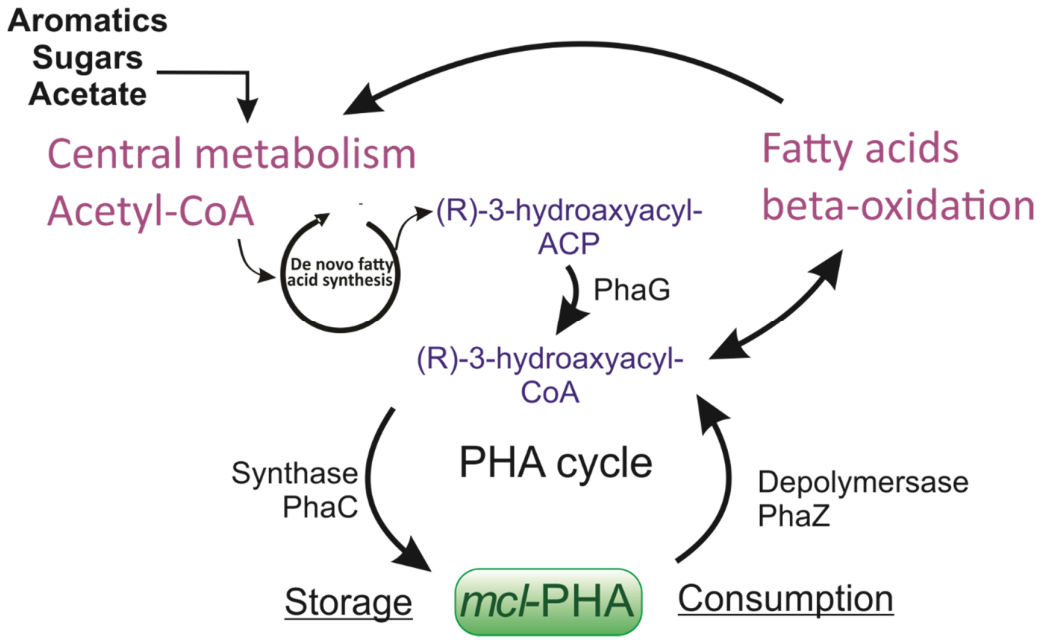

Fig. 1.6 Typical pathways for synthesis of *mcl*-PHA used by bacterial strains of *Pseudomonas sp.* Carbon sources like fatty acids can be degraded via β-oxidation process into (R)-3-hydroxyacyl-CoA. Structurally unrelated compounds like sugars, acetate, and aromatic compounds are converted into 3-hydroxyacyl precursors through central metabolism and *de novo* fatty acid biosynthesis.

Several *P. putida* strains have been recognized as efficient cell factories for *mcl*-PHA production, which have been fundamentally studied and optimized using conventional carbon sources (Poblete-Castro *et al.*, 2014a; Mozejko-Ciesielska *et al.*, 2019). However, the feedstocks being an important limiting factor for establishing cost effective *mcl*-PHA production, substrates coming from renewable and low-cost feedstocks like lignocellulosic biomass have been studied lately as sustainable foundation for cleaner production (Govil *et al.*, 2020). For this end, multiple fundamental and technical challenges need to be solved prior to establishing an efficient *mcl*-PHA value chain platform from the lignin fraction of lignocellulosic materials. Although several studies have demonstrated *mcl*-PHA production from single lignin aromatics and/or lignin-derived streams (Linger *et al.*, 2014; Jayakody *et al.*, 2018; Liu *et al.*, 2019; Salvachua *et al.*, 2020), obtaining real and reproducible liquors of lignin-derived aromatics as substrates is still difficult. Additionally, limited methods for analysis of the heterogeneous aromatic fractions and complex catabolic repression phenomena make a detailed physiological study of *mcl*-PHA production from lignin-derived aromatics very challenging. Thus, the majority of studies in *P. putida* have focused on evaluating aromatic monomers like benzoate (Xu *et al.*, 2019b; Borrero-de Acuña *et al.*, 2020), vanillate (Wang *et al.*, 2018), ferulate (Zhou *et al.*, 2020) or co-feeding some of them with glycerol (Xu *et al.*, 2021).

Thus, studies towards a physiological understanding of the uptake and conversion dynamics of defined aromatic mixtures into *mcl*-PHA are necessary. Finally, due to the importance of oxygen for the proper functioning of the aromatic catabolic pathways (Fig 1.5), a more

comprehensive understanding of the impact of oxygen transfer rates on *mcl*-PHA production from lignin aromatic mixtures is also a requirement.

1.7 Production of *cis,cis*-muconic acid from lignin aromatics

Muconic acid is a high value building block in the chemical industry. Due to its high reactivity, in the presence of catalysts, it can be converted to valuable industrial chemicals like adipic acid, terephthalic acid, and caprolactam (Carraher *et al.*, 2017; Skoog *et al.*, 2018). These molecules are widely used in the plastic, medical, cosmetic, and textile industry (Choi *et al.*, 2020). Because the production of most of these chemicals is petroleum-based and therefore generates hardazous waste products, in the last years the bio-based production of muconic acid based on microbes has gained high interest (Choi *et al.*, 2020).

Muconic acid is a six-carbon (C6) dicarboxylic acid with conjugated double bonds. It presents three isomeric forms *i.e., cis,cis*-, *cis,trans*- and *trans,trans*- (Fig 1.7). Depending on the culture pH, the first two forms are commonly found in microbial cultivations (Khalil *et al.*, 2020). The microbial production of *cis,cis*-muconic acid was first demonstrated from sugars like D-glucose using an engineered *Escherichia coli* strain (Draths and Frost, 1994). The authors connected a heterologous aromatic branch to a blocked shikimic acid pathway, reaching a conversion efficiency of 30%.

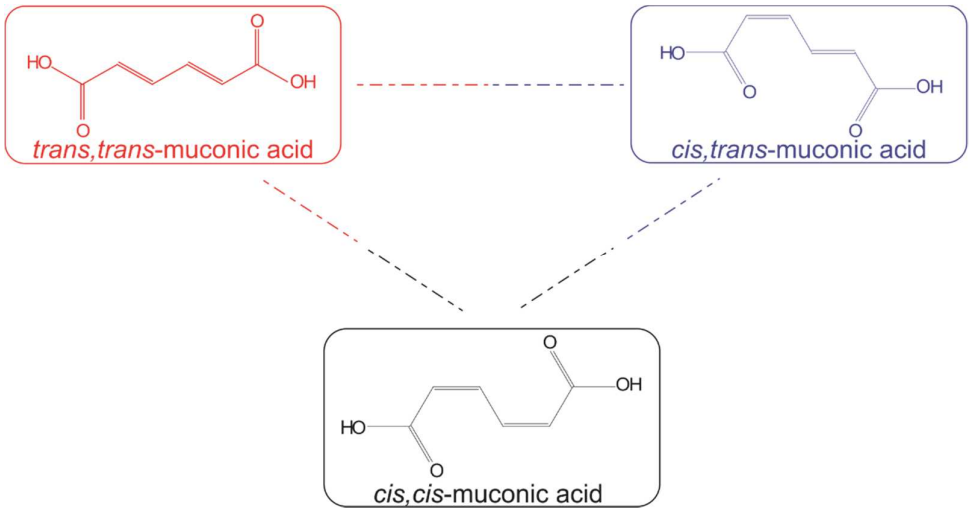

Fig. 1.7 Isomeric forms of muconic acid. Depending on the pH, *cis,cis*-muconic acid and *cis,trans*-muconic acid are commonly found in microbial cultivations. Adapted from Khalil *et al.*, 2020

Most of the microbial synthesis of *cis,cis*-muconic acid from lignin-aromatics has been achieved in bacterial strains like *P. putida*. In this case, the accumulation of *cis,cis*-muconic acid occurs upon disruption of the catabolic route at the *cis,cis*-muconate cycloisomerase point of the catechol degradation branch (Fig 1.5) (van Duuren *et al.*, 2011). Additional aromatic substrates like p-coumaric and ferulic acid can be converted linking the protocatechuate branch of the β-ketoadipate pathway with the catechol branch by metabolic

engineering (Vardon *et al.*, 2015). From these important contributions further approaches improved productivities in the same strains or other bacterial hosts, which have been well summarized in relevant reviews (Xie *et al.*, 2014; Becker and Wittmann, 2019; Choi *et al.*, 2020).

To achieve relevant production levels of *cis,cis*-muconic acid in *P. putida* from lignin aromatics, different fed-batch controlled bioprocess strategies have been implemented. Examples are the pH-stat fed-batch (van Duuren *et al.*, 2012; Kohlstedt *et al.*, 2018) and DO-stat fed-batch systems (Bang and Choi, 1995; Vardon *et al.*, 2015; Salvachúa *et al.*, 2018). Additionally, linear and high-pH feeding strategies and continuous cell recirculation systems also improved the process performance (Salvachúa *et al.*, 2018). Despite of the important progress to improve *cis,cis*-muconic acid production, a missing gap in this field is the implementation of proper strategies to overcome product inhibition.

Different studies have pointed out optimal *cis,cis*-muconic acid concentrations that promoted proper activity of the catechol 1,2-dioxygenase (Choi *et al.*, 1997). Other authors found detrimental conditions at high *cis,cis*-muconic acid levels for kinetic parameters like growth and substrate uptake rates (van Duuren *et al.*, 2012). Metabolic intermediates accumulation at *cis,cis*-muconic acid concentration higher than 25 g L^{-1} have been also reported (Salvachúa *et al.*, 2018). These observations suggest that there is still room for improvement by implementing strategies that maintain optimal *cis,cis*-muconic acid levels in the culture. One of the most utilized strategies to decrease the detrimental effect of product accumulation is the *in-line* extraction from the bioreactor.

1.7.1 In-line *product removal and recovery*

To alleviate the negative effects of product accumulation in biotechnological processes different systems promoting *in-line* product removal can be applied. A well-recognized integrated strategy is called *in-situ*/*in-stream* product recovery (ISPR), which has been applied to remove and recover a product of interest (Santos *et al.*, 2021). While during an *in-situ* recovery, the formation and separation steps occurs inside the bioreactor, in the *in-stream* or *in-line* system, the separation step takes place outside. Both *in-stream* and *in-situ* approaches can have significant advantages over conventional industrial biotechnology processes. With the advantages of increased concentrations and productivities at decreasing downstream operational costs, the implementation of these integrated systems is not new (Freeman *et al.*, 1993).

There are different configurations of integrated bioreactor systems performing *in-situ*/*in-stream* extraction, which used different operational units (*i.e.,* filtration, solvent extraction, reactive extraction, ion exchange chromatography, etc.) depending on the target molecule. Some of the most utilized systems are resumed in Fig. 1.8. Many specific cases and

configurations have been reported in the last decade, which have been well-reviewed (Van Hecke *et al.*, 2014).

To separate organic acids from fermentation broths, downstream process operations like chromatography, precipitation, membrane separation, liquid-liquid extraction, reactive extraction, distillation, etc. have been implemented (Li *et al.*, 2016). Based on the charges of non-protonated forms of organic acids, an attractive group of techniques based on electro-migration of ions through an ion exchange membranes (IEM) have been studied lately (López-Garzón and Straathof, 2014; Handojo *et al.*, 2019). Particularly, extractive membrane electrolysis stands out by its simple operation promoting the flux of charged products across a single IEM. It has been successfully integrated with mixed cultures producing carboxylates, enabling better process performance (Andersen *et al.*, 2014; Andersen *et al.*, 2015; Gildemyn *et al.*, 2015).

This novel process is driven by the electrolysis of water when applying a constant current between the cathode and the anode, while retaining solids or biomass by a selective IEM (see Fig. 1.9). If an anion exchange membrane AEM is implemented, the negatively charged molecules contained in the electrolyzed catholyte (for instance, carboxylates) migrate selectively to the anolyte. The flux of ions occurs against the applied current. The corresponding reactions at anode and cathode are oxidation ($2\ H_2O \rightarrow 4\ H^+ + O_2 + 4e^-$) and reduction ($2\ H_2O + 2e^- \rightarrow H_2 + 2\ OH^-$) of water, respectively. Thus, the extracted product could be accumulated in a clean and low pH anolyte while hydroxide ions could replace caustic soda management enabling *in-line* pH control of the fermentation broth. These advantages have been demonstrated in pure cultivation of *Basfia succiniciproducens* operated in fed-batch mode. In this case, the succinic acid productivity increased by 30% and the consumption of NaOH decresed (Pateraki *et al.*, 2019). Based on the possibility of selectively extracting *cis,cis*-muconate (which has two carboxylic groups) from a bioreactor, an integrated system should maintain proper product levels in the culture.

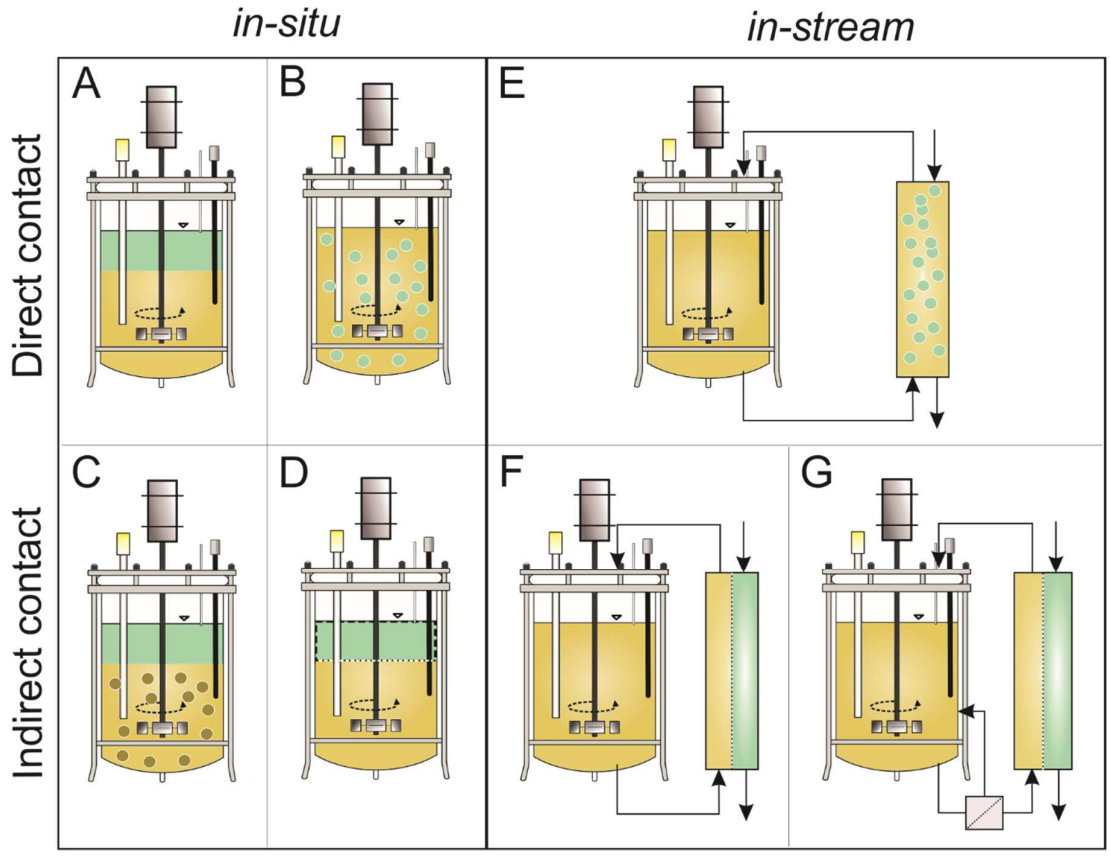

Fig. 1.8 Configurations of integrated product recovery strategies from bioreactors. *In-situ* extraction occurs inside the bioreactor: two-phase partitioning bioreactors (A), solvent-impregnated particles dispersed in culture medium (B) or indirect contact using immobilized cells (C) and internal pertraction (D). *In-stream* occurs outside of the bioreactor: direct contact fermentation broth pumped to a column packed with solvent-impregnated particles (E), external pertraction (F), or introducing microfiltration units to separate the biocatalyst from the fermentation broth before contact (G). Adapted from Sánchez-Castañeda *et al.*, 2020.

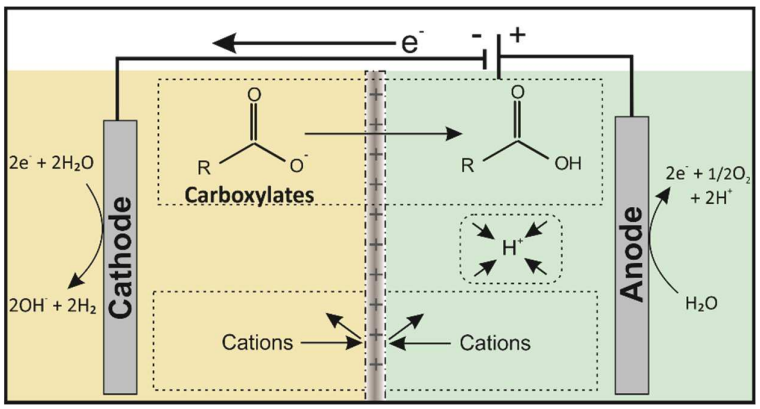

Fig. 1.9 Electrolytic extraction of carboxylates. This process is driven by the electrolysis of water when applying a constant current between the cathode and the anode. An anion exchange membrane AEM permits the selective movement of negatively charged anions from the catholyte to a low pH anolyte.

1.8 Scope and outline of the thesis

Lignin is a major component of lignocellulose biomass and represents the most abundant aromatic polymer on the planet. Therefore, it is a renewable source of bio-aromatics that promises to positively impact the development of the future biorefining processes. However, nowadays it is still widely underused for its material value. Inspired on overcoming the challenges related to efficient lignocellulose biomass conversion for building a circular bioeconomy, this thesis intends to implement novel strategies to promote the upgrading of lignin aromatics into valuable products like *mcl*-PHA and *cis,cis*-muconic acid.

To achieve this principal goal, the selection of a suitable biocatalyst (*i.e.,* microbial platform) is essential. It is known that the genus *Pseudomonas* stands out for having a great aromatic catabolic ability and a diverse and adaptable metabolic machinery. This capacity promises to ease the inherent aromatic heterogeneity found in lignin depolymerized streams and potentially to accumulate valuable metabolites. Thus, this study starts with a comprehensive screening campaign to select the most robust *Pseudomonas* from a group of wild type strains (**Chapter 3**). In a first approach, this group will be cultivated on diverse lignin derived monomers that have been reported to be present in aromatic liquors after lignin depolymerization. Once the most suitable strains and aromatic substrates are revealed, a second step will concentrate efforts on evaluating their valorization potential (*i.e.,* upgrading lignin aromatics into *mcl*-PHA). Being aware of the challenges related to obtaining reproducible amounts of aromatic liquors and the limitations on analytics to perform comparative studies, a mixture of aromatic compounds will be defined in a third step. Once the most robust strain has been selected through comparative cultivations in chapter 3, the balance of important process variables like oxygen, nitrogen and aromatics will be evaluated towards establishing a successful bioprocess (**Chapter 4**). Based on the optimal conditions for oxygen transfer rate and carbon to nitrogen ratios (C/N), scale-up in a bioreactor system will be performed. The last part of this chapter will focus on the increment on *mcl*-PHA production through implementing a strategy based on simultaneous optimization of the biocatalyst and the bioprocess conditions.

Cis,cis-muconic acid is another outstanding example of valuable product with a remarkable commercial potential. However, concentrations and productivities are still too low for implementing a fully-realized industrial process from lignin aromatics. An important limiting factor for achieving higher production is product toxicity and inhibition in cultivations of *Pseudomonas putida* KT2440. **Chapter 5** presents the process development for implementing an *in-line* extraction of *cis,cis*-muconate from a bioreactor. The final aim will be to alleviate the negative effects of product accumulation and thus, to enhance productivities. In a first stage, a suitable anion exchange membrane will be selected from a group of available commercial membranes. Then, the electrolytic extractive process will be characterized using synthetic media. This will enable to get extraction rates (flux) and coulombic efficiency of the

most relevant ions involved. Once the production rates of *cis,cis*-muconate are defined in a conventional bioreactor and the extraction conditions of fermentation broths are assessed, both processes will be coupled. After dealing with challenges related to process integration, parallel comparisons between a conventional process and the *in-line* extractive system will be performed.

A schematic representation of this research approach is shown in Fig 1.10.

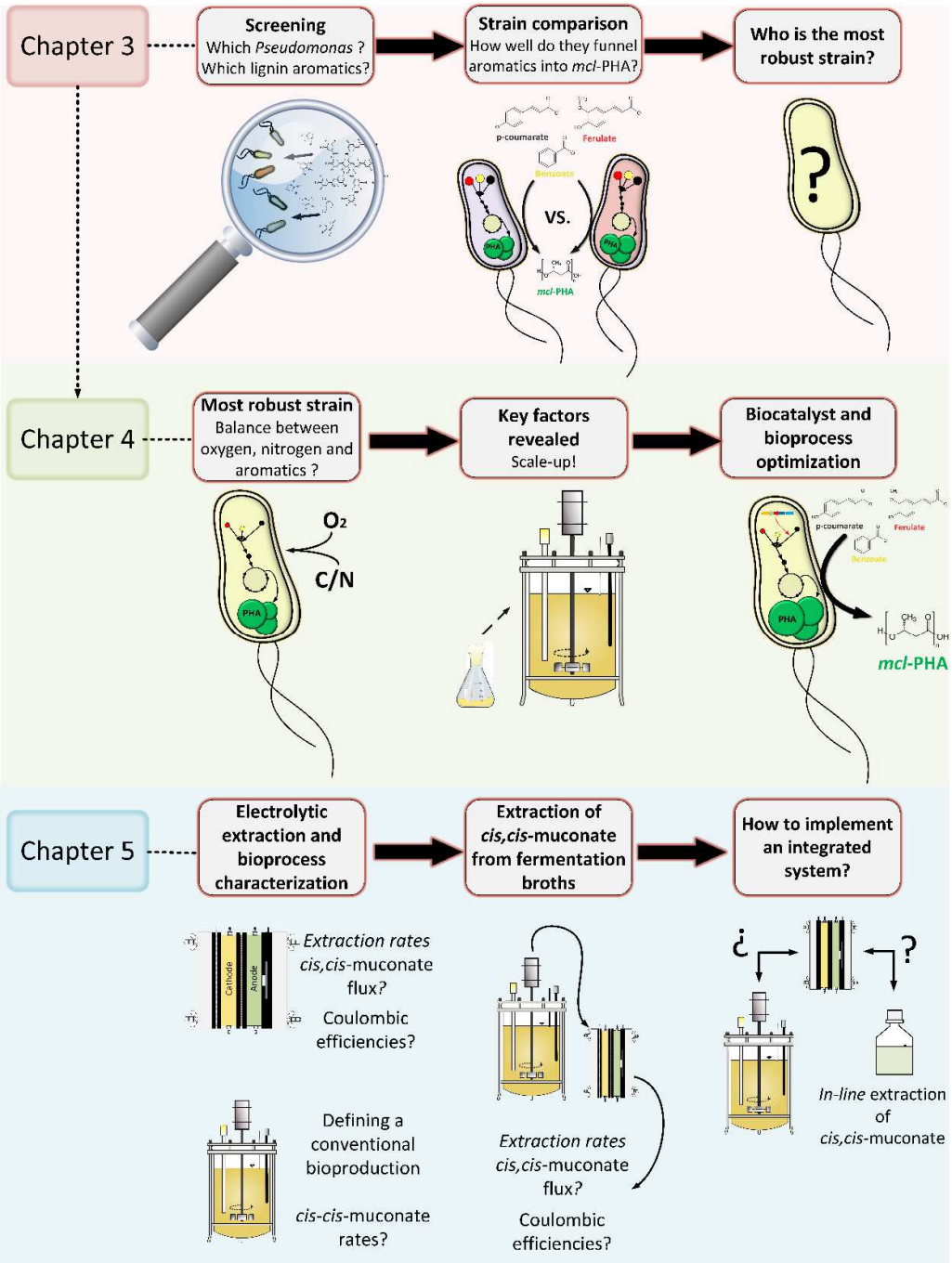

Fig. 1.10 Schematic representation of this research approach followed in every chapter of this the

Chapter 2: Materials and methods

Partially published as:

Ramírez-Morales J. E., Czichowski P., Besirlioglu V., Regestein L., Rabaey K., Blank L. M., Rosenbaum M. Lignin aromatics to PHA polymers: nitrogen and oxygen are the key factors for *Pseudomonas*. 2021. *ACS Sustainable Chemistry & Engineering*, 9, 31, 10579–10590. https://doi.org/10.1021/acssuschemeng.1c02682

Contributions:

Phillip Czichowski helped with genetic engineering procedures, strain screenings, and oxygen limited cultivations. Volkan Besirlioglu assisted with flow cytometry analysis. Mohammad Sanowar Hossain assisted in some electrolytic extractions and fermentation runs. Juan E. Ramírez implemented the majority of the set-ups and analytic techniques. Together with José M. Carvajal, Lars Regestein, Korneel Rabaey, Lars Blank and Miriam Rosenbaum, I designed the experiments and analyzed the results.

2.1 Bacterial strains

All wild type *Pseudomonas* strains used in this study, their relevant biotechnological features and sources are listed in Table 2.1. The genetically modified *Pseudomonas putida* strains generated during deletion and insertion of DNA procedures (described in the section 2.3), their main genotype/phenotype characteristics and sources are given in Table 2.2. Additional *E. coli* strains used during all cloning procedures can be found in the Appendix (Table S2.1).

Table 2.1 Wild type *Pseudomonas* strains used in this study. The relevant biotechnological features, source/reference and strain collection number of the institute of applied microbiology (iAMB, RWTH Aachen University) are given.

Wild type strain	Relevant biotechnological features	Source / Reference
Pseudomonas putida S12	Solvent tolerant, production of valuable aromatics	Hartmans *et al.*, 1989 (iAMB #2059)
Pseudomonas putida KT2440	Bioremediation, production of valuable chemical building blocks	DSM 6125 (iAMB #2058)
Pseudomonas putida F1	Catabolic properties for aromatic hydrocarbon utilization	DSM 6899
Pseudomonas taiwanensis VLB120	Solvent tolerant (styrene degrader), production of valuable aromatics	Park *et al.*, 2007 (iAMB #2060)
Pseudomonas aeruginosa PA14	Genes involved in the synthesis of several secondary metabolites	DSMZ 19882
Pseudomonas aeruginosa PAO1	Genes involved in the synthesis of several secondary metabolites	DSMZ 19880
Pseudomonas fluorescens	Bioremediation, biocontrol agent in agriculture	DSM 50090 (iAMB #2337)

Table 2.2 Genetically modified *Pseudomonas putida* strains generated in this study. The relevant genetic and phenotypic features, source/reference and strain collection number of the institute of applied microbiology (iAMB, RWTH Aachen University) are given.

Strain	Genotype/Phenotype	Source / Reference
P. putida		
KT2440-KOZ1	Deficient for *phaZ.* Higher *mcl*-PHA accumulation than wild type.	This study
KT2440-CCMA1	Deficient for *catRBC, catA* under control of $P_{tac.}$ Accumulation of cis,cis muconate from benzoate (catechol branch)	This study (iAMB #813)
KT2440-CCMA2	Derived from *P. putida* KT2440*ΔcatRBC::*P_{tac}. Deficient for *pcaHG,* carrying gene *aroY* under control of P_{tac}. Accumulation of cis,cis muconate from benzoate (catechol branch) and p-coumarate/ferulate (protocatechuate branch).	This study

2.2 General culture media and propagation

Pre-cultures were prepared from frozen glycerol stocks (final concentration of 35% v v^{-1}) kept at -80°C. They were cultivated in Lysogeny Broth (LB) medium (10 g L^{-1} peptone, 5 g L^{-1} yeast extract, 5 g L^{-1} NaCl) (Carl Roth®, Karlsruhe, Germany) and subsequently transferred into fresh mineral salt medium (MSM) in shake flasks (liquid kept at 10% of total volume) overnight at 200 rpm, throw of 50 mm and 30 °C. This procedure was repeated for all bacterial strains except for *P. aeruginosa* PA14, *P. aeruginosa* PAO1 and *E. coli* strains which were grown at 37°C. Prior to inoculation, the cells were harvested by centrifugation (12,000 g, 5 min), washed and resuspended in PBS solution. Then, they were then inoculated to an OD_{600} of 0.1. All experiments were performed using a defined MSM according to Hartmans *et al.*, 1989 containing 2.0 g L^{-1} $(NH_4)_2SO_4$, 3.88 g L^{-1} K_2HPO_4, 1.63 g L^{-1} NaH_2PO_4, 0.1 g L^{-1} $MgCl_2{\cdot}6H_2O$, 10 mg L^{-1} EDTA, 2 mg L^{-1} $ZnSO_4{\cdot}7\ H_2O$, 1 mg L^{-1} $CaCl_2{\cdot}2H_2O$, 5 mg L^{-1} $FeSO_4{\cdot}7\ H_2O$, 0.2 mg L^{-1} $Na_2MoO_4{\cdot}2H_2O$, 0.2 mg L^{-1} $CuSO_4{\cdot}5\ H_2O$, 0.4 mg L^{-1} $CoCl_2{\cdot}6\ H_2O$, 1 mg L^{-1} $MnCl_2{\cdot}2H_2O$. The media was supplemented with 20 mM glucose or the corresponding aromatic compound as carbon source.

During culture media preparation, corresponding amounts of separated stock solutions (phosphate buffer K_2HPO_4 + NaH_2PO_4, trace elements, nitrogen source $(NH_4)_2SO_4$ and glucose, each 100X concentrated and autoclaved) were added to sterile and double-distilled (bidest) water to reach the final volume of culture solution. The nitrogen source was added according to the carbon to nitrogen molar ratios (C/N of 4, 8, 40, 60 and 80). Solid media was prepared adding agar (1.5% w v^{-1}) and the corresponding antibiotic concentration. Autoclave sterilization was performed at 121 °C and 1 bar overpressure for 20 min.

The lignin-derived monomers were purchased from Carl Roth (Karlsruhe, Germany) or Sigma-Aldrich (St. Louis, MO, USA). Sterile stocks were prepared at 150 mM dissolving each compound in bidest water by increasing the pH with NaOH and then neutralizing to pH 7.1 with HCl. The aromatic stock solutions were sterilized by filtration (0.2 µm pore size) and stored at 4°C for short term usage.

2.3 Plasmid cloning and strain engineering procedures

All plasmids were constructed following the Gibson assembly (Gibson *et al.*, 2009) using the NEBuilder HiFi DNA Assembly master mix (New England Biolabs, Ipswich, MA, USA). Plasmid isolation was performed by Monarch® Plasmid Miniprep Kit (New England Biolabs, Ipswich, MA, USA). Primers were designed with Clone Manager Professional 9 (Sci-Ed, Denver, USA) or NEBuilder® Assembly Tool (New England Biolabs, Ipswich, USA). They were purchased from eurofins Genomics (Ebersberg, Germany), delivered freeze-dried and then diluted in nuclease-free water (Carl Roth®, Karlsruhe, Germany) according to corresponding instructions to reach a final concentration of 100 pmol μl^{-1}. Stocks of 10 µM were prepared and stored at -20 °C for

direct use during preparation of PCR reaction mixtures. Codon optimized DNA fragments were ordered and purchased from Integrated DNA Technologies (Coralville, USA). All DNA fragments were purified using the Monarch® PCR & DNA Cleanup Kit (New England Biolabs, Ipswich, USA). DNA concentration (*i.e.*, genomic DNA, plasmids and PCR fragments) was determined by NanoDrop™ One Microvolume UV-Vis Spectrophotometer (Thermo Fisher Scientific Inc., Waltham, USA).

2.3.1 General procedure for targeted editing of Pseudomonas *genomes*

Deletion and insertion of DNA molecules into *Pseudomonas* chromosomes was carried out by the methodology based on homologous recombination and I-SceI-based editing tool reported by Martínez-García and de Lorenzo, 2011. The general procedure followed for targeted editing of all the *Pseudomonas putida* genomes used in this study was based on the deletion vector pEMG and is summarized in Fig. 2.1. A general list of all plasmids, primers and synthetic DNA fragments involved during all genetic engineering procedures in this work can be found in the Appendix (Tables S2.2 and S2.3)(Fig. S2.1 and S2.2).

Targeted sequences of DNA (*i.e.*, TS1 and TS2 as the flanking regions of the gene of interest GOI) were amplified from genomic DNA by PCR using corresponding primers (carrying overlapping ends, which are homologous to the pEMG backbone) and the Q5 High-Fidelity Polymerase (New England Biolabs, Ipswich, USA). In parallel, *E. coli* DH5α-λpir containing the pEMG was grown in LB media containing 50 µg mL^{-1} kanamycin. After plasmid isolation and DNA quantification, the vector was linearized by restriction enzyme digestion in the site XbaI located in the multiple cloning site (MCS), which in turn is flanked by the recognition site I-SceI. Vector and insert were assembled with the Gibson Assembly method following the manufacturer's protocol.

Electrocompetent *E. coli* DH5α-λpir cells (50 µl) (Table S2.1) were transformed with approximately 100 ng of the assembled products in a pre-chilled electroporation cuvette with a gap width of 2 mm (Cell Projects, Harrietsham, England) at 2.5 kV, 200 Ω and 25 µF by a Gene Pulser Xcell™ electroporation system (Bio-Rad laboratories, Hercules, CA, USA). Soon after, 950 µl of LB media were added and the cells were incubated for 1 h at 37 °C and 200 rpm. The successful integration was verified via blue-white screening using LB agar plates containing kanamycin 50 µg mL^{-1}, 1 mM IPTG and 1% w v^{-1} X-gal. White colonies were picked and verified by colony PCR using OneTaq 2X Master mix (New England Biolabs, Ipswich, USA). In this step, the co-integrate resolution was triggered via DNA double-strand breaks (DSBs) in the recognition site I-SceI caused by the endonuclease expressed from the mobilized plasmid pSW-2. The self-reparation system via RecA-mediated homologous recombination re-circularize the bacterial chromosome and eliminate the vector backbone and GOI (or alternatively insertion of a DNA sequence). As a restoration of the wildtype genotype could have happened depending on the flanking region recombined, cell material was again resuspended and spread on Centrimide agar plates containing gentamycin 10 µg mL^{-1} to find

successful cases via colony PCR screening. Corresponding primers were used to amplify and sequence a region of interest by Sanger sequencing (performed by Eurofins Genomics, Ebersberg, Germany). Finally, the plasmid pSW-2 was cured by successively growing the new strain in media without antibiotic.

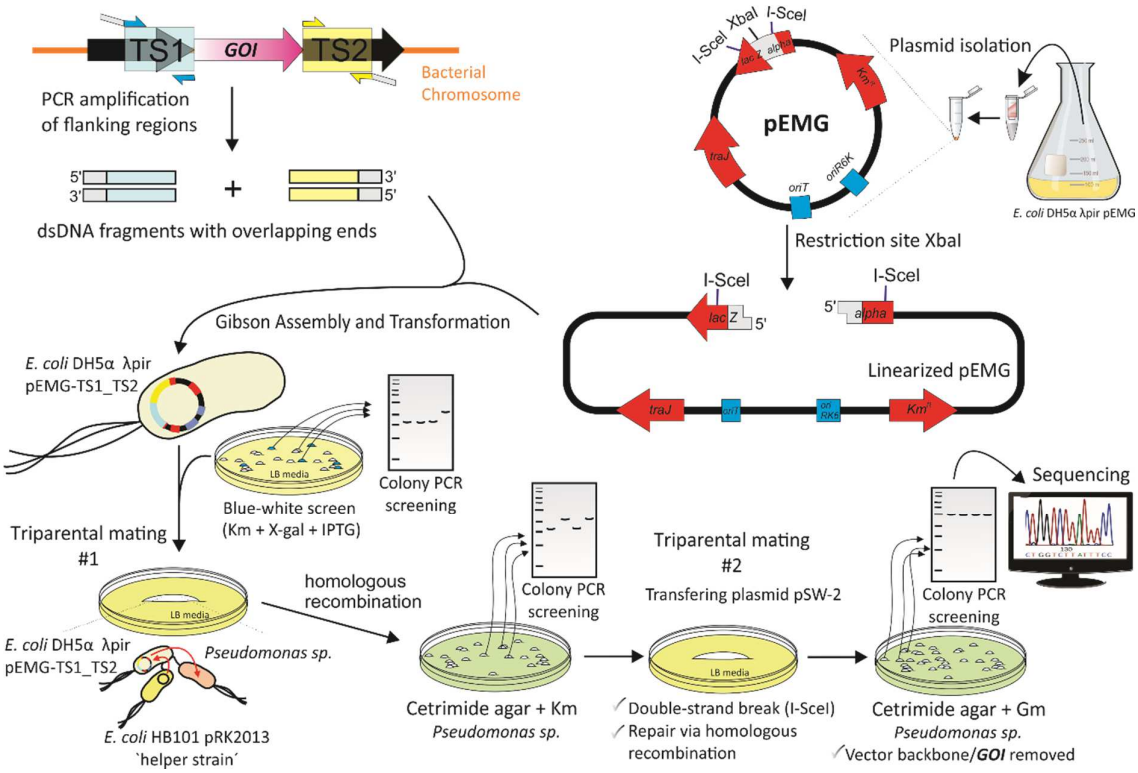

Fig. 2.1 General workflow used for targeted editing of *Pseudomonas* genomes. The procedure was based on homologous recombination and I-SceI-based editing tool reported by Martínez-García and de Lorenzo, 2011. Targeted DNA sequences (flanking regions TS1 and TS2 of the gene of interest GOI) were amplified by PCR using primers with overlapping ends and homologous to the vector pEMG. This plasmid was isolated from the strain *E. coli* DH5α-λpir pEMG and then linearized in the site XbaI. Through Gibson assembly, the dsDNA fragments and the linearized pEMG were assembled and the re-circularized vector pEMG-TS1_TS2 was transformed into competent cells of *E. coli* DH5α-λpir. The successful integration was verified both by blue-white screening using LB agar plates containing kanamycin (km), IPTG and X-gal and colony PCR. To mobilize pEMG-TS1_TS2 into *Pseudomonas*, triparental mating was performed. A helper strain *E. coli* HB101 harbouring the conjugative plasmid pRK2013 with complementary transfer features of pEMG-TS1_TS2 was used. After plating these three strains in LB media, the genome integration of pEMG-TS1_TS2 occurred via homologous recombination, and the *Pseudomonas* colonies were isolated in centrimide agar supplemented with Km and checked by colony PCR. In a second triparental mating, the plasmid pSW-2 was transferred to *Pseudomonas* and the double-strand brakes caused by the endonuclease I-SceI were self-repaired via homologous recombination. During this process the elimination of the vector backbone and GOI (or restoration of the wildtype genotype) occurred. Successful *Pseudomonas* colonies were selected in Centrmide agar supplemented with Gentamicin (Gm) and screened by colony PCR. Finally, verification of the edited genome was performed by DNA sequencing.

2.3.2 Construction of a higher mcl-PHA accumulating strain of P. putida KT2440

A strain of *P. putida* KT2440 deficient for the gene encoding for the intracellular *mcl*-PHA depolymerase (*i.e., P. putida* KT2440 Δ*phaZ)* was generated following the described workflow for targeted editing of *Pseudomonas* genomes (Fig. 2.1). This enzyme is known for being associated to biopolymer hydrolysis at surface of *mcl*-PHA granules, whose gene is located between two synthase-coding genes (*phaA* and *phaC*) in the *pha* gene cluster (de Eugenio *et al.*, 2007). An overview of the pathways for synthesis and depolymerisation of *mcl*-PHA in *P. putida* KT2440 from diverse substrates can be seen in Fig. 2.2A.

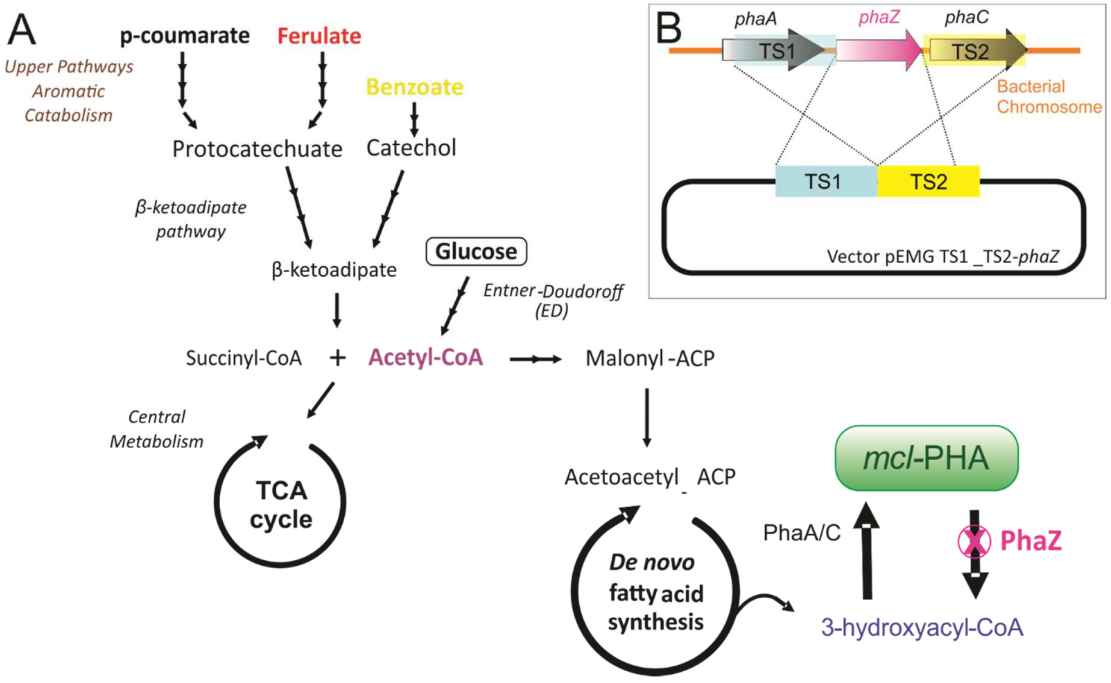

Fig. 2.2 Construction of a higher *mcl*-PHA accumulating strain of *P. putida* KT2440. Synthesis of *mcl*-PHA can be achieved from different aromatic substrates or glucose by the carbon flux generated in de novo fatty acid synthesis fed by acetyl-CoA (A). Two synthases PhaA and PhaC contributes to polymer accumulation, while PhaZ depolymerize it. Corresponding flanking regions TS1 and TS2 were joint into pEMG to delete *phaZ* while conserving sequences for correct terminal and starting transcription sites of both synthases.

Corresponding flanking regions TS1 and TS2 were selected to conserve the sequence of nucleotides up- and downstream of the start and terminal codons for the correct transcription of both *mcl*-PHA synthases (*i.e.,* terminators and ribosome binding sites RBSs) (Fig. 2.2B). These regions were cloned using the vector pEMG TS1 _TS2-*phaZ* (Fig. S2.1B), which was constructed and conjugated using the primers and auxiliary *E. coli* strains detailed in the Appendix (Tables S2.1, S2.3).

The selected clones were screened by colony PCR and verified by sequencing. Phenotypic characterization was carried out on different substrates like glucose, octanoate and aromatics under different nitrogen conditions. After clone screening, a selected strain (*P. putida*

KT2440-KOZ1) able to accumulate more *mcl*-PHA was selected. The results and the experimental details for strain selection based on the specific *mcl*-PHA fluorescence intensities are given in the Appendix (Fig. S2.3).

2.3.3 Construction of a metabolically engineered strain of P. putida *KT2440 to accumulate* cis,cis*-muconate from lignin aromatics*

A two-step procedure for the generation of *P. putida* KT2440 accumulating *cis,cis*-muconate from aromatics was adapted from (Vardon *et al.*, 2015) and following the previously described workflow for targeted editing of *Pseudomonas* genomes (Fig. 2.1). All plasmids, primers and auxiliary *E. coli* strains are detailed in the Appendix (Tables S2.1, S2.2 and S2.3) (Fig. S2.2).

First, the set of genes *catRBC* located in the gene cluster *catRABC* were deleted to block the conversion of *cis,cis*-muconate in the catechol branch of the β-ketoadipate pathway (see Fig. 2.3). Additionally, to enable strong and constitutive expression of catechol 1,2-dioxygenase (CatA), the native promoter for catBCA was replaced with the tac promoter (P_{tac}) (through pEMG TS1_*Ptac*_TS2), which is constitutively expressed in *P. putida* KT2440 (Fig. 2.3B). This procedure generated the a strain *P. putida* KT2440-CCMA1 (*P. putida* KT2440*ΔcatRBC::*P_{tac}), which accumulated *cis,cis*-muconate when converting benzoate and being provided with a secondary growth substrate lke glucose (see Fig. S2.4).

Secondly, the protocatechuate catechol branch of the β-ketoadipate pathway (*pcaHG* genes) was blocked (Fig. 2.3), and a simultaneous insertion of a heterologous protocatechuate descarboxilase (AroY) from *E. cloacae subsp. cloacae* ATCC 13047 was carried out by integration of the vector pEMG TS1_*aroY-Ptac*_TS2. The DNA sequence of the corresponding gene was codon-optimized, driven by P_{tac} and purchased as two fragments of synthetic DNA (gBlocks®) (Integrated DNA technologies, Coralville, USA) (see appendix for sequences). Both fragments had a homologous region and were joined during the Gibson assembly and flanked by the corresponding TS1 and TS2 regions. This procedure generated the strain *P. putida* KT2440-CCMA2 (*P. putida* KT2440ΔcatRBC::PtacΔpcaHG::aroY-Ptac). Thus, production of *cis,cis*-muconate from the aromatic monomers *p*-coumarate, ferulate, 4-hydroxybenzoate, and vanillate additionally to benzoate was enabled.

The selection of clones were also performed by the two-steps. First, the genotypes were verified in the different colonies selected, and the production of *cis,cis*-muconate (a yield of approximately 95%) from benzoate was verified by HPLC (Fig. S2.4). In a second step, the successful procedure for simultaneous insertion of *aroY*+P_{tac} and deletion of *pcaHG*, was verified by re-checking the ability to accumulate *cis,cis*-muconate from benzoate and then by evaluating the production from a mixture of benzoate and p-coumarate in shake flasks. These tests were complemented by online acquisition of the O_2 and CO_2 transfer rates (OTRs and CTRs) to correlate the time points where catabolic repression took place (see Fig 2.5BC)

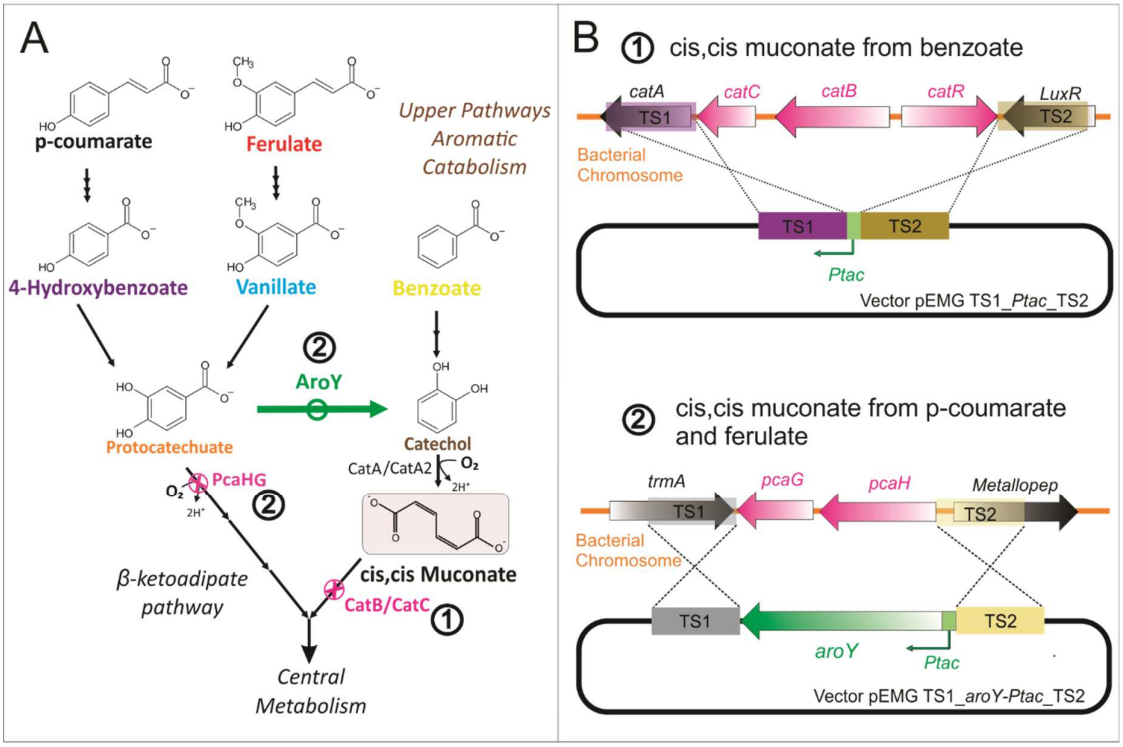

Fig. 2.3 Strain construction of a metabolically engineered *P. putida* KT2440 to accumulate *cis,cis*-muconate from aromatics. A two-step procedure for the generation of *P. putida* KT2440 accumulating *cis,cis*-muconate from aromatics was adapted from (Vardon *et al.*, 2015) (A), following workflow for targeted editing of *Pseudomonas* genomes (Fig 2.1) (B). First, the set of genes *catRBC* were deleted to block the conversion of *cis,cis*-muconate in the catechol branch of the β-ketoadipate pathway and the tac promoter P_{tac} was inserted enabling constitutive expression of catechol 1,2-dioxygenase (CatA). Thus, the production from benzoate was allowed by pEMG TS1_Ptac_TS2. Secondly, the protocatechuate catechol branch of the β-ketoadipate pathway (*pcaHG* genes) was blocked, and a simultaneous insertion of a heterologous protocatechuate descarboxilase (AroY) driven by P_{tac} was carried out. This later step expanded the production of *cis,cis*-muconate from p-coumarate and ferulate by pEMG TS1_aroY-Ptac_TS2.

2.4 Production of *mcl*-PHA from lignin-derived aromatics: cultivation conditions and operational procedures

Different system configurations were build and operated for setting up a final integrated process consisting of an electrolytic cell extraction unit and a fermenter. The next sections describe the devices, process flow diagrams and operational conditions used during the process development. Additionally, the main downstream process steps to recover *cis,cis*-muconic acid from a fermenter broth are described.

2.4.1 Strain screening in microtiter plates

Simultaneous on-line measurements of biomass formation was carried out via scattered light at 620 nm with the micro-bioreactor (MBR) system BioLector® I (m2p-labs GmbH, Baesweiler, Germany) (Fig. 2.4A) in 96 and 48 well plates. A total of 888 independent experimental units (wells) were taken in consideration during the three sequential step screening (Fig. 2.4B).

Each step started with a standardized inoculation procedure from cryogenic vials and two step shake flask cultivation in rich and MSM (glucose as sole carbon source) as described previously. The same composition of MSM was kept, except for the amount of nitrogen. All assays started at OD_{600} of 0.1 from a pre-washed cell suspension in PBS solution. Due to the amount of combinations derived of the number of strains and aromatic compounds involved, a general calibration of the BioLector® device was carried out using glucose for every strain and a suitable detector sensitivity (gain) of 50 was chosen for all other experiments. Initial blank scattered light values were obtained for every condition without inoculation to subtract the contribution of each media composition.

In step 1, seven wild type strains were screened on 15 aromatics and glucose (positive control) at 5 and 20 mM under nitrogen excess conditions (C/N of 4). Each strain was cultivated independently for 39 hours in a black 96 well-plate with an optical bottom from Greiner Bio-One GmbH (Solingen, Germany) and covered with an adhesive gas-permeable membrane (Greiner Bio-One, Solingen, Germany). Experiments were performed in triplicates with a filling volume of 190 µl, humidity controlled at 85%, and shaken at a frequency of 900 rpm. The temperature was 30 °C for all bacterial strains except for *P. aeruginosa* PA14 and *P. aeruginosa* PAO1, which were grown at 37°C. Details about the calculation of the normalized growth values are provided in section 2.7.1.

Screening step 2 focused on evaluation of the valorization potential of the best four performing strains from step 1. The selection was based on the highest average values of the normalized growth for all the aromatics at 20 mM. Four aromatic compounds were selected from the same ranking. The accumulation of *mcl*-PHA was evaluated under nitrogen excess (C/N of 4) and limited conditions (C/N of 40) after 48 hours. Endpoint sampling allowed measurements of final OD_{600}, aromatic composition and BODIPY-*mcl*-PHA fluorescence. To guarantee high oxygen transfer rates (OTRs), sufficient amount of cell broth, and to reduce evaporation, the essays were performed in 48 flower-like shaped microtiter plates (m2p-labs GmbH, Baesweiler, Germany) (Funke *et al.*, 2009). Experiments were performed in duplicates with a filling volume of 1800 µl, humidity controlled at 85%, and shaken at a frequency of 900 rpm. Proportionality between scattered light values and expected bacterial concentrations was obtained at a gain of 50 during internal calibration. Relevant biological parameters were obtained fitting an adapted version (re-parameterized) of the Gompertz model to microbial growth data as it is indicated in section 2.7.2, depending if biphasic or monophasic growth profiles were obtained. The theoretical oxygen transfer rate (OTR_{cap}) calculation in flower-like shaped microtiter plates was carried out by Eq. (4) (section 2.7.3).

Finally, screening step 3 was carried out under the same conditions in flower microtiter plates using the best three performing strains on aromatic valorization. This step compared the conversion capacity of a defined aromatic mixture into *mcl*-PHA by the strains. This time, the initial concentration of aromatics was set to 30 mM at a C/N of 80.

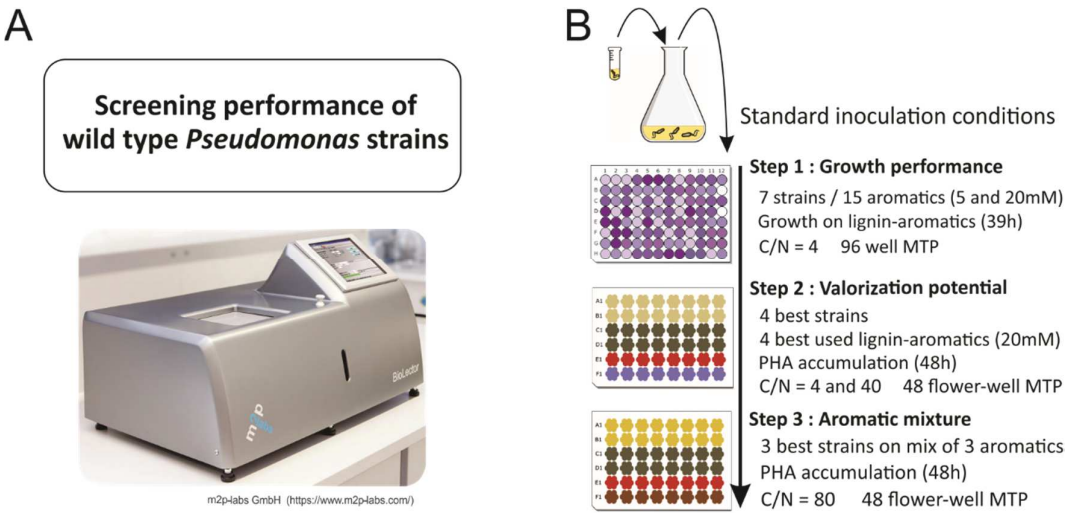

Fig. 2.4 Schematic overview of the experimental approach followed during strain screening in microtiter plates. On-line measurements of biomass formation of selected *Pseudomonas* strains was carried out via scattered light at 620 nm with the micro-bioreactor (MBR) system BioLector® (A). Three sequential steps were followed to evaluate the growth of seven wild type *Pseudomonas* strains on 15 lignin model compounds and the valorization potential of selected substrates and strains in microtiter plates (B).

2.4.2 Strain comparison in conventional shake flask and microaerobic bioreactors

The best two strains selected in the screening stage were cultivated in duplicates at 30 °C in conventional shake flask. In this case, 500 mL erlenmeyer flaks contained 50 ml culture media (diameter of 105 mm). The batch experiments started at a uniform inoculation OD_{600} of 0.1 and were shaken at 200 rpm for 124 h using a Multitron incubator shaker (Infors HT, Birsfelden, Switzerland) with an orbital throw of 2.5 cm (Fig 2.5A). The cultivations were carried out under atmospheric conditions (1 bar and 21 percent oxygen). The substrate consisted on the defined aromatic mixture of p-coumarate, ferulate and benzoate, each at 10 mM. The amount of $(NH_4)_2SO_4$ was adjusted to reach C/N ratios of 8 and 80. The corresponding OTR_{cap} for this experiments was calculated by Eq. (5), following the procedure explained in section 2.7.4 and using the osmolarity of each media (section 2.6.5). The mcl-PHA and aromatics involved in the cultivations were detected by flow cytometry and HPLC (Fig. 2.5B).

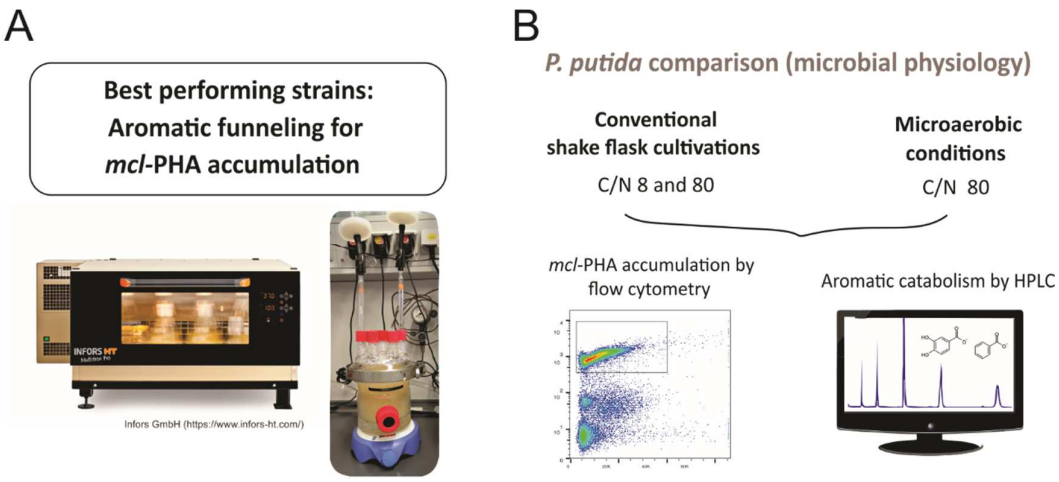

Fig. 2.5 Overview of the experimental approach to compare the best performing strains after the screening stage. The comparison was made in a conventional shake flask device (Infors HT) and using a microaerobic bioreactor (A). The microbial physiology of both strains was compared in terms of aromatic funneling capacity and *mcl*-PHA accumulation, which were monitored by HPLC and flow cytometry, respectively (B).

2.4.3 Oxygen limited cultivations

Bacterial strains were cultivated in batch duplicates under oxygen limited conditions in a lab-scale bioreactor set-up (Fig. 2.5A). It consisted of water jacketed glass vessels (custom-made, Gassner Glastechnik, Munich) with working volumes of 500 mL and sampling ports sealed with butyl rubber gasket septum. They were operated at 30 °C and stirred at 200 rpm. Microbial cultivations were carried out under two oxygen-limited conditions. Active aeration settings involved oxygen transfer via convection, where the head space was aerated at 30 ml min^{-1} by an aquarium air pump and controlled by a Flow Meter (Key Instruments, USA). Passive aeration was carried out by oxygen diffusion into the bioreactor opening the headspace to the atmosphere via 0.2 µm sterile PTFE vent filters (Millipore, Billerica, MA). The *mcl*-PHA and aromatics involved in the cultivations were detected by flow cytometry and HPLC The *mcl*-PHA and aromatics involved in the cultivations were detected by flow cytometry and HPLC (Fig. 2.5B).

2.4.4 On-line *measurements of the OTR in shake flask cultivations*

The methodology for obtaining the on-line respiratory activity and the dynamics of aromatic funnelling into *mcl*-PHA was adapted from a previous study evaluating production of other molecules (*Heyman et al., 2019*). The commercial shaker device TOM® (Adolf Kühner AG, Birsfelden, Switzerland) was used for on-line monitoring of the OTR (Fig. 2.6A). The general procedure was combined with parallel cultivations under identical conditions to take offline samples. For this, a Multitron orbitar shaker (Infors HT, Bottmingen, Switzerland) was used. Both devices were set with an orbital throw of 5 cm, 100 rpm, and 30 °C. The substrate consisted of the defined aromatic mixture described previously. Different amounts of $(NH_4)_2SO_4$ were adjusted to reach C/N ratios of 40, 60 and 80. For every of these nitrogen limited conditions a master mix was prepared. Cultivations were performed in unbaffled 250

mL shake flasks and filled with the corresponding master mix preparations, which were also inoculated with a common preculture. All cultivations started at an OD_{600nm} of 0.1. Different OTRs were set by changing the filling volumes (10, 20, 30 and 50ml) with each master mix. Thus, a combination of 12 different conditions were evaluated (Fig. 2.6B). Duplicates from every culture condition were evaluated in the TOM® device without disturbances up to 72 h, while every time a sampling flask was sacrificed in the conventional shaker for offline sampling. Compressed air was supplied to the TOM® device at concentrations of CO_2 and O_2 of 0.04% v v^{-1} and 20.95% v v^{-1}, respectively. The measured concentrations were corrected by an evaporation factor, which changed for every filling volume.

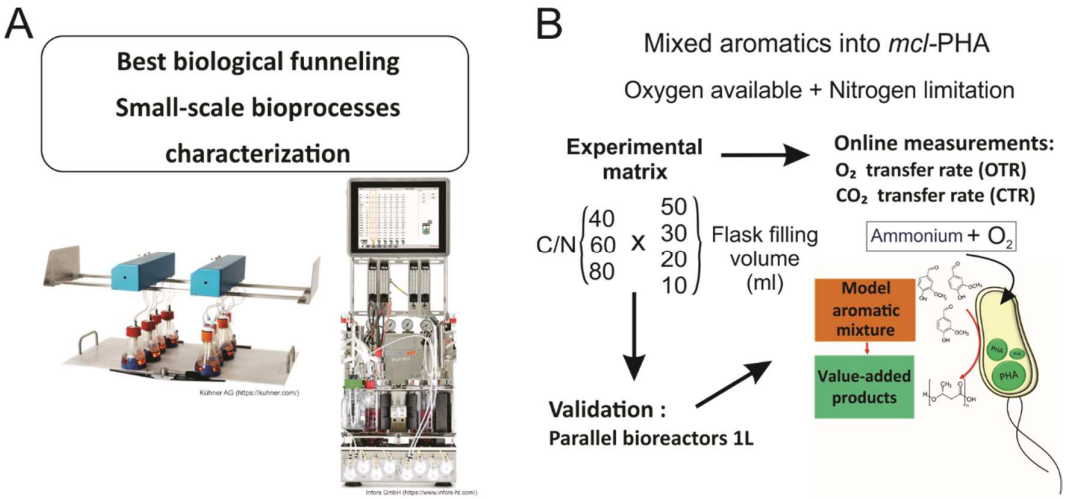

Fig. 2.6 Overview of the experimental approach followed for bioprocess characterization with the best strain. On-line measurements of the respiration were carried out by the device TOM® and by off-gas analysis in a bioreactor (A). First, the funnelling capacity at different oxygen and nitrogen availabilities were evaluated in flasks. Subsequently, the process was scaled to a 1-L stirred tank bioreactor at a proper OTR and C/N ratio to obtain a detailed dynamics of the bioprocess (B).

2.4.5 Cultivations in bench-top bioreactor system

Two parallel cultivations were conducted in two identical 1 L stirred-tank reactors Multifors 2 (Infors HT, Bottmingen, Switzerland) with a working volume of 0.7 L. The temperature was controlled at 30 °C during the bioprocess (Fig. 2.6). The preculture and mixed substrate preparation followed the same procedure as previously described. Before inoculation, 100 µL of Antifoam 204 (Sigma-Aldrich, St.Louis MO, USA) was added manually to each reactor. The initial stirring speed, pH and OD_{600nm} were 300 rpm, 0.1 and 7.1, respectively. To achieve the desired respiratory activity found in shake flasks, the reactors were aerated constantly with 0.175 L min^{-1} (0.25 vvm) pressurized air through mass-flow regulators. On-line O_2 and CO_2 concentrations were measured using parallel BlueInOne Cell gas analyzers (BlueSens GmbH, Herten, Germany). Initially, the dissolved oxygen concentration (DOT) was set to a minimum level of 50% in both reactors and was controlled automatically via stirrer speed controller. The on-line measurements of the gas outlet composition were taken and the OTR was calculated manually using Eq. (6) (section 2.7.5) Once the desired values were achieved for

every reactor, the control loop was opened and the stirrer speed was set at the corresponding constant value for the rest of the cultivation, completing 96 h. The carbon dioxide transfer rate (CTR) and the respiratory coefficient (RQ) were calculated according to Eq. (7) and Eq. (8) (section 2.7.5).

2.5 Production and electrochemical extraction of *cis,cis*-muconate : process configurations and operational conditions

Different system configurations were built and operated for a final integrated process consisting of a fermenter and an electrolytic cell extraction unit. The next sections describe the devices, process flow diagrams and operational conditions used during the process development. Additionally, the main downstream process steps to recover *cis,cis*-muconic acid from a fermentation broth are described.

2.5.1 Electrolytic membrane extraction of cis,cis*-muconate from synthetic solutions*

The first approach to extract *cis,cis*-muconate from synthetic media used a low volume two-chamber electrochemical cell separated by an anion exchange membrane (AEM) (Fig. 2.7). The membranes used were AM-7001S Anion Exchange Membranes, Membranes International Inc., Ringwood, USA; Fujifilm Type II (Fujifilm Europe GmbH, Germany); PC-200 D and PC-400 D, PCA Polymerchemie Altmeier GmbH / PCCell GmbH, Heusweiler, Germany) (Table 2.7). Each chamber had an internal dimension of 75 × 10 × 20 mm and 75 × 10 mm effective AEM area dimensions. Both chambers were built from square Perspex® frames and the cell was sealed using rubber and silicone gaskets. The iridium-coated anode consisted of a mixed metal oxide sheet of 10 mm × 10 mm, 0.5 mm thickness (Magneto Special Anodes, The Netherlands), 7 × 7 mm effective area dimensions, which was attached to a stainless steel sheet metal current collector. The cathode was a 316-L stainless steel mesh, 80 mm × 20 mm, mesh width: 564 µm; wire thickness: 140 µm (Solana, Belgium) and presented a 75 × 10 mm effective area.

Table 2.3 Commercial anion exchange membranes (AEMs) and their main characteristics.

Type of membrane	Functional group	Thickness [µm]	Resistance [Ω m^2]	Ion exchange cap. [meq g^{-1}]
AM-7001S	$-NR_3^+$	450	<40	1.3
Fujifilm Type II	$-NR_3^+$	160	5	1.08
PC-200 D	$-NR_3^+$	180-200	~2	1.24
PC-400	$-NR_3^+$	160-200	~10	0.66

The catholyte was prepared as synthetic fermentation broth using the same amount of components of based on the same defined MSM according to Hartmans *et al.*, 1989 and previously described (Section 2.2). In this case, different concentrations of commercial *cis,cis*-muconic acid (Sigma-Aldrich St. Louis, MO, USA) were added from fresh stock solutions

neutralized at pH 7.0. The anolyte was composed of 3g L^{-1} Na_2SO_4 and set to pH 2.0 with concentrated H_2SO_4.

Extraction experiments were carried out at 10, 25 and 50 mA at 20 °C. The tests were run in duplicates. The system set-up is shown in Fig. 2.8. In this configuration, the continuous flow of the anolyte was set to 3 L h^{-1} by a 530DU peristaltic pump (Watson Marlow, Falmouth, UK) and the spent solution was collected in a reservoir. The catholyte (100 ml) was recirculated at the same conditions ensuring turbulent mixing in a 250 ml glass flask. For this solution, hydroxide ions generated by water reduction were mitigated by adding drops of 1 M H_2SO_4. Different currents were applied by controlling the cell potential with a VSP-300 multichannel potentiostat (Biologic, Claix, France), which was run for 6 h in a galvanostatic mode. Samples of the anolyte were obtained every hour.

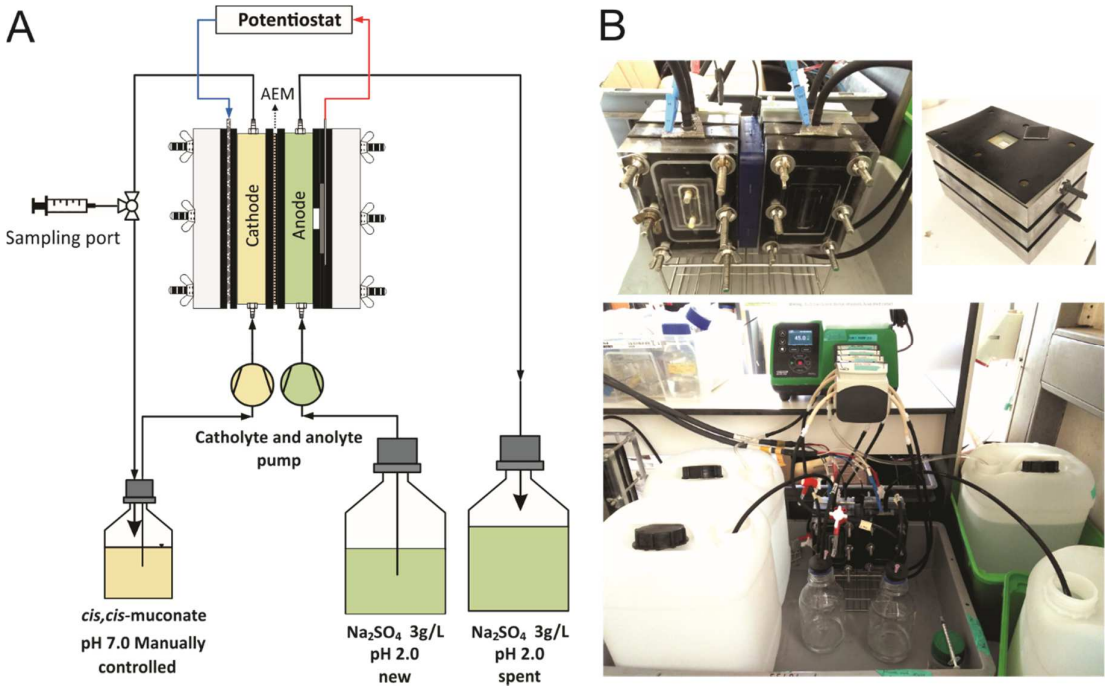

Fig. 2.8 Set-up for electrolytic membrane extraction of *cis,cis*-muconate from synthetic solutions (A). The system was run in duplicates using identical cells made of square Perspex® frames and rubber gaskets (B). The catholyte was manually controlled at pH 7.0 and anolyte was initially set to pH 2.0. The experiments were run at different current densities for 6 h.

2.5.2 Conventional bioprocess for cis,cis*-muconate production*

A 5 L Biostat® B-DCU bioreactor (Sartorious AG, Goettingen, Germany) was used for a fed-batch process carried out at 30 °C and pH 7.0 (Fig. 2.9). The process operation was adapted from Kohlstedt *et al.*, 2018. The pre-culture preparation was carried out as described above in Section 2.2. The batch operation started with a culture media composed by 10 g L^{-1} glucose, 5.6 g L^{-1} $(NH_4)_2SO_4$, 10.8 g L^{-1} K_2HPO_4, 4.5 g L^{-1} NaH_2PO_4, 0.28 g L^{-1} $MgCl_2{\cdot}6H_2O$, 28 mg L^{-1} EDTA, 5.6 mg L^{-1} $ZnSO_4{\cdot}7\ H_2O$, 2.8 mg L^{-1} $CaCl_2{\cdot}2H_2O$, 14 mg L^{-1} $FeSO_4{\cdot}7\ H_2O$, 0.56 mg L^{-1} $Na_2MoO_4{\cdot}2H_2O$, 0.56 mg L^{-1} $CuSO_4{\cdot}5\ H_2O$, 1.12 mg L^{-1} $CoCl_2{\cdot}6\ H_2O$, 2.8 mg L^{-1} $MnCl_2{\cdot}2H_2O$ and

0.01% of Antifoam 204 (Sigma-Aldrich St. Louis, MO, USA). It was inoculated to start at OD_{600} of 0.1. The initial aeration rate and stirring speed were set at 0.5 vvm and 300 rpm, respectively. The dissolved oxygen tension was maintained at 50 % air saturation by control of mixing and aeration rate. Automatic foam control added auxiliary Antifoam 204 (Sigma-Aldrich St. Louis, MO, USA) when needed. On-line O_2 and CO_2 concentrations were measured by BlueInOne Cell gas analyzers (BlueSens GmbH, Herten, Germany).

The subsequent fed-batch stage was operated in a pH-stat strategy to prevent benzoate overdo (van Duuren *et al.*, 2012). This technique was based on the pH drop induced by *cis,cis*-muconate formation, which was coupled to addition of a solution composed by of 2.9 M NaOH and 1.2 M benzoate. In parallel, a nutrient solution provided carbon, supplement elements and energy source to the culture. This solution contained: 600 g L^{-1} glucose, 50 g L^{-1} $(NH_4)_2SO_4$, , 3.88 g L^{-1} K_2HPO_4, 1.63 g L^{-1} NaH_2PO_4, 0.1 g L^{-1} $MgCl_2 \cdot 6H_2O$, 10 mg L^{-1} EDTA, 2 mg L^{-1} $ZnSO_4 \cdot 7\ H_2O$, 1 mg L^{-1} $CaCl_2 \cdot 2H_2O$, 5 mg L^{-1} $FeSO_4 \cdot 7\ H_2O$, 0.2 mg L^{-1} $Na_2MoO_4 \cdot 2H_2O$, 0.2 mg L^{-1} $CuSO_4 \cdot 5\ H_2O$, 0.4 mg L^{-1} $CoCl_2 \cdot 6\ H_2O$, 1 mg L^{-1} $MnCl_2 \cdot 2H_2O$. An exponential feeding rate of this solution was set to enable an specific growth rate (μ_{max}) of 0.04 h^{-1} using the Eq. (13), which was adapted from Kohlstedt *et al.*, 2018. The amount of benzoate and nutrient solution was recorded by coupling electronic balances to the control unit of the bioreactor.

2.5.3 Electrolytic membrane extraction of cis,cis-*muconate from fermentation broths*

Once real fermentation broths were obtained, new extraction experiments were performed. The general experimental procedures and set-up were the same as previously described (Fig. 2.10). This time, the concentration of the catholyte (fermentation broth) was diluted and set to 50 mM *cic,cis*-muconic acid. Initially, extraction experiments were carried out at 20 °C under manual pH control. For those tests, two lab-scale cells, one low volume (20 ml chamber) described above and a large volume cell (200 ml chamber) were compared.

The AEM membrane of the large volume cell was the AM-7001 (Membranes International Inc., Ringwood, USA) with effective area dimensions of 200 × 50mm. For this cell, each chamber had an internal dimension of 200 × 50 × 20 mm. Both chambers were built from square Perspex® frames and the cell was sealed using silicone gaskets. The anode consisted of an iridium oxide-coated titanium electrode IrO2/TaO_2; 0.65/0.35, 200 mm × 50 mm (Magneto Special Anodes, The Netherlands). Spacers (ElectroCell A/S, Denmark) were located at the membrane surface to avoid electrode contact and improve convection. The cathode was given by a 316L stainless steel mesh, 210 mm × 60 mm, mesh width: 564 µm; wire thickness: 140 µm (Solana, Belgium) and presented a 200 × 50 mm effective area.

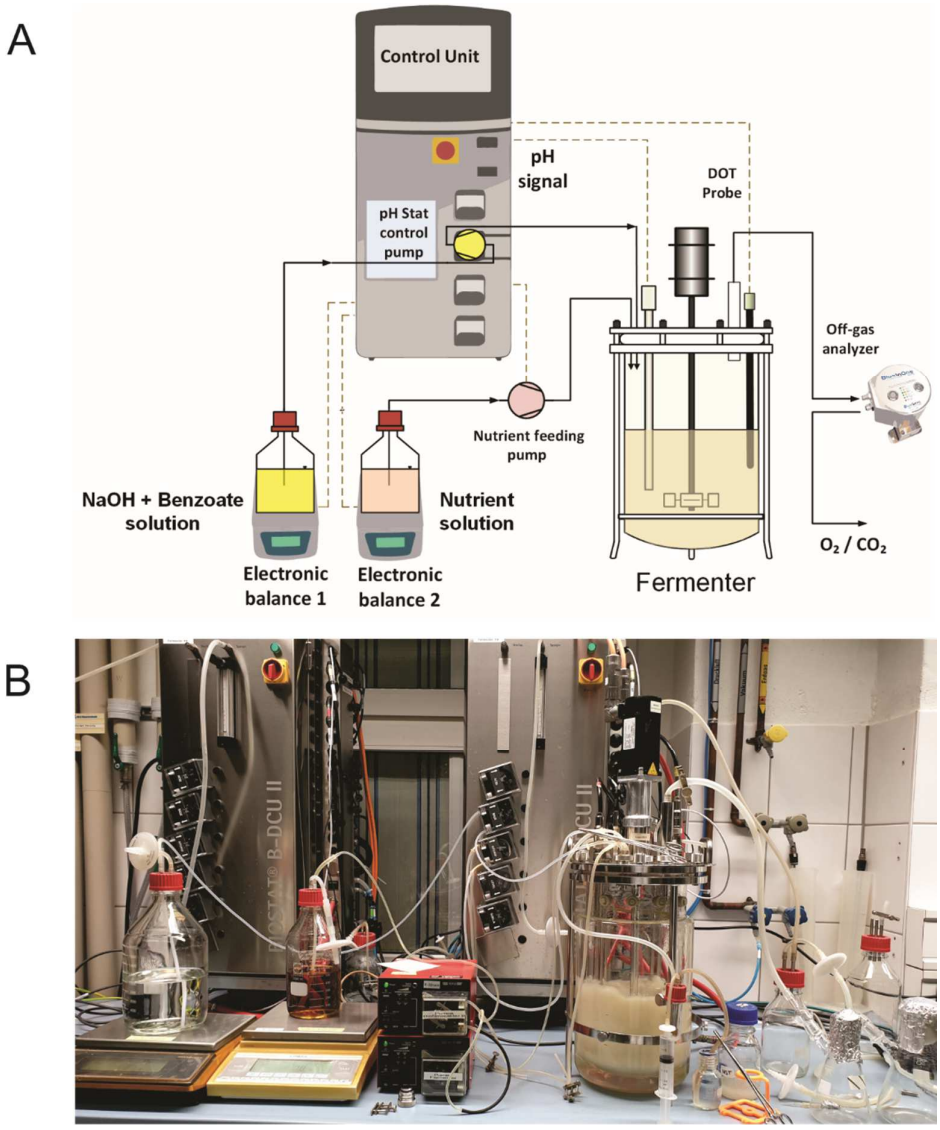

Fig. 2.9 Set-up of a conventional bioprocess for *cis,cis*-muconate production (A) and it's respective photo (B). A pH stat controlled fed-batch strategy was implemented to prevent benzoate overdoses. In this process, a solution of 1.2 M benzoate and 2.9 M NaOH was added when the pH dropped due to *cis,cis*-muconic acid formation. In addition, to provide a carbon and energy source, a nutrient solution was fed at an exponential rate to promote a specific growth rate of 0.04 h^{-1}.

Additional electrochemical extractions were performed at short (3 h) and long-term (24 h) at 333 mA using the large volume cell under automatic pH control and closed recirculation of both anolyte and catholyte. For this, an additional set-up and some specific conditions were modified (Fig. 2.10). The catholyte was prepared as previously described diluting a real fermentation broth to approximately 50mM *cis,cis*-muconic acid. The anolyte was composed of 3g L^{-1} Na_2SO_4 and set to pH 2.0 with concentrated H_2SO_4.

Extraction experiments were carried out in the cascade of 1-L lab-scale bioreactors Multifors 2 (Infors HT, Bottmingen, Switzerland), each with a working volume of 0.7 L. The pH of the

anolyte and catholyte were automatically controlled at 3.5 (adding 1 M NaOH) and 7.0 (adding 1 M H_2SO_4), respectively. In this configuration, the recirculated of both solutions was set at 3 L h^{-1} by using Sci-Q 300 series peristaltic pumps (Watson Marlow, Falmouth, UK). Additionally, the temperature and stirring speed were set at 30 °C and 300 rpm. All electrochemical experiments were controlled with a VSP-300 multichannel potentiostat (Biologic, Claix, France) and run in a galvanostatic mode.

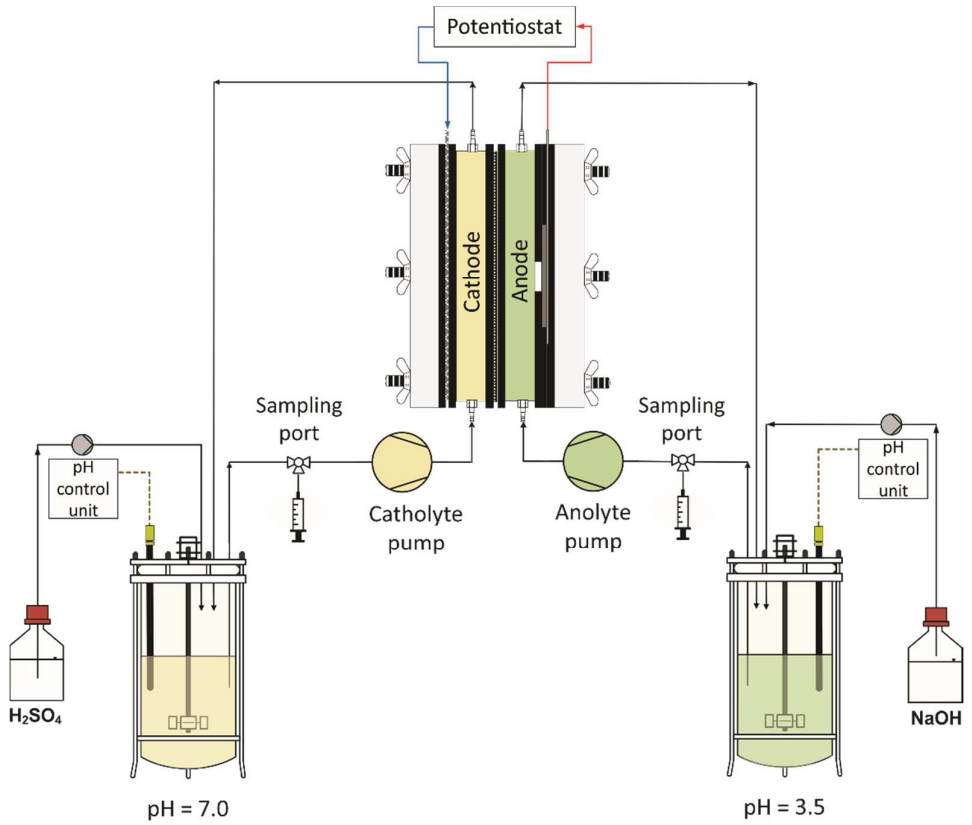

Fig. 2.10 Set-up for electrolytic membrane extraction of *cis,cis*-muconate from real fermentation broths using a large volume electrolytic cell (A). The extraction was performed under automatic control of pH, temperature, and stirring speed in both cell chambers.

2.5.4 Integrated bioprocess for in-line *electrolytic extraction of* cis,cis-*muconate*

The integrated system set-up with the large volume electrolytic cell coupled to a bioreactor is shown in Fig. 2.11. The operation was carried out in the cascade of 1-L lab-scale bioreactors Multifors 2 (Infors HT, Bottmingen, Switzerland). The culture conditions and bioreactor operation followed a similar procedure as described above for a conventional bioprocess.

In this particular case, two bioreactor systems were run in parallel to compare the behaviour of cultures with and without product removal by in-line electrochemical extraction. However, to achieve enough product removal from the culture, the initial batch volume was set to 0.5 L. This was planned in accordance to the anticipated removal of *cis,cis*-muconate by the cell and bioproduction rates obtained from previous experiments. Due to the hydroxide ions

generated by electrolytic water reduction in the catholyte (*i.e.,* bacterial culture), in this case it was not possible to establish a pH stat control system to feed benzoate. Therefore, similar flow rates of nutrient and benzoate solutions were imposed and corrected according to the new scale of production. For this, the corresponding feeding rates set by two 205U multichannel peristaltic pumps (Watson Marlow, Falmouth, UK) were manually controlled during the operation time. The amount of benzoate and nutrient solution was recorded manually by weighting the solution with an electronic balance. The pH of the catholyte and anolyte was automatically controlled at 7.0 and 3.5, respectively. Both solutions were recirculated at 3 L h^{-1} by Sci-Q 300 series peristaltic pumps (Watson Marlow, Falmouth, UK).

An additional dead-end filtration unit (perpendicular flow) was placed between the cell and the anolyte reservoir to promote *cis,cis*-muconic acid precipitation at the filter surface. For this, the pressure of the fed was increased by a Sci-Q 300 series peristaltic pump (Watson Marlow, Falmouth, UK) and monitored by a pressure gauge. The filtration unit consisted of a 142 mm stainless steel holder (Sartorious AG, Goettingen, Germany) with a 130 mm standard glass fiber pre-filter (Sartorious AG, Goettingen, Germany) and it was changed when a maximum pressure of 1 bar was achieved.

A reference electrode (RE Ag/AgCl) was attached to the electrolytic cell to monitor the potential of the catholyte (*i.e.,* bacterial culture). Prior to connection of the electrolytic cell to the fermenter, an alkaline solution of 0.1 M NaOH was introduced for 30 min to the cathodic chamber and corresponding tubing to inactivate residual microorganisms before operation. Then, the whole volume was replaced and washed several times with sterilized water under a laminar flow cabinet. The cell connection and operation started during a selected time point of the fed-batch and the potential was controlled and monitored via a VSP-300 multichannel potentiostat (Biologic, Claix, France). A maximum current of 333 mA was applied

Once the fermentation was finished, the culture broth was harvested and cooled at 4 °C. The biomass was separated by centrifugation at 10,000 rpm for 30 min with the large volume centrifuge Avanti® JXN-30 (Beckman Coulter, CA, USA). Then, to promote *cis,cis*-muconic acid precipitation, the supernatant was adjusted to a pH of 2.0 with concentrated H_2SO_4. During serial centrifugations and washing steps with on distilled water (pH 2.0), the crystals and precipitates were separated from solution. After a final step of lyophilisation carried out for 24 h, the final product was recovered.

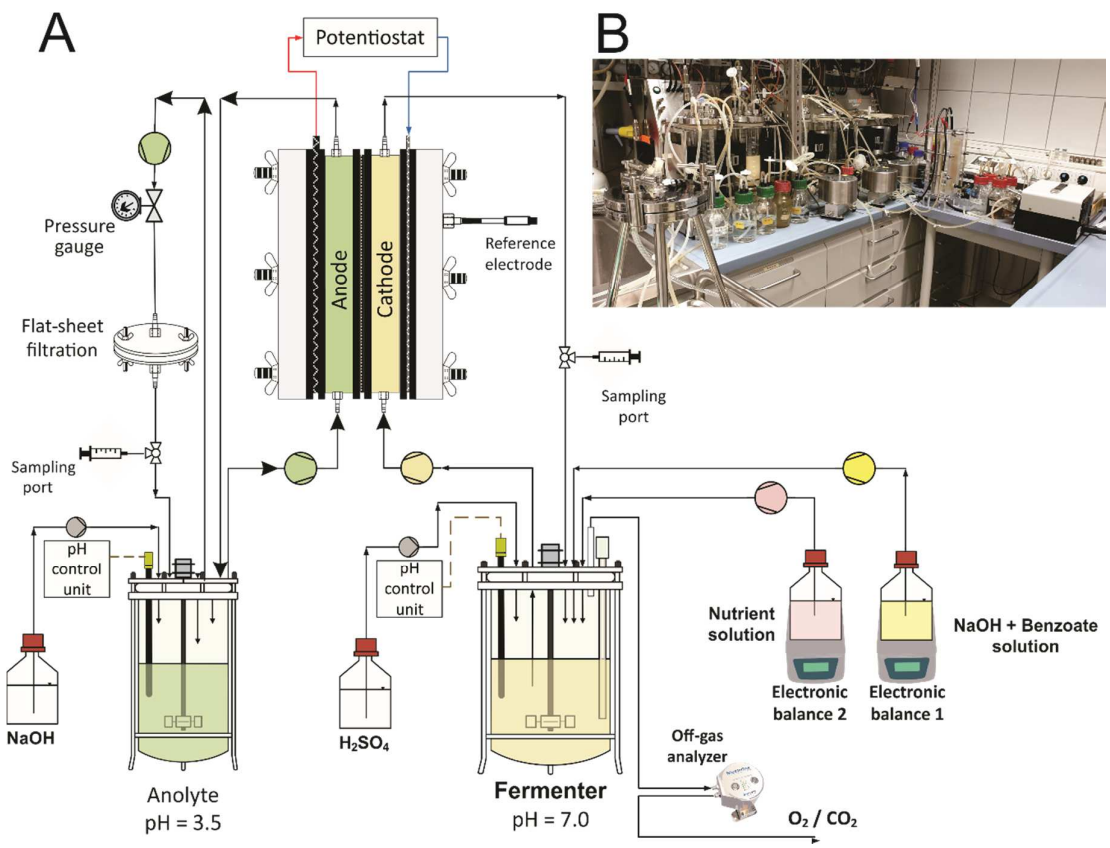

Fig. 2.11 Set-up of an integrated bioprocess for in-line electrolytic extraction of *cis,cis*-muconate (A) and respective photo (B). The culture was operated at 30 °C in a 1-L fermenter under DOT control. The initial working volume was 0.5 L. Bioproduction started during the fed-batch phase imposing exponential feeding rates of nutrient and benzoate solutions, which was supervised manually by electronic balances. The catholyte (bacterial culture) and anolyte were recirculated by peristaltic pumps at 3 L h^{-1} and their pH was controlled at 7.0 and 3.5, respectively. A filtration unit was placed between the anolyte reservoir and the cell to promote *cis,cis*-muconic acid precipitation at the filter surface. A reference electrode (RE Ag/AgCl) was attached to the electrolytic cell to monitor the potential of the catholyte.

2.6 Analytical methods

2.6.1 Bacterial growth determination

Cell growth was monitored using optical density at 600 nm (OD_{600}) with an Ultrospec 10 spectrophotometer (GE Healthcare, Chicago, IL, USA) and online measurements of back scattered light, carried out during the screening assays (details above). In cases where enough sample was available, cell dry weigh (CDW) was determined by a gravimetric procedure. Initially, 7 ml of sample was added into a pre-weighted conical bottom glass tube and centrifuged for 10 min at 3000 g. The cell pellet was washed two times by resuspension in 7 ml PBS buffer and centrifugation (10 min, 3000 g). Then, the sample was dried overnight at 80 °C until a constant weight was attained. The CDW was determined by subtracting the weight of the empty tube and the corresponding weight of the PBS salts contained in 7 ml. Alternatively, the cell pellet was also dried in plastic tubes but via lyophilisation for 24 h. A

correlation factor of CDW [g L^{-1}] = 0.57 × OD_{600} - 0.03 was determined for cultivations of the strain *P. putida* KT2440-CCMA1 on glucose and benzoate as substrates. In the case of wild type *P. putida* KT2440 growing on CFB aromatic mixture (30 mM, C/N 60), the correlation was: CDW [g L^{-1}] = 0.36 × OD_{600} - 0.16.

2.6.2 Mcl-*PHA determination*

Mcl-PHA fluorescence measurements were performed using BODIPY 493/503 (Thermo Fisher, USA), a green fluorescent dye very sensitive, specific and stable for staining PHA lipids with less background staining than Nile Red (Kacmar *et al.*, 2006). The staining procedure was modified from (Karmann *et al.*, 2016). The cells were harvested by centrifugation (12,000 g, 5 min), washed and resuspended in 300 µL of 50% v/v PBS buffer containing 5 mM EDTA to a final OD of 1.5. A stock solution of BODIPY 493/503 dissolved in DMSO was added to reach a final concentration of 0.67 µg ml^{-1} and incubated for 10 minutes in the dark at room temperature. A second step of washing and resuspension was carried out. The fluorescence intensity was measured in two technical replicates of 100 µL (final resuspension) in flat bottom 96 well plates (black) at 30 °C, delay of 0.1 s and gain of 50. Samples were excited at 488 nm and the signal collected at 525 nm using a Synergy™ MX microplate reader (BioTek, 258 Winooski, VT, USA).

A linear correlation between *mcl*-PHA fluorescence intensity and *mcl*-PHA concentration led to construct a standard curve to quantify the final product concentrations and calculate further process parameters. *P. putida KT2440* and *P. putida* F1 were cultured in parallel from the mixed aromatic substrate (CFB at 30mM) at a C/N ratio of 60 with the Hartmans's mineral media previously described. The total *mcl*-PHA produced was extracted from the biomass generated. The polymer isolation procedure was adapted from *Liu et al., 2019*. After centrifugation (12,000 g, 10 min) and lyophilization for 24 h, the dried cells were digested with chloroform (1:15 (w/v)) at 80 °C for 24 h in screw-cap glass tubes (thermoplastic polyester cap with PTFE faced sealing disc). The cell debris was separated by filtration (0.45 µm pore size) from the organic phase, which was concentrated by evaporation. The dissolved *mcl*-PHA was precipitated adding a 10-fold volume of ice-cold methanol twice to improve purity. The polymer was recovered by centrifugation (3,000 g, 30 min and 4 °C), dried and quantified by gravimetric analysis. The linear correlation between total fluorescence intensity and weight-determined *mcl*-PHA concentration for *P. putida KT2440* was: *mcl*-PHA [mg L^{-1}] = 0.0278 × (Fluorescence Intensity) - 24.048. For *P. putida* F1 it was: *mcl*-PHA [mg L^{-1}] = 0.0168 x (Fluorescence Intensity) – 6.663. Alternatively, cell populations accumulating mcl-PHA were identified by flow cytometry, as is described below.

2.6.3 Flow cytometry

All flow cytometry analyses were performed using a BD Influx flow cytometer (BD Biosciences). The *mcl*-PHA staining protocol was adapted from Karmann *et al.*, 2016. Bacterial cells were diluted to approx. 10^4 cells μL^{-1} in 50% v v^{-1} PBS buffer containing 5 mM EDTA. 500

µl of sample was stained with 5 µL of BODIPY 493-503 stock at 20 µg mL^{-1} (incubation for 5 min). Samples were analysed recording the forward scatter (FSC) and fluorescence intensity (λ_{ex} 488 nm - λ_{em} 530 nm). Gates (P1 and P2) were set from previously prepared samples containing *mcl*-PHA accumulating populations. Detailed information can be found in Fig. S2.7.

2.6.4 Microscopy

Fluorescence microscopy images of *P. putida* KT2440 were acquired using an Axio Imager A2 fluorescence microscope (Carl Zeiss Microscopy GmbH, Jena, Germany). The pictures captured were composed by an overlay of 3 images, a differential interference contrast (DIC) image, brightfield and fluorescence image with a corresponding filter set for BODIPY. The samples were diluted in bidest. water to obtain an OD_{600} of 1.5 . Then, the BODIPY 493/503 staining was carried out following the same procedure for *mcl*-PHA fluorescence measurements previously described. After this, 20 µL of cell suspensions was taken and immobilized in 1 % agarose, which was previously solidified and fixed on microscope slides.

2.6.5 Osmolarity

The corresponding osmolarity of the mixed aromatic substrates was determined using a Loeser™ Freezing Point Osmometer (Löser Messtechnik, Germany). Measurements of 0.16, 0.17 and 0.18 Osmol kg^{-1} were found for the substrate mixtures at C/N 80, 60 and 40, respectively. A detailed explanation of the OTR_{cap} calculation in conventional shake flask can be found in the section 2.7.4.

2.6.6 Glucose determination

The glucose concentration from cleared supernatants (*i.e.,* centrifuged at 12,000 g, 10 min and filtered by 0.22 µm) was determined automatically via an immobilized enzyme electrode assay using a 2900 Series Biochemistry Analyzer (YSI inc, Yellow Springs, USA).

2.6.7 Anions and cations determination

After centrifugation and filtration of samples (*i.e.,* centrifuged at 12,000 g, 10 min and filtered by 0.22µm), cations ($NH4^+$, K^+) and anions (PO_4^{3-}, SO_4^{2-}) were quantified using a Metrohm 761 and Metrohm 930 compact ion chromatographs, respectively (both equipped with a conductivity detector). For cation determination, the column used was Metrosep C6-250/4.0 (Metrohm, Switzerland). In the case of anions, the column was Metrosep A Supp 5-150/4.0 (Metrohm, Switzerland).

Alternatively, $NH4^+$ was also determined by steam distillation on a Vapodest 30 steam distillation unit (Gerhardt Analytical Systems, Königswinter, Germany). For low concentrations of $NH4^+$, a method based on the Berthelot reaction (Krom, 1980) was modified to be performed in microtiter plates. After centrifugation and filtration samples (*i.e.,* centrifuged at 12,000 g, 10 min and filtered by 0.22µm), 100 µl of diluted sample (in the range 0 – 10 mg L^{-1}) was combined with 50 µL of sodium citrate dihydrate (160 g L^{-1}),), 50 µL alkaline

dichloroisocyanurate (25 g L^{-1} NaOH + 2 g L^{-1} dichloroisocyanurate), 50 µL sodium nitroprusside dihydrate (1.2 g L^{-1}). After 10 min, the absorbance (at 650nm) of samples and corresponding calibration samples was measured in a Synergy™ MX microplate reader (BioTek, 258 Winooski, VT, USA).

2.6.8 Muconic acid and aromatic compounds determination

Muconic acid and all aromatic compounds were quantified by HPLC analysis in a Beckman System Gold 126 Solvent Module equipped with a System Gold 168 diode array detector (Beckman Coulter, Brea, CA, USA) and a reversed phase column (ISAspher 100–5 C18 BDS, ISERA, Düren, Germany). The method consisted of elution with 0.1% v v^{-1} trifluoroacetic acid (TFA) and 99.95% v v^{-1} methanol at a flow rate of 0.8 mL min^{-1} for 26 min at 40 °C. Both solutions were applied at an initial ratio of 5:95 (methanol:TFA) for the first 2 min. Subsequently, the proportion of methanol was linearly elevated to 25% during 18 min and then kept constant for 4 min, before it was progressively reduced again to 5% in 2 min. Aromatics and muconic acid were quantified with UV detection at a wavelength of 268 nm against standard curves prepared with commercial aromatic monomers. Eventually, pH samples of anolyte solutions containing mixed isomeric forms of muconic acid were diluted in alkaline water (pH 8.0) prior to analysis.

2.7 Calculations

2.7.1 Normalized bacterial growth

The value corresponding to the normalized bacterial growth during the screening step 1 was determined according to:

$$Normalized\ bacterial\ growth\ = \frac{\left(I_f - I_0\right)_i}{\left(I_f - I_0\right)_{max}} \quad (1)$$

where I_o and I_f stand for the initial and final (39 hours) average scattered light values. The fraction gives normalized data (≤ 1.0) for every experimental condition (*i*) respect to the maximum growth level (*max*) for both aromatic concentrations (5 and 20 mM), which enable a rescaling of data to facilitate comparison.

2.7.2 Modified Gompertz model

Meaningful growth parameters were obtained fitting a modified version of the re-parameterized Gompertz sigmoidal function (Zwietering *et al.*, 1990) to the experimental data (backscatter values) when the growth profile showed a typical monophasic shape:

$$\mathrm{y(t)} = \mathrm{A}\,\exp\left\{-\exp\left[\frac{\mu_{\max}\ \cdot\ \mathrm{e}}{\mathrm{A}}\,(\lambda - \mathrm{t}) + 1\right]\right\} \quad (2)$$

where *y(t)* is the dependent variable transformed into logarithm of the relative population size (*ln (N(t)/N₀)*, where N_0 is population size at $t = 0$), *A* represents the maximal growth value reached, μ_{max} the maximum specific growth rate [h^{-1}] at curve inflection and λ the lag time [h]. These parameters were estimated using the non-linear regression approach via the Solver ToolPak of MSExcel 2013 assuming the changes of population size *N(t)* as changes in the scattered light intensity *I(t)*. For every experimental unit, the data was manually treated to guarantee reliable parameter estimation excluding values corresponding to morphological changes associated with carbon depletion during late stationary phase (flocculation or biofilm formation), as shown in the Appendix (Fig. S2.6).

Eq. (2) was further adapted to describe a diauxic growth profile, containing two sequential sigmoid curves, similarly as it has been reported for other growth models (Tyrovouzis *et al.*, 2014).

$$y(t) = A_1 \exp\left\{-\exp\left[\frac{\mu_{(1)\max} \cdot e}{A_1}(\lambda_1 - t) + 1\right]\right\} + A_2 \exp\left\{-\exp\left[\frac{\mu_{(2)\max} \cdot e}{A_2}(\lambda_2 - t) + 1\right]\right\} \quad (3)$$

This new function was fitted to the experimental data when a biphasic profile was identified. Index 1 in Eq. (3) refers to the first sigmoid, while index 2 refers to the second. λ_1 and λ_2 account for the adaptation time from the start of the culture for both sigmoidal functions (Fig. S2.6). For monophasic profiles, only the first sigmoid was fitted to experimental data, Eq. (2).

2.7.3 OTR_{cap} estimation in flower-like shaped microplate wells

To calculate the OTR_{cap} [mmol O_2 L^{-1} h^{-1}] in microplate wells with a flower shape geometry, the empirical correlation found by *Lattermann et al., 2014* was used:

$$OTR_{cap} = 2.5 \cdot 10^{-7} \cdot Peri^{6.0} \cdot n^{2.37} \cdot V_L^{-0.64} + 3.3 \cdot 10^{-4} \quad (4)$$

where *Peri* corresponds to the relative perimeter of the well geometry (1.12 for 6-edged flower), *n* the shaking frequency [rpm] and V_L the filling volume [µl]. Eq. (4) was obtained in experiments carried out using the BioLector technique where the shaking diameter is 3 mm (*Lattermann et al., 2014*).

2.7.4 OTR_{cap} estimation in conventional shake flask

The OTR_{cap} [mmol O_2 L^{-1} h^{-1}] calculation in non-baffled shake flasks for an exhaustive range of shaking conditions has been developed and validated experimentally by *Meier et al., 2016* :

$$OTR_{cap} = 3.72 \cdot 10^{-7} \cdot Osmol^{0.05} \cdot n^{\left(1.18 - \frac{Osmol}{10.1}\right)} \cdot V_L^{-0.74} \cdot d_0^{0.33} \cdot d^{1.88} \cdot p_{abs} \cdot y_{O_2}^{*} \quad (5)$$

where *Osmol* stands for the Osmolarity [Osmol kg^{-1}], *n* the shaking frequency [rpm], V_L the filling volume, d_0 the orbital throw [cm], *d* the shake flask diameter [mm], p_{abs} the ambient pressure[bar], and y_{O2}* the gas phase oxygen concentration.

2.7.5 OTR and CTR calculations in stirred tank bioreactor

From the off-gas composition analysis in the bioreactors, the consumption of O_2 and formation of CO_2 were calculated via OTR [mmol O_2 L^{-1} h^{-1}] and carbon dioxide transfer rate CTR [mmol CO_2 L^{-1} h^{-1}], respectively (Peña-Ortiz *et al.*, 2020):

$$OTR = \frac{\dot{V}_G}{V_L \cdot V_{norm}} \left(y_{O_{2,in}} - \frac{1 - y_{O_{2,in}} - y_{CO_{2,in}}}{1 - y_{O_{2,out}} - y_{CO_{2,out}}} \cdot \ y_{O_{2,out}} \right) \quad (6)$$

$$CTR = \frac{\dot{V}_G}{V_L \cdot V_{norm}} \left(y_{CO_{2,out}} - \frac{1 - y_{O_{2,in}} - y_{CO_{2,in}}}{1 - y_{O_{2,out}} - y_{CO_{2,out}}} \cdot \ y_{CO_{2,out}} \right) \quad (7)$$

where $\dot{V}_G$ is the gas flow rate [L h^{-1}], V_L the filling volume of the reactor [L], V_{norm}, the molar volume of an ideal gas [mol L^{-1}], $y_{O2,in}$ the molar fraction of oxygen in the gas inlet, $y_{O2,out}$ the molar fraction of oxygen in the off gas, $y_{CO2,in}$ the molar fraction of carbon dioxide in the gas inlet and $y_{CO2,out}$ the molar fraction of carbon dioxide in the off gas.

Finally, the ratio of CTR and OTR defines the respiratory quotient (RQ):

$$RQ = \frac{CTR}{OTR} \quad (8)$$

2.7.6 Flux of charged molecules in the electrochemical cell

The flux (*J* [kg m^{-2} d^{-1}]) of a charged element (*i*) in the electrochemical cell was estimated as:

$$J_i = \frac{V}{A} \left(\frac{\Delta C_i}{\Delta t} \right) \times 1000 \quad (9)$$

where *V* is the volume of catholyte [L] and ΔC is the change of element concentration [M], *A* is the effective area of ion exchange membrane [m^{-2}] and Δt the time of process [d].

2.7.7 Coulombic efficiency in the electrolytic cell

The Coulombic or faradic efficiency (*CE* [%]) describes the proportion between the Coulombs invested in the movement of charged elements ($Q_{experimental}$) and the Coulombs supplied by the charge applied in the cell ($Q_{applied}$):

$$CE \ = \left(\frac{Q_{experimental}}{Q_{applied}} \right) \times 100 \quad (10)$$

From the Faraday's law of electrolysis, it is known that the mass of elements (*n*) transported is directly proportional to their charge ($Q_{experimental}$) :

$$CE = \frac{z \cdot F \cdot n}{Q_{applied}} \times 100 \quad (11)$$

where *z* is the valence of the element and *F* the Faraday constant (96,485 C mol^{-1}). Then, if the current applied (*I* [A]) is constant during the time of the process *Δt* [s] and *n* is related to the volume of catholyte *V* [L] and the change of element concentration *ΔC* [M]:

$$CE = \frac{z \cdot F \cdot V}{I} \left(\frac{\Delta C_i}{\Delta t}\right) \times 100 \quad (12)$$

2.7.8 Feeding rate of nutrient solution during fed-batch bioprocess

An exponential feeding (*F*) rate of the nutrient solution, [mL h^{-1}] was determined according to Kohlstedt *et al.*, 2018:

$$F = \left(\frac{\mu_{set}}{Y_{x/s}} + m_s \cdot e^{0.02(t-t_0)}\right) \cdot \frac{V_L \cdot X_0 \cdot e^{\mu_{set} \cdot (t-t_0)}}{S_0} \quad (13)$$

where μ_{set} is the specific growth rate (set at 0.04 h^{-1}), $Y_{x/s}$ the biomass yield of *P. putida* grown on glucose (0.4 g g^{-1}), m_s the maintenance coefficient (0.037 g g^{-1} h^{-1}), V_L the current working volume [ml], X_0 the cell dry weight at the beginning of fed-batch stage [g CDW L^{-1}] and S_0 the glucose concentration in the nutrient solution (600 g L^{-1}).

Chapter 3: Lignin-aromatics valorization by wild type *Pseudomonas*: aromatic funneling and *mcl*-polyhydroxyalkanoate accumulation

Partially published as:

Ramírez-Morales J. E., Czichowski P., Besirlioglu V., Regestein L., Rabaey K., Blank L. M., Rosenbaum M. Lignin aromatics to PHA polymers: nitrogen and oxygen are the key factors for *Pseudomonas*. 2021. *ACS Sustainable Chemistry & Engineering*, 9, 31, 10579–10590. https://doi.org/10.1021/acssuschemeng.1c02682

Contributions:

Phillip Czichowski performed some strain screenings and oxygen limited cultivations. Volkan Besirlioglu assisted on flow cytometry analysis. Juan E. Ramírez performed most of the experiments and together with Lars Regestein, Korneel Rabaey, Lars Blank and Miriam Rosenbaum designed the experiments and analyzed the result

3.1 Abstract

Many wild type *Pseudomonas* have the potential to contribute to the valorization of lignin in future biorefineries. Through a robust aromatic catabolism, *i.e.*, biofunneling capacity, they can ease the inherent aromatic heterogeneity found in lignin hydrolysates and accumulate naturally marketable biopolymer like *mcl*-polyhydroxyalkanoate (*mcl*-PHA) under nitrogen limitation. However, most of the strain screenings campaigns on lignin aromatic valorization have incorporated only particular *Pseudomonas* strains to compare them into a wider set of microbial species. This study present fundamental research to select the best *Pseudomonas* accumulating *mcl*-PHA from different lignin-derived aromatic monomers as single and mixed carbon sources when implementing sequential strain screening steps. After parallel cultivations in microtiter plates, essential differences between seven wild type *Pseudomonas* were found on lignin aromatic utilization. Unexpectedly, growth on sinapic acid by *P. putida* F1 and changes in scattered light values of *P. putida* S12 on tough molecules for biodegradation like syringol and 4-methylguiaiacol were found at low concentrations (5 mM). Additionally, the growth kinetics was characterized though meaningful parameters (*i.e.,* specific growth rates μ_{max} and lag times λ), identifying diauxic shifts in all *P. putida* when growing on a selected aromatic mixture of p-coumarate, ferulate and benzoate (CFB 30mM) under nitrogen limitation. Experiences at higher scale with the same mixture and in shake flask cultivations yielded a maximum *mcl*-PHA concentration of 497 ± 39 and 79.8 ± 7.1 mg L^{-1} at a C/N ratio of 80 for *P. putida* KT2240 and *P. putida* F1, respectively. Overall, this comparative evaluation led to select *P. putida* KT2240 as the most robust and best performing strain to valorize lignin aromatics into *mcl*-PHA under stressful environments. Furthermore, oxygen supply was identified as an important process parameter. Future work may focus on identifying the optimal balance between oxygen, nitrogen and aromatics to establish an efficient biocatalytic conversion through bioprocess development with this strain.

3.2 Introduction

Lignin, the most abundant aromatic polymer on the planet, promises to positively impact in the development of the future biorefining processes. This renewable source of bio-aromatics constitutes around 15-30 wt.% of lignocellulosic biomass and is generated in high volumes during the cellulose extraction in traditional lignocellulosic biorefineries, like the paper industry (Den *et al.*, 2018).

Despite being considered as a treasure from a chemical point of view, during the extraction process most of the lignin fraction suffers irreversible structural modifications, which makes it very recalcitrant and it is therefore mainly burned to obtain heat, power or applied as material in different sectors (Kim and Kim, 2018; Yu and Kim, 2020). However, in recent years chemical processes have advanced on fractionation and depolymerization to prevent structural lignin degradation (*i.e.*, to avoid formation of carbon–carbon bonds), preserve reactive ether bond structures enhancing functionality, and increase monomer yields (Rinaldi *et al.*, 2016; Renders *et al.*, 2017; Sun *et al.*, 2018; Zhang and Wang, 2020). Moreover, biochemical efforts on ligninolytic enzymes found in fungi and bacteria also promise to minimize energy demand and hazardous waste generation (Salvachúa *et al.*, 2016; Hämäläinen *et al.*, 2018; Liu *et al.*, 2019; Weiss *et al.*, 2020). Nevertheless, both approaches still generate complex lignin-derived aromatic mixtures and only few of the depolymerized products obtained can be directly considered as marketable chemicals without an additional down-stream transformation (Schutyser *et al.*, 2018).

To overcome both limitations, the concepts of chemocatalytic (Rinaldi *et al.*, 2016) and biological funneling (Linger *et al.*, 2014) have been introduced, encouraging the last upgrading stages towards generation of a full value chain from lignin. The concept of bio-catalytic funnelling is based on the ability of some bacterial species using catabolic upper-pathways to converge a plethora of lignin-derived aromatics into few central intermediates like catechol and protocatechuate, which are eventually cleaved and metabolized via the β-ketoadipate pathway to access the central carbon metabolism (Linger *et al.*, 2014). Versatile and tolerant bacterial strains from genera like *Pseudomonas, Sphingobium*, *Rhodococcus* and *Amycolatopsis* have evolved in synergy with other organisms like fungi in soils or forest environments where lignin depolymerisation and aromatic degradation naturally take place (Kamimura *et al.*, 2017; Lopez-Mondejar *et al.*, 2019). Furthermore, when establishing suitable microbial factories, additional bacterial properties related to a proper domestication like metabolic robustness, genetic accessibility, fast growth, and high productivities need to be also covered. Several of such characteristics have been identified in wild type *Pseudomonas* (Silby *et al.*, 2011; Zhou *et al.*, 2020). Especially, *Pseudomonas putida* stands out for its ability to adapt and tolerate stressful environmental conditions (Belda *et al.*, 2016; Nikel and de Lorenzo, 2018; Weimer *et al.*, 2020).

The number of research studies on isolates of wild type *Pseudomonas* able to degrade lignin-derived aromatics have been extensively reported in databases like eLignin (Brink *et al.*, 2019). A successful case for uptake of lignin-derived substrates and production of native or engineered value products is *Pseudomonas putida*, which has been renowned in the field of lignin biotechnology (Kohlstedt *et al.*, 2018; Salvachúa *et al.*, 2018; Becker and Wittmann, 2019; Johnson *et al.*, 2019). One of the native products of this bacterium are medium chain length polyhydroxyalkanoates (*mcl*-PHAs), which consist of biopolymers with multiple applications in the material and biomedicine sector (Prieto *et al.*, 2016). However, many other *Pseudomonas* strains can also accumulate this product from conventional substrates like sugars, carbohydrates, glycerol, acetate and fatty acids (Madison and Huisman, 1999; Mozejko-Ciesielska *et al.*, 2019). Except when the carbon source is a structurally related substrate (*i.e.,* medium chain length fatty acids), the accumulation of *mcl*-PHA takes place mainly under unbalanced growth conditions like nitrogen limitation (Prieto *et al.*, 2016). Several reports have shown *mcl*-PHA accumulation from lignin-derived streams (Linger *et al.*, 2014; Jayakody *et al.*, 2018; Liu *et al.*, 2019; Salvachua *et al.*, 2020) or single aromatics (Wang *et al.*, 2018; Xu *et al.*, 2019b; Borrero-de Acuña *et al.*, 2020; Zhou *et al.*, 2020; Xu *et al.*, 2021).

While some studies have incorporated some particular *Pseudomonas* strains into microbial screenings involving other non-related microorganisms for utilization of lignin derivates (Tomizawa *et al.*, 2014; Salvachúa *et al.*, 2016; Rodriguez *et al.*, 2017), evaluation of the *mcl*-PHA accumulation with a representative amount of strains in this genus has not been yet performed. Furthermore, being aware of the important advances achieved in bioprocess development for *mcl*-PHA production with several *Pseudomonas* using conventional substrates in the past years (Kim, 2002; Sun *et al.*, 2006; Poblete-Castro *et al.*, 2014a; Poblete-Castro *et al.*, 2014b; Mozejko-Ciesielska *et al.*, 2019), further microbial performance comparisons are necessary to select the suitable hosts with whom to achieve similar progress from lignin aromatics.

Therefore this chapter presents an experimental approach to select, compare and evaluate a group of *Pseudomonas* strains to accumulate *mcl*-PHA from different lignin-derived aromatic monomers as sole or mixed carbon sources. A 3-step sequential screening was implemented to evaluate the growth performance of seven wild type *Pseudomonas* on 15 lignin model compounds at two concentrations (5 and 20 mM). Additionally, different scenarios of nitrogen and oxygen availability were evaluated in shake flasks and oxygen limited cultivations to expose the changes in funneling capacity of selected strains when accumulating *mcl*-PHA from a mixture composed of representative lignin aromatics. From these experiences the selection of a robust and tolerant strain to hostile environmental conditions was possible.

3.3 Results and discussion

To find strains with a suitable catabolic activity on lignin-derived aromatics and an eventually ability to convert them into valuable products, rational procedures need to be implemented. Through several screening steps and strain comparison experiments, the next sections describe the selection of a robust strain able to convert an aromatic mixture into *mcl*-PHA.

3.3.1 Strain screenings reveal the different lignin valorization potentials of wild type Pseudomonas

A 3-step sequential strain screening was implemented to select suitable *Pseudomonas* strains by evaluating their degradation and conversion capacity on 15 lignin-model compounds (Fig 2.4). This group, included renowned strains in the field of lignin valorisation like *P. putida* KT2440 (Linger *et al.*, 2014), strains with solvent tolerant characteristics (*i.e., P. putida* S12 (Hartmans *et al.*, 1989) and *P. taiwanensis* VLB120 (Park *et al.*, 2007)), aromatic catabolic features (*i.e., P. putida* F1 (Hughes *et al.*, 2017)) and strains that are well known for their capacity to degrade polycyclic aromatic hydrocarbons PAHs (*i.e., P. aeruginosa* (Sangkharak *et al.*, 2020) and *P. fluorescens* (Whitman *et al.*, 1998)). A general summary of the main characteristics of these wild type strains can be found in Table 2.1.

The selection of the aromatic compounds was based on their prevalence in lignin depolymerisation extracts or identified as common intermediates found in aromatic upper pathways (Xu *et al.*, 2019a). Particularly, molecules like vanillyl alcohol (Behling *et al.*, 2016), acetovanillone (Das *et al.*, 2017) and 4-methylguaiacol (Kim *et al.*, 2018) have been found after catalytic oxidation and depolymerization processes, which also represent a challenge for biodegradation.

The first screening step evaluated the growth performance of the 7 wild type *Pseudomonas* on 15 lignin model compounds at two concentrations (5 and 20mM) under the same environmental conditions. The results are shown as a heat map representation of the normalized bacterial growth reached after 39 hours (Fig. 3.1A). The normalization enabled quantitative, visual comparison of growth phenotypes. It gives values between 0 and 1, in reference to the maximum scatter intensity values reached at 5 and 20 mM (183 and 578, respectively) which corresponds to *P. putida* KT2440 grown on benzoic acid and *P. aeruginosa* PAO1 grown on glucose, respectively.

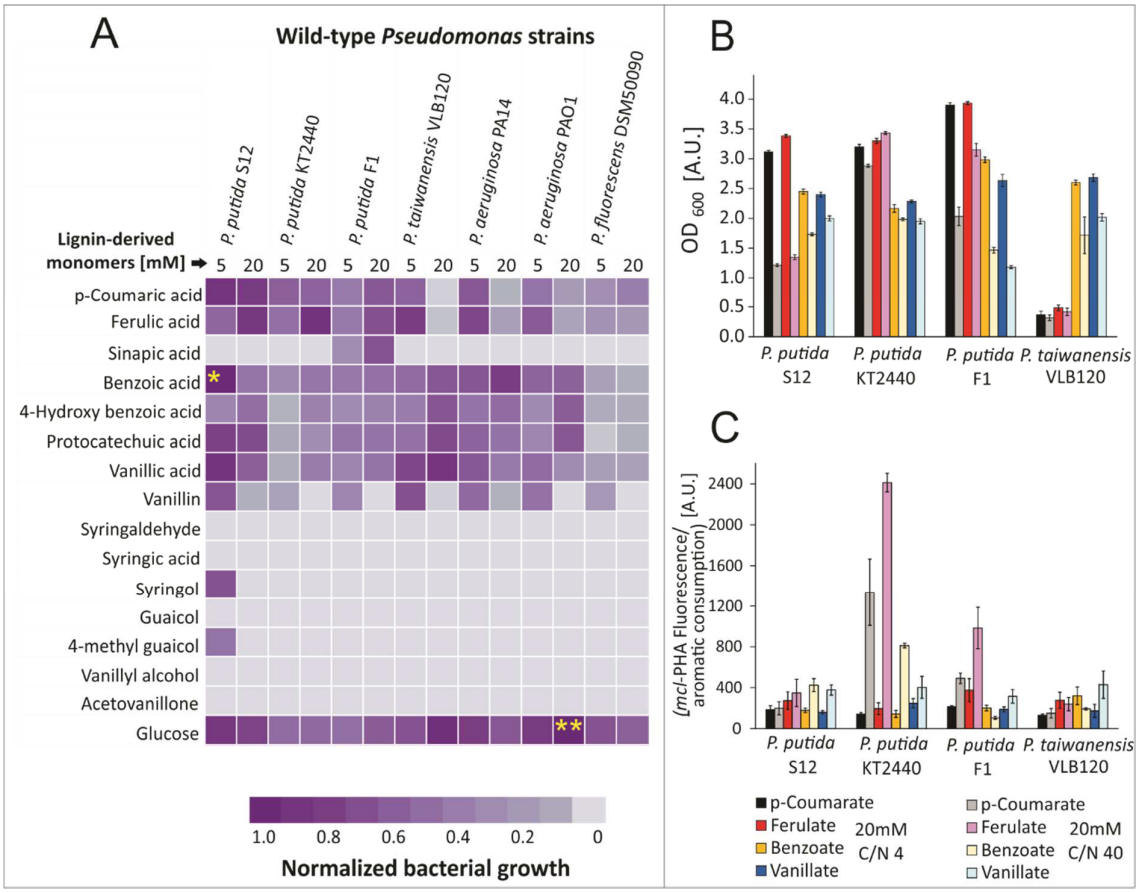

Fig. 3.1 Screening step 1 (A) and 2 (B), (C). The first is represented as a heat map of the growth performance of 7 wild type *Pseudomonas* strains on 15 lignin-derived monomers at two concentrations (5 and 20mM) (A). Glucose was used as reference carbon source and served as positive control. The strains were cultivated in microbioreactors (BioLector®) using 96-well plates under nitrogen excess (C/N = 4) in Hartman's mineral salt medium for 39 h. Normalized bacterial growth data (≤ 1.0) was calculated for every experimental condition (Eq. (1), section 2.7.1) in respect to the maximum scatter intensity value indicated as yellow asterisks for both aromatic concentrations (* for 5 mM: maximum scatter intensity = 183 and ** for 20 mM: maximum scatter intensity = 578). Experiments were performed in triplicates. The second screening stage states the valorisation potential of the best 4 performing strains and 4 selected aromatics at 20 mM aromatics from the output of screening step 1 (B-C). The strains were tested at two carbon to nitrogen ratios (C/N = 4 and 40) during cultivation in 48-well flower plates for 48 h. The final optical density (OD_{600}) was determined immediately after 48 h. (B) and the normalized mcl-PHA fluorescence intensity respect to the aromatic consumption (C) complemented the study. Error bars indicate the deviation from the mean (n = 2).

About half of the tested lignin-derived monomers were utilized for growth under the studied conditions. The other half, poorly or not utilized, corresponds to phenols with aldehyde, ketone and methoxy groups that are known to compromise the integrity of cell membranes (Machovina *et al.*, 2019). These groups have an increased inhibitory action compared to well-utilized phenolic acids. Recent efforts are trying to defeat this limitation by protein engineering of new promiscuous P450 aryl-O-demethylases and their heterologous expression in *Pseudomonas putida* (Tumen-Velasquez *et al.*, 2018; Machovina *et al.*, 2019).

Unexpectedly, *P. putida* F1 was able to grow on sinapic acid, which to our knowledge has not yet been reported. Additionally, *P. putida* S12, which was one of the best performing strains overall, and *P. taiwanensis* showed changes in scattered light values for challenging molecules like syringol and 4-methylguiaiacol at low concentrations (5 mM). However, a reliable cell growth was not possible for this strain on these molecules. Sinapic and syringic acid, together with syringaldehyde are syringyl related units of hardwood lignin. They are considered challenging molecules because of the two methoxy groups found in the aromatic rings (Xu *et al.*, 2019a). *P. putida* F1 is known for growing on several aromatic hydrocarbons, including benzene, toluene, ethylbenzene, xylene (BTEX) and *p* -cymene, possess a broad substrate toluene dioxygenase and has the ability to sense hydroxycinnamic acids like p-coumaric, caffeic and ferulic acid (Hughes *et al.*, 2017). Thus, considering that sinapic acid is also part of this shared structural group of phenolic acids and the potential applications from S-lignin valorization, additional studies should explore this interesting finding. Furthermore, they could also evidence a promising catabolic capacity of *P. putida* S12 on syringol and 4-methyl guiaiacol, which are extremely toxic lignin-related molecules. Interestingly, *P. putida* S12 is known to perform under highly toxic compounds like styrene (Kuepper *et al.*, 2015).

P. putida S12 and *P. taiwanensis* VLB120 also presented the highest growth values for other challenging molecules like vanillin at 5 mM. This compound has an aldehyde, hydroxyl, and ether functional group, which cause toxicity for most microorganisms even at low concentrations. Even *P. putida* KT2440 experiences long lag phases due to the necessary bioconversion of vanillin to vanillic acid by vanillin dehydrogenase (*Vdh)* (see Chapter 1, Fig. 1.5)*,* before it starts growing (Ravi *et al.*, 2017). At the high concentration of this molecule (20 mM), the toxic level was exceeded and none of the strains grew, which is in accordance with a recent study where the specific growth rate and lag phase of *P. taiwanensis* VLB120 were affected when vanillin was higher than 2 g/L (approx. 13 mM) (Wordofa and Kristensen, 2018). *P. taiwanensis* VLB120 grew well on vanillic acid and 4-hydroxy benzoic acid at 20 mM, but it did not yield growth with p-coumaric and ferulic acid at this concentration, in contrast to the *P. putida* strains, which grew remarkably well. Intermediate performance values were obtained for *P. putida* KT2440. However, final growth values could have been underestimated. It is known for this strain that optical density readings decrease due to morphological changes taking place after carbon depletion (Ravi *et al.*, 2017). Lastly, both strains of *P. aeruginosa* grew similarly and performed better than *P. fluorescens*, but less than the other strains.

Overall the best average normalized growth on lignin monomers at 20 mM were achieved with *P. putida* S12, *P. putida* F1, *P. putida* KT2440 and *P. taiwanensis* VLB120 and thus, these four strains were selected for the next step to evaluate their valorization potential into *mcl*-PHAs. This biopolymer is an intrinsic storage compound found in many *Pseudomonas* strains, which is produced under nutrient limitation and is, thus, a straight forward goal for valorization. To induce *mcl*-PHA formation, two carbon to nitrogen ratios (nitrogen excess C/N = 4 and nitrogen limited C/N = 40) were tested in 48-well flower plates providing suitable

oxygen transfer conditions and a higher working volume for additional analysis. The aromatics p-coumaric, ferulic, benzoic and vanillic acid at 20 mM, each, were selected from the first step as single substrates to proceed.

Regarding screening step 2, performance data to characterize the valorisation potential like the final growth (OD_{600}) and the aromatics utilized for *mcl*-PHA accumulation (*i.e.,* mcl-PHA fluorescence per aromatics consumed) are shown in Fig 3.1B-C. Further growth parameters like the maximum specific growth rates (μ_{max}) and lag times (λ) were obtained fitting the modified version of the Gompertz model (section 2.7.2, Eq. (2)). Depending if the growth profile showed one or two sigmoids, which can appear under nitrogen limitation, an additional model was fitted to the experimental data (section 2.7.2, Eq. (3)). For this, the scatter values were selected manually to exclude data corresponding to morphological changes like biofilm or floc formation. Then, the new function was fitted to the selected values obtaining kinetic parameters to the first (*i.e.,* $\mu_{(1)max}$, $\lambda_{(1)}$) and/or second sigmoid (*i.e.,* $\mu_{(2)max}$, $\lambda_{(2)}$) (see Appendix Fig S2.6). The complete data comparison of growth kinetic parameters and the final aromatic consumption for all conditions and strains evaluated can be found in Fig 3.2.

Each strain behaved differently regarding the different substrates under nitrogen excess conditions (C/N of 4). Biomass formation was highest for p-coumarate and ferulate in all *P. putida* strains, implying a high biomass yield from these compounds (Fig. 3.1A). The highest μ_{max} were obtained in *P. putida* S12 (0.54 ± 0.01 h^{-1}) and *P. putida* F1 (0.56 ± 0.02 h^{-1}) growing on benzoate and p-coumarate, respectively (Fig. 3.2A). Strain F1 also presented a high $\mu_{(1)max}$ growing on benzoate (0.50 ± 0.01 h^{-1}). *P. taiwanensis* VLB120 confirmed that was not able to grow on p-coumarate and ferulate at 20 mM (compare Fig. 3.1A and B). *P. putida* KT2440 presented intermediate $\mu_{(1)max}$ values between 0.33 ± 0.05 h^{-1} (vanillate) and 0.49 ± 0.01 h^{-1} (ferulate), which were higher than the values obtained by Ravi *et al.*, 2017, although they performed the cultivations at 5 mM in shake flask. The highest lag times were obtained for all strains on vanillate (Fig. 3.2C).

Alternatively, accumulation of *mcl*-PHA was promoted by reducing the initial amount of nitrogen source 10-fold (C/N = 40). The optical density of the bacterial strains was affected under this nitrogen limited condition, although less for *P. putida* KT2440 (Fig. 3.1B). The growth rate most affected was $\mu_{(1)max}$ for *P. putida* F1, with decreases of 30-80 % in respect to the nitrogen excess condition (Fig. 3.2A). Additionally, most of the strains presented a diauxic growth profile, which was reflected in the presence of a second growth rate ($\mu_{(2)max}$) and lag time (Fig. 3.2B and D). Strains like *P. putida* S12 and *P. putida* F1 showed big differences between both growth rates, while *P. putida* KT2440 only slightly changed the growth rate during the second sigmoidal growth on benzoate (for growth profile details see also Fig. S2.6B).

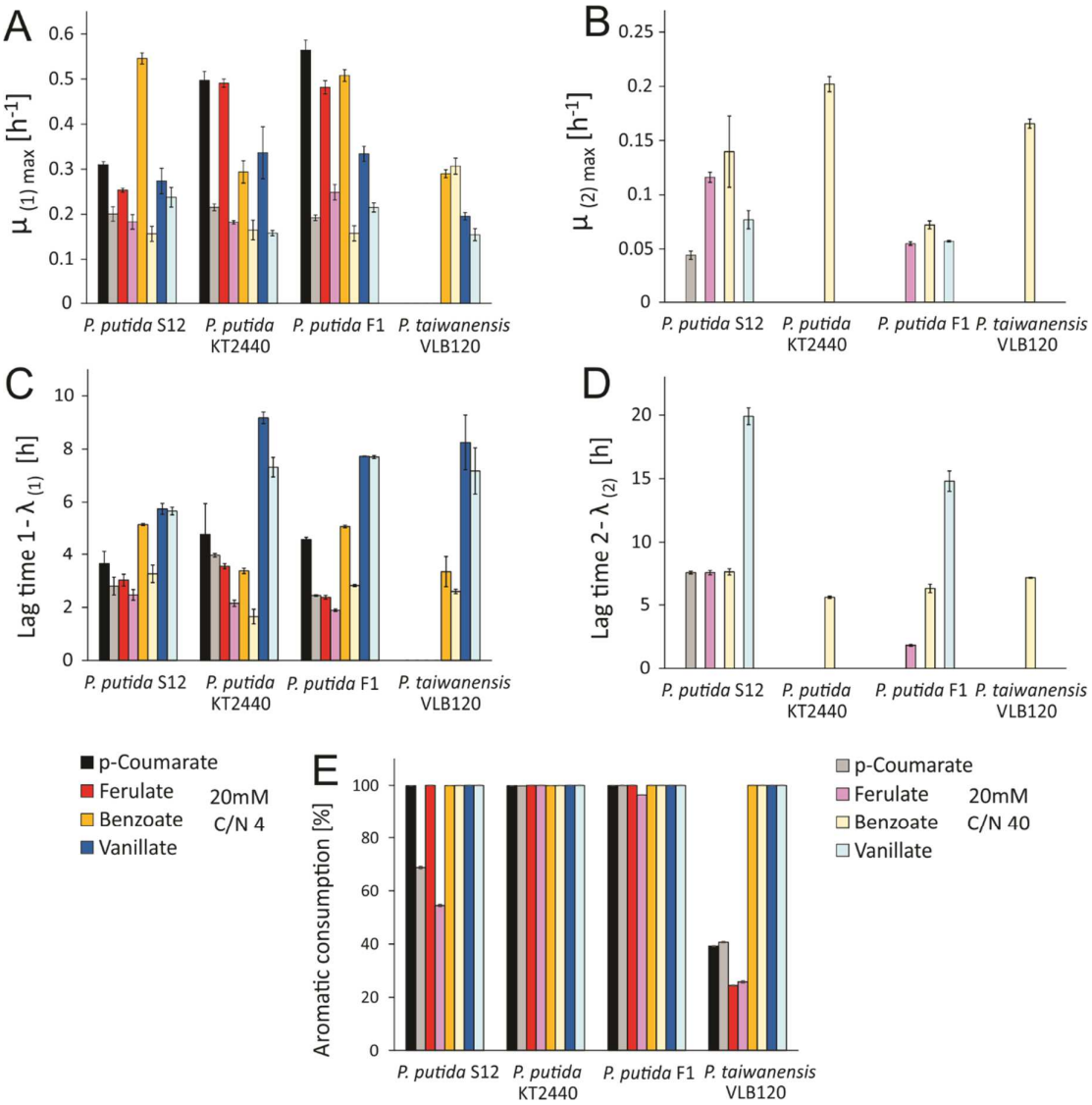

Fig. 3.2 Additional data from screening step 2. The maximum specific growth rates found in strains with one ($\mu_{(1)\,max}$) (A) and/or a second sigmoidal growth profile ($\mu_{(2)\,max}$) under nitrogen limitation C/N of 40 (B). These parameters and the lag times of strains showing a monophasic $\lambda_{(1)}$ [h] (C) and biphasic growth $\lambda_{(2)}$ [h] (D) were calculated from Eq. (2) or Eq. (3) and explained in Fig. S2.6B. The total aromatic consumption was estimated after 48 h (E). Error bars indicate deviation from the mean (n = 2).

Interestingly, *P. putida* KT2440 showed the highest valorization potential, described as the normalized *mcl*-PHA fluorescence in respect to the aromatic consumption (Fig. 3.1C). This was reflected especially for ferulate. All aromatics were completely consumed by this strain (Fig. 3.2E). The reduction of the nitrogen supply also had a positive effect on *P. putida* F1 *mcl*-PHA production, but almost no effect on *P. putida* S12. The same *P. putida* strains as in this study have been previously compared for *mcl*-PHA accumulation from crude glycerol, where *P. putida KT2440* was also the best producer (Poblete-Castro *et al.*, 2014a). *P. taiwanensis* VLB120 showed low *mcl*-PHA production capacity on the aromatics, which it could utilize.

From these results, the comparison of diverse *Pseudomonas* strains under identical conditions confirmed a high performance for aromatics degradation, especially for all three *P. putida* strains. Of them, the strain with the highest potential for lignin valorization under nitrogen limitations was *P. putida* KT2440. Therefore, only the three *P. putida* strains were included in step 3 to evaluate their aromatic funneling capacity from a defined aromatic mixture.

For the screening step 3, a mixture of p-coumarate, ferulate and benzoate further called CFB (each component at 10 mM) was selected as substrate in all *P. putida* strains with the nitrogen source even lower, corresponding to faster nutrient limitation (C/N = 80) (Fig. 3.3). As a control, the strains were also cultivated on the individual aromatics at the sum CFB aromatics concentration of 30 mM, each. The three components of the mixture were selected based on the growth performance and *mcl*-PHA accumulation, but also because they are representative lignin-derived monomers of three important upper pathways during aromatic catabolism; the coniferyl and p-coumaryl branch of the protocatechuate node and the benzoate funnelling pathway of the catechol node (see Chapter 1, Fig. 1.5).

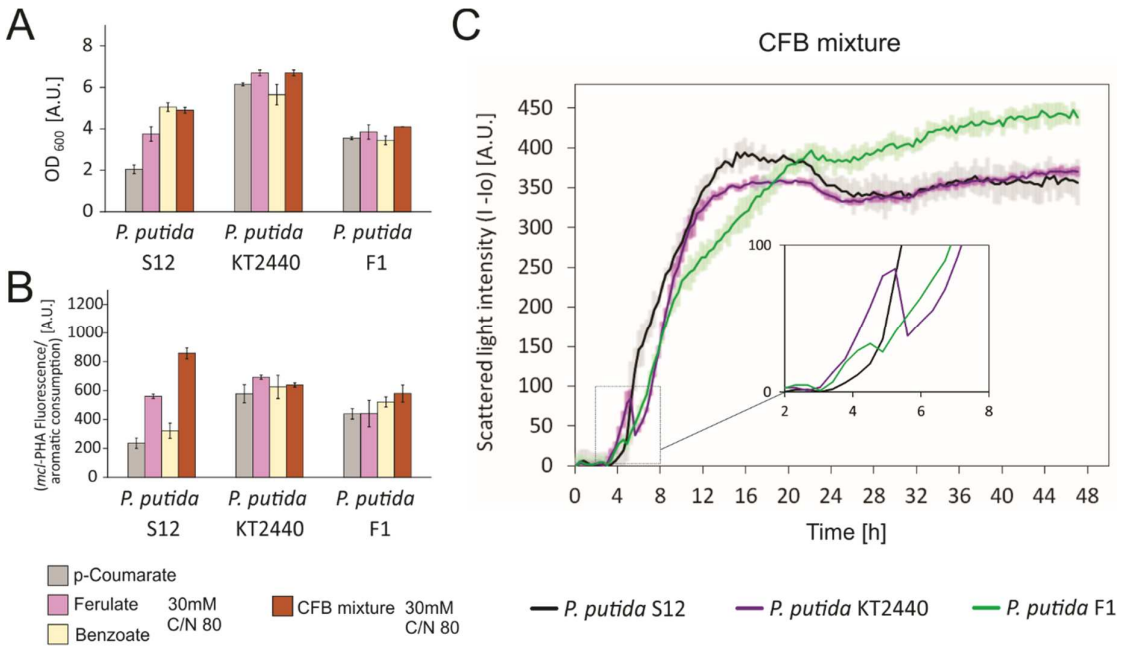

Fig. 3.3 Screening step 3. Aromatic mixture evaluation with the three most suitable strains from step 2, using a stronger nitrogen limitation (C/N = 80) and aromatic compounds as sole carbon sources or mixed (CFB), both at 30 mM in Hartman's mineral salt medium. The final optical density (OD_{600}) (A) and normalized *mcl*-PHA fluorescence intensity respect to the aromatic consumption (B) were measured using 48-well flower plates for 48h. For this step all the strains presented a diauxic shift, which is graphically detailed for the defined model mixture (C). Error bars indicate deviation from the mean (n = 2).

Compared to the growth obtained at 20 mM and C/N = 40 (Fig. 3.1B), the final OD_{600} values increased with more carbon source available, especially for *P. putida* KT2440 (approx. 2-fold) (Fig. 3.3A). The normalized *mcl*-PHA fluorescence did not change in respect to the previous

experiment with the single aromatic substrates (compare Fig. 3.3B vs. Fig. 3.1B). However, the intensity decreased in *P. putida* KT2440 for ferulate and p-coumarate, which could indicate a possible optimum condition around a C/N of 40 for these single aromatics.

All three *P. putida* strains presented a diauxic shift around 5 hours, which can be related to the nitrogen depletion due to the stronger limitation (C/N = 80) (zoom in Fig. 3.3C). The corresponding growth parameters obtained after model fitting can be found in Fig. 3.4.

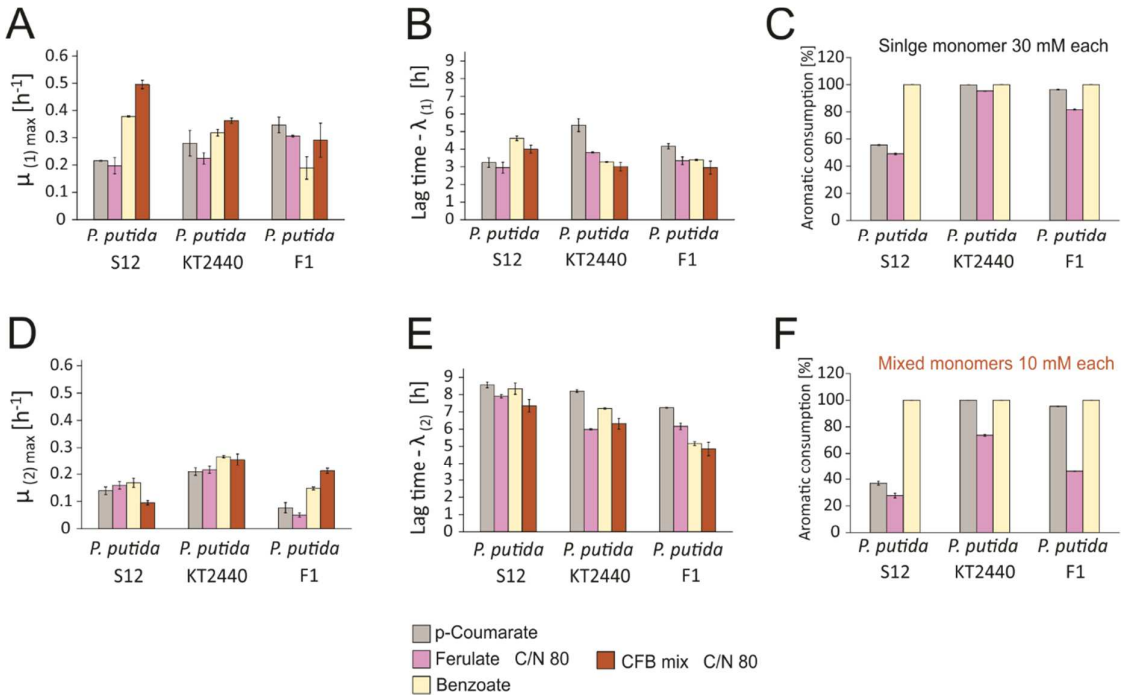

Fig 3.4 Additional data from screening step 3. Maximum specific growth rates (A, D) and lag times (B, E) with two sigmoidal growth profiles under nitrogen limitation (C/N of 80). These parameters were calculated from the Eq. (3). Total aromatic consumption after 48 h for single monomers substrates (C) and mixed substrates (F) were estimated after 48 h. Error bars indicate deviation from the mean (n = 2).

For *P. putida* KT2440 grown in the CFB mixture, μ_{max}, lag times, and final OD_{600} were overall not significantly altered compared to the values from growth on single aromatics, except for an increase of lag time for p-coumarate (30 mM) vs. CFB (30 mM) (Fig. 3.4B). In contrast, for the other two *P. putida* strains the $\mu_{(2)max}$ values were affected for all aromatics. The reason of this could be explained by a different kinetic of aromatic consumption, where the aromatic uptake of *P. putida* KT2440 under nitrogen limitation was clearly superior (Fig. 3.4C and F).

Quantitative biomass monitoring in microtiter plates is based on the linear correlation between scatter intensity and cell density, which has been validated even at high concentrations (Samorski *et al.*, 2005; Kensy *et al.*, 2009). However, factors like cell morphological changes (size and shape) during cultivation could hamper the practical comparison during screening campaigns (Kunze *et al.*, 2014). Also, the effect of the *mcl*-PHA

granules on reliable biomass quantification could interfere in the process. For this reason, aromatics consumption and *mcl*-PHA accumulation are more valid parameters to evaluate the success than biomass formation.

At this stage, the findings highlight that the funnelling capacity of the aromatics as well as the accumulation of *mcl*-PHAs depends strongly on availability of essential nutrients. Therefore, subsequent experiments were designed in a larger scale, where a hierarchical aromatic uptake under nutrient limited scenarios was possible to be discerned.

3.3.2 The funneling capacity in P. putida *is affected when* mcl-*PHA accumulation is triggered*

To reveal the time course of the microbial activity under nitrogen limitation, conventional shake flask cultivations were carried out with the CFB mixture using *P. putida* KT2440 and *P. putida* F1. The comparison of their aromatic funnelling capacity and *mcl*-PHA accumulation at two different nitrogen conditions (nitrogen excess C/N = 8 and limitation C/N = 80) is shown in Fig. 3.5.

Under nitrogen excess, both strains consumed all aromatic compounds within 24 hours utilizing 50% of the initial amount of ammonium. However, *P. putida* F1 yielded higher OD_{600} values and degraded benzoate slightly faster than *P. putida* KT2440 during the first 9 hours (50 vs. 30% consumed, respectively), which resulted in stronger initial growth of F1 (OD_{600} at 9 hours: 0.98 vs. 0.32) (Fig. 3.5B). While a typical order of uptake preference is known for *P. putida* KT2440 when nitrogen does not limit growth: benzoate > p-coumarate > ferulate (Ravi *et al.*, 2017), no hierarchical aromatic uptake was observed (or resolved with the sampling frequency) with nitrogen excess. However, under nitrogen limitation, the aromatic uptake hierarchy clearly became evident and followed the classical regulatory control (*i.e.,* catabolite repression by the Crc global regulator protein) known for *P. putida (*Nichols and Harwood, 1995; Morales *et al.*, 2004; Rojo, 2010). The consumption of benzoate was similar in both strains and correlated with the ammonium depletion. Afterwards, *P. putida* KT2240 showed a faster consumption of the other two substrates. Under this condition, the *mcl*-PHA concentration increased for *P. putida* KT2440 reaching a maximum of 497 mg L^{-1} after 72 hours. Contrarily, *P. putida* F1 did not trigger *mcl*-PHA formation after entering nitrogen limitation and overall showed a drastic reduction in growth, which contrasted to the results of the screening step 3. Furthermore, when comparing the aromatic consumption by *P. putida F1* in shake cultivations and 48-well flower plates, less amount of p-coumarate and ferulate was consumed at 48 hours. In the case of *P. putida* KT2240, ferulate uptake was also affected, suggesting that the aromatic catabolism of both strains behave different depending on the cultivation system utilized.

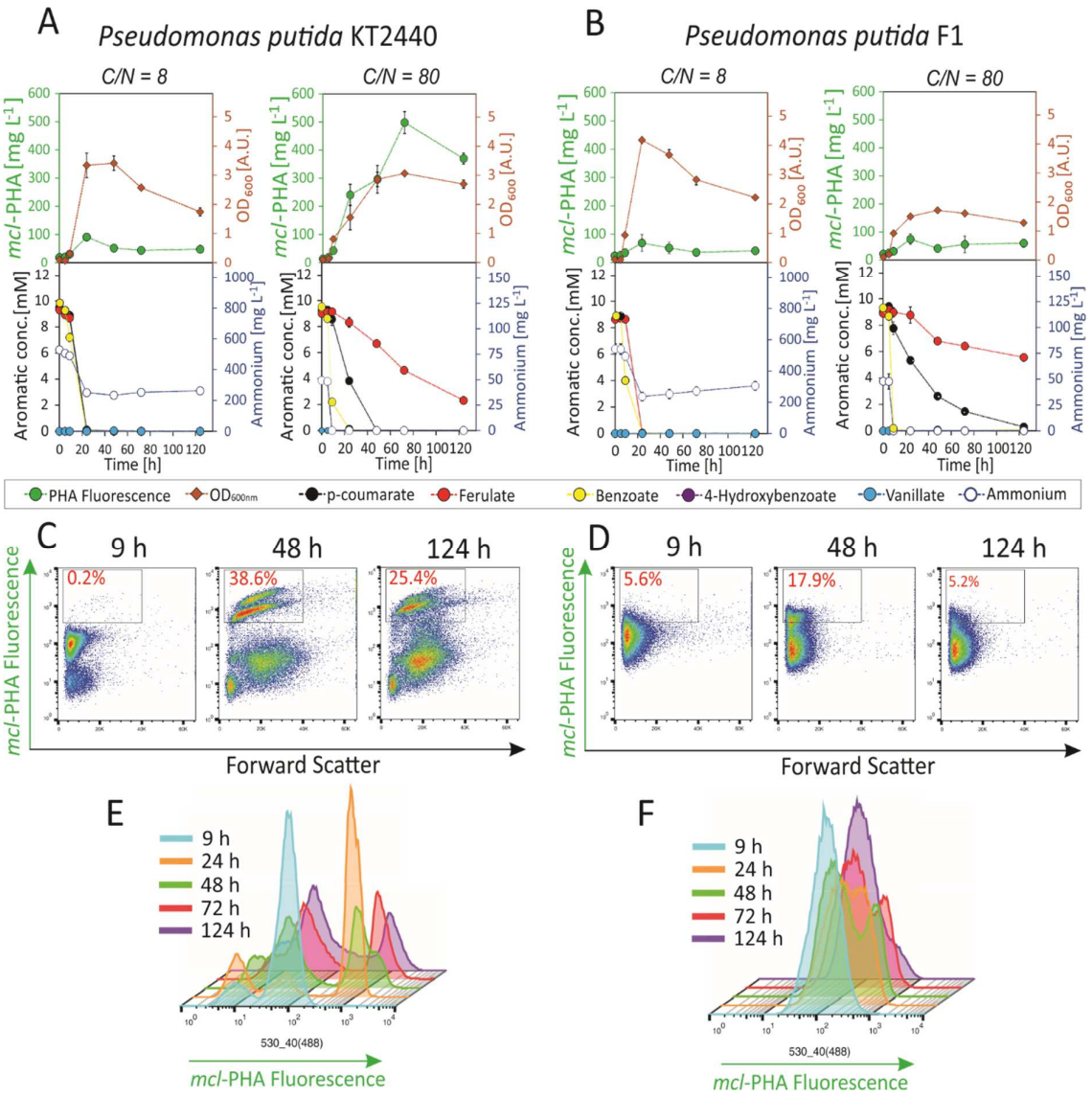

Fig. 3.5 Conventional shake flask cultivations. Comparison of the aromatic funnelling capacity and *mcl*-PHA formation at two different nitrogen concentrations. The defined lignin-derived monomer mixture (30 mM) consisted of 10 mM p-coumarate, ferulate and benzoate, each (dissolved in Hartman's mineral salt medium). Cell growth, *mcl*-PHA accumulation, aromatic consumption and ammonium utilization under nitrogen excess (C/N = 8) and nitrogen limitation (C/N = 80) for *P. putida* KT2440 (A) and *P. putida* F1 (B). Flow cytometry analysis of the bacterial populations developed by both strains during nitrogen limitation (C/N= 80). Fluorescence scatter plots for selected time points, *P. putida* KT2440 (C) and *P. putida* F1 (D) during 124 hours. The corresponding histograms representing the dynamic change of *mcl*-PHA accumulating cell for all the time points (E-F). Error bars indicate the deviation of the mean (n = 2).

The study of the dynamic *mcl*-PHA accumulation in both strains was complemented by flow cytometry (Fig. 3.5C-F). Initially, during the exponential growth of *P. putida* KT2440 (*i.e.*, 9 to 24 hours), a narrow *mcl*-PHA fluorescence peak was observed (Fig. 3.5E). This indicates a similar *mcl*-PHA content within the *mcl*-PHA sub-population. After 24 hours, when both benzoate and p-coumarate were consumed, the *mcl*-PHA-derived fluorescence peak became

first wider and then split into two cell clusters, possibly indicating partial *mcl*-PHA degradation. A similar behaviour has been previously reported by *Karmann et al., 2017*, who suggested a bistable behaviour when *P. putida* KT2440 depolymerize *mcl*-PHA during carbon limitation. In this case, the limited consumption of ferulate related to the lack of nitrogen could trigger *mcl*-PHA depolymerization to provide cell maintenance energy. On the contrary, *mcl*-PHA accumulating populations in *P. putida* F1 were only temporarily identified until p-coumarate was completely consumed, reaching a maximum of 17.9% of the total events at 48 hours, while for *P. putida* KT2440 was 38.6% (compare Fig. 3.5C-D).

From the time-resolved uptake of aromatics and the ammonium consumption, it was evident that the funneling capacity of both *P. putida* strains was affected. However, *P. putida* KT2440 partially metabolized the aromatic mixture into *mcl*-PHA, while *P. putida* F1 was drastically hindered by the nitrogen availability. The drastic interruption of carbon flux induced by nitrogen depletion limited *P. putida F1* to generate the needed central precursor (*i.e.,* acetyl-CoA) for biomass and *mcl*-PHA synthesis. From these observations, more questions were opened regarding the role of oxygen availability from the differences found in microtiter plate cultivations, where the oxygen transfer rate is different. At this point, it was hypothesized that oxygen availability could be responsible for the relevant differences found for *P. putida F1* in shake flasks compared to the screening in 48-well flower plates. Therefore, the maximum oxygen transfer rate capacity (OTR_{cap}) for these systems was calculated (Eq. 4 and 5 in the sections 2.7.3 and 2.7.4, respectively). Theoretical maximum OTR_{cap} of 40.9 and 16.1 mmol O_2 L^{-1} h^{-1} were found for the 48-well flower plates and shake flask, respectively, highlighting a great difference in maximum respiration capacity. The indifference of the *P. putida* KT2440 results also highlight the high tolerance of *P. putida* KT2240 towards stress generated during nitrogen depletion and lower OTRs, where *mcl*-PHA carbon storage formation occurs even although the funnelling capacity is affected.

However, to further understand and confirm how the aromatic metabolism is affected under low oxygen availability and evaluate the overall effect on *mcl*-PHA accumulation, additional cultivations were followed for both *P. putida* strains.

3.3.3 Oxygen-limited environments slows down the aromatic funneling capacity in P. putida *hindering* mcl-*PHA accumulation*

The oxygen availability in the microbial synthesis of PHA has been identified as key factor for process performance and economics, particularly when increasing production scale (Blunt *et al.*, 2018). Depending on the substrates, microbial cultures (pure or mixed), particular metabolism and type of PHA (short or medium chain length *scl/mcl*-PHA), the effect of low oxygen availability could positively affect the production. For example, it has been reported that *scl*-PHA can act as an electron sink, since the synthesis occurs though a reductive process where NADPH act as electron donor and ATP synthesis occurs via substrate-level phosphorylation during oxygen limitation. In this case, the disposal of excess reducing power

enable a balanced redox state on cell metabolism at low oxygen levels, which was first established in *Azotobacter beijerinckii* growing on glucose (Senior and Dawes, 1971; Senior *et al.*, 1972). Additionally, from the possibility of reducing mixing power input in the bioprocess, limiting oxygen has been an implemented strategy for *scl*-PHA accumulation from volatile fatty acids (VFAs) via β-oxidation in pure (Kek *et al.*, 2008; Cavalheiro *et al.*, 2012; Shantini *et al.*, 2015) and mixed cultures (Third *et al.*, 2003; Wang *et al.*, 2017). However, the effect of limited oxygen conditions on *mcl*-PHA has not been considered in detail. In particular, the effect on the biopolymer production using lignin-aromatic substrates to accumulate *mcl*-PHA by *P. putida* is unknown. Therefore, to evaluate the response of *P. putida* KT2240 and *P. putida* F1 under environments with low oxygen levels additional cultivations were implemented.

The comparison of the aromatic funnelling and *mcl*-PHA accumulation for both *P. putida* strains growing on the CFB mixture (30 mM) under simultaneous nitrogen (C/N = 80) and oxygen limitation is shown in Fig. 3.6. The passive aeration of the head space of a lab-scale bioreactor (working volume of 500 ml) was carried out by air diffusion via 0.2 µm sterile vent filters. The results indicate that *P. putida* is capable of not only survival, but also growth in low oxygen environments. However, the simultaneous limitation of oxygen and nitrogen drastically slowed the aromatic funnelling capacity of both strains, limiting the cell growth and promoting substrate intermediate accumulation. In the case of *P. putida* KT2440, the nitrogen source was completely consumed after 4 days while approximately half of the benzoate was still present (Fig. 3.6A). Right after this (day 5), the corresponding intermediates of the aromatic catabolism of p-coumarate (*i.e.,* 4-hydroxybenzoate) and ferulate (*i.e.,* vanillate) reached a concentration of 7 and 4.8 mM, respectively. From the residual amount p-coumarate and ferulate observed, it was clear that the carbon flux decreased considerably through the β-ketoadipate pathway (see Chapter 1, Fig. 1.5), limiting the generation of central intermediates like acetyl-CoA, which are essential for growth and *mcl*-PHA synthesis. The lack of nitrogen and oxygen could have limited the proper activation and/or production of oxygenases that incorporate oxygen and cleave the aromatic ring in the protocatechuate node. For example, a similar accumulation of intermediates has been observed in a *P. putida* lacking genes encoding the PCA dioxygenase (PcaHG) normally present in a native β-ketoadipate pathway (Johnson *et al.*, 2016). After 5 days, a further uptake of benzoate and 4-hydroxybenzoate continue with a corresponding slight increment of OD_{600} and *mcl*-PHA. Here, the consumption of 4-hydroxybenzoate only occurred after all p-coumarate was depleted, which is due to regulated transport mechanisms by catabolite repression managed from the β-ketoadipate pathway. The transport of 4-hydroxybenzoate is repressed by growth on benzoate as it has been demonstrated in *P. putida*, which was initially suggested as a communication between the two branches of the β-ketoadipate pathway at molecular level (*i.e.,* catechol and protocatechuate branches) by Nichols and Harwood, 1995. Later on, it was demonstrated that the Crc global regulator was the responsible for such control (Morales *et*

al., 2004) and when eliminating it´s action, the conversion of aromatics was enhanced in *P. putida* KT2440 (Johnson *et al.*, 2017).

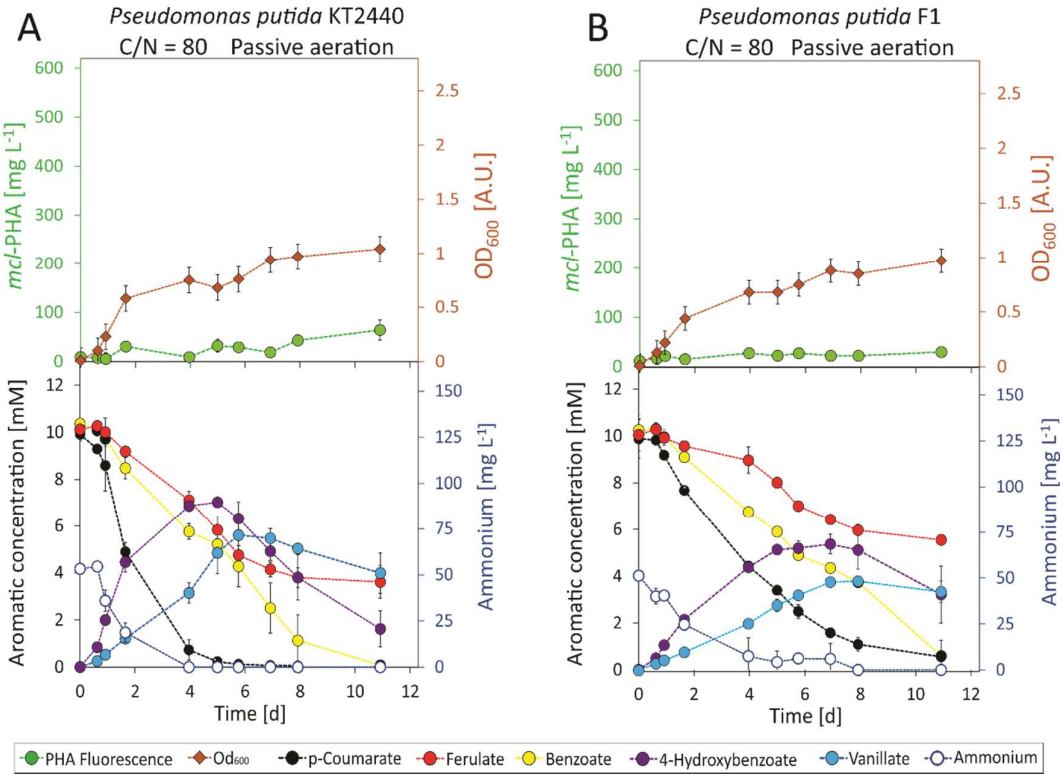

Fig. 3.6 Oxygen-limited cultivations of *P. putida* KT2440 (A) and *P. putida* F1 (B). The simultaneous effect of nitrogen and oxygen limitation was evaluated on the aromatic funnel capacity at C/N = 80 in lab-scale bioreactors with passive aeration (air diffusion into the headspace via 0.2 µm sterile vent filters). The defined lignin-derived monomer mixture CFB (30 mM) consisted on p-coumarate, ferulate acid and benzoate. Cell growth as OD_{600}, *mcl*-PHA concentration, aromatic composition and ammonium concentration were measured over time. Error bars indicate the deviation of the mean (n = 2).

In *P. putida* F1, a similar trend was observed, but with a slower uptake of aromatics and ammonium (Fig. 3.6B). For example, while *P. putida* KT2440 totally consumed the nitrogen source and converted all p-coumarate after 4 days, *P. putida* F1 took the double amount of time to achieve a similar result. From these observations, it was clear that an oxygen-limited environment with an additional nitrogen depletion slowed down the aromatic funneling in *P. putida* and hindered the *mcl*-PHA production. However, the strain KT2440 stands out over F1 as more tolerant to these stress conditions as previously found in the shake flask cultivations.

A final experiment under two aeration conditions and enabling nitrogen excess (C/N = 8) was implemented with *P. putida* KT2440 to evidence the single effect of oxygen but still under a limited availability (Fig 3.7). For this, a similar passive aeration was implemented as previously described (Fig 3.7A) and an additional active aeration condition was promoted by air flow though the headspace at 30 ml min^{-1} (Fig 3.7B).

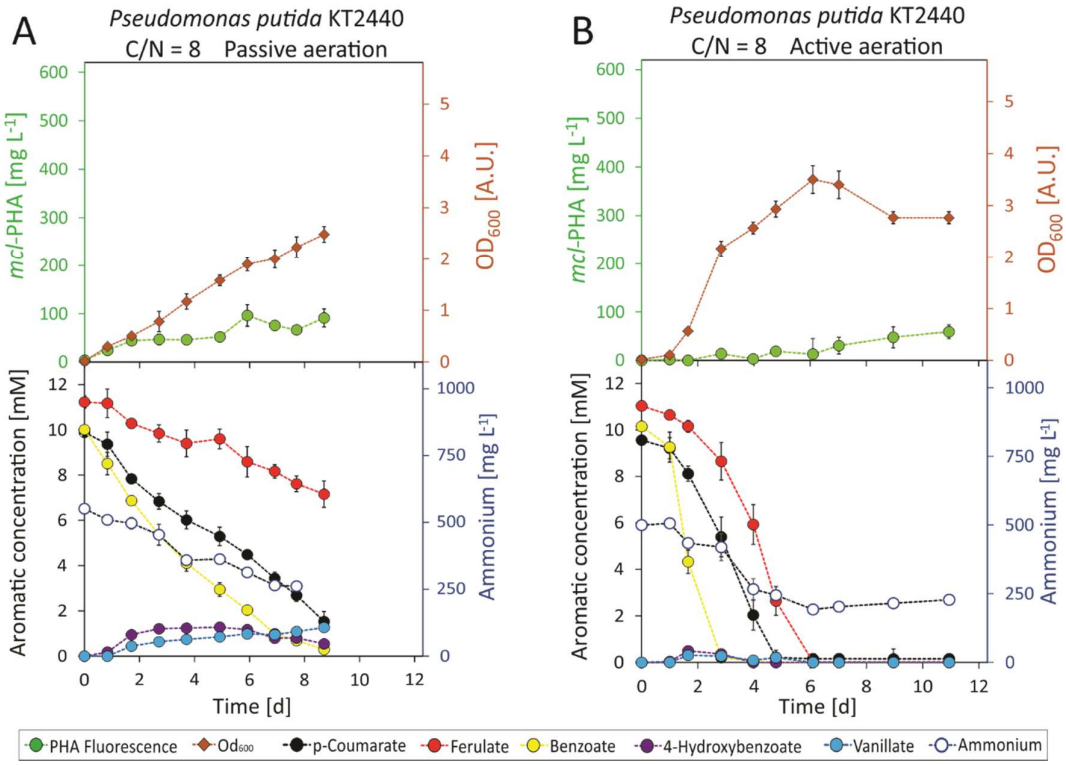

Fig. 3.7 Oxygen-limited cultivations of *P. putida* KT2440 under passive (A) and active aeration (B) and nitrogen excess (C/N = 8). The effect of the oxygen availability on the aromatic funnel capacity and *mcl*-PHA accumulation was carried out in lab-scale bioreactors. The oxygen availability was set promoting passive (air diffusion into the headspace via 0.2 µm sterile vent filters) and active aeration (air flow though the headspace at 30 ml min^{-1}). The defined lignin-derived monomer mixture CFB (30 mM) consisted on p-coumarate, ferulate acid and benzoate. Cell growth as OD_{600}, *mcl*-PHA concentration, aromatic composition and ammonium concentration were measured over time. Error bars indicate the deviation of the mean (n = 3).

This time, the accumulation of intermediates decreased drastically in all cases and the rates of aromatic uptake, growth and polymer accumulation correlated with the oxygen availability set by each cultivation. The carbon flux was more efficient than in the previous oxygen-limited cultivations with a simultaneous lack of nitrogen, resulting in a higher biomass formation. As detailed observation, the concentration of *mcl*-PHA was slightly higher in the culture under passive aeration even though higher residual levels of ferulate still remained unconsumed. This suggests a considerable increase in yield of *mcl*-PHA on aromatics and therefore a higher carbon flux pushed towards *mcl*-PHA than biomass. However, these differences did not represent a considerable increment of *mcl*-PHA under any limited oxygen availability tested, which can be explained by the mechanism of *mcl*-PHA accumulation from aromatic compounds in *Pseudomonas*.

Although *scl*-PHA can act as electron sink to maintain a balanced redox sate in the cell at low oxygen levels, the same evidence on *mcl*-PHA has been limited, especially from aromatic compounds. Only some studies using intermediates of the β-oxidation cycle like medium-chain fatty acids (C ≥ 6) have shown an improvement under low oxygen concentrations (Blunt *et al.*, 2018). For example, an increment on *mcl*-PHA production from fatty acids like octanoate in microaerophilic environments has been reported by the strain *P. putida* LS46 (Blunt *et al.*, 2017; Blunt *et al.*, 2018). However, this was not attributed as *mcl*-PHA acting as electron sink, since *Pseudomonas* utilizes the β-oxidation cycle to synthetize *mcl*-PHA via an oxidative process that uses NAD^+ and FAD as the electron acceptors. Alternatively, the increment of *mcl-PHA* accumulation from fatty acids is due to inhibition of key enzymes in the TCA cycle during redox imbalance induced under oxygen limitation. Thus, the cell may not be able to further metabolize the available acyl-CoA and the *mcl*-PHA occurs via carbon flux re-direction, leaving more available monomers that can be directly polymerized even without a strict nitrogen limitation (Prieto *et al.*, 2016). Thus, this is a mechanism for storing electrons as *mcl*-PHA to maintain a balanced redox state. In contrast, structurally unrelated compounds like carbohydrates, glycerol and aromatic molecules are converted into *mcl*-PHA by de novo fatty acid biosynthesis in *Pseudomonas,* where a previous biomass build-up stage is required along with a nutritional imbalance (Prieto *et al.*, 2016). This is a reductive process that uses NADPH as the electron donor and until now there is not yet evidence that occurs under oxygen limited conditions (Blunt *et al.*, 2018). Therefore, a considerable accumulation of *mcl*-PHA from aromatics was not expected in the oxygen-limited tests here presented.

Instead, it seems that providing a balanced nitrogen and oxygen supply promotes a better carbon flux into biopolymer, avoiding accumulation of aromatic intermediates. This assumption must be evidenced comparing accurate differences in oxygen availability. Finally, besides a very good performance in funneling a mixture of aromatic compounds and the superior performance in *mcl*-PHA formation compared to all tested strains, *P. putida* KT2440 also presents the most robust biocatalyst against process parameter deviations. This strain screening and parallel cultivations therefore, clearly supports the focus of the research field on *P. putida* KT2440 for a direct native production of *mcl*-PHA straight from lignin-mixed aromatics. In the next chapter, a detailed metabolic characterization of the funnelling process is performed for this strain.

3.4 Conclusion

Through a sequential experiment approach involving parallel strain screenings in microtiter plates, this study revealed essential differences between wild type *Pseudomonas* strains on lignin aromatics uptake and *mcl*-PHA accumulation. In these experiments, interesting results like growth on sinapic acid by *P. putida* F1 and changes in scattered light values of *P. putida* S12 on challenging molecules like syringol and 4-methylguiaiacol at low concentrations (5 mM) were obtained. Additionally, the growth kinetics was characterized though meaningful parameters (*i.e.,* specific growth rates μ_{max} and lag times λ), which were obtained by fitting a modified version of the Gompertz model to experimental data. Thus, it was possible to identify and compare diauxic shifts in all *P. putida* when growing on a selected aromatic mixture of p-coumarate, ferulate and benzoate (CFB 30mM) under nitrogen limitation. Later on, *P. putida* F1 and *P. putida* KT2240 were the two most suitable strains to convert the CFB mixture into *mcl*-PHA and therefore were compared in shake flask cultivations to obtain more detailed culture dynamics. This exposed that their funneling capacity was considerably affected when triggering *mcl*-PHA accumulation by nitrogen limitation. From the different microbial performance on lignin aromatic valorization between shake flasks and 48-microtiter plates cultivations, it was inferred that oxygen availability limit considerably the biocatalytic process. Further experiments were carried out under oxygen-limited conditions to understand to what extent the aromatic funneling and *mcl*-PHA accumulation were affected either by a simultaneous nitrogen limitation or without it. These experiments showed that a low oxygen availability slowed down the aromatic uptake, hindering *mcl*-PHA accumulation. Nevertheless, all this comparative evaluation led to select *P. putida* KT2240 as the most robust and best performing strain under stressful environments, identifying the oxygen supply as important process parameter. The next step should focus on identifying optimal C/N ratios and the proper oxygen availabilities by mean of further bioprocess development in *P. putida* KT2240.

Chapter 4: Oxygen and nitrogen availability as the key factors for funneling lignin-aromatic mixtures into *mcl*-polyhydroxyalkanoates in *Pseudomonas putida* KT2440

Partially published as:

Ramírez-Morales J. E., Czichowski P., Besirlioglu V., Regestein L., Rabaey K., Blank L. M., Rosenbaum M. Lignin aromatics to PHA polymers: nitrogen and oxygen are the key factors for *Pseudomonas*. 2021. *ACS Sustainable Chemistry & Engineering*, 9, 31, 10579–10590. https://doi.org/10.1021/acssuschemeng.1c02682

Contributions:

Juan E. Ramírez performed all the experiments and together with Lars Regestein, Lars Blank and Miriam Rosenbaum designed the experiments and analyzed the results

4.1 Abstract

Polyhydroxyalkanoates (PHAs) represent an alternative to petroleum-based plastics, which can be commercialized as biodegradable polymers in many applications. Although it is possible to produce PHA from several sources, low-costs feedstocks like lignocellulosic biomass promises to stimulate a more sustainable microbial production. *Pseudomonas putida,* a medium chain length PHA producer, is also recognized for having a versatile aromatic catabolism, which makes it quite suitable for upgrading lignin aromatics. However, there are two main challenges that prevent fundamental research on microbial physiology and bioprocess development: Complexity of aromatic liquors after lignin depolymerisation and limited analytics. In this study, the most robust and best performing strain selected in the last chapter (*i.e., P. putida* KT2440), was further evaluated to identify the optimal balance between oxygen, nitrogen and aromatics towards efficient biocatalytic conversion of lignin-aromatics into medium chain length PHA. From a defined aromatic mixture of p-coumarate, ferulate, and benzoate, the accumulation of polymer was improved in the wild type strain under technically relevant conditions by up to 43% (polymer content in cell biomass, mg *mcl*-PHA mg^{-1} CDW). The highest *mcl*-PHA concentration (582 ± 41 mg L^{-1}) was obtained for a C/N ratio of 60 for oxygen-unlimited conditions (oxygen transfer rate ≥ 20 mmol L^{-1} h^{-1}). In contrast, aromatic intermediates accumulated under oxygen-limited conditions at oxygen transfer rates below 10 mmol L^{-1} h^{-1}. The experimental conditions were scalable into a 1-L stirred tank bioreactor based on the oxygen transfer rate. Finally, through synergetic effects from implementing simultaneous biocatalyst and bioprocess optimization, a 1.9-fold increment in *mcl*-PHA concentration and a 1.5-fold increment in *mcl*-PHA content were obtained in a strain lacking PHA depolymerisation ability. This study contributes to deepening our understanding of the bio-catalytic capability of the promising *P. putida* KT2440 towards downstream microbial conversions of lignin aromatics for future biorefinery applications.

4.2 Introduction

Petroleum-based plastics consist of a great diversity of chemically synthetized polymers with versatile features that have led great societal benefits for health, safety, energy saving and material conservation (Andrady and Neal, 2009). Although they are utilized in every aspect of daily life, their disposal has become a global issue due to poor waste management, generating negative impacts like accumulation of microplastics in aquatic environments (Padervand *et al.*, 2020). In addition, being non-biodegradable and coming from non-renewable sources, important efforts have been focused on replacing them with analogue bio-based polymers (Nakajima *et al.*, 2017).

Polyhydroxyalkanoates (PHAs) are an alternative to fossil-based plastic and have been commercialized as biodegradable polymers in medical and industrial applications (Ali and Jamil, 2016; Muneer *et al.*, 2020). These biopolymers can be very versatile depending on molecular structure (*i.e.,* associated chemical groups and chain length of corresponding monomers) and therefore are classified on these features. The simplest and more common microbial PHA is poly-3-hydroxybutyrate (PHB), which is the most studied in wastewater-cultures (Amadu *et al.*, 2021). Additionally, there are three types of PHAs based on the carbon chain length: Short chain length PHAs (*scl*-PHAs, C3 to C5), medium chain length PHAs (*mcl*-PHAs, C6 to C14) and long chain length PHAs (*lcl*-PHAs, C>14) (Muneer *et al.*, 2020). The application of *scl*-PHAs is usually restricted to the production of soft plastic like packaging films, while *mcl*-PHAs present interesting properties like flexibility and elasticity (thermos-elastomeric). Thiese characteristics lead broader spectrum of applications for *mcl*-PHA as hot melt adhesives, medical devices and biocarriers for slow release of different substances (Prieto *et al.*, 2016).

Pseudomonas sp. are recognized to accumulate *mcl*-PHA from several feedstocks, changing the monomer composition and molecular weights of the polymers depending of the type of substrate (Dartiailh *et al.*, 2021). Structurally unrelated carbon sources like sugars, carbohydrates, glycerol, acetate or aromatics are converted into *mcl*-PHA by *de novo* fatty acid biosynthesis, where a nutritional imbalance and a biomass build-up stage prior to polymer accumulation are required (Prieto *et al.*, 2016). On the other hand, related structures like medium chain length fatty acids (MCFAs) are metabolized via β-oxidation and a strict nutrient limitation is not mandatory for polymer formation (Prieto *et al.*, 2016). Additionally, some studies have shown that promoting low oxygen levels led to an increased *mcl*-PHA accumulation from these related substrates, which represents a great advantage from an energy saving point of view (Blunt *et al.*, 2017; Blunt *et al.*, 2018). However, with the feedstocks being an important limiting factor for establishing cost effective *mcl*-PHA production, the low power consumption (*i.e.,* less aeration) advantages related to expensive substrates like MCFAs need to be re-evaluated. Thus, substrates coming from renewable and

low-cost feedstocks like lignocellulosic biomass have been studied lately as sustainable platform for cleaner production (Govil *et al.*, 2020).

However, multiple fundamental and technical challenges need to be solved prior to establishing an efficient *mcl*-PHA value chain platform from lignocellulosic materials. The lignin fraction being the most underutilized fraction of lignocellulosic feedstocks, great efforts have been focused on obtaining suitable lignin-derived substrates for microbial utilization (Sun *et al.*, 2018; Xu *et al.*, 2019a). In addition to being recognized as efficient cell factories for *mcl*-PHA production (Mozejko-Ciesielska *et al.*, 2019), *Pseudomonas putida* stands out for a versatile catabolism towards lignin aromatic compounds (Abdelaziz *et al.*, 2016; Becker and Wittmann, 2019; Brink *et al.*, 2019), which has led to intensive research on this bacterium.

Important proof-of-concept and cultivation studies for upgrading single lignin aromatics and/or lignin-derived streams into *mcl*-PHA in *P. putida* greatly improved production parameters (Linger *et al.*, 2014; Jayakody *et al.*, 2018; Liu *et al.*, 2019; Salvachua *et al.*, 2020). However, obtaining real and reproducible liquors of lignin-derived aromatics as substrates for biological funnelling studies in sufficient amounts is still difficult. Furthermore, limited methods for analysis of the heterogeneous aromatic fractions and complex catabolic repression phenomena make a detailed physiological study on *mcl*-PHA production from lignin-derived aromatics very challenging. Therefore, much of the physiological research thus far focused on the evaluation of single lignin-derived aromatic compounds like benzoate (Xu *et al.*, 2019b; Borrero-de Acuña *et al.*, 2020), vanillate (Wang *et al.*, 2018), ferulate (Zhou *et al.*, 2020) or co-feeding some of them with glycerol (Xu *et al.*, 2021). Thus, detailed studies towards a physiological understanding of the uptake and conversion dynamics of defined aromatic mixtures into *mcl*-PHA are necessary. Especially, knowledge on how the native funnelling capacity of *P. putida* is affected under nutrient limited conditions (*i.e.,* when triggering *mcl*-PHA accumulation) is required, as hierarchical aromatics consumption is likely to heavily affect productivities (Rojo, 2010). Finally, a more rigorous comprehension of the impact of oxygen transfer rates on *mcl*-PHA production from lignin aromatics is a relevant gap to be covered, especially to encourage a proper reporting criteria of oxygen transfer conditions, which has been identified as a long-standing problem in the PHA field (Blunt *et al.*, 2018).

In this chapter, *P. putida* KT24440 as the most robust biocatalyst to synthetize *mcl*-PHA from mixed lignin aromatics and which has been selected previously (see chapter 3), was further evaluated. Online measurements of the respiratory capacity via the oxygen transfer rate (OTR) and the dynamics of aromatic funneling into *mcl*-PHA facilitated a closer look to the bioprocess. After a comprehensive evaluation of the aromatics funneling, the main outcomes were transferable and scalable into a stirrer tank bioreactor. Finally, a partially optimized *P. putida* KT24440 PHA production strain was also characterized to demostrate that simultanous

optimization by metabolic engineering and bioprocess development leads to significant increments of product formation.

4.3 Results and discussion

To optimize the *mcl*-PHA accumulation in *P. putida* KT2440 from alternative carbon sources like lignin aromatic mixtures, it is necessary to find the key factors that promote an efficient bioconversion. The next sections show the determination of these factors though experiments combining oxygen and nitrogen availabilities, scaling-up cultivations and evaluation of a metabolically enhanced *P. putida KT2440*.

4.3.1 Online measurements of the oxygen consumption reveal the dynamics of aromatic funnelling into mcl-*PHA in* P. putida *KT2440*

Producing high levels of *mcl*-PHA is mandatory for establishing a cost-effective industrial process. Thus, constrains related to *mcl*-PHA commercialization and price competition with the conventional plastic industry may be overcome when increasing carbon conversion efficiencies. Thus, a similar progress like the one obtained on *mcl*-PHA optimization by metabolic engineering and process development in *P. putida* from conventional carbon sources (Poblete-Castro *et al.*, 2014a; Poblete-Castro *et al.*, 2014b; Mozejko-Ciesielska *et al.*, 2019), also needs to be achieved from lignin-derived aromatics. For this, optimization of production parameters like *mcl*-PHA concentration, content in biomass (% based on the total CDW) and product yields on lignin aromatics is required. Once the relevant factors are found, the bioprocess performance in terms of biopolymer production can be controlled.

As stated previously, some studies have found that *mcl*-PHA can be promoted under low oxygen levels using medium chain length fatty acids, which may save costs regarding energy consumption. However, as shown in the last study of this thesis (Chapter 3), enough oxygen supply seems to play an important role for promoting a correct carbon flux from lignin aromatics into *mcl*-PHA when nitrogen limits the growth in *P. putida*.

To fine tune the importance of oxygen and nitrogen, online measurements of the oxygen consumption at different combinations of oxygen and nitrogen availability were carried out to reveal the dynamics of aromatic funnelling into *mcl*-PHA during 72 h for *P. putida* KT2440. By changing the filling volumes (10, 20, 30 and 50 ml) of shake flasks for each nitrogen condition (C/N ratios of 40, 60, and 80), the maximum oxygen transfer capacity (as OTR_{cap}) was defined. The 12 possible combinations were run in duplicates and offline samples were taken sacrificing parallel flask cultivations. The time resolved dynamics of parameters evaluated for every C/N ratio facilitate a detailed comparison. An example for one unlimited and one limited oxygen consumption under nitrogen limitation (C/N 40) is shown in Fig. 4.1. The complete data set for all conditions can be found in the Appendix (Fig S4.1, S4.2 and S4.3).

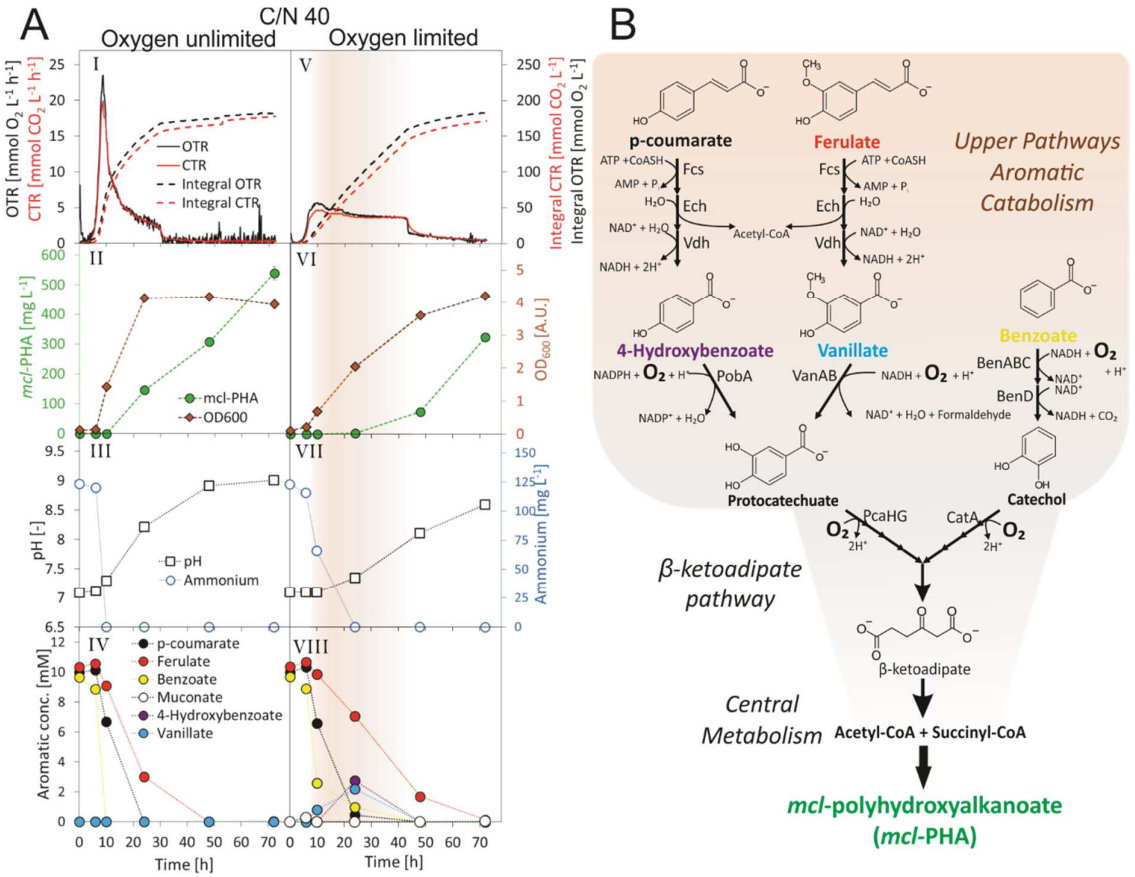

Fig. 4.1 Comparison of the dynamics of aromatics funnelling into *mcl*-PHA in *P. putida* KT2440 under oxygen unlimited (I – IV) and limited conditions (V – VIII), both under nitrogen limitation at C/N 40 and CFB 30 mM in Hartman's mineral salt medium (A). OTR_{max} of 23.5 and 5.7 mmol O_2 L^{-1} h^{-1} were achieved for filling volumes of 10 and 50 ml, respectively. Process parameters like the integral of OTR and CTR (I and V), *mcl*-PHA concentration and OD_{600} (II and VI), pH and ammonium concentration (III and VII), and aromatic concentration (IV and VIII) are reported. The shaded area indicates intermediate accumulation and oxygen limitation. Representative pathways of biocatalytic funneling of the CFB aromatic mixture into *mcl*-PHA by *P. putida* KT2440 (B). Adapted from (Nogales *et al.*, 2017; Ravi *et al.*, 2017). Through catabolic upper-pathways the lignin monomers converge into few central intermediates like catechol and protocatechuate, which are eventually cleaved and metabolized via the β-ketoadipate pathway to access the central carbon metabolism. Finally, part of the carbon flux excess accumulates as *mcl*-PHA under nitrogen limiting conditions. Fcs, feruloyl-CoA-synthase; Ech, feruloyl-CoA hydratase-lyase; Vdh, vanillin dehydrogenase; PobA, 4-hydroxybenzoate 3-monooxygenase; VanAB, vanillate O-demethylase; BenABC, benzoate 1,2-dioxygenase; BenD, benzoate 1,2-cis-dihydrodiol dehydrogenase; CatA, catechol 1,2-dioxygenase ; PcaHG, protocatechuate 3,4-dioxygenase.

The accumulation of *mcl*-PHA was affected negatively for all C/N ratios while the maximum oxygen transfer capacity decreased (Fig S4.1, S4.2 and S4.3). The aromatic analysis of the offline samples permitted to identify an OTR_{cap} of approx. 10 mmol O_2 L^{-1} h^{-1} where intermediates started to accumulate for every C/N ratio (also see pathway Fig. 4.1B). For values below this threshold, the simultaneous oxygen and nitrogen limitation became evident, where the shape of the OTRs curves presented a visible plateau, indicating a stable but low bacterial growth rate due to nutrient limitation. An example of this observation is

shown in Fig. 4.1A, where an OTR_{max} of 23.5 and 5.7 mmol O_2 L^{-1} h^{-1} were achieved at a C/N ratio of 40 for filling volumes of 10 and 50 ml, respectively. Overall, parameters like pH, OD_{600}, and integrated OTR and CTR followed a similar trend, which is related to the intrinsic metabolic activity of aerobic growth. The consumption of ammonium correlated well with the benzoate uptake for all conditions according to the typical uptake priority of *P. putida* previously discussed in Chapter 3.

Comparing the results with the previous flask cultivation at a C/N ratio of 80 (Chapter 3, OTR_{cap} of 16.1 mmol O_2 L^{-1} h^{-1}), an underestimation of the real potential of *P. putida* KT2440 was exposed. The aromatic funneling profiles and the final *mcl*-PHA concentration were well represented between the conditions 10 ml and 20 ml at a C/N of 80 (OTR_{max} = 18 ± 3.1 and 13.5 ± 0.4 mmol O_2 L^{-1} h^{-1}, respectively) (Fig. S4.3) but the maximum funneling performance of *P. putida* KT2440 was achieved at C/N of 60 or 40, where higher oxygen uptake rates were obtained. Hence, optimum conditions should be provided for a proper characterization or strain screening in nutrient limited lignin valorization studies. In this regard, reporting complete data of shaking conditions in conventional flask experiments should be a priority to be able to compare results across studies.

An overarching correlation of the oxygen availability (based on OTR_{max}) and the most relevant bioprocess parameters (*i.e., mcl*-PHA content and concentration) from this experiment is shown in Fig. 4.2. Additional process parameters like residual aromatics and *mcl*-PHA yield on substrate can be found in Table 4.1. For both product parameters, the linear tendency indicates a positive effect of increasing the oxygen respiratory capacity on the *mcl*-PHA accumulation for all evaluated nitrogen limited conditions. The biggest influence on *mcl*-PHA concentration was achieved for a C/N ratio of 40. Overall, the highest *mcl*-PHA concentration (582 ± 41 mg L^{-1}) was obtained for a C/N ratio of 60 at an OTR_{max} of 22.2 ± 2.8 mmol O_2 L^{-1} h^{-1}. The catabolic funneling was affected for all conditions with a C/N ratio of 80, which resulted in residual amounts of ferulate that could not be converted into biomass and product (Fig. S4.3 and Table 4.1). Thus, providing enough nitrogen for a correct function of the aromatic funneling pathways (*i.e.,* enzyme synthesis) but sufficiently low to trigger *mcl*-PHA accumulation at high OTRs, can effectively reveal the real bio-catalytic ability of promising strains with industrial relevance like *P. putida* KT2440. Therefore, increasing the oxygen supply in microbial cultivations is a proper strategy to overcome this trade-off that arises when the valorization of lignin needs to be performed under nitrogen limitation.

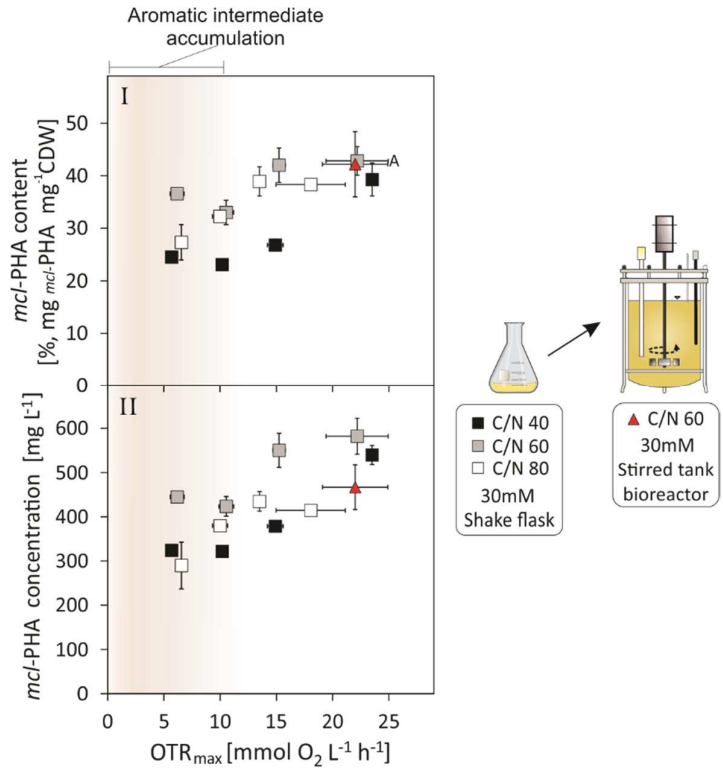

Fig. 4.2 Overall correlation of online measurements of the respiratory activity (OTR_{max}) and the *mcl*-PHA formation in *P. putida* KT2440. The *mcl*-PHA content (I) and concentration (II)) carried out in TOM®, an oxygen monitoring device for shake flasks (72h). The red triangle corresponds to the scale-up cultivation in a stirred tank bioreactor based on the OTR at C/N 60 and 30 mM of lignin aromatics (see section 4.3.2). The shaded area indicates where intermediates accumulation, which occurred below values of 10 mmol O2 L^{-1} h^{-1} . All measurements and dynamics can be found in the Apendix (Fig S4.1, S4.2 and S4.3). Additional process parameters can be found in Table 4.1.

The delicate balance between carbon sources (*i.e.,* lignin-derived aromatic mixture), oxygen availability, and nitrogen supply is coordinated in *P. putida* by fine-tuning adjustments of several global regulatory networks, which are induced under specific environmental conditions. They control particular catabolic pathways to optimize carbon metabolism and energy generation. In order to avoid intermediate accumulation, the proper nutrient balance must be provided. For example, the hierarchy of aromatic uptake is known to be controlled by the Crc global regulator protein (Nichols and Harwood, 1995; Morales *et al.*, 2004; Rojo, 2010; Johnson *et al.*, 2017). It was reported that Crc inhibits mRNA translation of *mcl*-PHA polymerase encoding gene *phaC1* and additionally hinders *mcl*-PHA synthesis in *P. putida* during exponential growth in media containing a balanced carbon source and nutrients (La Rosa *et al.*, 2014). Thus, the cultivations presented in this study with an equilibrated C/N ratio and proper oxygen availability promoted optimization of aerobic metabolism: Rapid initial growth and generation of an energy pool from benzoate reflects maximum energetic cost-benefit during nitrogen excess (*i.e.,* feast condition). Later, the benefits are used to encounter nitrogen scarcity and more complex aromatic catabolism, with the result of boosted *mcl*-PHA accumulation. The interaction of Crc with other regulatory systems involving nitrogen

regulation like NTR and regulation of terminal oxidases (by the oxygen sensor Anr and the Cyo terminal oxidase) may also interfere in the complex control of *mcl*-PHA accumulation from lignin-aromatics (Morales *et al.*, 2006; Mohanan *et al.*, 2019). Thus, further work is encouraged on evaluating key regulatory mechanisms by proteomic studies, acknowledging the possible targets for future metabolic engineering strategies or improvement by controlling key process operation parameters (Follonier *et al.*, 2013; Velázquez-Sánchez *et al.*, 2020).

Table 4.1. Most relevant bioprocess parameters obtained from the online measurements of the respiratory capacity and aromatic funnelling into *mcl*-PHA in *P. putida* KT2440.

Flask working volume [ml]	**C/N ratio**	**OTR_{max} [mmol O_2 L^{-1} h^{-1}]**	**CDW [mg L^{-1}]**	**Residual aromatics [mg L^{-1}]**	***mcl*-PHA conc. [mg L^{-1}]**	***mcl*-PHA content [%, mg *mcl*-PHA mg^{-1} CDW]**	**$Y^*_{mcl\text{-}PHA/aromatics}$ [mg *mcl*-PHA mg^{-1} aromatics]**
10	40	23.5 ± 0.3	1376 ± 55	0	539 ± 22	39.3 ± 3.1	0.11 ± 0
20		14.8 ± 0.7	1414 ± 52	0	378 ± 3	26.8 ± 1.1	0.08 ± 0
30		10.1 ± 0.4	1393 ± 6	0	321 ± 8	23.1 ± 0.7	0.07 ± 0
50		5.7 **	1322 ± 29	0	324 ± 5	24.5 ± 0.9	0.07 ± 0
10	60	22.2 ± 2.8	1359 ± 9	0	582 ± 41	42.8 ± 2.7	0.12 ± 0.01
20		15.2 ± 0.6	1311 ± 11	0	550 ± 39	42 ± 3.2	0.11 ± 0.01
30		10.5 ± 0.6	1284 ± 23	102 ± 3	423 ± 23	33 ± 2.3	0.08 ± 0
50		6.2 ± 0.6	1217 ± 20	277 ± 8	445 ± 4	36.6 ± 0.9	0.09 ± 0
10	80	18 ± 3.1	1081 ± 10	805 ± 85	414 ± 5	38.3 ± 0.7	0.1 ± 0
20		13.5 ± 0.4	1118 ± 23	586 ± 17	434 ± 22	38.9 ± 3	0.1 ± 0.01
30		10 ± 0.7	1178 ± 35	781 ± 23	380 ± 2	32.3 ± 1	0.09 ± 0
50		6.6 ± 0.1	1056 ± 64	670 ± 20	290 ± 53	27.3 ± 3.4	0.07 ± 0.01

**mcl*-PHA yield on substrate, **data from only one replicate

In addition to act as a final electron acceptor of energy metabolism to promote growth, molecular oxygen also plays an essential role in the aromatic catabolism. Specifically for the corresponding oxygenases during the catalytic activation (*i.e.,* debranching aromatic rings during the upper pathways) and cleavage of catechol and protocatechuate in the β-ketoadipate pathway (see oxygen-dependent reactions in Fig. 4.1B). In addition, a simultaneous lack of nitrogen and oxygen could limit the activation or expression levels of enzymes in the β-ketoadipate pathway overall. Recently, outer membrane vesicles (OMVs) were reported to act as extracellular cargo of catabolizing enzymes that turnover model lignin-derived aromatic compounds in *P. putida* KT2440 (Choi *et al.*, 2014; Salvachúa *et al.*, 2020). Through proteomics characterization, these two studies found extracellular evidence of most of the enzymes that metabolize all the single components of the CFB mixture. Thus, a deeper insight in this complex catabolic mechanism towards microbial host optimization is also necessary.

4.3.2 Scale-up based on the oxygen transfer rate

Finally, the optimum biocatalytic funneling of the CFB aromatic mixture into *mcl*-PHA by *P. putida* KT2440 was successfully scaled up and reproduced in a 1-L stirred tank bioreactor at an OTR_{max} of 22 ± 2.9 mmol O_2 L^{-1} h^{-1} and C/N of 60 (Fig. 4.3). The higher working volume in the bioreactor permitted to verify the biomass, substrate and product dynamics observed in previous experiments without sampling limitation. The parameters OTR, CTR, and respiratory quotient (RQ) were calculated from off-gas composition analysis using Eq. 6, 7, 8 (section 2.7.5). The OTR_{max} was obtained when ammonium was consumed, which correlated with a first stage of cell growth under nitrogen availability (*i.e.,* the first 8h), a complete benzoate consumption, and a bigger cell size (see Fig. 4.3B). At the same time, a diauxic shift, similar to the one observed in 48-well flower plates cultivations (Chapter 3, Fig. 3.3C), was associated with a change in the RQ. It reached a maximum value close to 1 and then decreased. This metabolic switch coincides with the sequential substrate utilization, changing from benzoate to p-coumarate. Additionally, it gives an idea of the metabolic reprograming from oxidative to reductive pathways (*i.e.,* strong decrease in respiration).

After this point, *mcl*-PHA started to increase reaching a maximum concentration and content at 48 h (*i.e.,* 467 ± 51 mg L^{-1} and 42.2 ± 6.6 % [mg *mcl*-PHA mg^{-1} CDW], respectively) (Fig. 4.3 III).These results are included in the Fig 4.2 as red triangles for comparison with the respective experiment in shake flask cultivations (i.e., the same OTR_{max} and C/N ratio). From the behaviour of biopolymer levels in the fermenter, a faster dynamic of *mcl*-PHA evolution was observed (*i.e.,* faster increment of *mcl*-PHA up to 48h and decrease after 72h) compared to the corresponding condition in flask experiments. This could be related to different mixing patterns established in bioreactor vs. shake flasks. This can influence a faster polymerization and depolymerisation of *mcl*-PHA (de Eugenio *et al.*, 2010; Arias *et al.*, 2013). This is also supported by the different numbers of polymer granules observed in some bacterial cells (see arrows at 48h Fig. 3.3C), which has been reported as bistable behavior of *P. putida* KT2440 depolymerizing *mcl*-PHA during carbon limitation (Karmann *et al.*, 2017).

Depending on the type of substrate (and initial its concentration), mode of cultivation, and native or engineered strain, different *mcl*-PHA production performances have been reported in previous studies. For example, in the seminal work of (Linger *et al.*, 2014) 150 mg L^{-1} mcl-PHA at 36 % CDW was achieved from a representative aromatic substrate (2 g L^{-1}) during a batch cultivation of a wild-type strain of *P. putida* KT2440. Recently, combining fed-batch cultivation and metabolic engineering of the same strain delivered 953 mg L^{-1} *mcl*-PHA at 54 % CDW from p-coumarate as single substrate (approx. 8 g L^{-1})(Salvachua *et al.*, 2020). The values obtained in this work (582 mg L^{-1} *mcl*-PHA at 43 % CDW) from mixed lignin aromatics (5 g L^{-1}) and performing only a batch cultivation with the native strain sit in the middle. However, through combining metabolic engineering and the presented process optimization strategy a further increase is very likely, which was proven in the next section.

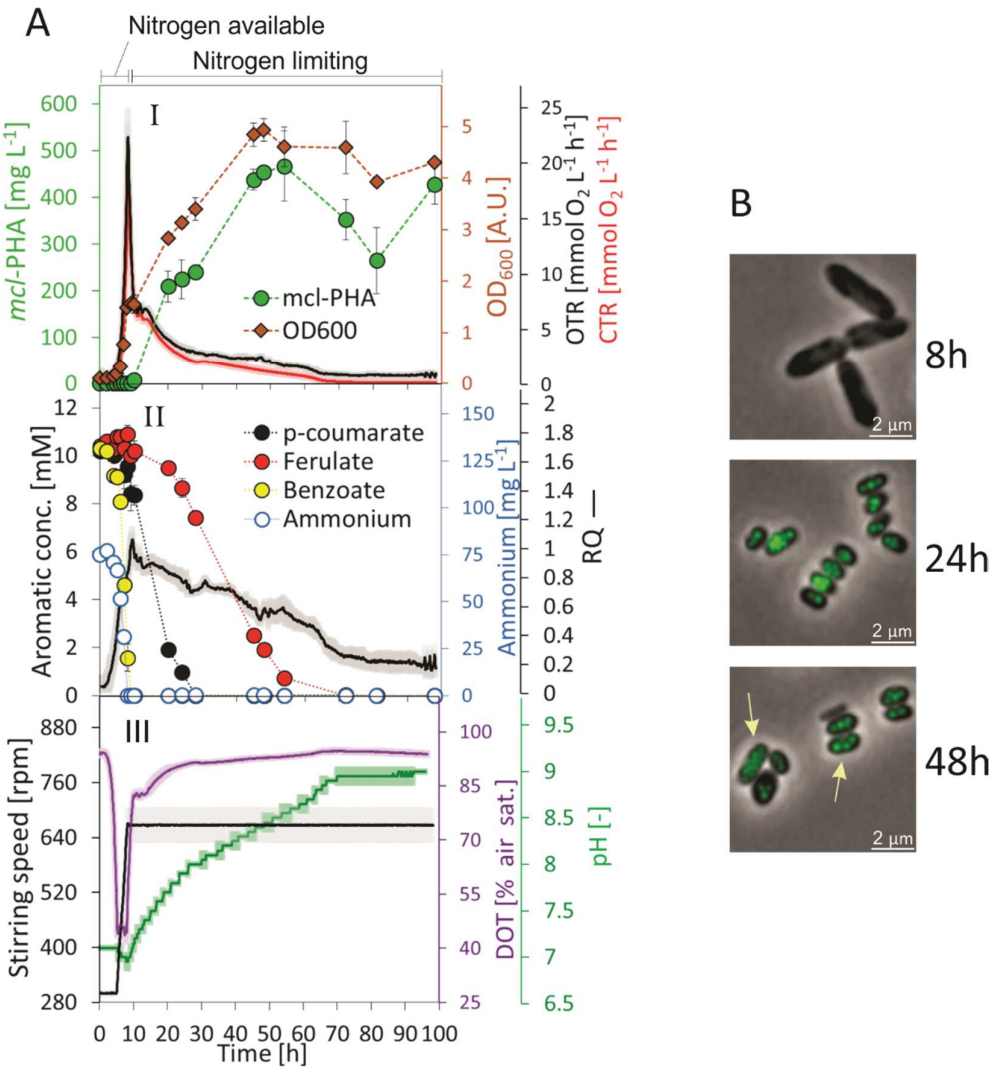

Fig 4.3 Scale-up based on the oxygen transfer rate in a stirred tank bioreactor. The dynamic change (A) of *mcl*-PHA concentration and OD_{600} (III), aromatic and ammonium concentration (IV) can be correlated to operational parameters like stirring speed, dissolved oxygen tension (DOT) and pH (V). The parameters OTR (III), CTR (III), and respiratory quotient (RQ) (IV) were calculated from off-gas composition analysis (section 2.7.5). Error bars indicate the deviation of the mean (n = 2). Microscopic captures of *mcl*-PHA accumulation at selected time points (C). Arrows at 48h indicate different number of *mcl*-PHA granules.

4.3.3 A case of simultaneous biocatalyst and bioprocess optimization

To optimize microbial metabolism towards higher *mcl*-PHA productivities and improved structural features, a diverse set of strategies have been implemented. Although modifications of regulatory circuits involved in the control of *mcl*-PHA metabolism have a great potential (Velázquez-Sánchez *et al.*, 2020), most of the predominant strategies have focused on improving the conversion efficiency, polymer quality and polymer storage capacity. Some of these include: Deletions or overexpression of key enzymes of the β oxidation pathway to redirect carbon flux (*i.e.,* monomers) and reducing equivalents (*i.e.,* NADH or NADPH), stabilization of polymer molecular weights, acceleration of cell growth,

improving cell morphology to increase granule storage and eliminating the ability of polymer self-degradation (Chen and Jiang, 2017; Chen and Jiang, 2018). In strains like *P. putida*, this last approach consist on deleting the *mcl*-PHA depolymerase gene *phaZ* (de Eugenio *et al.*, 2007), which has been reported to increase *mcl*-PHA production from conventional substrates like glycerol and octanoate (Cai *et al.*, 2009; de Eugenio *et al.*, 2010; Poblete-Castro *et al.*, 2014a).

As it was observed when comparing shake flask cultivations and bioreactor operation, faster dynamics involving *mcl*-PHA polymerization and depolymerisation can occur. This behaviour has been reported in *P. putida* as a tight regulation of PHA polymerase and depolymerase activities that act in synergy to provide polymer synthesis while ensuring optimal carbon source management (Arias *et al.*, 2013). Thus, the effect of *mcl*-PHA depolymerization can be more pronounced during carbon limitation (Karmann *et al.*, 2017). For this reason, a new strain with a deletion of the *mcl*-PHA depolymerase gene *phaZ* (*P. putida* KT2440-KOZ1) was generated as a first step to establish an optimized host (for strain construction see Chapter 2, section 2.3.2). Comparative cultivations were run under the two best conditions found during the online measurements of the respiratory activity (OTR_{max}) and C/N ratios. In this case, a high OTR was promoted by filling shake flask up to 10 ml in C/N ratios of 40 and 60 for the native and modified strain.

A comparative process dynamics when deleting the activity of PhaZ (*mcl*-PHA depolymerase) at a C/N of 40 and 60 is shown in Fig. 4.4 and Fig. 4.5, respectively. For a C/N ratio of 40 a similar dynamic was observed in respect to the previous experiment carried out at the same culture conditions with the wild type strain up to 72 h (compare Fig. 4.1A (I-IV) and Fig.4.4 (I-IV)). The differences in OTR_{max} (24.2 vs 23.5 mmol O_2 L^{-1} h^{-1}) reached were low, which highlight the reproducibility of the experiments. However, after 72 h, a rapid decrease of OD_{600} was observed. The drop of biomass signal is a common response to carbon depletion in *P. putida* KT2440, which is reflective of flocculation or biofilm formation and the changes in optical density are less reliable. Nevertheless, from the cell dry weight analysis, it was confirmed that biomass was indeed affected. The starvation stage that cells face led to a degradation of endogenous material, including *mcl*-PHA. Degradation of biomass and biopolymer was correlated with a linear increment of the integral OTR and CTR (Fig. 4.4 and 4.5 (I)). These parameters account for the accumulative consumption of oxygen and production of carbon dioxide, respectively and reflect the metabolic activity that was still slightly active after carbon depletion. The cultivation of the native strain at C/N 60 also showed a similar dynamic in respect to the previous experiment up to 72 h (compare Fig. S4.2A (I-IV) and Fig. 4.5 (I-IV)). But in this case, although a slight increment of integral OTR and CTR and the reduction of biomass and *mcl*-PHA also occurred, all were less pronounced, which indicates that the cultivation condition were less problematic after 72 h, which was not tested in the previous experiments. Possibly, the combination of aromatics, nitrogen and oxygen at this condition promoted an optimal carbon source management in terms of *mcl*-PHA accumulation.

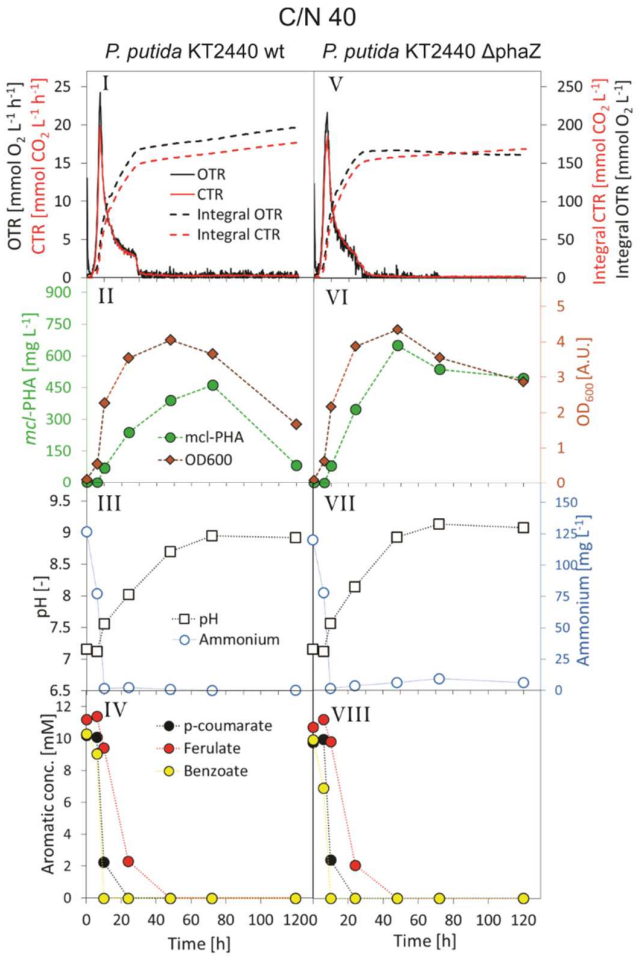

Fig. 4.4 Comparative process dynamics of deleting *phaZ* (*mcl*-PHA depolymerase) on *mcl*-PHA accumulation at a C/N of 40. Cultivations of *P. putida* KT2440 wt (I – IV) and *P. putida* KT2440 Δ*phaZ* (V – VIII) were out under nitrogen limitation with CFB 30 mM in Hartman's mineral salt medium. OTR_{max} of 24.2 and 21.6 mmol O_2 L^{-1} h^{-1} were achieved for filling volumes of 10 ml in both strains, respectively. Process parameters like the integral of OTR and CTR (I and V), *mcl*-PHA concentration and OD_{600} (II and VI), pH and ammonium concentration (III and VII), and aromatic concentration (IV and VIII) are reported.

The dynamics of the corresponding parallel cultivations with the strain lacking *mcl*-PHA depolymerase showed an increment on polymer accumulation up to 72 h in respect to the cultures of the wild type for both C/N ratios. As stated previously, depolymerisation is also active during the stages of prevalent *mcl*-PHA synthesis (Arias *et al.*, 2013) and the net effect was seen as higher polymer accumulation. Even better, after carbon source depletion (72 to 120 h), the endogenous polymer degradation was clearly avoided in comparison with the wild type strain for both C/N ratios. In this case, parameters like integral OTR and CTR (Fig. 4.4 and 4.5 (V)) did not show the same slight increment observed before for the wild type, which confirm the lack of metabolic activity while conserving the valuable product almost intact.

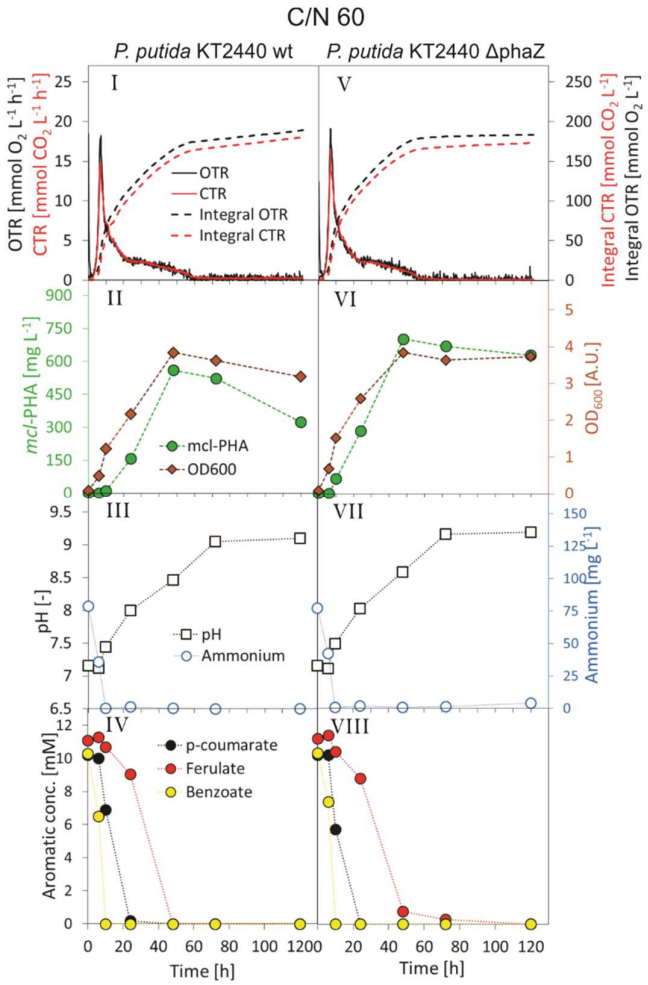

Fig. 4.5 Comparative process dynamics of deleting *phaZ* (*mcl*-PHA depolymerase) on *mcl*-PHA accumulation at a C/N of 60. Cultivations of *P. putida* KT2440 wt (I – IV) and *P. putida* KT2440 Δ*phaZ* (V – VIII) were out under nitrogen limitation with CFB 30 mM in Hartman's mineral salt medium. OTR_{max} of 18.2 and 19.1 mmol O_2 L^{-1} h^{-1} were achieved for filling volumes of 10 ml in both strains, respectively. Process parameters like the integral of OTR and CTR (I and V), *mcl*-PHA concentration and OD_{600} (II and VI), pH and ammonium concentration (III and VII), and aromatic concentration (IV and VIII) are reported.

Interestingly, for both ratios (although more pronounced for C/N of 40), residual amounts of ammonium were observed during the stationary phase (i.e., carbon starvation), which may be related to proteolysis during endogenous activity. Thus, the bacterial cultures lacking *mcl*-PHA depolymerise may not be able to easily re-consume the released ammonium due to lack of carbon (i.e., caused by a blocked capability to re-generate it from the polymer).

The overall effect of deleting *phaZ* on *mcl*-PHA concentration and content after 120 h is shown in Fig 4.6. A 5.8-fold increment in *mcl*-PHA concentration and a 3.5-fold increment in *mcl*-PHA content respect the wild type strain were obtained after 120 h for a C/N of 40. In the case of C/N 60, a 1.9-fold increment in *mcl*-PHA concentration and a 1.5-fold increment in *mcl*-PHA content were obtained after 120 h. For this last condition, it corresponded to a maximum *mcl*-

PHA concentration of 624 ± 9.2 mg L^{-1} and a maximum *mcl*-PHA content of 44.8± 9.2 % [mg *mcl*-PHA mg CDW] L^{-1}], respectively. These results demonstrate the benefits when simultaneous biocatalyst and bioprocess optimization strategies work along. Similar cases have been implemented in previous studies on lignin aromatics involving metabolic and process synergetic improvements. For instance, when applying deletions of the *mcl*-PHA depolymerase and the genes involved in β-oxidation (*fadBA1* and *fadBA2*) and overexpressing *phaG*, *alkK*, *phaC1* and *phaC2* in *P. putida* KT2440, Salvachua *et al.*, 2020 obtained 953 mg L^{-1} *mcl*-PHA at 54 % CDW from 8 g L^{-1} p-coumarate. In other study, a strain of *P. putida* H lacking *catA2* gene for balancing carbon flux between the parallel catechol-degrading routes enabled a *mcl*-PHA titre of 6.1 g L^{-1} in a fed-batch cultivation with stages of exponential and linear feeding of benzoate (Borrero-de Acuña *et al.*, 2020).

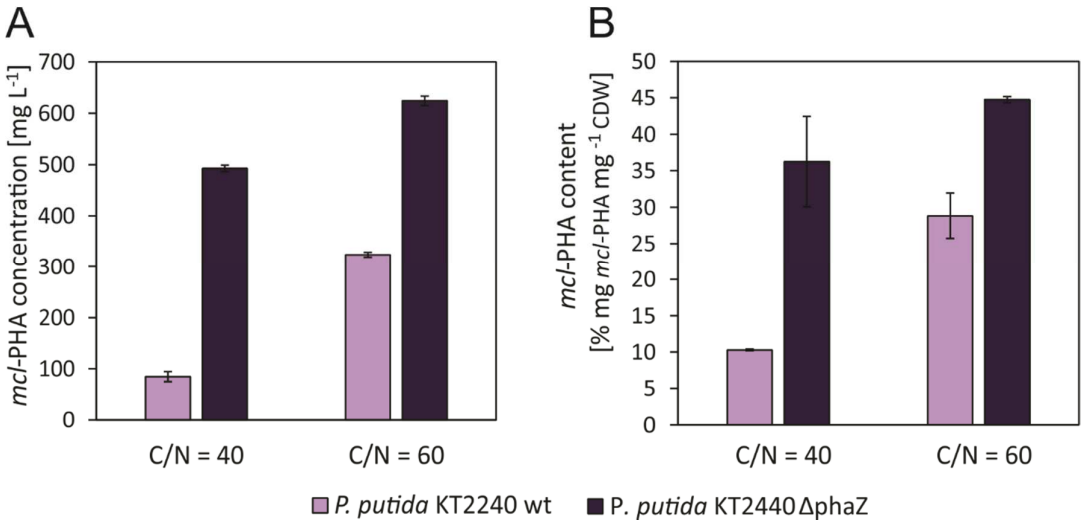

Fig. 4.6 Overall effect of deleting *phaZ* (*mcl*-PHA depolymerase) on *mcl*-PHA accumulation after 120 h. *mcl*-PHA concentration (A) and content (B) are presented. Cultivations of *P. putida* KT2440 wt and *P. putida* KT2440 ΔphaZ were carried out under nitrogen limitation at C/N 40 and 60 and CFB 30 mM in Hartman's mineral salt medium. Error bars indicate the deviation of the mean (n = 2).

4.4 Conclusion

Through a workflow involving different scale cultivations combined with online and offline performance analysis, this study acquired valuable information about the bio-catalytic capability in *P. putida* KT2440 for funneling lignin-derived aromatics into *mcl*-PHA. From careful bioprocess observation and control, the performance of cells funnelling a lignin aromatic mixture into *mcl*-PHAs under nitrogen limitation became predictable. Thus, the complexity of dealing with heterogeneous lignin-derived aromatic mixtures and simultaneous nutrient limitations can be greatly reduced. Additionally, the reproducibility should increase in future studies when warranting proper oxygen supply, especially during comparative microtiter and flask cultivations. By increasing the scale of production in bioreactors, the appropriate OTRs will be an important parameter for improving process performance and operational costs. Finally, the benefits of implementing simultaneous biocatalyst and bioprocess optimization strategies were demonstrated when obtaining a 1.9-fold increment in *mcl*-PHA concentration and a 1.5-fold increment in *mcl*-PHA content from lignin aromatics.

Chapter 5: *In-line* electrolytic membrane extraction of *cis,cis*-muconate produced by a metabolically engineered strain of *P. putida* KT2240

Contributions:

Phillip Czichowski assisted with genetic engineering procedures. Mohammad Sanowar Hossain performed clone selection experiments, executed electrolytic extractions using fermentation broths and assisted in fermentation runs. Juan E. Ramírez performed most of the experiments and together with José M. Carvajal, Korneel Rabaey and Miriam Rosenbaum designed the experiments and analyzed the results

5.1 Abstract

The development of sustainable and efficient processes to convert renewable feedstocks like lignocellulosic biomass into marketable chemicals is decisive for a successful transition into a biobased economy. Muconic acid has become an attractive alternative to fossil-based precursors of relevant molecules like adipic acid, terephthalic acid, and caprolactam, which are intensively used in the polymer industry. Through simultaneous efforts on metabolic engineering of *Pseudomonas putida* and bioprocess development, significant progress has been made on bioproduction of the isomer *cis,cis*-muconic acid from lignin-derived aromatic substrate. However, concentrations and productivities are still low for implementing an industrial process. High levels of *cis,cis*-muconic acid have been identified as a liming factor triggering product toxicity and inhibition in cultivations of *P. putida*. On this concern, this work presents an integrated bioprocess for in-line extraction of *cis,cis*-muconate from a bioreactor to alleviate the negative effect of product accumulation. Through a systematic approach, an extractive process and a conventional cultivation were characterized separately and then combined solving relevant technical drawbacks on the process development path. During the electrolytic extraction from a synthetic solution a maximum flux of *cis,cis*-muconate (2.54 Kg m^{-2} d^{-1}) was obtained at a current density of 66.7 mA m^{-2}, while the Coulombc efficiency was 59 %. With real fermentation broth, implementation of a pH controlled strategy avoided total precipitation of *cis,cis*-muconic acid in the anolyte and enabled it´s accumulation. In parallel, a conventional bioprocess with a metabolically engineered strain of *P. putida* KT440, reached a volumetric productivity of 1.74 g L^{-1} h^{-1} *cis,cis*-muconate from benzoate. Finally, by integrating the two systems the overall volumetric productivity of *cis,cis*-muconate increased 15.6 % in respect to a conventional bioprocess without extraction run in parallel. Although this first approach can still be further optimized, this study demonstrates for the first time the potential of *in-line* removal of *cis,cis*-muconic acid in a microbial cultivation and contributes as an important step towards implementing a cost-effective biological lignin valorization.

5.2 Introduction

A successful transition of the current chemical industry, which is grounded on fossil feedstocks, to a biobased economic model requires a substantial transformation of the production processes in conventional chemical chain supplies. A central bottleneck in this transition relies on the development of sustainable processes to generate new or advantaged molecules that compete with the oil-based analogues. Thus, considerable efforts have been focused towards efficient conversion of renewable feedstocks like lignocellulosic biomass into market relevant chemicals (Becker and Wittmann, 2019; Johnson *et al.*, 2019; Yu *et al.*, 2020).

Muconic acid is one of the outstanding examples with a remarkable potential to become a direct precursor of industrially relevant derivates (*i.e.,* chemical commodities for polymer synthesis) like adipic acid, terephthalic acid, and caprolactam (Carraher *et al.*, 2017; Skoog *et al.*, 2018). This compound presents a 6-carbon skeleton, two conjugated double bonds in the middle and two reactive carboxylic functional groups at both ends. These properties make it a high value-added molecule with a suitable chemical platform. Due to this potential, a global market rise to more than 110 million USD is expected in 2024 with an increasing demand of about 3 to 5% over the next five years in the industrial sector of textiles (Khalil *et al.*, 2020). However, traditional production ways of producing muconic acid or derivates like adipic acid relies on chemical transformation of non-renewable petroleum-based feedstocks. In addition, most of the precursors or by-products generated during such processes represent environmental hazards (*i.e.,* phenol, N_2O, cyclohexane, cyclohexanol, and cyclohexanone from benzene) (Aryapratama and Janssen, 2017; Skoog *et al.*, 2018). For these reasons, there is an eager motivation to establish less harmful and more sustainable processes that fit with the concept of biobased production.

Biological production of muconic acid could meet the requirements set by a growing bioeconomy when using the different fractions of lignocellulosic feedstocks as substrates. Consequently, important research efforts have been focused on establishing cost-effective biotechnological process. Muconic acid presents three isomeric configurations designated *cis,cis*-muconic acid, *cis,trans*-muconic acid and *trans,trans*-muconic acid, of which the first two forms are commonly found during microbial synthesis depending on the culture pH (Khalil *et al.*, 2020). The conversion of different aromatic substrates into *cis,cis*-muconic acid occurs via catechol ortho-cleavage pathway via the catechol 1,2-dioxygenase (EC 1.13.11.1, CatA), either through native aromatic catabolic pathways or by construction of artificial networks in different types of microorganisms (Xie *et al.*, 2014).

The biocatalytic synthesis of *cis,cis*-muconic acid from D-glucose was first demonstrated in an engineered *Escherichia coli* strain by Draths and Frost, 1994. They connected a heterologous aromatic branch to a blocked shikimic acid pathway, reaching a conversion efficiency of 30%. In addition to the potential pathways from sugars, microbial synthesis of *cis,cis*-muconic acid

from lignin-streams or aromatic compounds can be achieved in bacterial strains with a robust and native aromatic degradation ability like *Pseudomonas putida*. In this case, the accumulation of *cis,cis*-muconic acid occurs upon disruption of catabolic route at the *cis,cis*-muconate cycloisomerase point of the catechol degradation branch (van Duuren *et al.*, 2011). Additionally, a further range of aromatic substrates can be converted linking the protocatechuate branch of the β-ketoadipate pathway with the catechol branch by insertion of the gene *aroY* from *Enterobacter cloacae* and simultaneously disrupting the protocatechuate degradation (see Chapter 2, Fig. 2.3) (Vardon *et al.*, 2015). From these important contributions further approaches in metabolic engineering have been evaluated to improve the same strains or other bacterial hosts like *Saccharomyces cerevisiae*, *Corynebacterium glutamicum, Amycolatopsis sp., Sphingobium paucimobilis* and *Klebsiella pneumoniae*, which have been well summarized in relevant reviews (Xie *et al.*, 2014; Becker and Wittmann, 2019; Choi *et al.*, 2020).

The optimization of rational metabolic approaches to construct robust *P. putida* biocatalysts need to work concurrently with bioprocess development strategies to establish cost-effective biological lignin valorization. Thus, it is necessary to achieve relevant product concentration, yields, and productivities, similarly to the ones achieved from carbohydrate fractions of lignocellulosic biomass. In this regard, significant process advances have been achieved on *cis-,cis*-muconic acid production to avoid substrate toxicity by establishing fed-batch controlled strategies. DO-stat fed-batch systems have been applied for accurate dosing of aromatics based on the depletion of oxygen, reaching final *cis,cis*-muconic acid concentrations and volumetric productivities up to 50 g L^{-1} and 2.2 g L^{-1} h^{-1}, respectively (Bang and Choi, 1995; Vardon *et al.*, 2015; Salvachúa *et al.*, 2018). Analogously, feeding strategies to prevent substrate overdoses based on the pH drop induced by product formation (*i.e.,* pH-stat fed-batch) have been also established obtaining higher concentrations (64.2 g L^{-1}) and volumetric productivities (4.5 g L^{-1} h^{-1}) (van Duuren *et al.*, 2012; Kohlstedt *et al.*, 2018). Linear and high-pH feeding strategies also improved the process performance when using hydroxycinnamic acids like p-coumaric acid and ferulic acid (Salvachúa *et al.*, 2018). However, the highest volumetric productivity (*i.e.,* 5.5 g L^{-1} h^{-1}) has been obtained in a continuous mode system at high cell density based on membraned biomass retention (40g L^{-1}) yielding a *cis,cis*-muconic acid effluent of 12 g L^{-1} (Choi *et al.*, 1997). Finally, simultaneous efforts on bioprocess development and metabolic engineering achieved relevant progress on bottlenecks related to accumulation of intermediates like 4-hydroxybenzoate, vanillate and catechol (Kohlstedt *et al.*, 2018; Salvachúa *et al.*, 2018).

Despite of the important progress to improve *cis,cis*-muconic acid production, further efforts are necessary to evaluate product toxicity limits and strategies to overcome them. It is known that *P. putida* stands out as a highly tolerant strain to overcome some toxic aromatics and stressful environmental conditions (Belda *et al.*, 2016; Kusumawardhani *et al.*, 2018). Nevertheless, it's tolerance machinery and intrinsic aromatic catabolic regulation may be

seriously affected at high concentration of *cis,cis*-muconic acid (Salvachúa *et al.*, 2018). For instance, a study pointed out the effect of *cis,cis*-muconic acid concentration on the specific enzymatic activities of catechol 1,2-dioxygenase, finding an optimal concentration of 12 g L^{-1} and detrimental enzymatic synthesis at higher levels (Choi *et al.*, 1997). In other research, it was shown that the maximum specific growth rate of the strain *P. putida* KT2440-JD1 decreased by 50% at 300 mM (42 g L^{-1}) product concentration, while growth no longer occurred at concentrations higher than 84 g L^{-1} (van Duuren *et al.*, 2012). Additionally, they found an optimal specific uptake rate of benzoate (q_{sb}) at 14.2 g L^{-1} of *cis,cis*-muconic acid, after which q_{sb} decreased to become completely arrested at 34 g L^{-1}. Similarly, a recent study found metabolic intermediates accumulation at *cis,cis*-muconic acid concentrations higher than 25 g L^{-1} when increasing feeding rates of p-coumaric acid to improve volumetric productivities (Salvachúa *et al.*, 2018). These observations suggest that there is still room for improvement by implementing strategies that maintain optimal *cis,cis*-muconic acid levels in the culture, inducing relevant enzymatic activities and finally achieving higher production rates.

A well-established strategy to alleviate the effects of product accumulation through continuous removal during bioconversions is *in-situ/in-stream* product recovery (ISPR) process (Santos *et al.*, 2021). Several applications of extractive fermentations and ISPR led to significant increment in yields and productivities and the in-line integration of fermentation and separation decreased downstream operational costs (Van Hecke *et al.*, 2014). An attractive group of techniques that have been applied in recent years to separate organic acids are based on electro-migration of ions through selective ion exchange membranes (IEMs) (López-Garzón and Straathof, 2014; Handojo *et al.*, 2019). Particularly, extractive membrane electrolysis stands out by its simple operation promoting the flux of charged products across a single IEM. It has been successfully integrated with mixed cultures producing carboxylates (Andersen *et al.*, 2014; Andersen *et al.*, 2015; Gildemyn *et al.*, 2015). This novel process is driven by the electrolysis of water when applying a constant current between the cathode and the anode and retaining solids or biomass in the catholyte (see Fig. 5.2). Thus, the extracted product accumulates in a clean and low pH anolyte while hydroxide ions can replace caustic soda management enabling *in-line* pH control in a carboxylate producing fermentation. These advantages have been recently applied in a fed-batch fermentation of *Basfia succiniciproducens*, where the succinic acid productivity increased by 30% (Pateraki *et al.*, 2019).

In this chapter, a process development approach was implemented towards *in-line* electrolytic membrane extraction of *cis,cis*-muconate produced by a metabolically engineered strain of *P. putida* KT2240. First, the process performance of *cis-,cis*-muconic acid extraction was evaluated in terms of rates and efficiency. Later on, a conventional bioprocess for *cis,cis*-muconic acid was established and real fermentation broths were tested. Finally, a

set-up coupling the fermenter and extractive unit was performed and future improvements towards increasing productivities of the *in-line* integrated bioprocess are discussed.

5.3 Results and discussion

To integrate the electrolytic extraction of *cis,cis*-muconic acid to a bioreactor requires different steps of process development to warrant a proper operation of the combined system. The next sections describe these relevant steps, starting with the selection of a commercial AEM, defining a conventional bioproduction process, evaluating the electrolytic extraction from fermentation broths and finally coupling the cell to a bioreactor.

5.3.1 Characterization of cis,cis-*muconate extraction from synthetic media and selection of a commercial membrane*

On the market different anion exchange membranes are available and show advantageous characteristics for specific applications. Selective performance and chemical stability are some of the most relevant parameters (Hagesteijn *et al.*, 2018). For this reason, four suitable commercial AEMs (for specific features see Table 2.3) were evaluated in terms of flux and Coulombic efficiency for the main charged species involved in the electrolytic extraction (see Chapter 2, Fig. 2.8). Thus, a synthetic solution was prepared to simulate a model fermentation broth and the representative components *cis,cis*-muconate, PO_4^{3-}, SO_4^{2-}, and K^+ were evaluated. The Coulombic efficiency and flux of the most concentrated ionic species (*i.e., cis,cis*-muconate and PO_4^{3-}) during the extraction are shown for the four AEMs in Fig 5.1. The extractions were carried out using duplicate low volume cells at a current density of 33 A m^{-2}, 50 mM (7.1 g L^{-1}) *cis,cis*-muconic acid, 16mM (1.6 g L^{-1}) SO_4^{2-} and 32 mM (3.1 g L^{-1}) PO_4^{3-}. These conditions were similar to those expected in a final *in-line* extraction. However, to avoid mass transfer limitations created by reverse transport of *cis,cis*-muconate, continuous flow of anolyte was permitted.

The best performing membranes for the target molecule *cis,cis*-muconate were AM-7001S and Fujifilm Type II, presenting a very similar performance with transport efficiencies of 48.2 ± 1.9 and 49.7 ± 3.9%, respectively (Fig 5.1A). The flux for the same membranes were 1.02 ± 0.04 and 1.05 ± 0.08 Kg m^{-2} d^{-1}, respectively. The higher extraction efficiency of *cis,cis*-muconate was expected, as this component was present at higher molar concentration. The other two membranes performed worse for *cis,cis*-muconate, which was reflected in higher Coulombic efficiencies and flux of PO_4^{3-} (Fig 5.1B), especially for the membrane PC-200 D. Although its use is recommended with medium sized organic anions (information found in the technical data sheet), it is not totally clear why it resulted more selective for PO_4^{3-}. Other relevant concentrations of ions in the catholyte like SO_4^{2-} and K^+ are shown in Fig. 5.2A and 5.2B. During the first 2 h, the levels of SO_4^{2-} changed slightly. However, after this, the concentration started to raise reaching values 65% higher than the starting conditions. In the case of K^+, the concentrations were kept constant for all membranes.

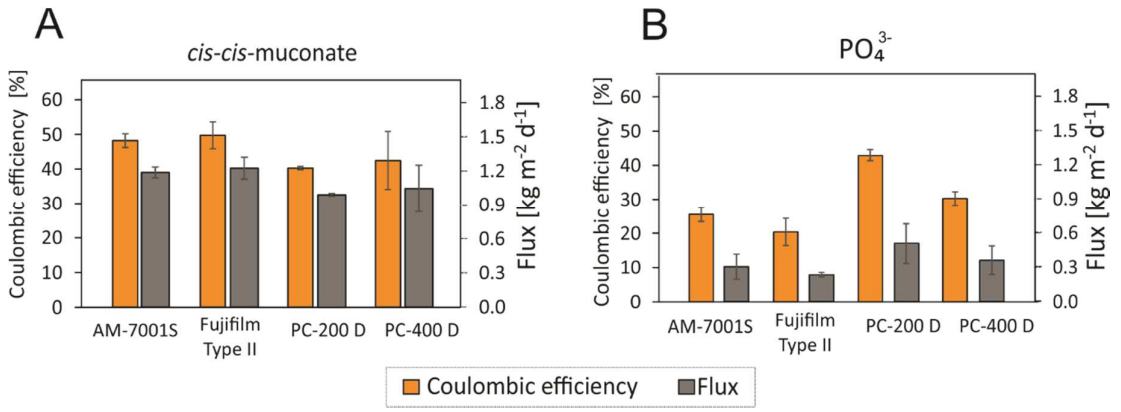

Fig. 5.1 Electrolytic extraction of *cis,cis*-muconate (A) and PO_4^{3-}(B) from the same solution using different commercial anion exchange membranes (AEMs). Tests were run at 33 A m^{-2} and 50 mM (7.1 g L^{-1}) *cis,cis*-muconic acid. Solution flow was 3 L h^{-1}. The initial concentration of PO_4^{3-} was 32 mM (3.1 g L^{-1}). Error bars indicate the deviation of the mean (n = 2).

Although it is apparent that higher molecular availability (molar concentration) of *cis,cis*-muconate (50 mM) vs. PO_4^{3-}(32 mM) promoted higher flux and Coulombic efficiencies of the target anion, special care must be taken when providing phosphorous sources in the culture media or feed solutions. With its simultaneous function as buffer component and essential nutrient for microorganisms, future process optimization may denote differences on the cultivation performance in the integrated bioprocess. The flux mechanisms and accumulation of relevant ions are shown in Fig. 5.2C. The flux of *cis,cis*-muconate, SO_4^{2-} and PO_4^{3-} (Fig. 5.2C (I)) is a result of the charge balance promoted by the applied current. The amount of Coulombs invested to transport these species resulted in the different extraction efficiencies observed. In addition to the net diffusion effect, accumulation of SO_4^{2-} after 2 h occurred also due to addition of H_2SO_4 to neutralize the OH^- produced at the cathode. Here, a proton flux from the anolyte was promoted to balance the accumulation of SO_4^{2-}, which may limit Coulombic efficiencies due to more ion competition (Fig. 5.2C (II)). This occurred because all the commercial membranes used are susceptible to proton flux. Finally, cations like K^+ or Na^+ are nearly blocked by the selective feature of all commercial AEMs Fig. 5.2C (III).

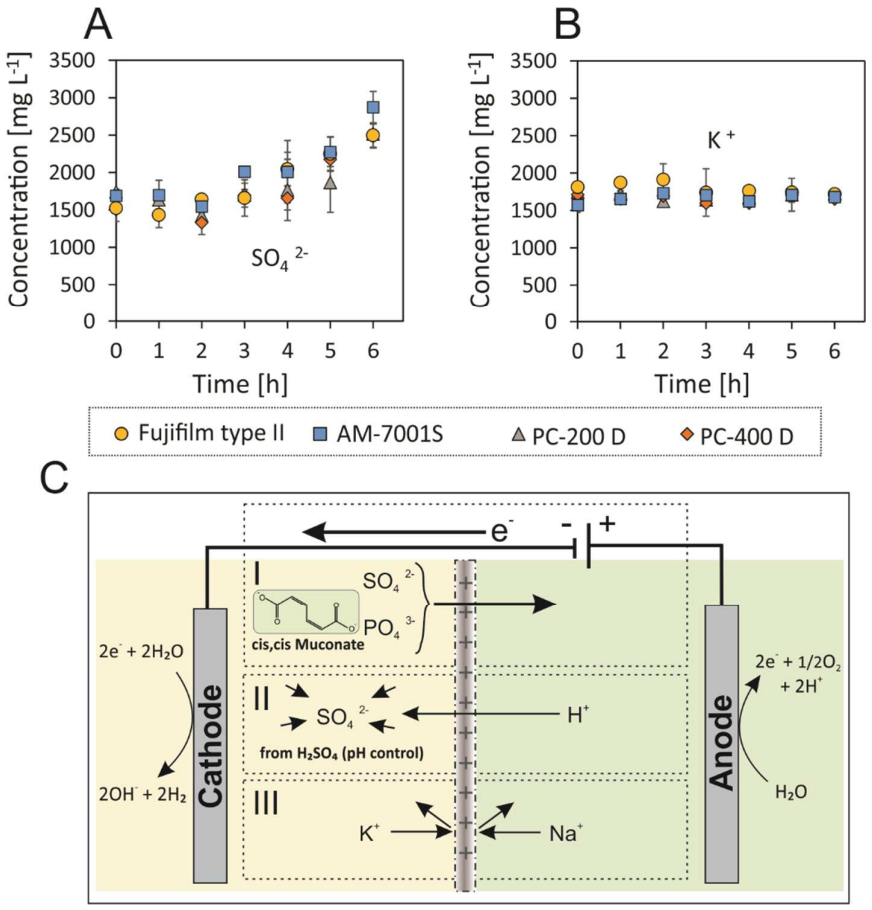

Fig. 5.2 Concentration profile of SO_4^{2-} (A) and K^+ (B) in the catholyte using different commercial anion exchange membranes. Tests were run at 33 A m^{-2} and 50 mM *cis,cis*-muconic acid. Solution flow was 3 L h^{-1}.Transport and accumulation of the main charged species involved (C) were adapted from Andersen *et al.*, 2014. Error bars indicate the deviation of the mean (n = 2).

Due to the small difference in extraction performance between the AM-7001S and Fujifilm Type II membranes, the first membrane was selected based on stock availability and reliable experience. With this membrane, an additional range of concentrations and current densities were evaluated. The obtained flux and extraction efficiencies profiles are sown in Fig. 5.3.

Increments of *cis,cis*-muconate flux were achieved when the initial concentration and current densities were increased (*i.e.,* from 20 to 100 mM and 13.3 to 66.7 mA m^{-2}, respectively). A maximum flux of 2.54 ± 0.18 kg m^{-2} d^{-1} was obtained at 66.7 mA m^{-2} and a starting concentration of 100 mM (14.2 g L^{-1}). This rate of extraction at this concentration is a relevant parameter for the process design and development. It can be used to estimate the effective area of the extractive cell for a specific extraction requirement to promote product removal for optimal bioproduction. In fact, at 100 mM (14.2 g L^{-1}) *cis,cis*-muconate, two previous studies have reported the best enzymatic performance of catechol 1,2-dioxygenase (catechol cleavage to *cis,cis*-muconate) and optimal specific uptake rate of benzoate (q_{sb}) in a *P. putida* production processes (Choi *et al.*, 1997; van Duuren *et al.*, 2012). The Coulombic efficiency also increased at the higher initial *cis,cis*-muconate concentrations. A maximum value of 67 ±

1.2 % was obtained at 13.3 mA m^{-2} and 100 mM *cis,cis*-muconate. At higher current densities the Coulombic efficiency slightly decreased for all concentrations evaluated. To overcome this issue and manage higher Coulombic efficiencies, proton-blocking AEMs membranes like FumaTech fumasep (FAB) can be implemented and the salinity of the anolyte can be increased (Andersen *et al.*, 2014). In this way, less ion competition will promote higher extraction efficiencies.

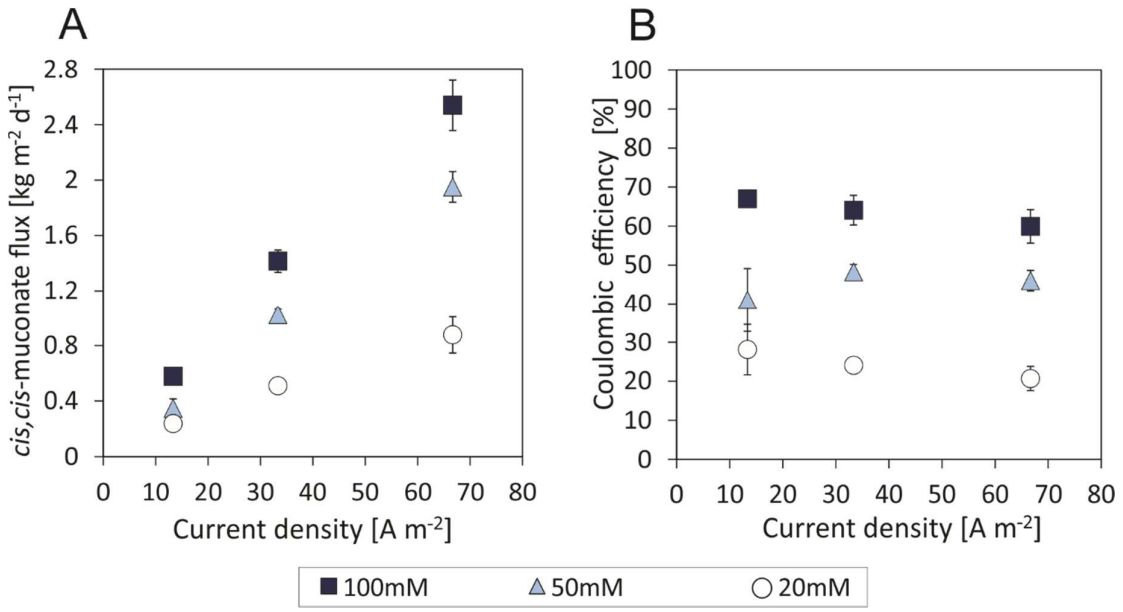

Fig. 5.3 Profiles of flux (A) and Coulombic efficiencies (B) during electrolytic extraction of *cis,cis*-muconate from synthetic salt medium at different starting concentrations and current densities (Section 2.5, Fig 2.8). The extractions were performed using the commercial membrane AM-7001S (effective area of 7.5 cm^2) at 20 °C, controlling the catholyte pH (7.0) and under continuous flow of anolyte (3 L h^{-1}) to avoid mass transfer limitations.

The recovery of *cis,cis*-muconate is frequently carried out after precipitation in acidic conditions (pH = 2.0) where it is fully protonated (Vardon *et al.*, 2015; Kohlstedt *et al.*, 2018). During and after extraction experiments, *cis,cis*-muconic acid precipitates were found at the walls of the anodic chamber, anode and membrane surface, which represented a considerable technical drawback. It can create transport limitations as the membrane resistance can increase due to scaling and promote undesired side reactions at the anode surface. Additional experiments evaluated the extraction performance of new, cleaned, and dirty membranes at 20 mM *cis,cis*-muconate and 33.3 mA m^{-2} (see Appendix Fig. S5.1). The cleaned ones corresponded to used membranes washed with a solution of 0.1 M NaOH for 20 min after one extraction test. Comparing the Coulombic efficiency and flux of the new and dirty membrane, both performance parameters decreased 17%, and the cleaned membrane sat in the middle. However, this loss of performance may be negatively amplified if the objective is to accumulate *cis,cis*-muconic acid in the anolyte. Thus, further strategies were implemented in the next sections to avoid total precipitation of the product at the different cell unit surfaces.

5.3.2 Defining a conventional bioprocess for cis,cis*-muconate production*

To accumulate *cis,cis*-muconate at high concentrations, fed-batch bioprocess operations have been established in combination with a controlled dose of aromatic substrates, which can be toxic at certain levels for *P. putida* (van Duuren *et al.*, 2012; Calero *et al.*, 2018). DO-stat feeding strategies have been applied previously to reach high *cis,cis*-muconate concentrations relying on the dissolved oxygen tension (Bang and Choi, 1995; Vardon *et al.*, 2015; Salvachúa *et al.*, 2018). However, the process productivities in this feeding strategy can be limited due to dead times corresponding to intervals where the dissolved oxygen tension increases after substrate consumption. For this reason, constant feeding strategies have been studied, setting a proper proportion of feeding solutions (*i.e.,* carbon and energy source and aromatics) to achieve faster bioproduction (Salvachúa *et al.*, 2018). A pH-stat strategy is advantageous for decoupling the feeding of aromatics from the nutrient solution (containing carbon and energy source). Thus, the aromatic substrate is replenished when the pH drops by *cis,cis*-muconate formation and the uncoupled feeding of the nutrient solution enables objective biomass growth achieving desired conversion rates (van Duuren *et al.*, 2011; Kohlstedt *et al.*, 2018). For these reasons, a pH-stat strategy was selected to characterize the production of *cis,cis*-muconate from benzoate by a metabolically engineered strain of *P. putida* KT2440 with glucose as carbon and energy source.

The used fed-batch system is shown in Fig. 2.9. The molecular biology procedures to generate the corresponding metabolically engineered biocatalyst (*i.e., P. putida* KT2440-CCMA1) can be found in Section 2.3.3. An exponential feeding rate of the nutrient solution was imposed to promote a specific growth rate (μ_{max}) of 0.04 h^{-1} using Eq. (13). Through the pH control, responding to *cis,cis*-muconate production, the feeding of benzoate was expected to be exponential too as a result of the bacterial self-regulation. The bioprocess performance over time is shown in Fig. 5.4A. The starting OD_{600} was 0.1 and after 3 h of batch operation, 1 mM of benzoate was added to induce *cis,cis*-muconate production (van Duuren *et al.*, 2012). The feeding stage started after 8 h (when O_2 off-gas started to rise, indicating glucose depletion) and continued up to 34 h. During this time catechol was not detected by the HPLC. The acidification of the culture was continuously neutralized by the addition of the alkaline benzoate solution (2.9 M NaOH) resulting in an exponential profile at the initial hours, which was recorded by an electronic balance. However, after 25 h, this profile turned automatically into a linear profile, which also coincided with abrupt changes in other parameters like O_2, CO_2, DOT, and stirring speed. At this point, the concentration of *cis,cis*-muconate was 195 mM (27.7 g L^{-1}), which increased to a maximum of 245 mM (34.8 g L^{-1}) at 28 h (100% conversion yield). After this point, benzoate and glucose started to accumulate in the media. Additional biomass growth occurred up to 31 h.

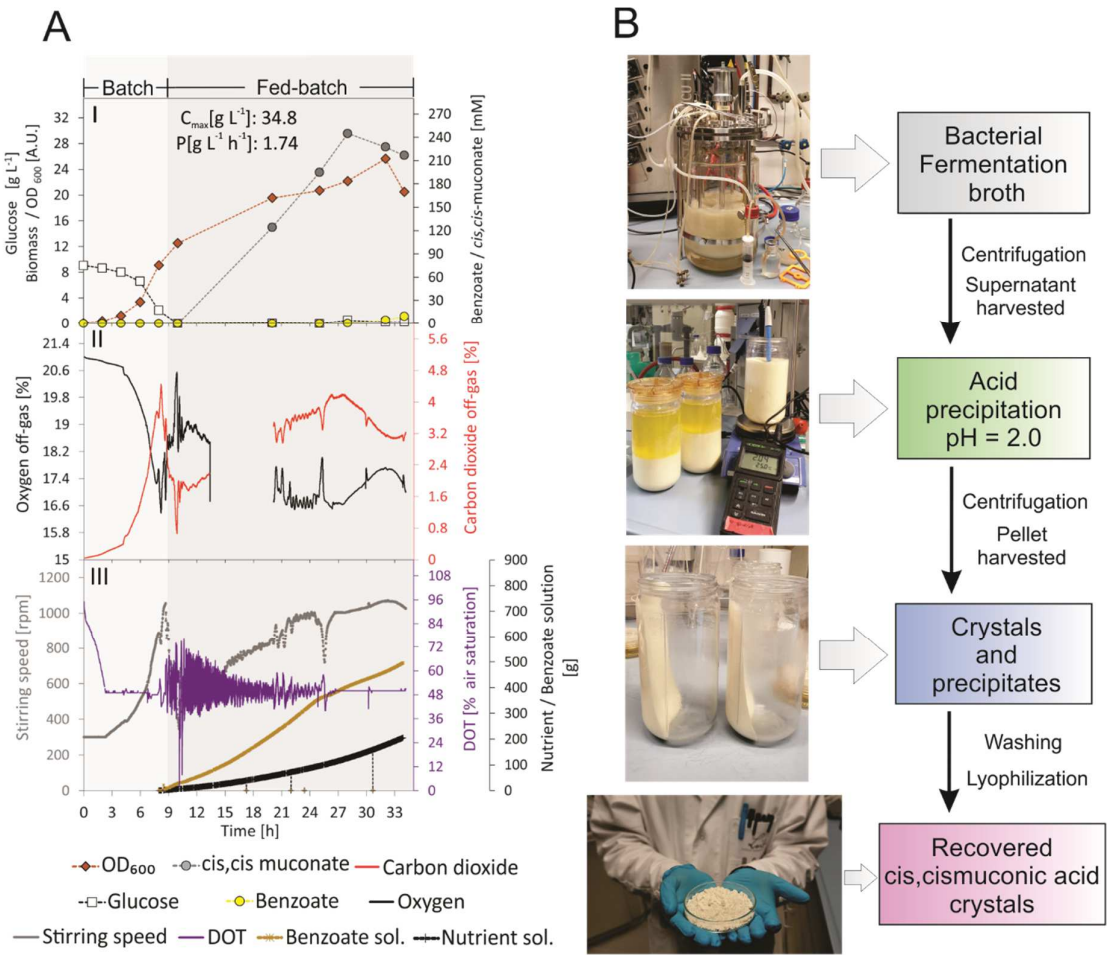

Fig. 5.4 Operational data of a conventional bioprocess for *cis,cis*-muconate production (A) and general workflow during downstream product separation (B). The pH-stat cultivation was carried out at 30 °C and an exponential feeding rate of nutrient solution was imposed to promote a specific growth rate (μ_{max}) of 0.04 h^{-1}. Maximum concentration (C_{max}) and volumetric productivities (P) are shown in graph (I). Additional operational parameters like off-gas composition (II) and stirring speed, dissolved oxygen tension (DOT), and continuous monitoring of feed solutions (III) were recorded. Off-gas data adquisition failed between 12 and 20h.

A comparison of the bioprocess performance with other similar studies involving *P. putida* as biocatalyst, fed-batch cultivation mode, and using benzoate as substrate is shown in Table 5.1. Although, this study achieved the highest volumetric (1.74 g L^{-1} h^{-1}) and a middle range final *cis,cis*-muconate concentration, the cell specific productivity was low (0.15 g L^{-1} h^{-1}) compared to studies that report this parameter, like van Duuren *et al.*, 2012. The difference may be related to the initial glucose concentration used here, which was 5 times more than other studies. In this way, it was able to start the feeding stage with higher biomass concentration and achieve higher volumetric productivities. The difference of the maximum *cis,cis*-concentration achieved may also be due to genotype variations of the strain. For example, the concentration achieved in the pH-stat system implemented by Kohlstedt *et al.*, 2018 with the strain *P. putida* KT2440 MA-1 was approximately 1.4 more than in this study. Their strain was generated by elimination of the genes *catBC*. However, in this study an

additional gene was deleted (*i.e., catR*) because of intended further strain development for additional aromatic utilization, similarly to Vardon *et al.*, 2015. This gene encodes for the regulatory protein CatR, which enables increased expression of the *catBCA* operon through binding to the promoter region (Rothmel *et al.*, 1991). This functions in paralell to the self-induction of the *catBCA* operon by *cis, cis*-muconate. Mutants deficient in CatR have shown accumulation of *cis, cis*-muconate from benzoate due to induction of *catA2*, an alternative catechol 1,2-dioxygenase besides the usual *catA* (van Duuren *et al.*, 2011; Jiménez *et al.*, 2014). In this work, the native promoter of the *catBCA* operon was replaced by the constitutive promoter $P_{tac,}$ to keep a strong expression of *catA*. Nevertheless, *P. putida* KT2440 MA-1 that holds the native *cat* promoter P_{cat} and *catR* seemed to achieve higher concentrations of *cis,cis*-muconate from benzoate. Although this strain can be susceptible to the intermediate catechol, this issue was elegantly solved by the authors including an additional *catA2* gene under P_{cat} control, enabling continuous induction by *cis,cis*-muconate (Kohlstedt *et al.*, 2018).

Table 5.1 Bioprocess performance of other studies involving *P. putida* as biocatalyst, fed-batch mode, and benzoate as aromatic substrate.

Strain	Fed-batch mode	Max. concentration [g L^{-1}]	Cell specific productivity [g g_{CDW}^{-1} h^{-1}]	Volumetric Productivity [g L^{-1} h^{-1}]	Reference
P. putida KT2440-JD1	pH-stat	18.5	0.6	0.8	van Duuren *et al.*, 2012
P. putida KT2440 MA-1	pH-stat	48	-	~0.88	Kohlstedt *et al.*, 2018
P. putida BM014	DO-stat	32.4	-	1.4	Bang and Choi, 1995
P. putida KT2440-CJ102	DO-stat	34.5	-	0.28	Vardon *et al.*, 2016
P. putida KT2440-CJ242	DO-stat	52.3	-	0.26	Salvachúa *et al.*, 2018
P. putida KT2440-CCMA1	pH-stat	34.8	0.15	1.74	This study

The bioprocess performance obtained in this step helped to plan the final in-line extraction process. The rate of *cis,cis*-muconate production during the fed-batch stage defines the needs for the electrolytic extraction. From the previous electrolytic process characterization (*i.e., cis,cis*-muconate flux) and the available effective AEM area, it is possible to estimate the current to be applied for maintaining proper *cis,cis*-muconate levels in an integrated culture with a defined bioreactor volume. However, until this point, the extraction tests were performed only on synthetic media and for this reason more extractions were conducted with real fermentation broths obtained from this stage. Therefore, part of the harvested supernatant was saved at 4 °C for further electrochemical extraction tests. The remaining culture broth was used for traditional downstream processing steps including acid precipitation and lyophilisation. This enabled a recovery and purity of 86% and 92% *cis,cis*-

muconate, respectively (Fig. 5.4B). The rest of the components corresponded to residual benzoic acid and salts.

5.3.3 Electrolytic extractions of cis,cis*-muconate from fermentation broths*

Once the bioprocess production rates were characterized and a real fermentation broth was available, a new lab-scale electrolytic cell with a higher volume chamber (200 ml) and surface area (100 cm^2) was evaluated. In a first step, the extraction performance between the new devices (*i.e.,* large volume or ``big cell´´) and the low volume cell (``small cell´´) previously evaluated with synthetic solutions were compared (Fig. 5.5). The extractions were carried out at an initial concentration of 50 mM *cis,cis*-muconate, 33 mA m^{-2} applied current density, and a flow of anolytes and catholytes of 3 L h^{-1}. A higher flux (1.29 ± 0.0 kg m^{-2} d^{-1}) and Coulombic efficiencies (61.34 ± 0.34 %) were obtained from a real fermentation broth respect to the tests performed with synthetic solution at the same starting *cis,cis*-muconate concentration in the small cell (Fig. 5.3). This may be linked with higher available *cis,cis*-muconate in respect to other important ions like PO_4^{3-}, which are consumed as phosphorous source during the cultivation. However, with the increase of scale, the extraction performance decreased by 33 %, with a flux of 0.86 ± 0.07 kg m^{-2} d^{-1} and 40.7 ± 3.6 % Coulombic efficiency. A possible explanation may be associated with mass transfer limitations promoted by the different hydrodynamic conditions that can establish at the same solution flow in the big cell. Limiting a turbulent flow tends to enlarge the diffusion boundary layer that develops at the membrane surface in the big cell, decreasing the extraction performance, similar to as it has been observed in low salt concentration systems (Długołęcki *et al.*, 2010). Higher flow rates of solution should maintain performance with the scale-up of the cell, although it must be technically evaluated in terms of pump capacity and maximum operating pressure of the cell casing.

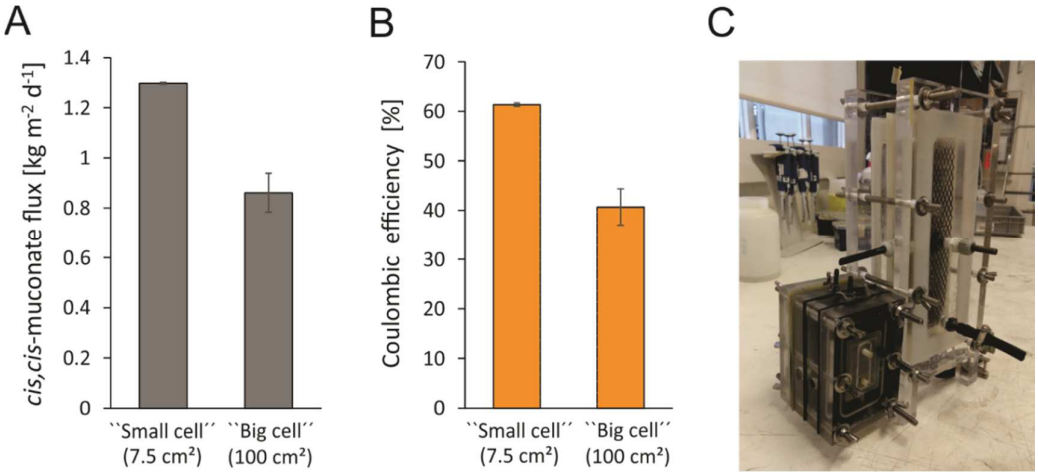

Fig. 5.5 Electrolytic extraction of *cis,cis*-muconate from a real fermentation broth using two lab-scale cells. Flux (A) and columbic efficiencies (B) for both cells were estimated from extractions carried out at 50 mM initial *cis,cis*-muconate, 33 mA m^{-2} applied current density, and a solution flow of a 3 L h^{-1} (Section 2.5, Fig 2.8). Error bars indicate the deviation of the mean (n = 2).

Because of the observed *cis,cis*-muconic acid precipitation at the equipment surfaces of (*i.e.,* tubing, cell chamber, membrane, anode and anolyte reservoir), an additional experiment was performed. The goal was to define a proper anolyte pH that enabled partial accumulation of the ionized form of *cis,cis*-muconate (*i.e., cis,cis*-muconic acid) in the anolyte but avoiding total precipitation at extreme low pH. For this the dissociation reactions were studied by titrating 60 mM of neutralized *cis,cis*-muconate with concentrated sulfuric acid to pH 2.0. The profile of the muconate forms (determined by HPLC) present in the supernatant is shown in the Appendix (Fig. S5.2). A typical sigmoid curve of pH-dependence was obtained for *cis,cis*-muconate speciation (Fig. S5.2A). At first side, an inflection point corresponding to the pH where the non-dissociated acid and dissociated form are in equilibrium (*i.e.,* acid dissociation constant or pK_a) was close to 4. However, an additional peak appeared in the HPLC chromatographs and the specific area presented a maximum level at the same pH. From knowledge recently generated regarding muconic acid isomeration, it was possible to determine that this peak corresponded to the isomeric form *cis,trans*-muconate. For example, similar findings were achieved in other studies stating that isomerization can be easily overlooked as both isomers present similar retention times during HPLC analysis. Additionally, they emphasized that the consequences are significant as the *cis*,*trans* isomer is five times more soluble at room temperature under acidic conditions than *cis*,*cis*-muconic acid (Carraher *et al.*, 2016). In a later study, the identity of this peak was confirmed by ^{1}H NMR spectra (Carraher *et al.*, 2017). Although, the last authors were unsuccessful to measure the corresponding acid dissociation constants (K_{a1} and K_{a2}) for both isomeric forms by titration, they were able to obtain the experimental K_{obs} from a first order kinetic model. In this way, ranges for pK_{a1} and pK_{a2} of 2.8 – 4.4 and 4.2 – 5.0 were estimated for *cis,cis*-muconic acid at 22.5 °C. From this and the observations found in Fig. S5.2, a mixture of dissociated and non-dissociated (but not precipitated) isomeric forms of *cis,cis* and *cis-trans* muconic acid are the most common species to be found between a pH of 3 and 4, which may be a fitting range for anolyte operation. For this reason, a pH set-point of 3.5 was selected for anolyte pH control. Because this can imply a sacrifice on Coulombic efficiency due to the presence of ionic forms, a final process evaluation was carried out with the big cell and fermentation broth (45 mM *cis,cis*-muconate) in a long term experiment (24 h). The concentration profile in the anolyte and catholyte is shown in Fig. 5.6. This time, the extraction set-up was modified with a recirculation of the anolyte to enable *cis,cis*-muconic acid accumulation by automatic pH control at 3.5 (see Chapter 2, Fig. 2.10). To quantify the amount of the target ion, HPLC samples were neutralized, ensuring that all muconate was in the *cis,cis* form.

As expected, a negative effect on the cell performance was observed by the presence of ionic forms of muconic acid in the anolyte at pH 3.5. During the first 7.5 h, the Coulombic efficiency (22 %) and flux (0.46 kg m^{-2} d^{-1}) decreased almost to 50% of the values obtained previously (see big cell in Fig. 5.5A and 5.5B). However, in this case it was possible to accumulate *cis,cis*-muconic acid in the anolyte with a high recovery respect to the initial amount that the catholyte contained (*i.e.,* mass recovery, accounting for 97 and 63 % after 7.5 and 24 h,

respectively). Thus, at a decrease of 18 % Coulombic efficiency the target molecule still accumulated in the anolyte while avoiding total precipitation and obtaining good recovery values during the first 7.5 h.

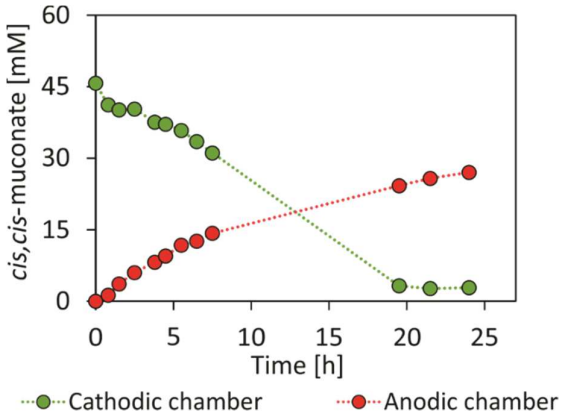

Fig. 5.6 Long-term extraction of *cis,cis*-muconate from a real fermentation broth. A current density of 33 mA m^{-2} was applied and the anolyte and cathoyte pH was automatically controlled at 3.5 and 7.0 by addition of 1M NaOH and 1M H_2SO_4, respectively.

5.3.4 In-line *electrolytic membrane extraction of* cis,cis-*muconate as integrated bioprocess*

From the process characterization of bioproduction and electrolytic extraction and of *cis,cis*-muconate, an *in-line* integrated bioprocess was implemented. Additionally, the technical issues related to *cis,cis*-muconate precipitation in the anolyte compartments were taken into account and a new set-up was developed (see Chapter 2, Fig. 2.11). This time, the starting working volume of the culture was reduced to 0.5 L and was implemented in a different 1-L bioreactor system (Section 2.5.4) to be able to work with the small electrolytic cell (and avoid any internal cell mixing issues at this point). An additional filter unit was placed between the anolyte reservoir and the cell to promote *cis,cis*-muconic acid precipitation at the filter surface, increasing the pressure of the filter feeding line. In this manner, it may be possible to decreased the concentration of ionized *cis,cis*-muconic acid in the anolyte and reduce precipitation on other surfaces. The pH-stat feeding strategy could not be implemented due to non-compatibility with the cell extraction. The electrolytic process generates OH^- and therefore conflicts with the feeding of alkaline benzoate solution (2.9 M NaOH). Instead, exponential feeding rates of benzoate and nutrient solution from the previous experiment were recalculated to fit the new bioreactor volume. Then, the feeding profiles were manually applied by corresponding low volume peristaltic pumps and monitored discontinuously by an electronic balance.

The operational data of two parallel bioprocesses (*i.e.,* conventional vs. extractive) is shown in Fig. 5.7. The microbial cells were induced at 1 mM benzoate after 4 h. Later, at 8 h of batch operation, the fed-batch stage started. The physiological behaviour of both cultures was very similar up to 14 h. However, at 22 h, parameters like O_2, CO_2, DOT, and stirring speed changed momentarily in both cases. At this point, the concentration of *cis,cis*-muconate of the

conventional and extractive process (both run under the same condition until this point) were 142 and 135 mM, respectively. This point seemed to correspond to the same perturbation point observed at 195 mM *cis,cis*-muconate in the previous 2-L conventional bioprocess (see 25 h in Fig. 5.4). After 22h, the concentration of *cis,cis*-muconate started to reach a maximum level in both processes.

The extractive cell was connected after 24 h and initially a current density of 13 mA m^{-2} was applied, which corresponded to a cell potential of 2.8 V (Fig. 5.7B II). At this point, the potential of the catholyte was -0.95 V, which was determined against $Ag/AgCl_{sat}$ reference electrode placed in the cathodic chamber. After 26 h, benzoate started to accumulate in both cultures and low amounts of unconsumed glucose were also observed. At 29 h, the current density was increased to 33 mA m^{-2} (cell potential of 4.0 V) and the cathode potential was -1.02 V (RE Ag/AgCl). Extraction of *cis,cis*-muconate was observed in the anolyte from the beginning of the cell operation, reaching a final concentration of 17.4 mM in the anolythe at the end (31.5 h). Additionally, some traces of benzoate were also detected in the anolyte as expected. Flux and Coulombic efficiencies of 0.52 Kg L^{-1} h^{-1} and 25 %, were estimated from the *cis,cis*-muconate quantified in the anolyte. Both values were slightly higher than the previous extraction on fermentation broth, which started with lower *cis,cis*-muconate concentration (*i.e.,* 45 mM) (Fig 5.6).

Some negative effects were detected on the cell culture performance during the cell extraction, such as a higher glucose accumulation after the extractive process was started (see differences, white squares in 5.7A and 5.7B graph I). In combination with the already high *cis,cis*-muconate built-up in the culture, other issues related to harmful reductive potential on the cells and oxygen limited environments built in the cathodic chamber seemed to have an additional harmful influence. The reductive potential (-1 V, RE Ag/AgCl) may cause problems in the cell membrane potential and substrate transport across, decreasing the overall performance. In addition, poor oxygen levels in the cathodic chamber established as consequence of limited mass transfer phenomena and scavenging effects due to the hydrogen evolution, may affect this bioconversion process that is heavily dependent on proper oxygen supply. These negative impacts were also observed in an additional parallel operation, which can be found in the Appendix (Fig. S5.3). This second approach was an attempt to couple the electrolytic cell earlier (at 17 h), however an immediate increase of the cell potential led to a rapid accumulation of benzoate and glucose in the cell culture (Fig. S5.3B). Additionally, another process drawback during the *in-line* extraction corresponded to a different mixing regime recorded for the integrated system, where the stirring speed increased up to 1100 rpm to maintain the DOT at 50 % air saturation (see Fig. 5.7 III). The limited oxygen transfer to the volume of cell culture flowing through lines and the cathodic chamber needed to be compensated inside the bioreactor by better mixing, possibly increasing shear stress on the cells. In a next run, a higher level of aeration (as vessel volumes per minute, vvm) should be provided to avoid such high stirring speed.

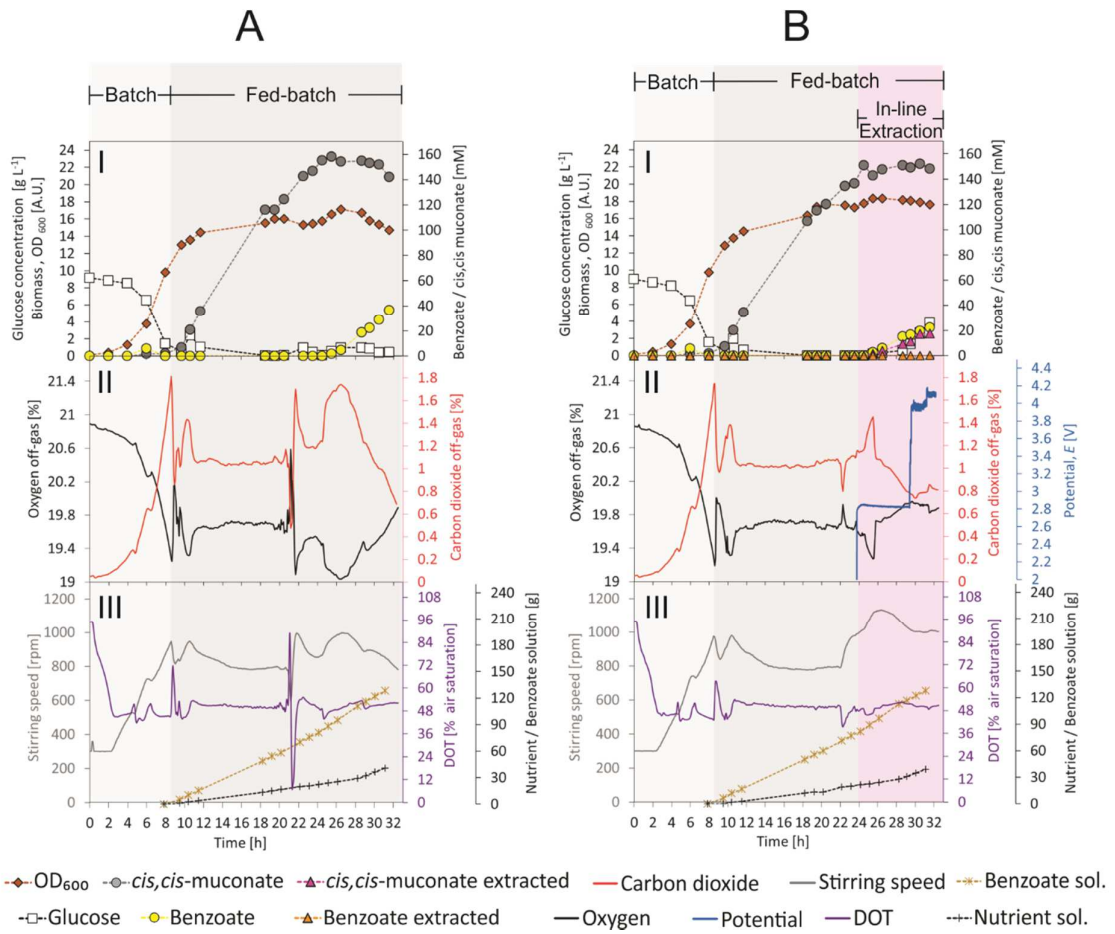

Fig. 5.7 Operational data of two parallel bioprocess for *cis,cis*-muconate production. Both, conventional bioporecess (A) and an integrated bioprocess with in-line electrolytic membrane extraction of *cis,cis*-muconate (B) were operated at 30 °C under DOT control at 50 % air saturation. Both systems were fed by the same benzoate (1.2 M) and nutrient solutions (600 g glucose L^{-1}). The extractive cell was connected after 24 h. Additional operational parameters like off-gas composition and cell potential (II) and stirring speed, dissolved oxygen tension (DOT) and amount of fed solutions (III) were recorded.

Despite the above limitations, the global effect of the cell extraction led to an increase in the process performance compared to the conventional system (Fig. 5.8). The in-line extraction enabled a rise of 15.6 % in volumetric productivity, counting the mass of *cis-,cis*-muconic acid obtained in the cell culture, anolyte and precipitates collected by the filter unit (Fig. 5.9B). Fractions of precipitates were also found at the anode surface, but they were difficult to recover (Fig. 5.9A). The increase of productivity may be related to a better benzoate uptake and later conversion to *cis,cis*-muconate as benzoate accumulation in the extractive system was the half of the conventional system (Fig. 5.9A). Additionally, the biomass concentration (OD_{600}) in the extractive bioprocess did not decrease abruptly at the last hours as observed for the conventional bioproduction. In accordance, negative effects of high *cis,cis*-muconate concentrations on the specific benzoate uptake rate and growth of *P. putida* has been

previously reported (van Duuren *et al.*, 2012; Salvachúa *et al.*, 2018). Thus, it is very likely that the cell extraction partially alleviated toxic effects generated by high *cis,cis*-muconate levels.

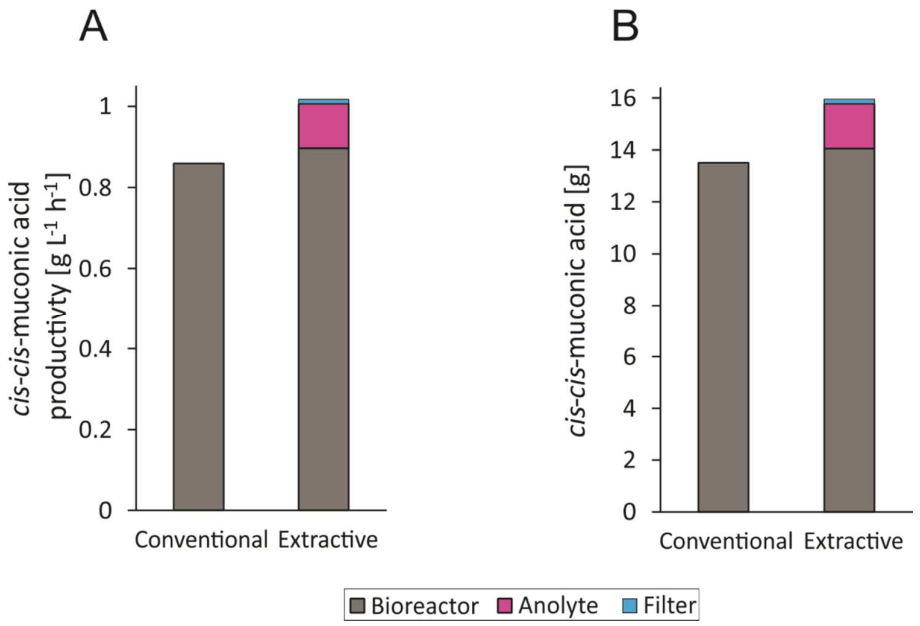

Fig. 5.8 Overal performance of a conventional bioproecess and extractive system for *cis,cis*-muconate production. Volumentric productivity (A) and quantified *cis,cis*-muconic acid were estimated for the different process units (bioreactor, anolyte and filter).

Although the overall improvement of bioprocess performance was not all that high, there is still room for improvement. Through advanced set-up configurations and further process optimization, higher productivities can be achieved. For example, a cell retention unit like an microfiltration module can be implemented to avoid bacterial contact with the cathode. In addition, an automatic control could ease process operation. In a final system, an integrated cell extraction operation could be simplified by a closed-loop control strategy based on changes of process signals related to *cis,cis*-muconate accumulation to non-desired levels (for instance, relevant changes in the off-gas analysis). If the pH control is also coupled to the automatic control, hydroxide ions produced by water splitting can also replace caustic soda management. Similar systems with an integrated membrane electrolysis unit have been reported in mixed fermentative cultures, where the cathodic conditions had a positive influence on process performance. These systems improved product recovery, reduced the amount of base added, and increased the overall production rates of diverse carboxylic acids (Andersen *et al.*, 2015; Xu *et al.*, 2015; Khor *et al.*, 2017; Verbeeck *et al.*, 2018; Carvajal-Arroyo *et al.*, 2020). In a particular case of a pure culture, a direct electrochemical extraction of succinic acid from a fermentation carried out by *Basfia succiniciproducens* resulted in 33 % less NaOH usage and the productivity improved by 30 % when H_2 generated at the cathode provided additional biological reducing power (Pateraki *et al.*, 2019).

Finally, a further optimized *in-line* extractive system may also offer advantages for improving concentrations and productivities with further metabolically optimized strains that accumulate *cis,cis*-muconate from other aromatic sources or even real lignin-depolymerized substrates (Kohlstedt *et al.*, 2018; Salvachúa *et al.*, 2018). In those cases, the combined effects of the product removal and enhanced metabolic features of the biocatalysts may help to achieve industrial relevant concentrations. Analogous approaches to produce carboxylic acids from sugars were able to build up to 220 g L^{-1} of product (Hosseinpour Tehrani *et al.*, 2019). Thus, further studies based on rational metabolic improvement working alongside with an *in-situ*/*in-stream* extractive bioprocess to promote cost-effective lignin valorization approaches are strongly encouraged.

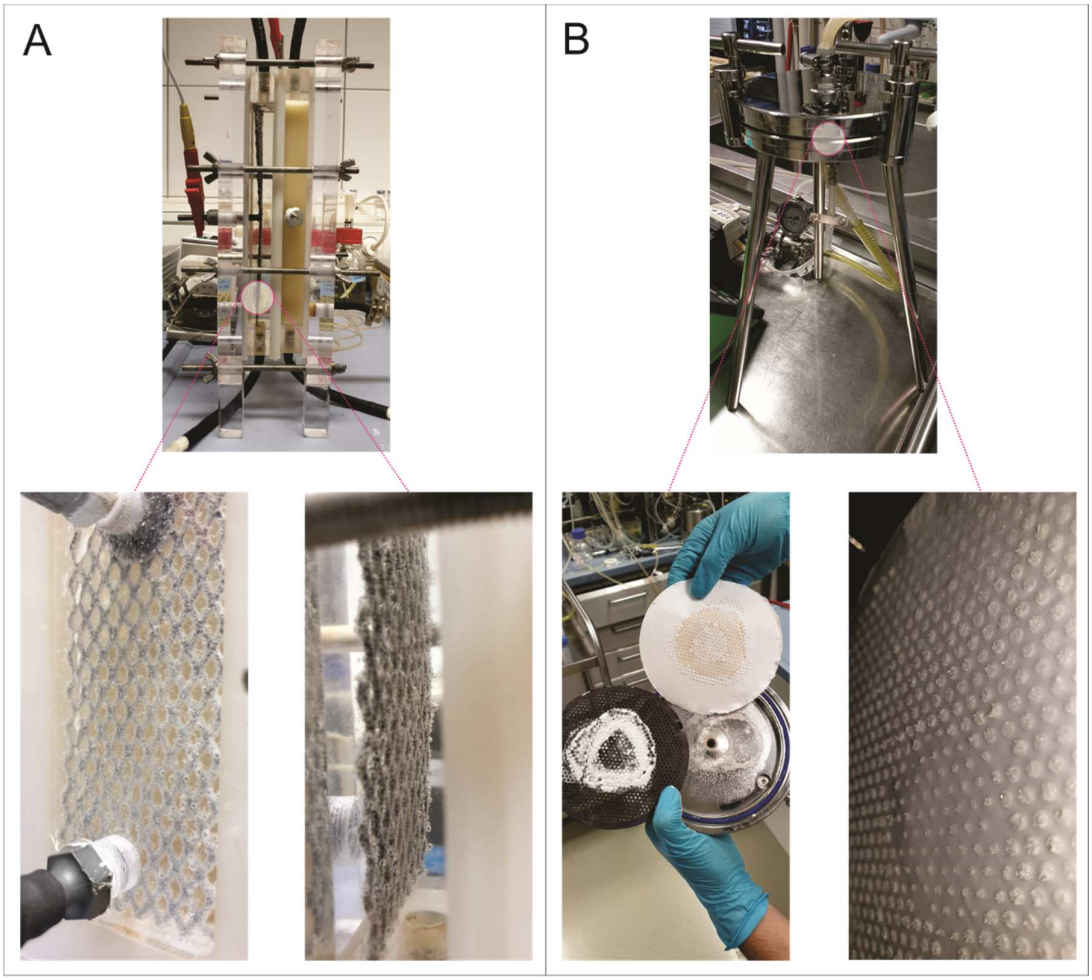

Fig. 5.9 Photos showing *cis,cis*-muconic acid precipitation at the anode (A) and filter (B).

5.4 Conclusion

Through a systematic approach, an *in-line* extraction of *cis,cis*-muconate was implemented solving technical challenges along the process development path. After a suitable anion exchange membrane was selected (AM-7001S, membrane International Inc.), the electrolytic extraction of *cis,cis*-muconate was characterized in terms of flux and Coulombic efficiency from synthetic solutions. The flux of *cis,cis*-muconate increased up to 2.54 Kg m^{-2} d^{-1} at a current density of 66.7 mA m^{-2} while the Coulombc efficiency was 59 %. These values corresponded to starting concentration of 100 mM (14.2 g L^{-1}) *cis,cis*-muconate, which has been reported in previous studies as a threshold level for optimal bioproduction. In our reference bioprocess, a volumetric productivity and concentration of 1.74 g L^{-1} h^{-1} and 245 mM (34.8 g L^{-1}) *cis,cis*-muconate were obtained, respectively. From these parameters an advanced extractive system was evaluated with real fermentation broths. Further process development with a bigger electrolytic cell set-up largely prevented *cis,cis*-muconic acid precipitation in the anolyte by implementing a pH control. Finally, the cell was coupled to a bioreactor and with an additional precipitation filter unit, the extractive system enabled an increase of 15.6 % in volumetric productivity for *cis,cis*-muconate production in respect to the conventional process. Although there is still much opportunity for optimization, the combination of this in-line *cis,cis*-muconte removal approach and further metabolic engineering approaches promises to boost technical and economic feasibility of biological lignin valorization.

Chapter 6: Final conclusions and outlook

6.1 Summary and main outcomes

From the need of establishing efficient bioconversions of lignin into valuable products, this thesis demonstrated an increased production of *mcl*-PHA and *cis,cis*-muconic acid from lignin aromatics. This was possible through fundamental understanding of the key factors involved during the biocatalytic lignin aromatics upgrading and applying this knowledge to implement innovative bioprocess strategies.

Pseudomonas is a recognized bacterial genus to ease the inherent aromatic heterogeneity of lignin-based aromatic mixtures and synthetize naturally marketable biopolymers like *mcl*-PHA (Kumar *et al.*, 2021). However, due to the great diversity of this genus, a representative group of wild type strains were evaluated as requisite for selecting a suitable biocatalyst (**Chapter 3**). Through a 3-step sequential screening in microtiter plates, the different lignin valorization potentials of the strains were revealed. Remarkably, during parallel cultivations in 96 microtiter plates, growth on tough molecules for biodegradation like sinapic acid and changes in scattered light values on 4-methylguiaiacol and syringol were detected at low concentrations (5 mM) in *P. putida F1* and *P. putida S12*, respectively. Despite these interesting findings, and keeping in mind the ultimate goal of converting lignin aromatics into biopolymer, other molecules like ferulate, p-coumarate, vanillate and benzoate were selected for further evaluation in 48 microtiter plates. These aromatics were tested on biocatalyst like P*. putida F1*, *P. putida S12*, *P. putida* KT2440 and *P. taiwanensis* VLB120. Because of the challenges related to obtaining reproducible amounts of aromatic liquors and the limitations of analytics to perform comparative studies with heterogeneous lignin derivates, a lignin-aromatic mixture composed of p-coumarate, ferulate and benzoate was selected for further evaluation in the best performing strains (*i.e,* a group of *P. putida*). As main outcome, the most robust and best performing strain under stressful enviroments in terms of *mcl*-PHA accumulation from this lignin aromatic mixture was *P. putida* KT2440. However, from differences on aromatic funneling into *mcl*-PHA observed in *P. putida* F1 and *P. putida* KT2440 under simultaneous nitrogen and oxygen-limited conditions, it was inferred that oxygen availability limited considerably the biocatalytic process. For this reason, identification of optimal C/N ratios and oxygen availabilities was proposed. This objective was assessed in the *P. putida* KT2240 by means of further bioprocess development in **Chapter 4**. Effectively, oxygen and nitrogen availability were confirmed as the key factors for funneling the lignin-aromatic mixture into *mcl*-PHA for this strain. In this particular study, the detailed dynamics of lignin aromatic funneling and biopolymer accumulation was revealed during online measurements of the oxygen consumption. Overall, the accumulation of *mcl*-PHA was improved in the wild type strain under technically relevant conditions by up to 43% (polymer content mg *mcl*-PHA mg^{-1} CDW). The highest *mcl*-PHA concentration (582 mg L^{-1}) was obtained for a C/N ratio of 60 for oxygen-unlimited conditions (oxygen transfer rate ≥ 20 mmol L^{-1} h^{-1}). In contrast, aromatic intermediates accumulated under oxygen-limited conditions at oxygen transfer rates below 10 mmol L^{-1} h^{-1}. Through this bioprocess

characterization, the performance of the biocatalytic funneling in *P. putida* KT2440 became predictable and thus, the experimental conditions were scalable into a 1-L stirred tank bioreactor based on the oxygen transfer rate. Finally, the benefits of implementing simultaneous biocatalyst and bioprocess optimization strategies were demonstrated. A 1.9-fold increment in *mcl*-PHA concentration and a 1.5-fold increment in *mcl*-PHA content were obtained from lignin aromatics. Overall, **Chapter 3** and **Chapter 4** contributed to deepening the understanding about the biocatalytic capability of the promising *P. putida* KT2440 towards efficient conversions of lignin aromatics for future biorefinery applications. A graphical representation of the research followed approach and the main outcomes obtained in these chapters are shown in Fig. 6.1.

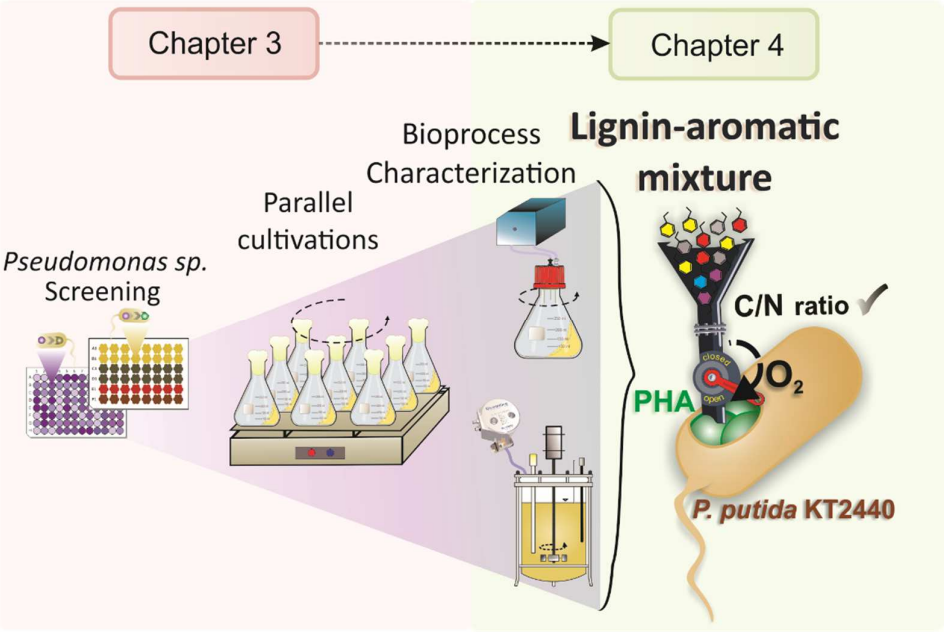

Fig. 6.1 Graphical representation of chapters 3 and 4. These chapters followed a research approach that consisted of step-wise screenings of wild type *Pseudomonas* in microtiter plates, parallel cultivations in shake flask and bioprocess characterization from online measurements of the oxygen consumption. As main outcome, nitrogen and oxygen were identified as the key factors for funneling a mixture of lignin aromatics into *mcl*-PHA in *P. putida* KT2240.

Cis,cis-muconic acid, another valuable precursor in the polymer industry, is synthetized via the catechol ortho-cleavage pathway in *P. putida* KT2240. Although this strain is recognized for its tolerance machinery and flexible aromatic catabolism, recent studies on bioprocess development identified that product toxicity is a limiting factor for achieving industrial relevant levels (Salvachúa *et al.*, 2018). For this reason, in **Chapter 5**, an *in-line* electrolytic extraction of *cis,cis*-muconic acid was implemented. First, the extraction of *cis,cis*-muconate was characterized from a synthetic media in an electrolytic cell that contained a suitable commercial anion exchange membrane. The flux of *cis,cis*-muconate increased up to 2.54 Kg m^{-2} d^{-1} at a current density of 66.7 mA m^{-2}, while the Coulombic efficiency obtained was 59 %. In parallel, a metabolically engineered strain was generated to accumulate *cis,cis*-muconic

acid from benzoate. With this strain, a conventional bioprocess was characterized in terms of production rates and the negative effect of *cis,cis*-muconic acid accumulation was confirmed at concentrations higher than 195 mM (27.7 g L^{-1}). Once fermentation broths were available in sufficient amounts, long term extractions were performed in a bigger electrolytic cell. After identifying technical drawbacks regarding muconic acid precipitation in the anodic chamber, a solution based on pH control (3.5) was implemented. This was essential to enable the higher muconate accumulation in the anolyte solution. From the knowledge obtained separately in both electrolytic extraction and bioprocess units, a final integration was carried out. An additional filtration unit was introduced to the integrated system to encourage muconic acid precipitation at the filter surface by the pressure built in the feed line, thus competing with non-desirable precipitation at the anode. Finally, by implementing the *in-line* extraction, the volumetric productivity of *cis,cis*-muconate was increased 15.6 % in respect to a conventional bioprocess run in parallel. This approach demonstrated for the first time the potential of *in-line* removal of *cis,cis*-muconic acid in a microbial cultivation and contributed as an important step towards implementing a cost-effective bioproduction. A graphical representation of the integrated system is shown in Fig. 6.2.

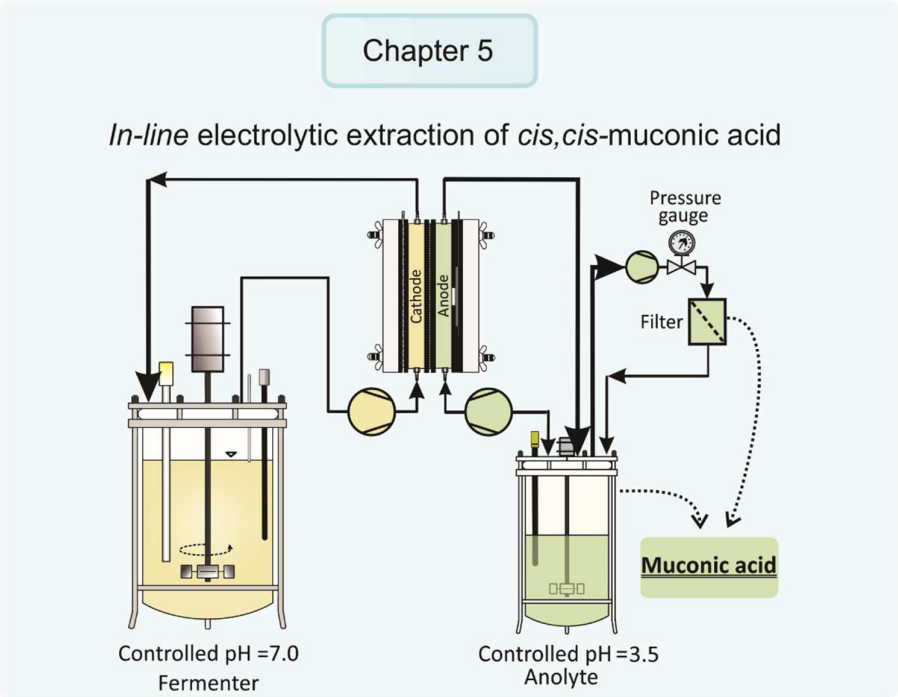

Fig. 6.2 In-line electrolytic membrane extraction of *cis,cis*-muconate produced by a metabolically engineered strain of *P. putida* KT2240. Through pH control (3.5) in the anolyte and promoting precipitation in a filter unit, accumulation of extracted muconic acid was enabled. For this system, the volumetric productivity of *cis,cis*-muconate was increased 15.6 % in respect to a conventional bioprocess run in parallel.

This thesis demonstrates the possibility of getting value form unexploited carbon sources like lignin aromatics, expanding the actual knowledge on the biocatalytic bioconversion and enhancing the process by applying biotechnological innovations. To continue walking in the

roadmap for building a circular bioeconomy and towards an effective implementation of the next sustainable bio-production systems, future research based on system upgrading is encouraged. In this regard, the next section discuss the possible improvements.

6.2 General discussion and future prospects

6.2.1 Lignin status quo and evolution: shifting paradigms towards future biorefineries

Since lignin was first mentioned (de Candolle, 1813) and was later studied for understanding how to perform pulp processing, it has been considered a subordinate fraction of lignocellulosic biomass. However, the minor role that lignin fraction always played in traditional lignocellulosic biorefineries is now being re-evaluated. With the aim of establishing a circular bioeconomy, the research progress of the last decade has pushed a tremendous progress to better integrate lignin valorization concepts into future biorefineries. The paradigm of having cellulose and hemicellulose as main focus is now shifting towards considering lignin as the first character in many bio-based production processes (Renders *et al.*, 2017; Korányi *et al.*, 2020). Acknowledging lignin as a primary valorisation target but also as a complex aromatic polymer, the future directions for establishing lignin biorefineries will depend on the interplay of three essential operational units: Biomass fractionation, lignin depolymerization and aromatic upgrading (Schutyser *et al.*, 2018).

Regarding biomass fractionation and lignin depolymerization, important research is underway in preserving the native lignin structure through reductive catalytic fractionation approaches, looking for stabilizing reactive linkages to facilitate depolymerization (*i.e.,* concept of lignin-first). There is now a general understanding of this technology, which has been established utilizing native biomass. Recently, through a techno-economic analysis and a life-cycle assessment, an integrated biorefinery concept fully converting wood into useful chemicals for ink production predicted competitiveness while estimating a low-carbon footprint relative to fossil-based production (Liao *et al.*, 2020). The future directions on this technology are now moving towards applying this technology for valorization of genetically engineered plants and waste biomass. This will require a huge interdisciplinary and collaborative effort to embrace the essential tasks that lie ahead, which is now being evaluated (Renders *et al.*, 2019). Concerning the processes for aromatic upgrading, which need to be also integrated to biomass fractionation and lignin depolymerization steps, the research on chemo- and bio-catalytic funnels should then look in the direction of planning ahead. Then, a total process integration should evaluate the type of biomass feedstock from the beginning. In any case, the product value chain would need to adapt to the specific case of biomass supply, while ensuring atom efficiency (*i.e.,* enough conversion efficiency) towards sustainable production. As first approach, advances on analysis of the chemical composition of whole biomass feedstocks and experimental standardization across laboratories will eventually speed up the research progress towards industrial implementation. This issue has been recently proposed in detail (Abu-Omar *et al.*, 2021). For instance, in the case of having

waste biomass, the concept of lignin-first could help to establish efficient cascades processes for producing and recovering target products with middle range value like fertilizers, bulk chemicals or fuels. In the case of engineered biomass feedstocks having a higher abundance of readily cleaved linkages, more andanced planning will be necesary. Here, the upstream modifications would affect the downstream processes and therefore specific fractionation, depolymerization and aromatic upgrading processes will need a solid design and development. However, if the process development on lignin-first concepts is combined along biocatalytic upgrading approaches, quality products located on top of the value scale like biodegradable polymers, bioactive compounds and pharmaceuticals can be effectively synthetized. Additionally, limitations related to toxic compounds generated during conventional depolymerizations could be prevented from a proper integrated process design. Thus, development of new technologies for system integration will play an eesential role and future research is encouraged in this direction. The next two sections focus on future developments and possibilities to be applied from the progress obtained in this thesis.

6.2.2 Further developments on lignin aromatics valorization

This thesis started with a comprehensive screening involving multiple lignin monomers and wild type *Pseudomonas* strains. From the interesting finding that *P. putida F1* could utilize sinapic acid for growth, future research should explore this capability. Sinapic acid is a derivate monomer of S-lignin. Thus, potential valorization opportunities will open if the genes involved are integrated into the genomes of most robust biocatalyst for *mcl*-PHA accumulation from lignin aromatics like *P. putida* KT2440. Additionally, this strain present less safety requirements for industrial cultivations (Kampers *et al.*, 2019). In fact, other challenging molecules for biodegradation like guaiacol and syringol are now considered for valorization from the research progress on new promiscuous P450 aryl-O-demethylases and their heterologous expression in *P. putida KT2440* (Tumen-Velasquez *et al.*, 2018; Machovina *et al.*, 2019). Thus, future work on continuous strain development with enhanced aromatic capabilities is expected.

In addition to sinapic acid, other aromatic molecules of the group of hydroxycinnamic acids like p-coumarate and ferulate were widely utilized in most of the *Pseudomonas* strains, while aromatics with aldehyde and methoxy functional groups were poorly used for biomass synthesis. This has also found in other studies and confirm why lignin depolymerized solutions containing these compounds have been frequently considered in the field of biological lignin valorization. One example is the alkaline pretreatment liquor (APL), which can be obtained from herbaceous sources like waste crops (Karlen *et al.*, 2020). New approaches like reductive catalytic fractionation (Anderson *et al.*, 2016) and lignin-first concepts are now being evaluated for increasing the efficiency on hydroxycinnamic acids (Johnston *et al.*, 2020). This represent a promising step towards integrating new progress on upstream lignin processing with biocatalytic applications, as discusses previously.

The effect of oxygen availability and the biocatalytic funneling of *P. putida* KT2440 was also explored in this study. As oxygen transfer rates increased, the funneling of the aromatic mixture was improved for all the nitrogen availabilities evaluated, and therefore more *mcl*-PHA accumulation was obtained. The role of oxygen was suspected from differences observed in different cultivation systems. For example, *P. putida* F1 consumed higher amounts of aromatic and accumulated more *mcl*-PHA in flower shape microtiter plates. On the other way, the consumption of ferulate and production of *mcl*-PHA was totally limited in shake flask cultivations where oxygen availabilities were not enough. For this reason, future screening campaigns should consider seriously proper oxygen availabilities to avoid underestimation of the real aromatic capabilities of many other strains.

A bottleneck that was also identified was intermediate aromatics accumulation under simultaneous nitrogen and oxygen-limited conditions, which was observed at oxygen transfer rates below 10 mmol L^{-1} h^{-1}. Thus, the carbon flux was temporally trapped before dioxygenase cleavage and could not be directed through the β ketoadipate pathway. Although this represent a serious constraint for proper synthesis of *mcl*-PHA from lignin aromatics, it can be utilized as possible strategy for accumulating target aromatic molecules like vanillic acid and 4-hydroxy benzoic acid from alkaline depolymerized liquors containing hydroxycinnamic acids like p-coumaric acid and ferulate. Especially, the accumulation of these intermediates was considerable in oxygen limited cultivations carried out in cultivations set at low mixing rates and poor air supply. Although specific applications should be defined, strategies for funneling aromatic mixtures into few aromatic targets under low energy consumption could compete with strain development strategies where blocking metabolic pathways by genetic engineering generate unavoidable metabolic constrains and unnwanted side effects. Cost-benefit analyses need to be in consideration.

Finally, together with ongoing important metabolic engineering efforts for strain development on improving lignin aromatic uptake and avoiding *mcl*-PHA re-assimilation (de Eugenio *et al.*, 2010; Arias *et al.*, 2013; Johnson *et al.*, 2017; Kohlstedt *et al.*, 2018; Borrero-de Acuña *et al.*, 2020; Salvachua *et al.*, 2020; Zhou *et al.*, 2020) , this study encourage future research on linking aspects like: media formulation (*i.e.,* optimization of nutrients like nitrogen amount to ratio of real mixed lignin fractions)(Salvachúa *et al.*, 2016), oxygen fine-tuned feeding strategies (*i.e.,* DO stat fed batch cultivations)(Poblete-Castro *et al.*, 2014b) to improve *mcl*-PHA concentrations and minimize diauxic aromatic uptake profiles during different nitrogen availability, synergistic co-carbon feeding strategies to balance metabolic energy (Liu *et al.*, 2017; Liu *et al.*, 2019; Xu *et al.*, 2021) and ensuring final product quality (*i.e.,* detailed studies on polymer monomers for enhancing *mcl*-PHA material properties)(Mozejko-Ciesielska *et al.*, 2019). The outcomes of this in depth bioprocess understanding may also benefit the production of other value compounds than *mcl*-PHA from lignin aromatics. For all future bioprocess engineering efforts, a balance between lignin, oxygen, and nitrogen supply

will be essential. Eventually, the proposed combination of biocatalyst and bioprocess characterization and optimization will increase the efficiency and economics of lignin valorization in the next generation biorefineries.

6.2.3 Additional developments towards in-line *extraction of* cis,cis-*muconic acid*

The first version of the *in-line* extraction system developed in chapter 5 can be further improved by integration of new operational units and process developments. The first improvement aspect should focus on the implementation of a microfiltration module for biomass retention in the fermenter. Thus, the negative effect of the oxygen scavenged by hydrogen evolution and the limitations on mass transfer in the cathodic chamber can be avoided. It was also mentioned that implementation of an automatic control based on changes in the off-gas composition and culture pH to tune the electrolytic extraction may reduce the NaOH consumption. In this case, a DO-stat fed-batch will be required to not intervene with the pH control, as a pH-stat strategy does. In addition to these enhancements, a focus on the reaction phenomena occurring in the anolyte should be further explored. During the operation runs, anolyte color changes were observed over time. Additionally, after harvesting, the precipitation of muconic acid from the anolyte required higher amounts of concentrated sulfuric acid to reach a pH of 2.0. Although the involved isomeric form *cis,trans* muconic acid is known to be five times more soluble at room temperature under acidic conditions than *cis,cis*-muconic acid (Carraher *et al.*, 2016), additional side reactions must be considered. Other electrochemically-induced reactions at the anode can be promoted as muconic acid precipitate at the surface. For example, reactions like irreversible ring closing of muconic acid to produce lactones (Khalil *et al.*, 2020) or electrocatalytic-induced isomerization to *trans,trans*-muconic acid (Matthiesen *et al.*, 2016) will need to take into consideration. Although isomerization phenomena of muconic acid is not totally clear yet, new research progress on this topic will enable better understanding towards increasing muconic acid accumulation in the anolyte.

As the research on selective extraction of muconic acid continues, other integrated systems may be implemented. For example, the advances on reactive extraction of other dicarboxylic acids like itaconic acid promoted *in-situ* crystallization with $CaCO_3$, improving bioconversion performance and reaching industrially relevant concentrations (Hosseinpour Tehrani *et al.*, 2019). A similar bioreactor configuration like the one graphically showed in Fig. 1.8B (see Chapter 1) may promote precipitation as calcium muconate crystals. In addition, processes on reactive extraction of muconic acid using biocompatible organic solvents (Gorden *et al.*, 2015) and re-extraction strategies (Gorden *et al.*, 2016) will be useful to implement new *in-situ*/*in-stream* product recovery configurations.

Finally, a future techno-economic analysis would state if the presented integrated system is economically competitive in relation to conventional muconic acid production process. In this

work, the substrate utilized consisted on benzoate and glucose. However, the final analysis should take into account results obtained from operations carried out with cheaper substrates like real lignin depolymerized liquors. In that case, the presence of other relevant compounds and ionic species generated during lignin fractionation/depolymerization steps would need to be considered. In addition to the price of substrate, other aspects that involve important cost-operative factors like membrane maintenance/replacement, downstream operations for recovery of muconic acid and coulombic efficiencies will need to be carefully included.

Appendix

Supplementary information for chapter 2

Table S2.1 List of *E.coli* strains involved during all genetic engineering procedures.

Strain	Characteristics	Reference	iAMB strain collection number
E. coli			
DH5α-λpir	Host for cloning vectors with R6K origin of replication. λpir lysogen of DH5α	de Lorenzo and Timmis, 1994	2072
DH5α-λpir pEMG	Host strain carrying the plasmid pEMG. Km^R	de Lorenzo and Timmis, 1994	2075
HB101 pRK2013	Helper conjugative plasmid pRK2013. Km^R	Boyer and Roulland-Dussoix, 1969	2037
DH5α pSW-2	Strain harbouring plasmid PSW-2. Gm^R.	Martínez-García and de Lorenzo, 2011	2404
DH5α-λpir pEMG TS1 _TS2-*phaZ*	Donor strain harbouring mobilizable plasmid pEMG TS1 _TS2-*phaZ* . Km^R .	This study	-
DH5α-λpir pEMG TS1_*Ptac*_TS2	Donor strain harbouring mobilizable plasmid pEMG TS1_*Ptac*_TS2. Km^R.	This study	-
DH5α-λpir pEMG TS1_*aroY-Ptac*_TS2	Donor strain harbouring mobilizable plasmid pEMG TS1_*aroY-Ptac*_TS2 Km^R.	This study	-

Table S2.2 List of plasmids and their relevant characteristics during all genetic engineering procedures.

Plasmid	Characteristics	Reference
pEMG	Km^R, *oriV*(R6K), *lacZ*α-MCS flanked by two I-SceI. Sites oriT for mobilization with a helper strain (Fig. S2.1A)	Martínez-García and de Lorenzo, 2011
pRK2013	Helper plasmid for conjugational transfer; Km^R, *ori* (RK2/ColE1), mob^+ tra^+	Boyer and Roulland-Dussoix, 1969
pSW-2	Gm^R, xylS, *Pm* → I-SceI promiscuous *ori*RK2/trfA origin of replication, *ori*T for mobilization with a helper strain.	Martínez-García and de Lorenzo, 2011
pEMG TS1 _TS2-*phaZ*	Deletion delivery vector. Km^R. pEMG bearing flanking sequences TS1 and TS2 of *phaZ* (Fig. S2.1B)	This study
pEMG TS1_*Ptac*_TS2	Deletion delivery vector. Km^R. pEMG bearing flanking sequences TS1 and TS2 of *catRBC* and tac promotor. (Fig. S2.2B)	This study
pEMG TS1_*aroY-Ptac*_TS2	Deletion delivery vector. Km^R. pEMG bearing flanking sequences TS1 and TS2 of *pcaHG* and *aroY* plus tac promotor. (Fig. S2.2C)	This study

Table S2.3 List of oligonucleotides used during all genetic engineering procedures. The designation, sequence, description and PCR fragment size are shown. Lower case letters indicate overhangs, while the binding sequence is capitalized. The colors follow the same pattern shown in Fig. S2.1 and 2.2.

Primer designation	5´-> 3´ sequence	Description	Size (bp)
P1_phaZ_fwd	gctcggtacccggggatcctGCATCACTTGTACCGCACTG	TS1 *phaZ* forward	847
P2_phaZ _rev	cgcagctgttGCACGTGACTCTTGGGTGAAG	TS1 *phaZ* reverse	
P3_phaZ_fwd	agtcacgtgcAACAGCTGCGGCCTGACAGG	TS2 *phaZ* forward	874
P4_phaZ_rev	tgcatgcctgcaggtcgactCTCCAGGGCTTGCACATAGC	TS2 *phaZ* reverse	
P5_phaZ_fwd	GCAGCAGCAGACCTTCATCATC	Verification deletion	2907
P6_phaZ_rev	CTTTCGAACTTGCTGTCCAGC	Verification deletion	WT
BW_013_fwd	TTTGCACTGCCGGTAGAAC	Verification sequence	-
BW_014_rev	AATACGCAAACCGCCTCTC	Verification sequence	-
P1_catRBC_fwd	ttcgagctcggtacccggggatcctGTGACATAACCTCGAACTCAG	TS1 *catRBC* forward	1010
P2_catRBC_rev	tcacttaaaaaggACAATACGAGGTAAGCACGATG	TS1 *catRBC* reverse	

Table S2.3 (Continued)

Primer designation	**5´-> 3´ sequence**	**Description**	**Size (bp)**
P3_catRBC_fwd	tacctcgtattgtCCTTTTTAAGTGAACTTGGGCC	Upstream *Ptac* forward	186
P4_catRBC_rev	gcagggctatacaTGCGTTCGGTCAAGGTTCTG	Downstream *Ptac* reverse	
P5_catRBC_fwd	ttgaccgaacgcaTGTATAGCCCTGCCCTATTGG	TS2 *catRBC* forward	1100
P6_catRBC_rev	aagcttgcatgcctgcaggtcgactCATCATTGAGACCGCGCGTG	TS2 *catRBC* reverse	
P7_catRBC_fwd	GTGCTCCTCGTGGATGTAG	Verification deletion-insertion	4845 in
P8_catRBC_rev	CATGCACCTGAACGTGATG	Verification deletion-insertion	WT
P1_pcaHG_fwd	ttcgagctcggtacccggggatcctCGATGCGATGATCACGATGTGC	TS1 *pcaHG* forward	901
P2_ pcaHG_rev	GGTGAAGCTTGGGGCCGC	TS1 *pcaHG* reverse	
P3_ pcaHG _fwd	GGAATTGTGAGAACGCCTG	TS2 *pcaHG* forward	881
P4_ pcaHG _rev	aagcttgcatgcctgcaggtcgactGTTTCTGCGCCTGGTAGG	TS2 *pcaHG* reverse	
P5_ pcaHG _fwd	CGAGAAGCACAAGGCAATC	Verification deletion-insertion forward	3361 in
P6_ pcaHG _rev	GAAGTGCCATGGGTGAAGG	Verification deletion-insertion reverse	WT
P7_ ptac+aroY _fwd	GAGCGGCCCCAAGCTTCAC	Verification insert forward	1621
P8_ ptac+aroY _rev	CCAGGCGTTCTCACAATTCCAG	Verification insert reverse	
S1_pcaH_veri_ rev	CTTACGCCTGACTACAAGAC	Verification insert reverse with P5_ pcaHG _fwd	2303 In WT
S2_aroY_veri_ rev	CCACCTACAGCGAGCTGAAG	Verification insert reverse with P5_ pcaHG _fwd	1354 In aroY
JS1_seq_rev	CGAGCGTGAAACAAGAAGAC	Verification sequence	-

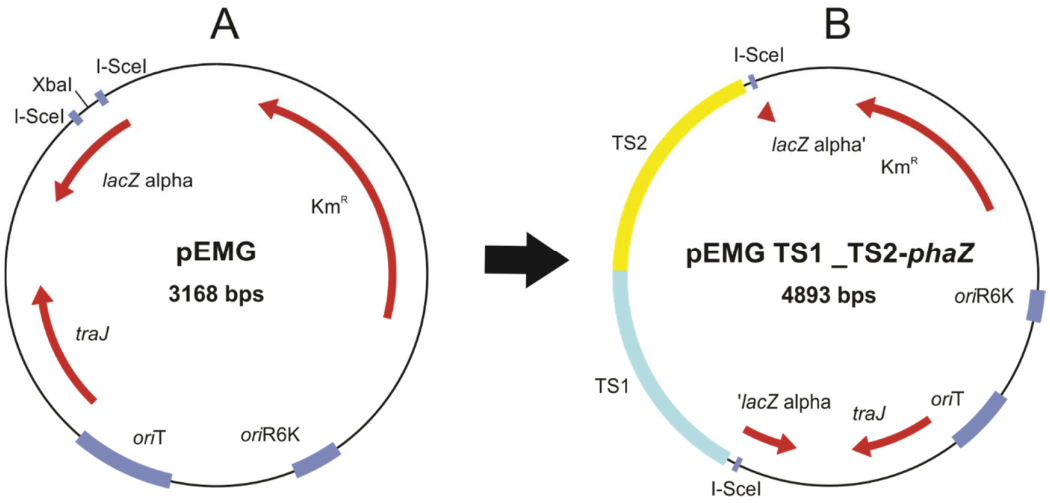

Fig. S2.1 Vector construction for deletion of the gene encoding for *mcl*-PHA depolymerase (*phaZ*). The suicide vector pEMG (A) harbors an origin of replication *ori*R6K (dependent on the π protein from phage lamda and not recognized by *Pseudomonas*) that enable isolation of chromosomally co-integrated clones. The origin of transfer *ori*T is recognized by a relaxase (key protein in conjugation), *traJ* gene – encodes a regulation transfer component required for conjugation, *lacZ* alpha – enable blue and white screening and Km^R encodes for a aminoglycoside 3-phosphotransferase conferring kanamycin resistance. During triparental mating, a homing endonuclease (carried by the plasmid DH5α pSW-2) recognises the sites I-SceI, enabling cleavage of the vector backbone from the bacterial genome. Two flanking regions (TS1 and TS2) corresponding to the up- and downstream of *phaZ* were fused and cloned into the multiple cloning site (MCS), where XbaI was used to open the vector. The resulting deletion vector pEMG TS1_TS2-phaZ (B) was delivered into *P. putida* KT2240 by conjugation.

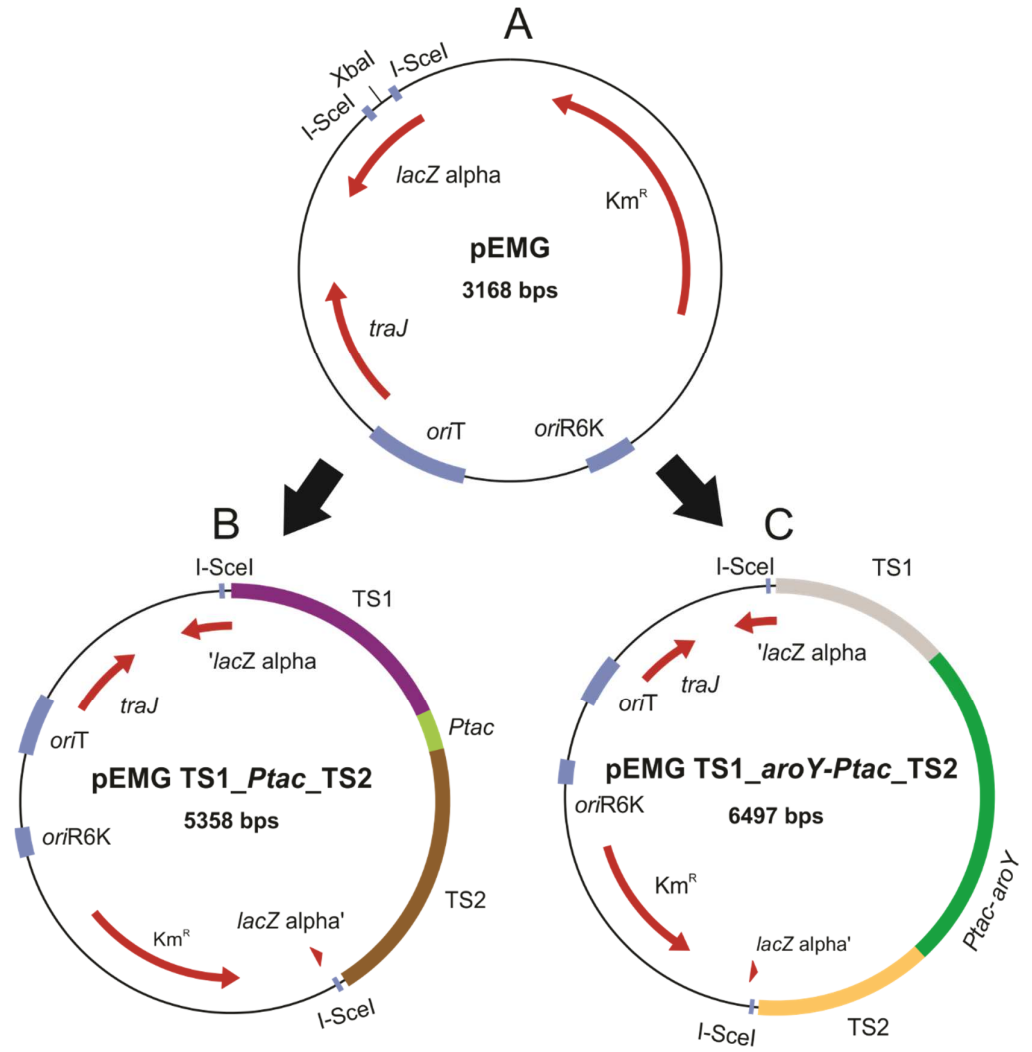

Fig. S2.2 Vector construction for deletions and insertions of corresponding genes during the generation of muconate producing strains from aromatics. The suicide vector pEMG (A) harbors an origin of replication *ori*R6K (dependent on the π protein from phage lamda and not recognized by *Pseudomonas*) that enable isolation of chromosomally co-integrated clones. The origin of transfer *ori*T is recognized by a relaxase (key protein in conjugation), *traJ* gene – encodes a regulation transfer component required for conjugation, *lacZ* alpha – enable blue and white screening and Km^R encodes for a aminoglycoside 3-phosphotransferase conferring kanamycin resistance. During triparental mating, a homing endonuclease (carried by the plasmid DH5α pSW-2) recognises the sites I-SceI, enabling cleavage of the vector backbone from the bacterial genome. Two flanking regions (TS1 and TS2) corresponding to the up- and downstream of the genes of interests were fused and cloned into the multiple cloning site (MCS), where XbaI was used to open the vector. The resulting deletion and insetion vectors pEMG TS1_*Ptac*_TS2 (B) and pEMG TS1_*aroY-Ptac*_TS2(C) were delivered sequentially in two steps into *P. putida* KT2240 by conjugation. The vector pEMG TS1_*Ptac*_TS2 deletes *catRBC* and inserts the tac promoter (*Ptac*). Otherwise, pEMG TS1_*aroY-Ptac*_TS2 deletes *pcaHG* and inserts *aroY* with *Ptac*. The resulting strains *P. putida* KT2440Δ*catRBC::Ptac* and *P.putida* KT2440Δ*catRBC::Ptac*Δ*pcaHG::aroY::Ptac* can produce muconate from benzoate and the mixture CFB, respectively.

Codon-optimized gene (*aroY* + *Ptac*)

It was ordered as two fragments of synthetic DNA (gBlocks®, integrated DNA technologies) for generation of *P. putida* KT2440*ΔcatRBC::PtacΔpcaHG::aroY-Ptac*. Lower case letters indicate overhangs. The colors follow the same pattern shown in Fig. S2.2C.

Fragment MAF1 (5´-> 3´):

ggccacacccagctcgttgtAGCCGAACGGGGTGGTTGGCGCTTCGAAGCAGGCACCGATGTAGATGGCT
GGGTCCAGGCCCATGTTGATGGTCACCGGCAGCGGCTTACCGGCGGCTTCGGCCTTCTTGCGGAAC
ACCTCGATGTGGCGACCGGCGGCCAGGAACATGCTCAGCTCGTCGCGCTCTTGCACGCACAGGCGG
TGGATGGTCACGTCGGTCAGGCTGGTATCTTCCGGGTCGCTCGCCAGCACCAGGCCCAGGCAGAAG
AACGGACCGGCATCGATCGGGGTGTTGGTTGGGGCTGGCAGCAGCTTGCGCAGGTCGAAGTCCGG
GTCGTCGGCGTAGAACACCTGTTCTTGGCATGGGGCTTGGCTGGCTGGCACCACCACTGGGGCCAC
CGGGTTCTTCACGGCCTGGCCCACGTGCTGCGCCAGTTTGCTTGGCACGCAGCCCAGCAGCAGGGC
GGCACGTTCACGGCTGGCGTGCATGCCCACCAGGATGCGGCTGCCTGGGTAGCCCTTCACGCTGTT
GAACATCATGGCTGGACCGGTGCGGGTCGGACGTTTCACGGTGCCACCCGCACCGATGTGGCGGTA
CACACCGGCCAGTTCGGCGTTCGGGTCGACCGGGTGGTCGGTTTCGATGTAGTGACCCGGATGGCG
TTGCAGCAGCGCGATCGCGGAGCGCAGGTCGTTGATCGGGTTCTGCATTCTCCCTCCTCTGTGTGAA
ATTGTTATCCGCTCACAATTCCACACATTATACGAGCCGATGATTAATTGTCAACAGCTCAGATCTGG
AATTGTGAGAACGCCTGG

Fragment MAF2 (5´-> 3´):

GAGCGGCCCCAAGCTTCACCGCGGCCGCTCACTTCTTGTCGCTGAACAGCTCTGGGGCCCACGGGG
TCGGGTCCACTTCCATGAATGGGGCACGCTCGAAACGGGCTTTCAGGGCCCACGGCACGGTGCAGT
CGAAGATGGTCTTGCAGCTGATGCCGTTGCCACGGATGCTGGTGCTGTAGTCTGGGCTCTGGCTCG
GGTCCAGCTGATGGCCACGGATGCCTGGCAGGGTGGTGATGCTCACGTCGCCCTGCATGCGGGTGG
TCATGGCCCACAGGATGTCGTCGCTGTCGAAGATGTCCACGTCCTCGTCCACCAGGATGATGTTCTT
CAGCTCGCTGTAGGTGGCCAGGGCGATCAGGGCGGCTTGGCCCTGACGGCCTTCGTCGCTCGGCTG
GCGCTTCTTGACCTGCAGGATGCCCAGGAACTTACCGCCACCGGCGGTGTGGGCGTACACGTTCTGC
AGGAAGCCTGGGATCGCCTCTTCCACGGCGTTGCGGATGCTGGCTTCGGTCGGCAGACCCGCCAGG
GTGGTGTGTTCCTCACCCGGACCCACCAGGGTCTGCAGGATGGCGTGGTTGCGCATGGTCACGGCC
TTCACCTTGATCACCGGCAGGCTCGGGTTGGCCTCACCGCAGTAGCCTGGGAATTCCGGCATGGCGT
GACCGGTGTTGGTGTGCTGATCTTCGCGCACGCGCACGCCTGGCAGCAGTTCGCCCTCGATGATGAT
CTCGGCACGCGCGATCGCCTTCTCTTTCACGGCCACGCCCTGCACCAGTTCCACCGGTTGCTGACGCA
GGGCACCggccacacccagctcgttgt

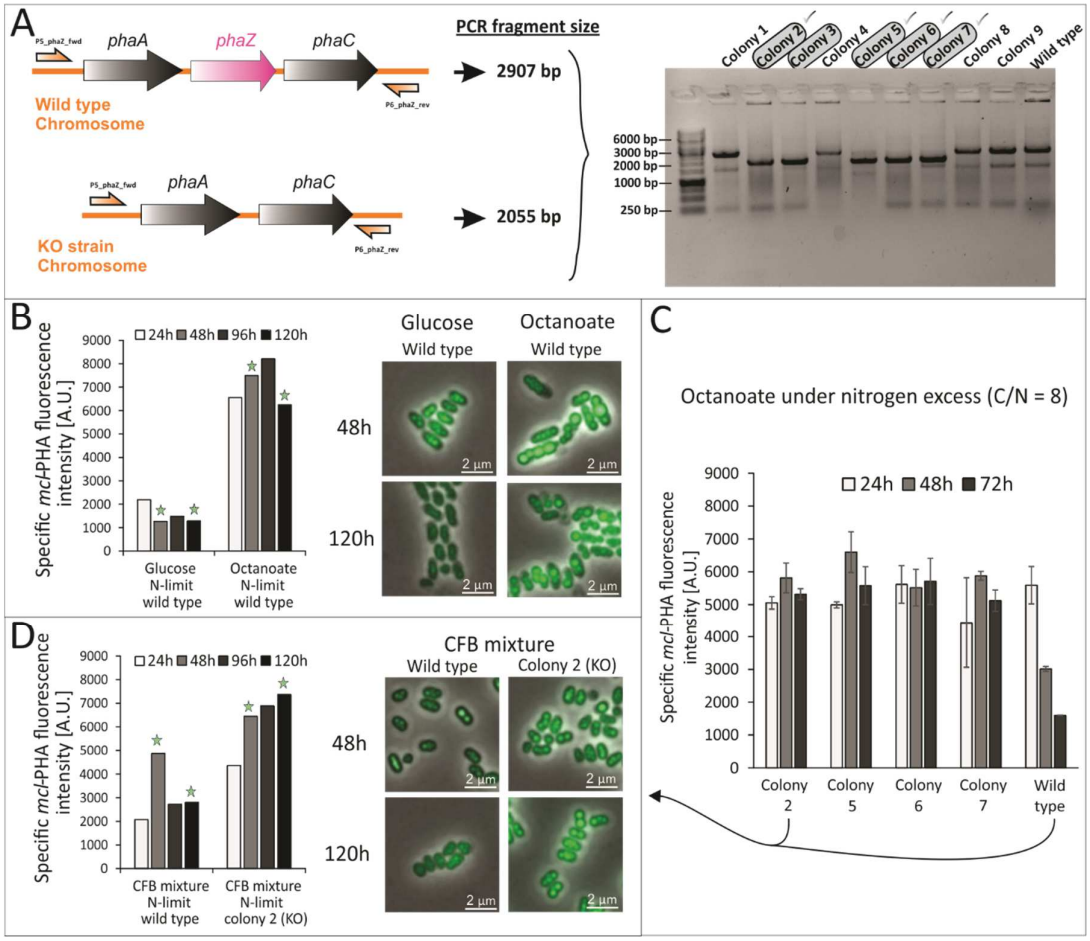

Figure S2.3 Genotypic and phenotypic characterization of the knock out (KO) strain *P. putida* KT2440-KOZ1 or *P. putida* KT2440 Δ*phaZ*. The genomic deletion of the gene *phaZ* was confirmed by gel electrophoresis, comparing the size of PCR fragments of selected colonies and the wild type strain using the same pair of primers P5_phaZ_fwd and P5_phaZ_rev (A). The wild type strain was phenotypically characterized for specific *mcl*-PHA fluorescence production (OD_{600} normalized *mcl*-PHA fluorescence) growing on glucose and octanoate to evaluate *mcl*-PHA depolymerisation under nitrogen limitation (C/N of 80) for 120 h. The selected colonies were also compared with the wild type strain on octanoate to confirm differences on *mcl*-PHA depolymerization when nitrogen was available (*i.e.* nitrogen excess, C/N of 8) (C). Finally, colony 2 was compared with the wild type growing on the CFB aromatic mixture under nitrogen limitation (C/N of 80). Colony number 2 was selected after verifying a higher *mcl*-PHA accumulation respect to the wild type. The fluorescence microscopy pictures showing differences in *mcl*-PHA fluorescence were captured under the same imaging conditions. Error bars indicate the deviation from the mean (n = 2).

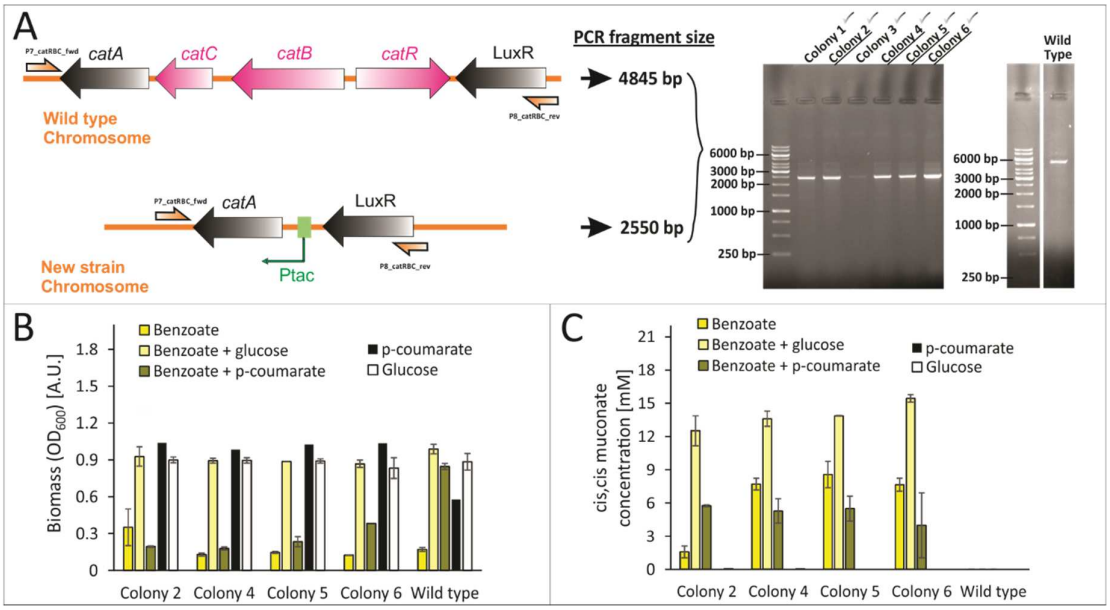

Figure S2.4 Genotypic and phenotypic characterization of the knock out (KO) strain *P. putida* KT2440-CCMA1 or *P. putida* KT2440Δ*catRBC::Ptac*. The genomic deletion of the gene *catRBC* and simultaneous insertion of the tac promoter (*Ptac*) was confirmed by gel electrophoresis, comparing the size of PCR fragments of selected colonies and the wild type strain using the same pair of primers P7_*catRBC*_fwd and P8_*catRBC*_rev (A). The selected colonies and wild type strain were phenotypically characterized by growth as OD_{600} (B) and *cis,cis* muconate production (C) on different substrates (each at 15 mM). Colony number 5 was selected after verifying the small differences between other colonies and the conversion around 95% of benzoate into *cis,cis*-muconate. Error bars indicate the deviation from the mean (n = 2).

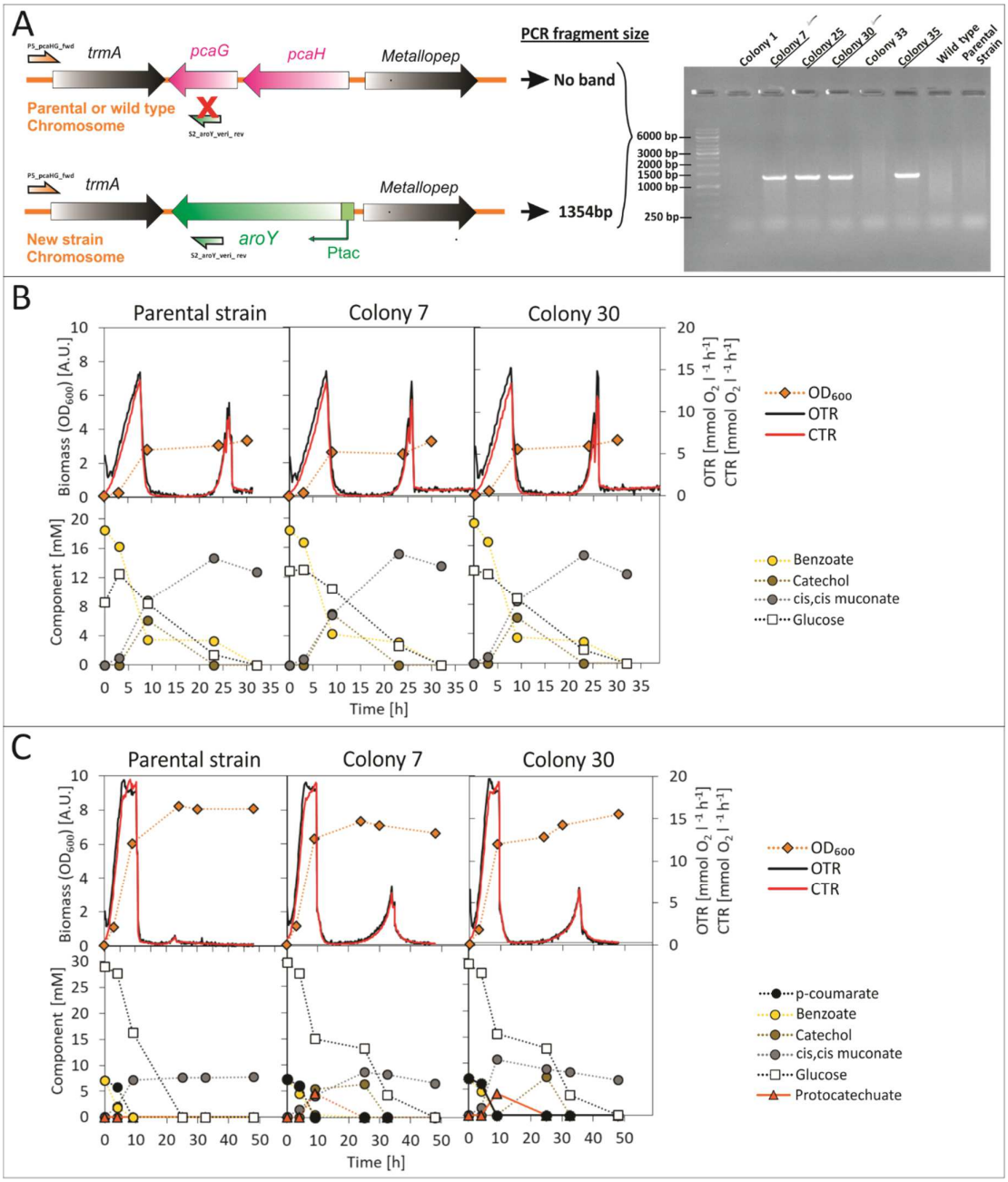

Figure S2.5 Genotypic and phenotypic characterization the strain *P. putida* KT2440-CCMA2 or *P. putida* KT2440*ΔcatRBC::PtacΔpcaHG::aroY-Ptac*. The genomic deletion of the gene *pcaHG* and simultaneous insertion of *aroY* and the tac promoter (*Ptac*) was confirmed by gel electrophoresis, comparing the size of PCR fragments of selected colonies, the wild type and the parental strain *P. putida* KT2440-CCMA1 (*P. putida* KT2440Δ*catRBC::Ptac*). The pair of primers P5_ *pcaHG* _fwd and S2_*aroY*_veri_ rev (binds inside the *aroY* gene) generated a PCR product of 1345 bp only in the successful cases (A). The selected colonies and parental strain were phenotypically characterized for *cis,cis*-muconate production, growth profiles (OD_{600}) and O_2/CO_2 transfer rates from media containing benzoate (15mM) and supplemented with glucose (15mM) (B). Similarly, production of *cis,cis*-muconate was confirmed from a mixture of benzoate (7.5 mM) and p-coumarate (7.5 mM) supplemented with glucose (30 mM) (C).

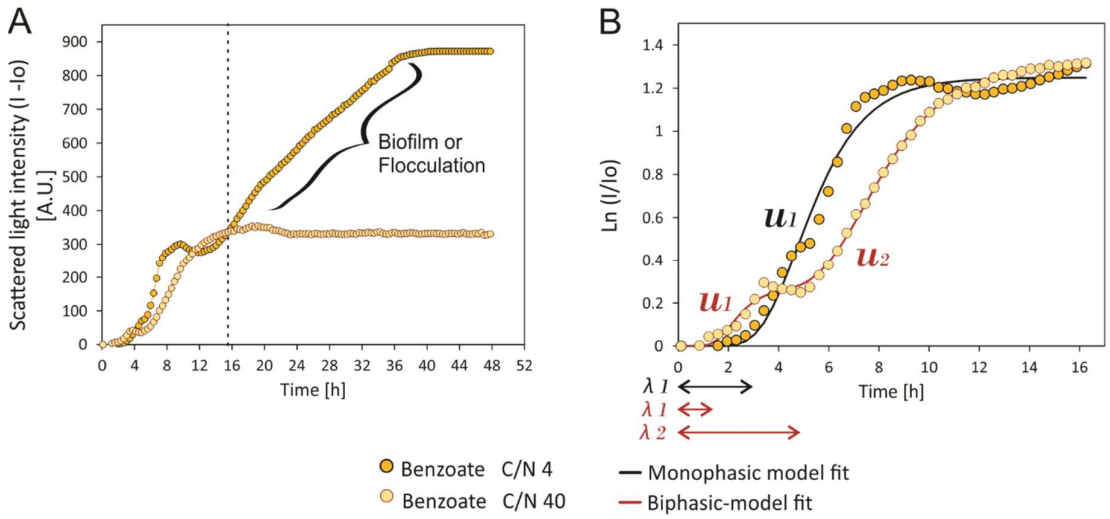

Fig. S2.6 Example of the procedure followed when fitting online measurements of scattered light with the modified Gompertz model (section 2.7.2, Eq. (2)) to obtain relevant growth parameters (maximum specific growth rate μ_{max} [h^{-1}] and lag times λ [h]). This particular case shows the growth profile of *P. putida* KT2440 on benzoate under excess (C/N of 4) and limited (C/N of 40) nitrogen conditions. Scattered light intensity values over 400 were related to biofilm or flocs formation due to carbon depletion under nitrogen excess (A) (error bars not included, n = 3). Zoom into the first 16 hours (B), which have been used for growth parameter determination. When a biphasic profile was identified, an adapted version of the growth model (Eq. (3)) was implemented, obtaining the parameters for two sequential sigmoid curves.

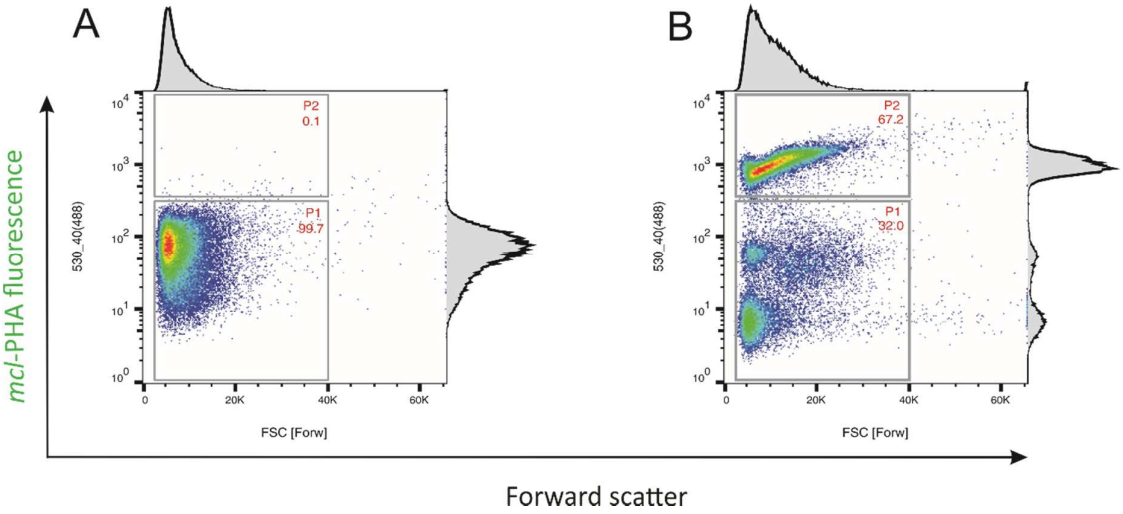

Fig. S2.7 Fluorescence scatter plots and histograms during gate definition for identifying *mcl*-PHA accumulating populations in *P. putida*. Negative control under nitrogen excess (C/N of 8) (A). The gate P2 corresponded to bacterial populations with a common characteristic (green fluorescence values higher than 350) and was defined using *mcl*-PHA accumulating biomass after 24 hours under nitrogen limitation, C/N of 80 (B).

Supplementary information for Chapter 4

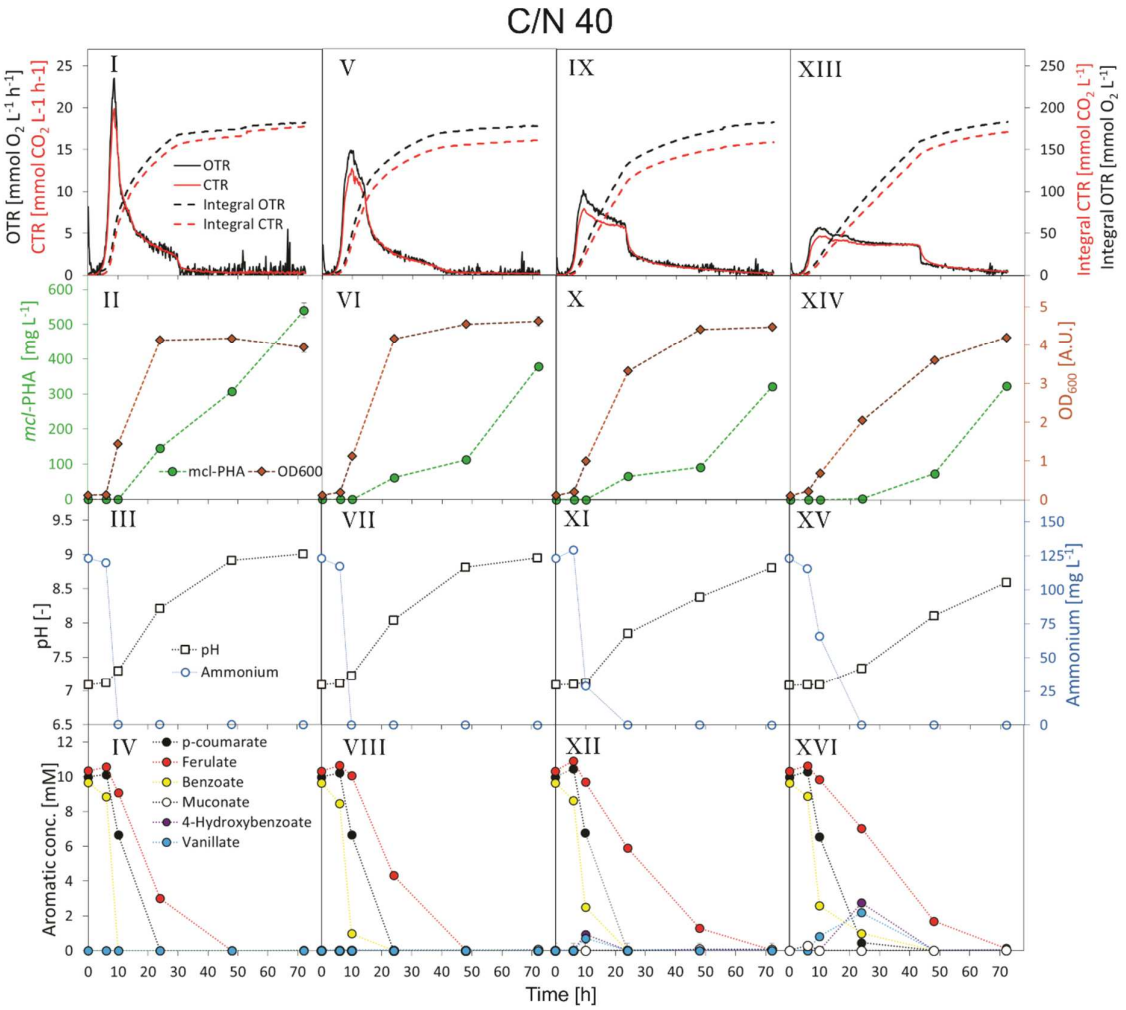

Fig. S4.1 Dynamics of aromatic funneling and *mcl*-PHA accumulation in *P. putida* KT2440 at different oxygen transfer rates (OTRs) under nitrogen limitation (C/N of 40). Different OTRs were set by changing the filling volumes 10 (I - IV), 20 (V - VIII), 30 (IX - XII) and 50 ml (XIII - XVI) of a master mix in shake flasks for online monitored cultivations. Process parameters like the integral of OTR and CTR (I,V,IX,XIII), *mcl*-PHA concentration and OD_{600} (II,VI,X,XIV), pH and ammonium concentration (III,VII,XI,XV) and aromatic concentration (IV,VIII,XII,XVI) are reported. Duplicates were evaluated in the TOM® device without disturbances up to 72 h, while samplings flasks were sacrificed in a conventional shaker for offline sampling.

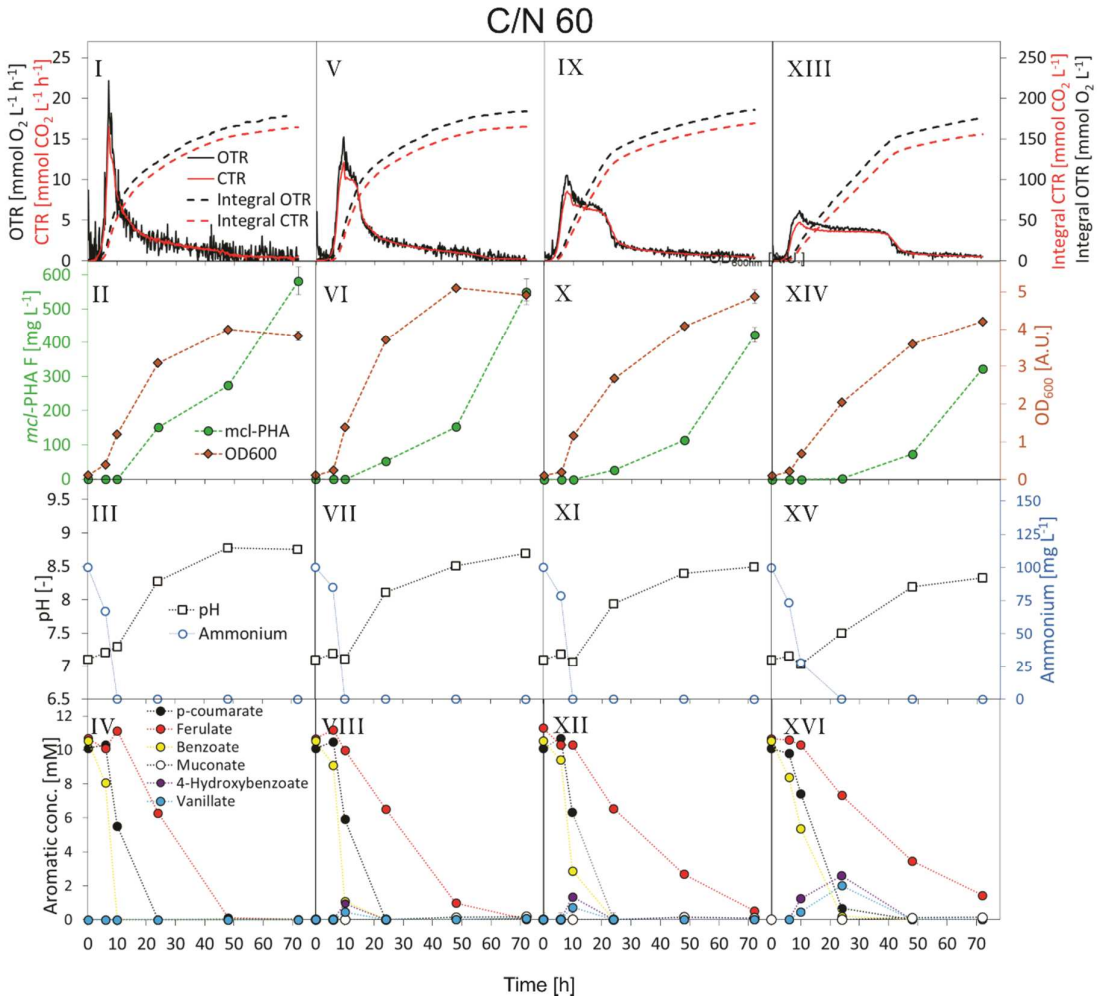

Fig. S4.2 Dynamics of aromatic funneling and *mcl*-PHA accumulation in *P. putida* KT2440 at different oxygen transfer rates (OTRs) under nitrogen limitation C/N 60. Different OTRs were set by changing the filling volumes 10 (I - IV), 20 (V - VIII), 30 (IX - XII) and 50 ml (XIII - XVI) of a master mix in shake flasks for online monitored cultivations. Process parameters like the integral of OTR and CTR (I,V,IX,XIII), *mcl*-PHA concentration and OD_{600} (II,VI,X,XIV), pH and ammonium concentration (III,VII,XI,XV) and aromatic concentration (IV,VIII,XII,XVI) are reported. Duplicates were evaluated in the TOM® device without disturbances up to 72 h, while samplings flasks were sacrificed in a conventional shaker for offline sampling.

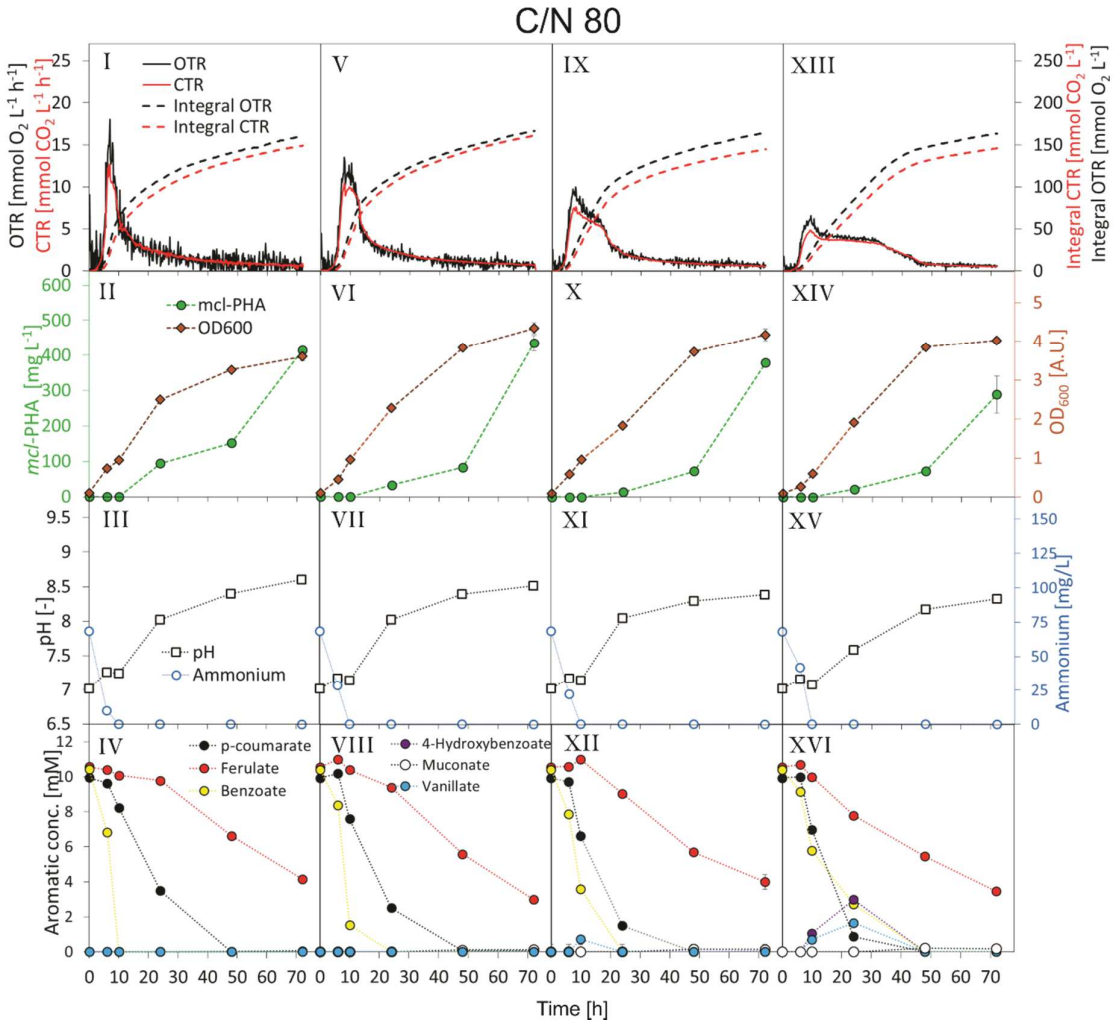

Fig. S4.3 Dynamics of aromatic funneling and *mcl*-PHA accumulation in *P. putida* KT2440 at different oxygen transfer rates (OTRs) under nitrogen limitation C/N 80. Different OTRs were set by changing the filling volumes 10 (I - IV), 20 (V - VIII), 30 (IX - XII) and 50 ml (XIII - XVI) of a master mix in shake flasks for online monitored cultivations. Process parameters like the integral of OTR and CTR (I,V,IX,XIII), *mcl*-PHA concentration and OD_{600} (II,VI,X,XIV), pH and ammonium concentration (III,VII,XI,XV) and aromatic concentration (IV,VIII,XII,XVI) are reported. Duplicates were evaluated in the TOM® device without disturbances up to 72 h, while samplings flasks were sacrificed in a conventional shaker for offline sampling.

Supplementary information for Chapter 5

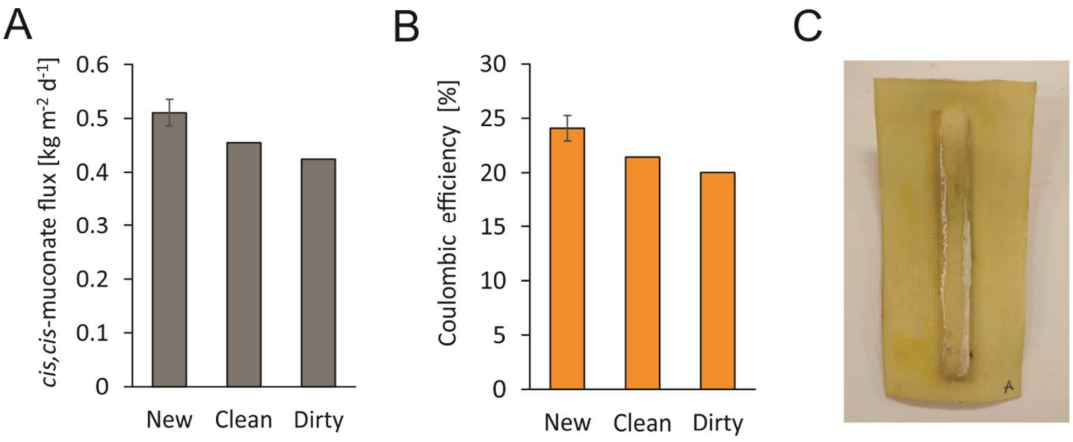

Fig. S5.1 Electrolytic extraction of *cis,cis*-muconate in different membrane conditions in terms of flux (A) and coulombic efficiency (B). The ''new'' term states for brand new membrane, ''dirty'' corresponds to a one time reused membrane and ''clean'' corresponds to a one time reused membrane cleaned through washing with 0.1M NaOH. The photo shows precipitation of *cis,cis*-muconic acid and salt at the AEM surface after one extraction (dirty membrane) (C).

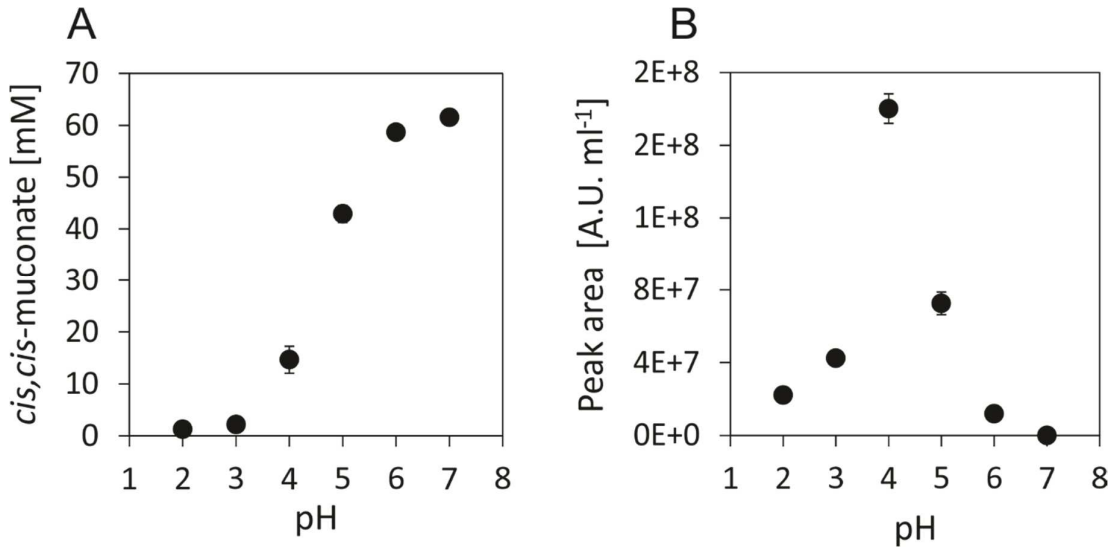

Fig. S5.2 Profiles of dissolved *cis,cis*-muconate (A) and corresponding peak area of *cis-trans*-muconate in solution when the pH of a fermentation broth is decreased from 7.0 to 2.0. Samples were taken from the supernatant.

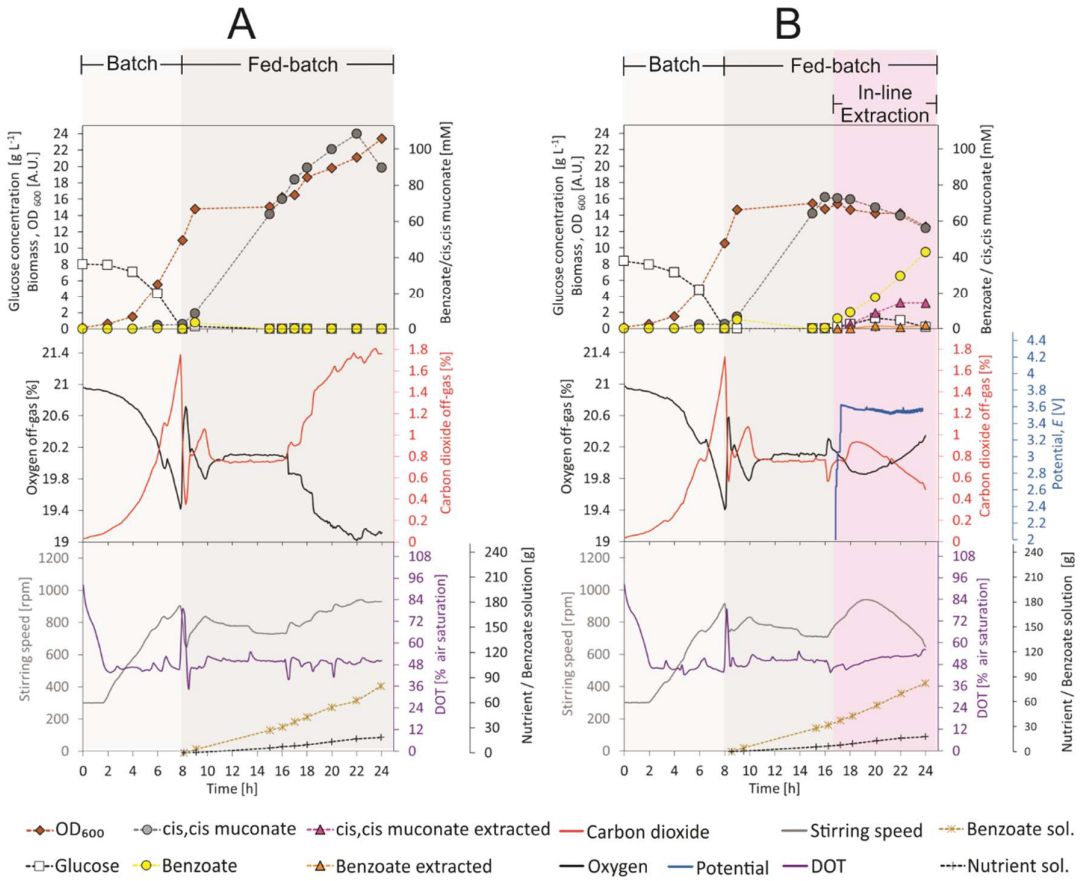

Fig. S5.3 Operational data of two parallel bioprocesses for *cis,cis*-muconate production. Both, conventional bioprocess (A) and an integrated bioprocess for *in-line* electrolytic membrane extraction of *cis,cis*-muconate (B) were operated at 30 °C under DOT control at 50 % air saturation. Both systems were fed by a same benzoate (1.2 M) and nutrient solutions (600 g glucose L^{-1}). The extractive cell was coupled after 16 h. Additional operational parameters like off-gas composition and cell potential and stirring speed, dissolved oxygen tension (DOT) and amount of fed solutions were recorded.

References

Abdelaziz, O.Y., D.P. Brink, J. Prothmann, K. Ravi, M. Sun*, et al.* 2016. Biological valorization of low molecular weight lignin. *Biotechnology Advances*. 34 (8):1318-1346.

Abu-Omar, M.M., K. Barta, G.T. Beckham, J.S. Luterbacher, J. Ralph*, et al.* 2021. Guidelines for performing lignin-first biorefining. *Energy & Environmental Science*. 14 (1):262-292.

Adler, E. 1957. Structural elements of lignin. *Industrial & Engineering Chemistry*. 49 (9):1377-1383.

Ali, I. and N. Jamil. 2016. Polyhydroxyalkanoates: Current applications in the medical field. *Frontiers in Biology*. 11 (1):19-27.

Amadu, A.A., S. Qiu, S. Ge, G.N.D. Addico, G.K. Ameka*, et al.* 2021. A review of biopolymer (poly-β-hydroxybutyrate) synthesis in microbes cultivated on wastewater. *Science of The Total Environment*. 756 143729.

Andersen, S.J., T. Hennebel, S. Gildemyn, M. Coma, J. Desloover*, et al.* 2014. Electrolytic membrane extraction enables production of fine chemicals from biorefinery sidestreams. *Environmental Science & Technology*. 48 (12):7135-7142.

Andersen, S.J., P. Candry, T. Basadre, W.C. Khor, H. Roume*, et al.* 2015. Electrolytic extraction drives volatile fatty acid chain elongation through lactic acid and replaces chemical ph control in thin stillage fermentation. *Biotechnology for Biofuels*. 8 (1):221.

Anderson, E.M., R. Katahira, M. Reed, M.G. Resch, E.M. Karp*, et al.* 2016. Reductive catalytic fractionation of corn stover lignin. *ACS Sustainable Chemistry & Engineering*. 4 (12):6940-6950.

Anderson, E.M., M.L. Stone, R. Katahira, M. Reed, G.T. Beckham*, et al.* 2017. Flowthrough reductive catalytic fractionation of biomass. *Joule*. 1 (3):613-622.

Andrady, A.L. and M.A. Neal. 2009. Applications and societal benefits of plastics. *Philosophical transactions of the Royal Society of London. Series B, Biological sciences*. 364 (1526):1977-1984.

Arias, S., M. Bassas-Galia, G. Molinari and K.N. Timmis. 2013. Tight coupling of polymerization and depolymerization of polyhydroxyalkanoates ensures efficient management of carbon resources in *Pseudomonas putida*. *Microbial Biotechnology*. 6 (5):551-563.

Aryapratama, R. and M. Janssen. 2017. Prospective life cycle assessment of bio-based adipic acid production from forest residues. *Journal of Cleaner Production*. 164 434-443.

Bang, S.-G. and C.Y. Choi. 1995. Do-stat fed-batch production of *cis, cis*-muconic acid from benzoic acid by *Pseudomonas putida* BM014. *Journal of Fermentation and Bioengineering*. 79 (4):381-383.

Becker, J. and C. Wittmann. 2019. A field of dreams: Lignin valorization into chemicals, materials, fuels, and health-care products. *Biotechnology Advances*. 37 (6):107360.

Behling, R., S. Valange and G. Chatel. 2016. Heterogeneous catalytic oxidation for lignin valorization into valuable chemicals: What results? What limitations? What trends? *Green Chemistry*. 18 (7):1839-1854.

Belda, E., R.G.A. van Heck, M. José Lopez-Sanchez, S. Cruveiller, V. Barbe*, et al.* 2016. The revisited genome of *Pseudomonas putida* KT2440 enlightens its value as a robust metabolic chassis. *Environmental Microbiology*. 18 (10):3403-3424.

Berner, R.A. 2003. The long-term carbon cycle, fossil fuels and atmospheric composition. *Nature*. 426 (6964):323-326.

Bhatia, S.K., S.S. Jagtap, A.A. Bedekar, R.K. Bhatia, K. Rajendran*, et al.* 2021. Renewable biohydrogen production from lignocellulosic biomass using fermentation and integration of systems with other energy generation technologies. *Science of The Total Environment*. 765 144429.

Biorizon Align project launched: Developing bio-aromatics from lignin. https://www.biorizon.eu/news/align-project-launched-developing-bio-aromatics-from-lignin (accessed 02-05-2021).

Birgen, C., P. Dürre, H.A. Preisig and A. Wentzel. 2019. Butanol production from lignocellulosic biomass: Revisiting fermentation performance indicators with exploratory data analysis. *Biotechnology for Biofuels*. 12 (1):167.

Blank, L.M., B.E. Ebert, K. Buehler and B. Bühler. 2010. Redox biocatalysis and metabolism: Molecular mechanisms and metabolic network analysis. *Antioxidants & Redox Signaling*. 13 (3):349-394.

Blunt, W., C. Dartiailh, R. Sparling, D. Gapes, D.B. Levin*, et al.* 2017. Microaerophilic environments improve the productivity of medium chain length polyhydroxyalkanoate biosynthesis from fatty acids in Pseudomonas putida LS46. *Process Biochemistry*. 59 18-25.

Blunt, W., R. Sparling, D.J. Gapes, D.B. Levin and N. Cicek. 2018. The role of dissolved oxygen content as a modulator of microbial polyhydroxyalkanoate synthesis. *World Journal of Microbiology and Biotechnology*. 34 (8):106.

Borrero-de Acuña, J.M., I. Gutierrez-Urrutia, C. Hidalgo-Dumont, C. Aravena-Carrasco, M. Orellana-Saez*, et al.* 2020. Channelling carbon flux through the meta-cleavage route for improved poly(3-hydroxyalkanoate) production from benzoate and lignin-based aromatics in *Pseudomonas putida* H. *Microbial Biotechnology*. n/a (n/a):

Boyer, H.W. and D. Roulland-Dussoix. 1969. A complementation analysis of the restriction and modification of DNA in *Escherichia coli*. *Journal of Molecular Biology* 41 (3):459-472.

Brink, D.P., K. Ravi, G. Liden and M.F. Gorwa-Grauslund. 2019. Mapping the diversity of microbial lignin catabolism: Experiences from the elignin database. *Applied Microbiology and Biotechnology* 103 (10):3979-4002.

Cai, L., M.Q. Yuan, F. Liu, J. Jian and G.Q. Chen. 2009. Enhanced production of medium-chain-length polyhydroxyalkanoates (PHA) by *pha* depolymerase knockout mutant of *Pseudomonas putida* KT2442. *Bioresource Technology*. 100 (7):2265-2270.

Calero, P., S.I. Jensen, K. Bojanovič, R.M. Lennen, A. Koza*, et al.* 2018. Genome-wide identification of tolerance mechanisms toward p-coumaric acid in *Pseudomonas putida*. *Biotechnology and Bioengineering*. 115 (3):762-774.

Cao, L., I.K.M. Yu, Y. Liu, X. Ruan, D.C.W. Tsang*, et al.* 2018. Lignin valorization for the production of renewable chemicals: State-of-the-art review and future prospects. *Bioresource Technology*. 269 465-475.

Cao, Y., S.S. Chen, S. Zhang, Y.S. Ok, B.M. Matsagar*, et al.* 2019. Advances in lignin valorization towards bio-based chemicals and fuels: Lignin biorefinery. *Bioresource Technology*. 291 121878.

Carraher, J.M., J.E. Matthiesen and J.-P. Tessonnier. 2016. Comments on "thermodynamics of *cis,cis*-muconic acid solubility in various polar solvents at low temperature range". *Journal of Molecular Liquids*. 224 420-422.

Carraher, J.M., T. Pfennig, R.G. Rao, B.H. Shanks and J.-P. Tessonnier. 2017. Cis,cis-muconic acid isomerization and catalytic conversion to biobased cyclic-c6-1,4-diacid monomers. *Green Chemistry*. 19 (13):3042-3050.

Carvajal-Arroyo, J.M., S.J. Andersen, R. Ganigué, R.A. Rozendal, L.T. Angenent*, et al.* 2020. Production and extraction of medium chain carboxylic acids at a semi-pilot scale. *Chemical Engineering Journal*. 127886.

Cavalheiro, J.M.B.T., R.S. Raposo, M.C.M.D. de Almeida, M. Teresa Cesário, C. Sevrin*, et al.* 2012. Effect of cultivation parameters on the production of poly(3-hydroxybutyrate-co-4-hydroxybutyrate) and poly(3-hydroxybutyrate-4-hydroxybutyrate-3-hydroxyvalerate) by *Cupriavidus necator* using waste glycerol. *Bioresource Technology*. 111 391-397.

Chan, J.C., M. Paice and X. Zhang. 2020. Enzymatic oxidation of lignin: Challenges and barriers toward practical applications. *ChemCatChem*. 12 (2):401-425.

Chen, G.-Q. and X.-R. Jiang. 2017. Engineering bacteria for enhanced polyhydroxyalkanoates (PHA) biosynthesis. *Synthetic and Systems Biotechnology*. 2 (3):192-197.

Chen, G.-Q. and X.-R. Jiang. 2018. Engineering microorganisms for improving polyhydroxyalkanoate biosynthesis. *Current Opinion in Biotechnology*. 53 20-25.

Choi, C.-W., E.C. Park, S.H. Yun, S.-Y. Lee, Y.G. Lee*, et al.* 2014. Proteomic characterization of the outer membrane vesicle of *Pseudomonas putida* KT2440. *Journal of Proteome Research*. 13 (10):4298-4309.

Choi, S., H.-N. Lee, E. Park, S.-J. Lee and E.-S. Kim. 2020. Recent advances in microbial production of cis,cis-muconic acid. *Biomolecules*. 10 (9):1238.

Choi, W.J., E.Y. Lee, M.H. Cho and C.Y. Choi. 1997. Enhanced production of cis,cis-muconate in a cell-recycle bioreactor. *Journal of Fermentation and Bioengineering*. 84 (1):70-76.

Crafts, N. 2000. Globalization and growth in the twentieth century. *IMF Working Paper*. (No. 00/44):Available at SSRN: https://ssrn.com/abstract=879431.

Dartiailh, C., W. Blunt, P.K. Sharma, S. Liu, N. Cicek*, et al.* 2021. The thermal and mechanical properties of medium chain-length polyhydroxyalkanoates produced by *Pseudomonas putida* LS46 on various substrates. *Frontiers in Bioengineering and Biotechnology*. 8 617489-617489.

Das, L., S. Xu and J. Shi. 2017. Catalytic oxidation and depolymerization of lignin in aqueous ionic liquid. *Frontiers in Energy Research*. 5 (21):

de Candolle, A.P. 1813. Theorie elementaire de la botanique ou exposition des principes de la classification naturelle et de l'art de decrire et d'etudier les vegetaux. *Paris, Déterville*. See p. 417.

de Eugenio, L.I., P. Garcia, J.M. Luengo, J.M. Sanz, J.S. Roman*, et al.* 2007. Biochemical evidence that *phaz* gene encodes a specific intracellular medium chain length polyhydroxyalkanoate depolymerase in *Pseudomonas putida* KT2442: Characterzation of a paradigmatic enzyme. *Journal of Biological Chemistry*. 282 (7):4951-4962.

de Eugenio, L.I., I.F. Escapa, V. Morales, N. Dinjaski, B. Galán*, et al.* 2010. The turnover of medium-chain-length polyhydroxyalkanoates in *Pseudomonas putida* KT2442 and the fundamental role of Phaz depolymerase for the metabolic balance. *Environmental Microbiology*. 12 (1):207-221.

de Gonzalo, G., D.I. Colpa, M.H.M. Habib and M.W. Fraaije. 2016. Bacterial enzymes involved in lignin degradation. *Journal of Biotechnology*. 236 110-119.

de Lorenzo, V. and K.N. Timmis. 1994. Analysis and construction of stable phenotypes in gram-negative bacteria with tn5- and tn10-derived minitransposons. *Methods in Enzymology*. 235 386-405.

de Oliveira, D.M., A. Finger-Teixeira, T. Rodrigues Mota, V.H. Salvador, F.C. Moreira-Vilar*, et al.* 2015. Ferulic acid: A key component in grass lignocellulose recalcitrance to hydrolysis. *Plant Biotechnology Journal*. 13 (9):1224-1232.

Den, W., V.K. Sharma, M. Lee, G. Nadadur and R.S. Varma. 2018. Lignocellulosic biomass transformations via greener oxidative pretreatment processes: Access to energy and value-added chemicals. *Frontiers in Chemistry*. 6 141.

Długołęcki, P., B. Anet, S.J. Metz, K. Nijmeijer and M. Wessling. 2010. Transport limitations in ion exchange membranes at low salt concentrations. *Journal of Membrane Science*. 346 (1):163-171.

Dos Santos, V.A.P.M., S. Heim, E.R.B. Moore, M. Strätz and K.N. Timmis. 2004. Insights into the genomic basis of niche specificity of *Pseudomonas putida* KT2440. *Environmental Microbiology*. 6 (12):1264-1286.

Draths, K.M. and J.W. Frost. 1994. Environmentally compatible synthesis of adipic acid from d-glucose. *Journal of the American Chemical Society*. 116 (1):399-400.

ElMekawy, A., L. Diels, H. De Wever and D. Pant. 2013. Valorization of cereal based biorefinery byproducts: Reality and expectations. *Environmental Science & Technology*. 47 (16):9014-9027.

European-Commission. 2012. Innovating for sustainable growth: A bioeconomy for europe. *Press conference, Brussels*. 13

European-Commission. 2015. Closing the loop-an eu action plan for the circular economy. *COM (2015) 614 final*.

European-Commission. 2018. A sustainable bioeconomy for europe: Strengthening the connection between economy, society and the environment. *European Commission.–2018.–URL: https://ec. europa. eu/research/bioeconomy/pdf/ec_bioeconomy_strategy_2018. pdf (Consulted 25.02. 2020)*.

Fan, Z., Chapter 7 - Consolidated bioprocessing for ethanol production. In *Biorefineries*, Nasib Qureshi, David B. Hodge and Alain A. Vertès, Eds. Elsevier: Amsterdam, 2014; pp 141-160.

Fernández-Rodríguez, J., X. Erdocia, C. Sánchez, M. González Alriols and J. Labidi. 2017. Lignin depolymerization for phenolic monomers production by sustainable processes. *Journal of Energy Chemistry*. 26 (4):622-631.

Follonier, S., I.F. Escapa, P.M. Fonseca, B. Henes, S. Panke*, et al.* 2013. New insights on the reorganization of gene transcription in *Pseudomonas putida* KT2440 at elevated pressure. *Microbial Cell Factories*. 12 (1):30.

Freeman, A., J.M. Woodley and M.D. Lilly. 1993. *In situ* product removal as a tool for bioprocessing. *Biotechnology (N Y)*. 11 (9):1007-1012.

Funke, M., S. Diederichs, F. Kensy, C. Muller and J. Buchs. 2009. The baffled microtiter plate: Increased oxygen transfer and improved online monitoring in small scale fermentations. *Biotechnology & Bioengineering* 103 (6):1118-1128.

Gibson, D.G., L. Young, R.-Y. Chuang, J.C. Venter, C.A. Hutchison*, et al.* 2009. Enzymatic assembly of DNA molecules up to several hundred kilobases. *Nature Methods*. 6 (5):343-345.

Gildemyn, S., K. Verbeeck, R. Slabbinck, S.J. Andersen, A. Prévoteau*, et al.* 2015. Integrated production, extraction, and concentration of acetic acid from CO_2 through microbial electrosynthesis. *Environmental Science & Technology Letters*. 2 (11):325-328.

Glasser, W.G. 2019. About making lignin great again—some lessons from the past. *Frontiers in Chemistry*. 7 (565):

Gorden, J., T. Zeiner and C. Brandenbusch. 2015. Reactive extraction of *cis,cis*-muconic acid. *Fluid Phase Equilibria*. 393 78-84.

Gorden, J., T. Zeiner, G. Sadowski and C. Brandenbusch. 2016. Recovery of *cis,cis*-muconic acid from organic phase after reactive extraction. *Separation and Purification Technology*. 169 1-8.

Govil, T., J. Wang, D. Samanta, A. David, A. Tripathi*, et al.* 2020. Lignocellulosic feedstock: A review of a sustainable platform for cleaner production of nature's plastics. *Journal of Cleaner Production*. 270 122521.

Hagesteijn, K.F.L., S. Jiang and B.P. Ladewig. 2018. A review of the synthesis and characterization of anion exchange membranes. *Journal of Materials Science*. 53 (16):11131-11150.

Hämäläinen, V., T. Grönroos, A. Suonpää, M.W. Heikkilä, B. Romein*, et al.* 2018. Enzymatic processes to unlock the lignin value. *Frontiers in Bioengineering and Biotechnology*. 6 20-20.

Handojo, L., A.K. Wardani, D. Regina, C. Bella, M.T.A.P. Kresnowati*, et al.* 2019. Electro-membrane processes for organic acid recovery. *RSC Advances*. 9 (14):7854-7869.

Hartmans, S., J.P. Smits, M.J. van der Werf, F. Volkering and J.A.M. de Bont. 1989. Metabolism of styrene oxide and 2-phenylethanol in the styrene-degrading *Xanthobacter strain* 124X. *Applied and Environmental Microbiology*. 55 (11):2850-2855.

Hayes, D.J.M., Chapter 2 - biomass composition and its relevance to biorefining. In *The role of Catalysis for the Sustainable Production of Bio-fuels and Bio-chemicals*, Kostas S. Triantafyllidis and Angelos A. Lappasand Michael Stöcker, Eds. Elsevier: Amsterdam, 2013; pp 27-65.

Hemmilä, V., S. Adamopoulos, O. Karlsson and A. Kumar. 2017. Development of sustainable bio-adhesives for engineered wood panels – a review. *RSC Advances*. 7 (61):38604-38630.

Heyman, B., R. Lamm, H. Tulke, L. Regestein and J. Büchs. 2019. Shake flask methodology for assessing the influence of the maximum oxygen transfer capacity on 2,3-butanediol production. *Microbial Cell Factories*. 18 (1):78.

Hosseinpour Tehrani, H., J. Becker, I. Bator, K. Saur, S. Meyer*, et al.* 2019. Integrated strain- and process design enable production of 220 g l−1 itaconic acid with *Ustilago maydis*. *Biotechnology for Biofuels*. 12 (1):263.

Houghton, R.A., F. Hall and S.J. Goetz. 2009. Importance of biomass in the global carbon cycle. *Journal of Geophysical Research: Biogeosciences*. 114 (G2):

Hughes, J.G., X. Zhang, J.V. Parales, J.L. Ditty and R.E. Parales. 2017. *Pseudomonas putida* F1 uses energy taxis to sense hydroxycinnamic acids. *Microbiology*. 163 (10):1490-1501.

Jardim, J.M., P.W. Hart, L. Lucia and H. Jameel. 2020. Insights into the potential of hardwood kraft lignin to be a green platform material for emergence of the biorefinery. *Polymers*. 12 (8):1795.

Jarre, M., A. Petit-Boix, C. Priefer, R. Meyer and S. Leipold. 2020. Transforming the bio-based sector towards a circular economy - what can we learn from wood cascading? *Forest Policy and Economics*. 110 101872.

Jayakody, L.N., C.W. Johnson, J.M. Whitham, R.J. Giannone, B.A. Black*, et al.* 2018. Thermochemical wastewater valorization via enhanced microbial toxicity tolerance. *Energy & Environmental Science*. 11 (6):1625-1638.

Jendrossek, D. and D. Pfeiffer. 2014. New insights in the formation of polyhydroxyalkanoate granules (carbonosomes) and novel functions of poly(3-hydroxybutyrate). *Environmental Microbiology*. 16 (8):2357-2373.

Jiménez, J.I., J. Nogales, J.L. García and E. Díaz, A genomic view of the catabolism of aromatic compounds in *Pseudomonas*. In *Handbook of hydrocarbon and lipid microbiology*, Kenneth N. Timmis, Ed. Springer Berlin Heidelberg: Berlin, Heidelberg, 2010; pp 1297-1325.

Jiménez, J.I., D. Pérez-Pantoja, M. Chavarría, E. Díaz and V. de Lorenzo. 2014. A second chromosomal copy of the cata gene endows *Pseudomonas putida* mt-2 with an enzymatic safety valve for excess of catechol. *Environmental Microbiology*. 16 (6):1767-1778.

Johnson, C.W. and G.T. Beckham. 2015. Aromatic catabolic pathway selection for optimal production of pyruvate and lactate from lignin. *Metabolic Engineering*. 28 240-247.

Johnson, C.W., D. Salvachúa, P. Khanna, H. Smith, D.J. Peterson*, et al.* 2016. Enhancing muconic acid production from glucose and lignin-derived aromatic compounds via

increased protocatechuate decarboxylase activity. *Metabolic Engineering Communications*. 3 111-119.

Johnson, C.W., P.E. Abraham, J.G. Linger, P. Khanna, R.L. Hettich*, et al.* 2017. Eliminating a global regulator of carbon catabolite repression enhances the conversion of aromatic lignin monomers to muconate in *Pseudomonas putida* KT2440. *Metabolic Engineering Communications*. 5 19-25.

Johnson, C.W., D. Salvachúa, N.A. Rorrer, B.A. Black, D.R. Vardon*, et al.* 2019. Innovative chemicals and materials from bacterial aromatic catabolic pathways. *Joule*. 3 (6):1523-1537.

Johnston, P.A., H. Zhou, A. Aui, M.M. Wright, Z. Wen*, et al.* 2020. A lignin-first strategy to recover hydroxycinnamic acids and improve cellulosic ethanol production from corn stover. *Biomass and Bioenergy*. 138 105579.

Kacmar, J., R. Carlson, S.J. Balogh and F. Srienc. 2006. Staining and quantification of poly-3-hydroxybutyrate in *Saccharomyces cerevisiae* and *Cupriavidus necator* cell populations using automated flow cytometry. *Cytometry Part A*. 69A (1):27-35.

Kamimura, N., K. Takahashi, K. Mori, T. Araki, M. Fujita*, et al.* 2017. Bacterial catabolism of lignin-derived aromatics: New findings in a recent decade: Update on bacterial lignin catabolism. *Environmental Microbiology Reports*. 9 (6):679-705.

Kampers, L.F.C., R.J.M. Volkers and V.A.P. Martins Dos Santos. 2019. *Pseudomonas putida* KT2440 is HV1 certified, not GRAS. *Microbial Biotechnology*. 12 (5):845-848.

Karlen, S.D., P. Fasahati, M. Mazaheri, J. Serate, R.A. Smith*, et al.* 2020. Assessing the viability of recovery of hydroxycinnamic acids from lignocellulosic biorefinery alkaline pretreatment waste streams. *ChemSusChem*. 13 (8):2012-2024.

Karmann, S., S. Follonier, M. Bassas-Galia, S. Panke and M. Zinn. 2016. Robust at-line quantification of poly(3-hydroxyalkanoate) biosynthesis by flow cytometry using a BODIPY 493/503-SYTO 62 double-staining. *Journal of Microbiological Methods*. 131 166-171.

Karmann, S., S. Panke and M. Zinn. 2017. The bistable behaviour of *Pseudomonas putida* KT2440 during PHA depolymerization under carbon limitation. *Bioengineering*. 4 (2):58.

Kek, Y.-K., W.-H. Lee and K. Sudesh. 2008. Efficient bioconversion of palm acid oil and palm kernel acid oil to poly(3-hydroxybutyrate) by cupriavidus necator. *Canadian Journal of Chemistry*. 86 (6):533-539.

Kensy, F., E. Zang, C. Faulhammer, R.-K. Tan and J. Büchs. 2009. Validation of a high-throughput fermentation system based on online monitoring of biomass and fluorescence in continuously shaken microtiter plates. *Microbial Cell Factories*. 8 (1):31.

Khalil, I., G. Quintens, T. Junkers and M. Dusselier. 2020. Muconic acid isomers as platform chemicals and monomers in the biobased economy. *Green Chemistry*. 22 (5):1517-1541.

Khor, W.C., S. Andersen, H. Vervaeren and K. Rabaey. 2017. Electricity-assisted production of caproic acid from grass. *Biotechnology for Biofuels*. 10 (1):180.

Kim, B.S. 2002. Production of medium chain length polyhydroxyalkanoates by fed-batch culture of *Pseudomonas oleovorans*. *Biotechnology Letters*. 24 (2):125-130.

Kim, J.-Y., S.Y. Park, I.-G. Choi and J.W. Choi. 2018. Evaluation of ruxni1-x/sba-15 catalysts for depolymerization features of lignin macromolecule into monomeric phenols. *Chemical Engineering Journal*. 336 640-648.

Kim, K.H. and C.S. Kim. 2018. Recent efforts to prevent undesirable reactions from fractionation to depolymerization of lignin: Toward maximizing the value from lignin. *Frontiers in Energy Research*. 6 (92):

Kim, Y.H., K. Cho, S.H. Yun, J.Y. Kim, K.H. Kwon*, et al.* 2006. Analysis of aromatic catabolic pathways in *Pseudomonas putida* KT2440 using a combined proteomic approach: 2-de/ms and cleavable isotope-coded affinity tag analysis. *Proteomics*. 6 (4):1301-1318.

Kohlstedt, M., S. Starck, N. Barton, J. Stolzenberger, M. Selzer*, et al.* 2018. From lignin to nylon: Cascaded chemical and biochemical conversion using metabolically engineered pseudomonas putida. *Metabolic Engineering*. 47 279-293.

Korányi, T.I., B. Fridrich, A. Pineda and K. Barta. 2020. Development of 'lignin-first' approaches for the valorization of lignocellulosic biomass. *Molecules (Basel, Switzerland)*. 25 (12):2815.

Krom, M.D. 1980. Spectrophotometric determination of ammonia: A study of a modified berthelot reaction using salicylate and dichloroisocyanurate. *Analyst*. 105 (1249):305-316.

Kuepper, J., H.J. Ruijssenaars, L.M. Blank, J.H. de Winde and N. Wierckx. 2015. Complete genome sequence of solvent-tolerant *Pseudomonas putida* S12 including megaplasmid ptts12. *Journal of Biotechnology*. 200 17-18.

Kumar, M., S. You, J. Beiyuan, G. Luo, J. Gupta*, et al.* 2021. Lignin valorization by bacterial genus *Pseudomonas*: State-of-the-art review and prospects. *Bioresource Technology*. 320 124412.

Kunze, M., S. Roth, E. Gartz and J. Büchs. 2014. Pitfalls in optical on-line monitoring for high-throughput screening of microbial systems. *Microbial Cell Factories*. 13 (1):53.

Kusumawardhani, H., R. Hosseini and J.H. de Winde. 2018. Solvent tolerance in bacteria: Fulfilling the promise of the biotech era? *Trends in Biotechnology*. 36 (10):1025-1039.

La Rosa, R., F. de la Peña, M.A. Prieto and F. Rojo. 2014. The Crc protein inhibits the production of polyhydroxyalkanoates in *Pseudomonas putida* under balanced carbon/nitrogen growth conditions. *Environmental Microbiology*. 16 (1):278-290.

Lattermann, C., M. Funke, S. Hansen, S. Diederichs and J. Büchs. 2014. Cross-section perimeter is a suitable parameter to describe the effects of different baffle geometries in shaken microtiter plates. *Journal of Biological Engineering*. 8 (1):18.

Leipold, S. and A. Petit-Boix. 2018. The circular economy and the bio-based sector - perspectives of european and german stakeholders. *Journal of Cleaner Production*. 201 1125-1137.

Li, Q.Z., X.L. Jiang, X.J. Feng, J.M. Wang, C. Sun*, et al.* 2016. Recovery processes of organic acids from fermentation broths in the biomass-based industry. *Journal of Microbiology and Biotechnology*. 26 (1):1-8.

Liao, Y., S.-F. Koelewijn, G. Van den Bossche, J. Van Aelst, S. Van den Bosch*, et al.* 2020. A sustainable wood biorefinery for low–carbon footprint chemicals production. *Science*. 367 (6484):1385-1390.

Lin, L., X. Wang, L. Cao and M. Xu. 2019. Lignin catabolic pathways reveal unique characteristics of dye-decolorizing peroxidases in *Pseudomonas putida*. *Environmental Microbiology*. 21 (5):1847-1863.

Linger, J.G., D.R. Vardon, M.T. Guarnieri, E.M. Karp, G.B. Hunsinger*, et al.* 2014. Lignin valorization through integrated biological funneling and chemical catalysis. *Proceedings of the National Academy of Sciences of the United States of America*. 111 (33):12013-12018.

Liu, Q., L. Luo and L. Zheng. 2018. Lignins: Biosynthesis and biological functions in plants. *International Journal of Molecular Sciences*. 19 (2):335.

Liu, X., F.P. Bouxin, J. Fan, V.L. Budarin, C. Hu*, et al.* 2020. Recent advances in the catalytic depolymerization of lignin towards phenolic chemicals: A review. *ChemSusChem*. 13 (17):4296-4317.

Liu, Z.-H., M.L. Olson, S. Shinde, X. Wang, N. Hao*, et al.* 2017. Synergistic maximization of the carbohydrate output and lignin processability by combinatorial pretreatment. *Green Chemistry*. 19 (20):4939-4955.

Liu, Z.-H., S. Shinde, S. Xie, N. Hao, F. Lin*, et al.* 2019. Cooperative valorization of lignin and residual sugar to polyhydroxyalkanoate (PHA) for enhanced yield and carbon utilization in biorefineries. *Sustainable Energy & Fuels*. 3 (8):2024-2037.

López-Garzón, C.S. and A.J.J. Straathof. 2014. Recovery of carboxylic acids produced by fermentation. *Biotechnology Advances*. 32 (5):873-904.

Lopez-Mondejar, R., C. Algora and P. Baldrian. 2019. Lignocellulolytic systems of soil bacteria: A vast and diverse toolbox for biotechnological conversion processes. *Biotechnology Advances*. 37 (6):107374.

Lyu, G., C.G. Yoo and X. Pan. 2018. Alkaline oxidative cracking for effective depolymerization of biorefining lignin to mono-aromatic compounds and organic acids with molecular oxygen. *Biomass and Bioenergy*. 108 7-14.

Machovina, M.M., S.J.B. Mallinson, B.C. Knott, A.W. Meyers, M. Garcia-Borras*, et al.* 2019. Enabling microbial syringol conversion through structure-guided protein engineering. *Proceedings of the National Academy of Sciences, USA*. 116 (28):13970-13976.

Madison, L.L. and G.W. Huisman. 1999. Metabolic engineering of poly(3-hydroxyalkanoates): From DNA to plastic. *Microbiology and Molecular Biology Reviews : MMBR*. 63 (1):21-53.

Martínez-García, E. and V. de Lorenzo. 2011. Engineering multiple genomic deletions in gram-negative bacteria: Analysis of the multi-resistant antibiotic profile of *Pseudomonas putida* KT2440. *Environmental Microbiology*. 13 (10):2702-2716.

Martínez-García, E. and V. de Lorenzo. 2017. Molecular tools and emerging strategies for deep genetic/genomic refactoring of *Pseudomonas*. *Current Opinion in Biotechnology*. 47 120-132.

Martone, P.T., J.M. Estevez, F. Lu, K. Ruel, M.W. Denny*, et al.* 2009. Discovery of lignin in seaweed reveals convergent evolution of cell-wall architecture. *Current Biology*. 19 (2):169-175.

Masai, E., N. Kamimura, D. Kasai, A. Oguchi, A. Ankai*, et al.* 2012. Complete genome sequence of *Sphingobium sp. strain* SYK-6, a degrader of lignin-derived biaryls and monoaryls. *Journal of Bacteriology*. 194 (2):534-535.

Matthiesen, J.E., J.M. Carraher, M. Vasiliu, D.A. Dixon and J.-P. Tessonnier. 2016. Electrochemical conversion of muconic acid to biobased diacid monomers. *ACS Sustainable Chemistry & Engineering*. 4 (6):3575-3585.

Meier, K., W. Klöckner, B. Bonhage, E. Antonov, L. Regestein*, et al.* 2016. Correlation for the maximum oxygen transfer capacity in shake flasks for a wide range of operating conditions and for different culture media. *Biochemical Engineering Journal*. 109 228-235.

Migula, W. 1894. Über ein neues System der Bakterien. Arbeiten aus dem Bakteriologischen Institut der Technischen Hochschule zu Karlsruhe; 1:235-238.

Migula, W. 1900. System der Bakterien. Vol. 2. Gustav Fischer. Jena, Germany.

Mohanan, N., A. Gislason, P.K. Sharma, A. Ghergab, J. Plouffe*, et al.* 2019. Quorum sensing and the anaerobic regulator (Anr) control polyhydroxyalkanoate (PHA) production in *Pseudomonas chlororaphis* PA23. *FEMS Microbiology Letters*. 366 (18):

Morales, G., J.F. Linares, A. Beloso, J.P. Albar, J.L. Martínez*, et al.* 2004. The *Pseudomonas putida* Crc global regulator controls the expression of genes from several chromosomal catabolic pathways for aromatic compounds. *Journal of Bacteriology*. 186 (5):1337-1344.

Morales, G., A. Ugidos and F. Rojo. 2006. Inactivation of the *Pseudomonas putida* cytochrome o ubiquinol oxidase leads to a significant change in the transcriptome and to increased expression of the CIO and cbb3-1 terminal oxidases. *Environmental Microbiology*. 8 (10):1764-1774.

Mozejko-Ciesielska, J., K. Szacherska and P. Marciniak. 2019. *Pseudomonas* species as producers of eco-friendly polyhydroxyalkanoates. *Journal of Polymers and the Environment*. 27 (6):1151-1166.

Mu, W., H. Ben, A. Ragauskas and Y. Deng. 2013. Lignin pyrolysis components and upgrading—technology review. *BioEnergy Research*. 6 (4):1183-1204.

Muneer, F., I. Rasul, F. Azeem, M.H. Siddique, M. Zubair*, et al.* 2020. Microbial polyhydroxyalkanoates (PHAs): Efficient replacement of synthetic polymers. *Journal of Polymers and the Environment*. 28 (9):2301-2323.

Mycroft, Z., M. Gomis, P. Mines, P. Law and T.D.H. Bugg. 2015. Biocatalytic conversion of lignin to aromatic dicarboxylic acids in *Rhodococcus jostii* RHA1 by re-routing aromatic degradation pathways. *Green Chemistry*. 17 (11):4974-4979.

Nakajima, H., P. Dijkstra and K. Loos. 2017. The recent developments in biobased polymers toward general and engineering applications: Polymers that are upgraded from biodegradable polymers, analogous to petroleum-derived polymers, and newly developed. *Polymers*. 9 (10):523.

Nichols, N.N. and C.S. Harwood. 1995. Repression of 4-hydroxybenzoate transport and degradation by benzoate: A new layer of regulatory control in the *Pseudomonas putida* beta-ketoadipate pathway. *Journal of Bacteriology*. 177 (24):7033-7040.

Nikel, P.I., E. Martínez-García and V. de Lorenzo. 2014. Biotechnological domestication of pseudomonads using synthetic biology. *Nature Reviews Microbiology*. 12 (5):368-379.

Nikel, P.I. and V. de Lorenzo. 2018. *Pseudomonas putida* as a functional chassis for industrial biocatalysis: From native biochemistry to trans-metabolism. *Metabolic Engineering*. 50 142-155.

Nogales, J., J.L. García and E. Díaz, Degradation of aromatic compounds in *Pseudomonas*: A systems biology view. In *Aerobic utilization of hydrocarbons, oils and lipids*, Fernando Rojo, Ed. Cham, 2017; pp 1-49.

Olguin-Maciel, E., A. Singh, R. Chable-Villacis, R. Tapia-Tussell and H.A. Ruiz. 2020. Consolidated bioprocessing, an innovative strategy towards sustainability for biofuels production from crop residues: An overview. *Agronomy*. 10 (11):1834.

Padervand, M., E. Lichtfouse, D. Robert and C. Wang. 2020. Removal of microplastics from the environment. A review. *Environmental Chemistry Letters*. 18 (3):807-828.

Palleroni, N.J. 2010. The *Pseudomonas* story. *Environmental Microbiology*. 12 (6):1377-1383.

Paone, E., T. Tabanelli and F. Mauriello. 2020. The rise of lignin biorefinery. *Current Opinion in Green and Sustainable Chemistry*. 24 1-6.

Park, J.-B., B. Bühler, S. Panke, B. Witholt and A. Schmid. 2007. Carbon metabolism and product inhibition determine the epoxidation efficiency of solvent-tolerant *Pseudomonas sp.* Strain VLB120. *Biotechnology and Bioengineering*. 98 (6):1219-1229.

Pateraki, C., S.J. Andersen, D. Ladakis, A. Koutinas and K. Rabaey. 2019. Direct electrochemical extraction increases microbial succinic acid production from spent sulphite liquor. *Green Chemistry*. 21 (9):2401-2411.

Paul, V., D.C. Rai, R.L. T.S, S.K. Srivastava and A.D. Tripathi. 2021. A comprehensive review on vanillin: Its microbial synthesis, isolation and recovery. *Food Biotechnology*. 35 (1):22-49.

Peña-Ortiz, L., I. Schlembach, G. Lackner and L. Regestein. 2020. Impact of oxygen supply and scale up on mycobacterium smegmatis cultivation and mycofactocin formation. *Frontiers in Bioengineering and Biotechnology*. 8 (1399):

Perez, J.M., W.S. Kontur, M. Alherech, J. Coplien, S.D. Karlen*, et al.* 2019. Funneling aromatic products of chemically depolymerized lignin into 2-pyrone-4-6-dicarboxylic acid with *Novosphingobium aromaticivorans*. *Green Chemistry*. 21 (6):1340-1350.

Pfitzer, C., N. Dahmen, N. Tröger, F. Weirich, J. Sauer*, et al.* 2016. Fast pyrolysis of wheat straw in the bioliq pilot plant. *Energy & Fuels*. 30 (10):8047-8054.

Poblete-Castro, I., D. Binger, R. Oehlert and M. Rohde. 2014a. Comparison of *mcl*-poly(3-hydroxyalkanoates) synthesis by different *Pseudomonas putida* strains from crude glycerol: Citrate accumulates at high titer under PHA-producing conditions. *BMC Biotechnology*. 14 (1):962.

Poblete-Castro, I., A.L. Rodriguez, C.M. Lam and W. Kessler. 2014b. Improved production of medium-chain-length polyhydroxyalkanoates in glucose-based fed-batch cultivations of metabolically engineered *Pseudomonas putida* strains. *Journal of Microbiology and Biotechnology*. 24 (1):59-69.

Prieto, A., I.F. Escapa, V. Martínez, N. Dinjaski, C. Herencias*, et al.* 2016. A holistic view of polyhydroxyalkanoate metabolism in *Pseudomonas putida*. *Environmental Microbiology*. 18 (2):341-357.

Ragauskas, A.J., G.T. Beckham, M.J. Biddy, R. Chandra, F. Chen*, et al.* 2014. Lignin valorization: Improving lignin processing in the biorefinery. *Science*. 344 (6185):1246843.

Ravi, K., J. Garcia-Hidalgo, M.F. Gorwa-Grauslund and G. Liden. 2017. Conversion of lignin model compounds by *Pseudomonas putida* KT2440 and isolates from compost. *Applied Microbiology and Biotechnology*. 101 (12):5059-5070.

Renders, T., S. Van den Bosch, S.F. Koelewijn, W. Schutyser and B.F. Sels. 2017. Lignin-first biomass fractionation: The advent of active stabilisation strategies. *Energy & Environmental Science*. 10 (7):1551-1557.

Renders, T., G. Van den Bossche, T. Vangeel, K. Van Aelst and B. Sels. 2019. Reductive catalytic fractionation: State of the art of the lignin-first biorefinery. *Current Opinion in Biotechnology*. 56 193-201.

Rinaldi, R., R. Jastrzebski, M.T. Clough, J. Ralph, M. Kennema*, et al.* 2016. Paving the way for lignin valorisation: Recent advances in bioengineering, biorefining and catalysis. *Angewandte Chemie International Edition*. 55 (29):8164-8215.

Roddy, D.J. 2013. Biomass in a petrochemical world. *Interface focus*. 3 (1):20120038-20120038.

Rodriguez, A., D. Salvachúa, R. Katahira, B.A. Black, N.S. Cleveland*, et al.* 2017. Base-catalyzed depolymerization of solid lignin-rich streams enables microbial conversion. *ACS Sustainable Chemistry & Engineering*. 5 (9):8171-8180.

Rojo, F. 2010. Carbon catabolite repression in *Pseudomonas*: Optimizing metabolic versatility and interactions with the environment. *FEMS Microbiology Reviews*. 34 (5):658-684.

Rothmel, R.K., D.L. Shinabarger, M.R. Parsek, T.L. Aldrich and A.M. Chakrabarty. 1991. Functional analysis of the *Pseudomonas putida* regulatory protein Catr: Transcriptional studies and determination of the Catr DNA-binding site by hydroxyl-radical footprinting. *Journal of Bacteriology*. 173 (15):4717-4724.

Sainsbury, P.D., E.M. Hardiman, M. Ahmad, H. Otani, N. Seghezzi*, et al.* 2013. Breaking down lignin to high-value chemicals: The conversion of lignocellulose to vanillin in a gene deletion mutant of *Rhodococcus jostii* RHA1. *ACS Chemical Biology* 8(10):2151-2156.

Salvachua, D., T. Rydzak, R. Auwae, A. De Capite, B.A. Black*, et al.* 2020. Metabolic engineering of *Pseudomonas putida* for increased polyhydroxyalkanoate production from lignin. *Microbial Biotechnology*. 13 (1):290-298.

Salvachúa, D., R. Katahira, N.S. Cleveland, P. Khanna, M.G. Resch*, et al.* 2016. Lignin depolymerization by fungal secretomes and a microbial sink. *Green Chemistry*. 18 (22):6046-6062.

Salvachúa, D., C.W. Johnson, C.A. Singer, H. Rohrer, D.J. Peterson*, et al.* 2018. Bioprocess development for muconic acid production from aromatic compounds and lignin. *Green Chemistry*. 20 (21):5007-5019.

Salvachúa, D., A.Z. Werner, I. Pardo, M. Michalska, B.A. Black*, et al.* 2020. Outer membrane vesicles catabolize lignin-derived aromatic compounds in *Pseudomonas putida* KT2440. *Proceedings of the National Academy of Sciences*. 117 (17):9302-9310.

Samorski, M., G. Müller-Newen and J. Büchs. 2005. Quasi-continuous combined scattered light and fluorescence measurements: A novel measurement technique for shaken microtiter plates. *Biotechnology and Bioengineering*. 92 (1):61-68.

Sánchez-Castañeda, A.K., M. Moussa, L. Ngansop, I.C. Trelea and V. Athès. 2020. Organic phase screening for in-stream reactive extraction of bio-based 3-hydroxypropionic acid: Biocompatibility and extraction performances. *Journal of Chemical Technology & Biotechnology*. 95 (4):1046-1056.

Sangkharak, K., A. Choonut, T. Rakkan and P. Prasertsan. 2020. The degradation of phenanthrene, pyrene, and fluoranthene and its conversion into medium-chain-length polyhydroxyalkanoate by novel polycyclic aromatic hydrocarbon-degrading bacteria. *Current Microbiology*. 77 (6):897-909.

Santos, A.G., T.L. de Albuquerque, B.D. Ribeiro and M.A.Z. Coelho. 2021. *In situ* product recovery techniques aiming to obtain biotechnological products: A glance to current knowledge. *Biotechnology and Applied Biochemistry*. n/a (n/a):

Schutyser, W., T. Renders, G. Van den Bossche, S. Van den Bosch, S.-F. Koelewijn*, et al.*, Catalysis in lignocellulosic biorefineries: The case of lignin conversion. In *Nanotechnology in catalysis*, 2017; pp 537-584.

Schutyser, W., T. Renders, S. Van den Bosch, S.F. Koelewijn, G.T. Beckham*, et al.* 2018. Chemicals from lignin: An interplay of lignocellulose fractionation, depolymerisation, and upgrading. *Chemical Society Reviews*. 47 (3):852-908.

Senior, P.J. and E.A. Dawes. 1971. Poly-hydroxybutyrate biosynthesis and the regulation of glucose metabolism in *Azotobacter beijerinckii*. *The Biochemical Journal*. 125 (1):55-66.

Senior, P.J., G.A. Beech, G.A. Ritchie and E.A. Dawes. 1972. The role of oxygen limitation in the formation of poly-hydroxybutyrate during batch and continuous culture of *Azotobacter beijerinckii*. *The Biochemical Journal*. 128 (5):1193-1201.

Shantini, K., A.R. Yahya and A.A. Amirul. 2015. Influence of feeding and controlled dissolved oxygen level on the production of poly(3-hydroxybutyrate-co-3-hydroxyvalerate) copolymer by *Cupriavidus sp.* USMAA2-4 and its characterization. *Journal of Microbiological Methods*. 176 (5):1315-1334.

Sheldon, R.A. 2007. The E factor: Fifteen years on. *Green Chemistry*. 9 (12):1273-1283.

Sheldon, R.A. 2012. Fundamentals of green chemistry: Efficiency in reaction design. *Chemical Society Reviews*. 41 (4):1437-1451.

Shin, S.K., Y.J. Ko, J.E. Hyeon and S.O. Han. 2019. Studies of advanced lignin valorization based on various types of lignolytic enzymes and microbes. *Bioresource Technology*. 289 121728.

Shuai, L., M.T. Amiri, Y.M. Questell-Santiago, F. Héroguel, Y. Li*, et al.* 2016. Formaldehyde stabilization facilitates lignin monomer production during biomass depolymerization. *Science*. 354 (6310):329-333.

Silby, M.W., C. Winstanley, S.A.C. Godfrey, S.B. Levy and R.W. Jackson. 2011. *Pseudomonas* genomes: Diverse and adaptable. *FEMS Microbiology Reviews*. 35 (4):652-680.

Skoog, E., J.H. Shin, V. Saez-Jimenez, V. Mapelli and L. Olsson. 2018. Biobased adipic acid – the challenge of developing the production host. *Biotechnology Advances*. 36 (8):2248-2263.

Stegmann, P., M. Londo and M. Junginger. 2020. The circular bioeconomy: Its elements and role in european bioeconomy clusters. *Resources, Conservation & Recycling: X*. 6 100029.

Stern, D.I. 2011. The role of energy in economic growth. *Annals of the New York Academy of Sciences*. 1219 (1):26-51.

Sudarsanam, P., D. Ruijten, Y. Liao, T. Renders, S.-F. Koelewijn*, et al.* 2020. Towards lignin-derived chemicals using atom-efficient catalytic routes. *Trends in Chemistry*. 2 (10):898-913.

Sun, Z., J.A. Ramsay, M. Guay and B.A. Ramsay. 2006. Automated feeding strategies for high-cell-density fed-batch cultivation of *Pseudomonas putida* KT2440. *Applied Microbiology and Biotechnology*. 71 (4):423-431.

Sun, Z., B. Fridrich, A. de Santi, S. Elangovan and K. Barta. 2018. Bright side of lignin depolymerization: Toward new platform chemicals. *Chemical Reviews* 118 (2):614-678.

Takkellapati, S., T. Li and M.A. Gonzalez. 2018. An overview of biorefinery derived platform chemicals from a cellulose and hemicellulose biorefinery. *Clean Technologies and Environmental Policy*. 20 (7):1615-1630.

Taylor, S. 2009. Wealth, health and equity: Convergence to divergence in late 20th century globalization. *British Medical Bulletin*. 91 (1):29-48.

Third, K.A., M. Newland and R. Cord-Ruwisch. 2003. The effect of dissolved oxygen on PHB accumulation in activated sludge cultures. *Biotechnology and Bioengineering*. 82 (2):238-250.

Thoresen, P.P., L. Matsakas, U. Rova and P. Christakopoulos. 2020. Recent advances in organosolv fractionation: Towards biomass fractionation technology of the future. *Bioresource Technology*. 306 123189.

Tian, D., J. Hu, J. Bao, R.P. Chandra, J.N. Saddler*, et al.* 2017. Lignin valorization: Lignin nanoparticles as high-value bio-additive for multifunctional nanocomposites. *Biotechnology for Biofuels*. 10 (1):192.

Tomizawa, S., J.-A. Chuah, K. Matsumoto, Y. Doi and K. Numata. 2014. Understanding the limitations in the biosynthesis of polyhydroxyalkanoate (PHA) from lignin derivatives. *ACS Sustainable Chemistry & Engineering*. 2 (5):1106-1113.

Tumen-Velasquez, M., C.W. Johnson, A. Ahmed, G. Dominick, E.M. Fulk*, et al.* 2018. Accelerating pathway evolution by increasing the gene dosage of chromosomal segments. *Proceedings of the National Academy of Sciences, USA*. 115 (27):7105.

Tyrovouzis, N.A., A.S. Angelidis and N.G. Stoforos. 2014. Bi-phasic growth of listeria monocytogenes in chemically defined medium at low temperatures. *International Journal of Food Microbiology*. 186 110-119.

van Duuren, J.B., D. Wijte, A. Leprince, B. Karge, J. Puchałka*, et al.* 2011. Generation of a *catR* deficient mutant of *P. putida* KT2440 that produces *cis, cis*-muconate from benzoate at high rate and yield. *Journal of Bacteriology*. 156 (3):163-172.

van Duuren, J.B., D. Wijte, B. Karge, V.A. dos Santos, Y. Yang*, et al.* 2012. PH-stat fed-batch process to enhance the production of *cis, cis*-muconate from benzoate by *Pseudomonas putida* KT2440-JD1. *Biotechnology Progress*. 28 (1):85-92.

Van Hecke, W., G. Kaur and H. De Wever. 2014. Advances in in-situ product recovery (ISPR) in whole cell biotechnology during the last decade. *Biotechnology Advances*. 32 (7):1245-1255.

Vardon, D.R., M.A. Franden, C.W. Johnson, E.M. Karp, M.T. Guarnieri*, et al.* 2015. Adipic acid production from lignin. *Energy & Environmental Science*. 8 (2):617-628.

Vardon, D.R., N.A. Rorrer, D. Salvachúa, A.E. Settle, C.W. Johnson*, et al.* 2016. *Cis,cis*-muconic acid: Separation and catalysis to bio-adipic acid for nylon-6,6 polymerization. *Green Chemistry*. 18 (11):3397-3413.

Velázquez-Sánchez, C., G. Espín, C. Peña and D. Segura. 2020. The modification of regulatory circuits involved in the control of polyhydroxyalkanoates metabolism to improve their production. *Frontiers in Bioengineering and Biotechnology*. 8 (386):

Verbeeck, K., S. Gildemyn and K. Rabaey. 2018. Membrane electrolysis assisted gas fermentation for enhanced acetic acid production. *Frontiers in Energy Research*. 6 (88):

Wang, H., Y. Pu, A. Ragauskas and B. Yang. 2019. From lignin to valuable products–strategies, challenges, and prospects. *Bioresource Technology*. 271 449-461.

Wang, X., A. Oehmen, E.B. Freitas, G. Carvalho and M.A.M. Reis. 2017. The link of feast-phase dissolved oxygen (DO) with substrate competition and microbial selection in PHA production. *Water Research*. 112 269-278.

Wang, X., L. Lin, J. Dong, J. Ling, W. Wang*, et al.* 2018. Simultaneous improvements of cell growth and polyhydroxyalkanoate production from a lignin derivative for lignin-consolidated bioprocessing. *Applied and Environmental Microbiology*. 84 (18):e01469-01418.

Weimer, A., M. Kohlstedt, D.C. Volke, P.I. Nikel and C. Wittmann. 2020. Industrial biotechnology of *Pseudomonas putida*: Advances and prospects. *Applied Microbiology and Biotechnology*. 104 (18):7745-7766.

Weiss, R., G.M. Guebitz, A. Pellis and G.S. Nyanhongo. 2020. Harnessing the power of enzymes for tailoring and valorizing lignin. *Trends in Biotechnology*. 38 (11):1215-1231.

Whitman, B.E., D.R. Lueking and J.R. Mihelcic. 1998. Naphthalene uptake by a *Pseudomonas fluorescens* isolate. *Canadian Journal of Microbiology*. 44 (11):1086-1093.

Wilkes, R.A. and L. Aristilde. 2017. Degradation and metabolism of synthetic plastics and associated products by *Pseudomonas sp.*: Capabilities and challenges. *Journal of Applied Microbiology*. 123 (3):582-593.

Winsor, G.L., E.J. Griffiths, R. Lo, B.K. Dhillon, J.A. Shay*, et al.* 2016. Enhanced annotations and features for comparing thousands of *Pseudomonas* genomes in the *Pseudomonas* genome database. *Nucleic acids research*. 44 (D1):D646-D653.

Wong, S.S., R. Shu, J. Zhang, H. Liu and N. Yan. 2020. Downstream processing of lignin derived feedstock into end products. *Chemical Society Reviews*. 49 (15):5510-5560.

Wordofa, G.G. and M. Kristensen. 2018. Tolerance and metabolic response of *Pseudomonas taiwanensis* VLB120 towards biomass hydrolysate-derived inhibitors. *Biotechnology for Biofuels*. 11 199.

Xie, N.-Z., H. Liang, R.-B. Huang and P. Xu. 2014. Biotechnological production of muconic acid: Current status and future prospects. *Biotechnology Advances*. 32 (3):615-622.

Xu, J., J.J.L. Guzman, S.J. Andersen, K. Rabaey and L.T. Angenent. 2015. *In-line* and selective phase separation of medium-chain carboxylic acids using membrane electrolysis. *Chemical Communications*. 51 (31):6847-6850.

Xu, Z., P. Lei, R. Zhai, Z. Wen and M. Jin. 2019a. Recent advances in lignin valorization with bacterial cultures: Microorganisms, metabolic pathways, and bio-products. *Biotechnology for Biofuels*. 12 32.

Xu, Z., X. Li, N. Hao, C. Pan, L. de la Torre*, et al.* 2019b. Kinetic understanding of nitrogen supply condition on biosynthesis of polyhydroxyalkanoate from benzoate by *Pseudomonas putida* KT2440. *Bioresource Technology*. 273 538-544.

Xu, Z., C. Pan, X. Li, N. Hao, T. Zhang*, et al.* 2021. Enhancement of polyhydroxyalkanoate production by co-feeding lignin derivatives with glycerol in *Pseudomonas putida* KT2440. *Biotechnology for Biofuels*. 14 (1):11.

Yao, X., R. Yasmeen, I.U.H. Padda, W.U.H. Shah and M.A. Kamal. 2020. Inequalities by energy sources: An assessment of environmental quality. *PLOS ONE*. 15 (3):e0230503.

Yoshikawa, N., S. Mizuno, K. Ohta and M. Suzuki. 1990. Microbial production of *cis,cis*-muconic acid. *Journal of Biotechnology*. 14 (2):203-210.

Yousuf, A. 2012. Biodiesel from lignocellulosic biomass – prospects and challenges. *Waste Management*. 32 (11):2061-2067.

Yu, I.K.M., H. Chen, F. Abeln, H. Auta, J. Fan*, et al.* 2020. Chemicals from lignocellulosic biomass: A critical comparison between biochemical, microwave and thermochemical conversion methods. *Critical Reviews in Environmental Science and Technology*. 1-54.

Yu, O. and K.H. Kim. 2020. Lignin to materials: A focused review on recent novel lignin applications. *Applied Sciences*. 10 (13):4626.

Zakzeski, J., P.C.A. Bruijnincx, A.L. Jongerius and B.M. Weckhuysen. 2010. The catalytic valorization of lignin for the production of renewable chemicals. *Chemical Reviews*. 110 (6):3552-3599.

Zhang, C. and F. Wang. 2020. Catalytic lignin depolymerization to aromatic chemicals. *Accounts of Chemical Research*. 53 (2):470-484.

Zhang, Y. and M. Naebe. 2021. Lignin: A review on structure, properties, and applications as a light-colored uv absorber. *ACS Sustainable Chemistry & Engineering*. 9 (4):1427-1442.

Zhao, C., S. Xie, Y. Pu, R. Zhang, F. Huang*, et al.* 2016. Synergistic enzymatic and microbial lignin conversion. *Green Chemistry*. 18 (5):1306-1312.

Zhou, Y., L. Lin, H. Wang, Z. Zhang, J. Zhou*, et al.* 2020. Development of a CRISPR/Cas9n-based tool for metabolic engineering of *Pseudomonas putida* for ferulic acid-to-polyhydroxyalkanoate bioconversion. *Communications Biology*. 3 (1):98.

Zhou, Z., F. Lei, P. Li and J. Jiang. 2018. Lignocellulosic biomass to biofuels and biochemicals: A comprehensive review with a focus on ethanol organosolv pretreatment technology. *Biotechnology & Bioengineering* 115 (11):2683-2702.

Zoghlami, A. and G. Paës. 2019. Lignocellulosic biomass: Understanding recalcitrance and predicting hydrolysis. *Frontiers in Chemistry*. 7 874-874.

Zwietering, M.H., I. Jongenburger, F.M. Rombouts and K. van 't Riet. 1990. Modeling of the bacterial growth curve. *Applied and Environmental Microbiology*. 56 (6):1875-1881.

Curriculum Vitae

Personal information

Name	: Juan Esteban Ramírez Morales
Permanent address	: Nollendorfer str. 9A, 07743 Jena, Germany
Telephone	: +49 1707890549
E-mail	: jeramir3@gmail.com juan.ramirez@leibniz-hki.de
Passport number	: AR016021
Nationality	: Colombian
Date of birth	: 1986-04-25

Education

10/2016-10/2021	European Joint Doctorate (Marie Skłodowska-Curie Actions) Doctor of Natural Science – RWTH Aachen University, Germany Doctor of Bioscience engineering – Ghent University, Belgium Doctoral Training Programme on Sustainable Product, Energy and Resource Recovery from Wastewater (SuPER-W) Doctoral Thesis : „Lignin aromatics valorization by *Pseudomonas putida*: novel strategies to increase the production of *mcl*-polyhydroxyalkanoate and cis,cis-muconic acid„
03/2010-03/2012	Master of Science in Biochemical Engineering (MSc). Pontifical Catholic University of Valparaíso. Valparaiso. Chile. Master thesis: „Improvement of hydrogen production via anaerobic digestion through an extractive membrane bioreactor„
01/2003-12/2008	Bachelor of Science in Biological Engineering (BSc). National University of Colombia. Medellín. Colombia. Bachelor thesis: „Biological production of hydrogen from wastewaters„

Professional experience

01/2020-Actual	Doctoral researcher. Bio Pilot Plant department. Leibniz Institute for Natural Product Research and Infection Biology (HKI), Jena, Germany
10/2016-12/2019	Marie Curie fellow. Joint PhD researcher. Project: Lignin aromatics valorization by *Pseudomonas putida*: novel strategies to increase the production of *mcl*-polyhydroxyalkanoate and *cis,cis*-muconic acid. RWTH Aachen University. Aachen, Germany. Ghent University, Ghent, Belgium.
09/2019-11/2019	Industrial internship at Paques biotechnology. Biological treatment of toxic wastewaters (aromatic streams). Balk, The Netherlands
06/2016-10/2016	Research assistant. Project: Occurrence and Fate of Analgesic/Anti-inflammatory compounds during wastewater treatment using advanced oxidation processes. University of Antioquia. Medellin. Colombia
06/2015-11/2015	Advisor for primary and high school research projects in the field of natural sciences (biology and chemistry). Program Ferias CT+I (Science, technology and innovation). Parque Explora. Medellin. Colombia.
08/2014-12/2014	Participation in the research topic: ORP vs. dissolved oxygen as parameters for controlling biological sulfide oxidation by a biofilm formed under microaerobic conditions. Universidad de la Frontera. Temuco. Chile.
06/2014- 08/2014	Participation in the research project GRAIL. European Commission (FP7 Programme). "Glycerol Biorefinery Approach for the Production of High Quality Products of Industrial Value". Pontifical Catholic University of Valparaíso. Chile.
06/2013-05/2014	Early Stage Researcher. Project Marie Curie-IRSES ALGAENET (GA-2011- 295165) "Renewable energy production through microalgae cultivation: closing material cycles". Institute of Chemical Technology (ICT) in Prague. Prague. The Czech Republic.
01/2013-04/2013	Researcher in the Bioenergy research line of the Project innovaChile CORFO FCR-CSB 09CEII-699. Fraunhofer Chile Research. Valparaíso. Chile.
04/2012-10/2012	Research assistant in the Project SEP-CONACYT (100298): "Real time optimization to improve the fermentative hydrogen production in a continuous reactor". Laboratory for Research on Advanced Processes for Water Treatment. National Autonomous University of Mexico. Quéretaro, México.
10/2011-11/2012	Research assistant in the project FONDEF D10ER1007. "Development of a demonstrative plant for producing biogas from agricultural and domestic wastes to improve quality of life and access of a renewable energy source to families in the rural sector". ". Pontifical Catholic University of Valparaíso. Chile.

06/2010-03/2012	Research assistant. Project Fondecyt N°1090482: "Development of a novel extractive membrane bioreactor to improve Bio-hydrogen production as a ready-to-use renew energy source". School of biochemical engineering. Pontifical Catholic University of Valparaíso. Chile.
10/2007-11/2008	Participation in the research Project: "Feasibility of bio-hydrogen production from wastewater". Laboratory of Bioconversions. National University of Colombia. Medellin. Colombia.
04/2006-09/2007	Participation in the research Project: "Isolation, purification and characterization of an alpha-amylase produced by a native strain of *Bacillus spp*". Laboratory of Industrial Microbiology. National University of Colombia. Medellin. Colombia.

Teaching Experience

06/2015- 11/2015	Workshops and courses on scientific research methodology for high school students. Parque Explora, Medellin, Colombia.
03/2011-07/2011	Teaching assistant of the course "Environmental engineering laboratory". School of Biochemical Engineering. Pontifical Catholic University of Valparaíso. Chile.
02/2007-11/2007	Teaching assistant of the course "Genetic engineering". National University of Colombia. Medellin. Colombia.

Research Advising

11/2019-03/2021	Mohammad Sanowar (Master thesis). Development of a novel biotechnological approach for production and separation of muconic acid from lignin derived aromatics generated by a metabolically engineered strain of *Pseudomonas putida* KT2440. Friedrich Schiller University Jena, Jena, Germany.
11/2019-03/2021	Onyi Agogbua (Master thesis). Promoting anodic interaction to enhance lignin aromatic uptake and *mcl*-PHA accumulation in *Pseudomonas putida* KT2440. Friedrich Schiller University Jena, Jena, Germany.
12/2017-06/2018	Phillip Czichowski (Master Thesis). Screening of wild type *Pseudomonas sp*. for biological valorization of lignin-derived-aromatic waste streams. RWTH Aachen University, Aachen, Germany.
11/2017-04/2018	Richard Braun (Bachelor Internship). Growth screening of wild type *Pseudomonas* on lignin aromatic solutions. RWTH Aachen University, Aachen, Germany.

05/2017-10/2017	Boniface Leufak (Master thesis). Electrochemical depolymerisation of lignin followed by a microbial culture to enhance the product spectra in downstream processing operations. RWTH Aachen University, Aachen, Germany.
06/2015- 11/2015	Advising of High School Students on scientific research methodology with research projects related to biosciences and chemistry. Program Ferias CT+I (Science, technology and innovation). Parque Explora. Medellin. Colombia
07/2011-03/2012	Ramiro Gutiérrez Cerda (Bachelor thesis). Technical-economic evaluation of a wastewater treatment system by two-phase anaerobic digestion. Pontifical Catholic University of Valparaíso. Chile.

Fellowships, Scholarships and Awards

10/2016–Actual	Early Stage Researcher (ESR03) in the Marie Skłodowska-Curie ITN European Training Network SuPER-W.
06/2013–05/2014	Fellowship. Project IRSES ALGAENET (GA-2011- 295165). Institute of Chemical Technology (ICT) in Prague. Prague. The Czech Republic.
04/2012–10/2012	Fellowship. Awarded with the scholarship Ing. Horst Otterstetter. Institute of engineering (II-UNAM) and Interamerican Sanitary and Environmental Engineering Association. México DF. México.
10/2011	Best Poster Presentation: “Selection of gas extractive membranes to improve hydrogen production by anaerobic digestion”. X Latin American Workshop and Symposium on Anaerobic Digestion X DAAL. Ouro Preto, Minas Gerais-Brazil.
03/2010–03/2012	Tuition Exemption Scholarship for master studies. Pontifical Catholic University of Valparaíso. Chile.
10/2008	Best Poster Presentation: Isolation, purification and characterization of an alpha-amylase produced by a native strain of *Bacillus spp*. First Colombian Congress on Clinical, Industrial, Environmental Microbiology and Bioanalysis. Medellín-Colombia.

Languages

Spanish: Native or bilingual proficiency
English: Professional working proficiency
German: Limited working proficiency

Peer-Reviewed Publications

Juan E. Ramírez-Morales, Phillip Czichowski, Volkan Besirlioglu, Lars Regestein, Korneel Rabaey, Lars M. Blank, and Miriam A. Rosenbaum. 2021. Lignin aromatics to PHA polymers: nitrogen and oxygen are the key factors for *Pseudomonas*. *ACS Sustainable Chemistry & Engineering*, 9, 31, 10579–10590.

JE Ramirez-Morales, E Tapia-Venegas, JL Campos, G Ruiz-Filippi 2019. Operational behavior of a hydrogen extractive membrane bioreactor (HEMB) during mixed culture acidogenic fermentation. *International Journal of Hydrogen Energy* 44 (47), 25565-25574

Estela Tapia-Venegas, **Juan Esteban Ramirez-Morales** , Fernando Silva , Javiera Toledo-Alarcón, Florian Paillet, Renaud Escudie , Chyi-How Lay, Chen-Yeon Chu, Hoang-Jyh Leu , Antonella Marone , Chiu-Yue Lin , Dong-Hoon Kim , Eric Trably , Gonzalo Ruiz-Filippi. 2015. Biohydrogen production by dark fermentation: scaling-up and technologies integration for a sustainable system. *Reviews in Environmental Science and Bio/technology*. DOI: 10.1007/s11157-015-9383-5

Juan E. Ramírez-Morales, Ixbalank Torres Zúñiga, Germán Buitrón. 2015. On-line heuristic optimization strategy to maximize the hydrogen production rate in a continuous stirred tank reactor. *Process Biochemistry*. 50(6):893-900. DOI:10.1016/j.procbio.2015.03.003.

Juan E. Ramírez-Morales, Estela Tapia-Venegas, Javiera Toledo-Alarcón, Gonzalo RuizFilippi. 2015. Review: Simultaneous production and separation of biohydrogen in mixed culture systems by continuous dark fermentation. *Water Science and Technology*. 71(9):1271-85. DOI:10.2166/wst.2015.104

J.E. Ramírez-Morales, E. Tapia-Venegas, N. Nemestóthy b, P. Bakonyi, K. Bélafi Bakó, G. Ruiz-Filippi. 2013. Evaluation of two gas membrane modules for fermentative hydrogen separation. *International Journal of Hydrogen Energy*, 38 (32), 14042-14052. DOI: 10.1016/j.ijhydene.2013.08.092.

Estela Tapia-Venegas, **Juan-Esteban Ramírez**, Cesar Zamorano, Andrés Donoso-Bravo, Lorena Jorquera, Rolando Chamy, Jean-Phillipe Steyer, Gonzalo Ruiz-Filippi.2012. Bio-hydrogen production during acidogenic fermentation in a multistage stirred tank reactor. *International Journal of Hydrogen Energy*, 38 (5), 2185 - 2190. DOI: 10.1016/j.ijhydene.2012.11.077.

P. Bakonyi, N. Nemestothy, **J. Ramirez**, G. Ruiz-Filippi , K. Belafi-Bako.2012. Escherichia coli (XL1-BLUE) for continuous fermentation of bioH2 and its separation by polyimide membrane. *International Journal of Hydrogen Energy*. 37(7): 5623–5630. DOI: 10.1016/j.ijhydene.2012.01.009.

P. Bakonyi, N. Nemestothy, **J. Ramirez**, G. Ruiz-Filippi , K. Belafi-Bako.2011. Feasibility study of gas separation membranes for biohydrogen separation. *Hungarian journal of industrial chemistry* Veszprém . ISSN: 0133-0276. 39(3) pp. 331-333.

Bedoya A., Castrillon J.C., **Ramírez J.E.**, Vásquez J.E., Arias M. 2008. Producción biológica de hidrógeno: una aproximación al estado del arte. *Dyna*. Revista de la facultad de Minas - Universidad Nacional de Colombia - Sede Medellín. ISSN 0012-7353. 75 (154):137-157.

Presentations at Conferences

Oral:

Juan E. Ramírez-Morales, L. M. Blank, K. Rabaey, M. A. Rosenbaum. 2018 Biological valorization of lignin model compounds by wild-type *Pseudomonas*: Substrate and strain screening. 1st Pseudomonas grassroots meeting. Frankfurt. Germany

Ramírez J.E., Torres I., Buitrón G. 2012. Real time optimization for fermentative hydrogen production in a continuous reactor. III Latinamerican congress on Biorefineries. Pucón – Chile.

Ramírez J.E, Tapia E., Nemestothy N., Bélafi-Bakó K., Chamy R. y Ruiz G. 2011. Evaluation of extractive membranes to improve the hydrogen production via anaerobic digestion". XIX Chilean congress on environmental and sanitary engineering AIDIS. Concepción-Chile.

Tapia E., **Ramírez J.E.**, Ruiz G. y Chamy R. 2010. Stable and continuous operation of a hydrogen production process via anaerobic digestion in a two-serial reactor system. XXXII Interamerican congress on environmental and sanitary engineering AIDIS. Punta Cana - Dominican Republic.

Poster:

Juan E. Ramírez-Morales, L. M. Blank, K. Rabaey, M. A. Rosenbaum. 2019. Biotechnological approach for the valorization of synthetic Lignin wastewater in a bioelectrochemical system by *Pseudomonas putida* KT2441 3rd IWA Resource Recovery Conference. Venice, Italy

Juan E. Ramírez-Morales, P. Czichowski, R. Braun, L. M. Blank, K. Rabaey, M. A. Rosenbaum. 2018 Growth screening of wild type *Pseudomonas* strains for biological valorization of lignin model compounds. 14th International Conference on Renewable Resources and Biorefineries. Ghent . Belgium.

Juan E. Ramírez-Morales, P. Czichowski, L. M. Blank, K. Rabaey, M. A. Rosenbaum. 2018. Evaluation of two wild-type *Pseudomonas putida* strains for anodic production of polyhydroxyalkanoates (PHAs) using lignin-derived aromatic compounds. International Society for Microbial Electrochemistry and Technology, 4th European Meeting. Newcastle. England

J.E. Ramírez-Morales, E. Tapia-Venegas, C. Contreras, G. Ruiz-Filippi. 2015. A simple methodology for kinetic determination: Application to hydrogen-producing mixed culture under different glycerol concentrations. 14th World Congress on Anaerobic Digestion (AD14). Viña del Mar, Chile.

N. Anferova, **J.E. Ramirez Morales**, J. Bartáček, P. Jeníček, D. Jeison. 2015. ORP vs. Dissolved oxygen as parameters for controlling biological sulfide oxidation by a biofilm formed under microaerobic conditions. 14th World Congress on Anaerobic Digestion (AD14). Viña del Mar, Chile.

N. Anferova, **J.E. Ramirez Morales**, J. Bartáček, P. Jeníček, D. Jeison. 2015. Efficient Growth of Sulfide-Oxidizing Bacteria (SOB) in a Moving Bed Biofilm Reactor (MBBR) under Microaerobic Conditions (LWWTP-0136). 12th IWA Specialised Conference on Design, Operation and Economics of "Large Wastewater Treatment Plants". Prague, Czech Republic.

Ramírez J.E., E. Tapia, N. Nemestothy, K. Bélafi-Bakó, R. Chamy, G. Ruiz. 2013. Behaviour of an extractive membrane bio-reactor for fermentative hydrogen production. 13th World Congress on Anaerobic Digestion (AD13). Santiago de Compostela , Spain.

R. Gutiérrez, **Ramírez J.E.**, E. Tapia, C. Zamorano, G. Ruiz-Filippi.2012. Energy production from wastewater with high sugar content. XXXII interamerican congress on enviromental and sanitary engineering AIDIS. Salvador Bahía - Brazil.

Ramírez J.E, Tapia E., Nemestothy N., Bélafi-Bakó K., Chamy R. and Ruiz G. 2011. Selection of gas extractive membranes to improve hydrogen production by anaerobic digestion. X Latin American Workshop and Symposium on Anaerobic Digestion X DAAL. Ouro Preto, Minas Gerais-Brazil.

Tapia E., **Ramírez J.E.**, Chamy R. y Ruiz G. 2010. Biohydrogen production with glycerol as substrate with continuous and non continuous hydrogen extraction. 12th World Congress on Anaerobic Digestion (AD12). Guadalajara-México.

Quintero M., **Ramírez J.E.**, Catrillon J.C., Pareja A., Montoya O., Gutiérrez P. 2008. Isolation, purification and characterization of an alpha-amylase produced by a native strain of *Bacillus spp*. First Colombian Congress on Clinical, Industrial, Environmental Microbiology and Bioanalysis. Medellín-Colombia.